Protoclusters associated with distant radio galaxies

Protoclusters associated with distant radio galaxies

Proefschrift

ter verkrijging van
de graad van Doctor aan de Universiteit Leiden,
op gezag van de Rector Magnificus Dr. D.D. Breimer,
hoogleraar in de faculteit der Wiskunde en
Natuurwetenschappen en die der Geneeskunde,
volgens besluit van het College voor Promoties
te verdedigen op woensdag 27 april 2005
te klokke 16.15 uur

door

Bram Pieter Venemans

geboren te Hoorn
in 1977

Promotiecommissie

Promotor:	Prof. dr. G. K. Miley
Co-promotor:	Dr. H. J. A. Röttgering
Referent:	Dr. S. A. Stanford (IGPP/LLNL & UC Davis, USA)
Overige leden:	Prof. dr. P. T. de Zeeuw
	Prof. dr. M. Franx
	Prof. dr. M. A. M. van de Weygaert (Rijksuniversiteit Groningen)
	Dr. P. N. Best (University of Edinburgh, UK)
	Dr. I. A. G. Snellen

The cover shows a narrow-band (*left*) and a broad-band (*right*) image of the radio galaxy TN J1338–1942 and its surroundings. Galaxies that appear bright in the narrow-band image but that are faint in the broad-band image are members of a forming cluster near the radio galaxy.

Op de omslag staat een opname gemaakt in een smalband filter (*links*) en een gemaakt in een breedband filter (*rechts*). De opnames tonen het radio sterrenstelsel genaamd TN J1338–1942 en zijn omgeving. Sterrenstelsels die helder zijn op de smalband opname maar veel zwakker zijn op de breed-band opname zijn leden van een groep van sterrenstelsels in de buurt van het radiostelsel.

Table of contents

Chapter 1

Introduction

1.1 Clusters of galaxies

I N Cold Dark Matter (CDM) scenarios the first stars and stellar systems form through gravitational infall of primordial gas in large CDM halos (e.g., White & Rees 1978). Numerical simulations suggest that, as these halos merge, they form vast, web-like networks (filaments) of young galaxies and ionized gas, surrounded by large, nearly empty voids (e.g., Baugh et al. 1998). At the intersection of the filaments are clusters of galaxies. These clusters of galaxies are the largest and most massive discrete structures that formed in the Universe. This makes them unique and important laboratories for investigating a number of questions in astronomy.

For example, the observed present-day number density of massive clusters of galaxies places strong constraints on cosmology, especially on the fundamental parameters Ω_M (the matter density) and σ_8 (the mass fluctuation on scales of ~ 8 Mpc). The observed present-day abundance of rich clusters allows either a Universe with a high density parameter and low fluctuation or a low density Universe with large mass fluctuations (e.g., Bahcall & Cen 1992; White et al. 1993; Eke et al. 1996). The *evolution* of cluster abundances with redshift, however, depends primarily Ω_M (e.g., Eke et al. 1996). Therefore, the number density of rich clusters at $z > 0.5$ can be used to constrain the matter density in the Universe and the strength of the mass fluctuations, as shown by e.g., Fan et al. (1997) and Bahcall & Fan (1998).

Several studies of massive clusters with redshifts up to $z = 1.3$ have found very little evolution in the cluster properties (Tozzi et al. 2003; Hashimoto et al. 2004; Maughan et al. 2004; Rosati et al. 2004). Despite the large lookback times, clusters at $z \sim 1$ appear to be very similar to local clusters. The high redshift clusters have thermodynamical properties and metallicities that are very similar to those of lower redshift clusters.

A second reason to study distant clusters is that they supply large numbers of galaxies at specific redshifts, making them excellent laboratories with which to investigate the formation and evolution of galaxies. For example, the analysis of galaxies in $z \sim 1$ clusters showed that the stars in massive, early-type galaxies formed at $2 < z < 3$ (e.g., Ellis et al. 1997; Stanford et al. 1998; van Dokkum & Stanford 2003; Holden et al. 2005). Investigating the galaxy population of (forming) clusters at $z > 2$ could provide knowledge on the formation process of such massive galaxies (e.g., Eggen et al. 1962; Baugh & Gaztanaga 1996). Also because clusters are the most extreme overdense regions in the Universe, they allow an efficient investigation of the interaction between galaxies and their environment (e.g., Miles et al. 2004; Tanaka et al. 2004; van Zee et al. 2004; Goto 2005; Nakata et al. 2005; Tran et al. 2005).

There are many intriguing questions in astronomy of which the answers involve studies of clusters of galaxies. These include:

- What is the mass function of high redshift clusters and how does this evolve with redshift?
- How do cluster X-ray scaling relations such as the mass-temperature relation and the luminosity-temperature relation evolve at high redshift?
- What is the origin of the minimum entropy of the intracluster medium (e.g., Valageas et al. 2003; Nath 2004)?
- How and when did the massive galaxies form that populate the cores of low redshift clusters?
- How does the environment influence the formation and evolution of galaxies?

To start answering these questions, a sample of high redshift clusters of galaxies is needed. Unfortunately, using conventional optical and X-ray techniques, the detection of clusters with $z > 1$ is difficult. Searches for extended X-ray sources become very challenging as the surface brightness of the X-ray emission fades as $(1 + z)^4$. And while optical surveys have been very successful in identifying galaxy clusters at $z \lesssim 1$ by searching for concentrations of red galaxies (e.g., Gladders 2002), to search for $z > 1$ clusters with the same method would require sensitive, wide field near-infrared cameras which are not (yet) available. In the future, surveys exploiting the Sunyaev-Zeldovich (SZ) effect (e.g., Carlstrom et al. 2002) will be able to detect clusters of galaxies at $z \gg 1$. However, at this moment the sensitivity of SZ surveys is not sufficient to detect any known clusters at $z > 1$.

This thesis adopts a different approach to search for distant clusters, namely to look for galaxy concentrations near distant luminous radio galaxies, which are presumed to be tracers of high-density regions in the Universe.

1.2   Distant luminous radio galaxies: tracers of overdense regions

During the last decade, multi wavelength studies of the most powerful high redshift radio galaxies (HzRGs; $z > 2$) have produced strong evidence that they are massive galaxies in the process of formation, and that they are probably the ancestors of dominant cluster galaxies. Supporting evidence includes:

- HzRGs trace the bright envelope in the infrared Hubble diagram (Lilly & Longair 1982; Jarvis et al. 2001; De Breuck et al. 2002; Zirm et al. 2003). At each redshift, HzRGs are amongst the brightest objects, implying that they are amid the most *massive* galaxies at high redshift (see also Rocca-Volmerange et al. 2004).
- HzRGs undergo vigorous star formation, with star formation rates frequently $\gg 100\,M_\odot\,\mathrm{yr}^{-1}$. For example, based on the UV continuum luminosity, Zirm et al. (2005) estimate that the radio galaxy TN J1338–1942 is forming $200\,M_\odot$ of stars each year. Using deep spectropolarimetric observations obtained with the Keck telescope of several radio galaxies at $2 < z < 4$, Dey et al. (1997) and Vernet et al. (2001) found that for some of the radio galaxies the contribution of the AGN to the UV continuum is small, and that the emission is dominated by young stars. The implied high star formation rate in these galaxies of up to $\sim 1000\,M_\odot\,\mathrm{yr}^{-1}$ is supported by the detection of dust and extended CO emission in HzRGs (e.g.,

Papadopoulos et al. 2000; Archibald et al. 2001; De Breuck et al. 2003a,b; Stevens et al. 2003; Greve et al. 2004; Reuland et al. 2004; De Breuck et al. 2005), which is likely caused by bursts of star formation (e.g., Papadopoulos et al. 2000; Reuland et al. 2004).

- HzRGs appear extremely clumpy on high resolution images taken with *Hubble Space Telescope (HST)*, and look strikingly similar to simulations from hierarchical models of forming massive galaxies (e.g., Pentericci et al. 1998, 1999). The sizes, profiles and luminosities of the clumps are comparable to those of high redshift UV bright, star forming galaxies (Lyman Break Galaxies, e.g., Giavalisco 2002).

Further evidence that (at least a fraction of) HzRGs reside in cluster environments is the extreme radio rotation measures ($> 1000\ \mathrm{rad\,m^{-2}}$) that 20% of the HzRGs possess (Carilli et al. 1997; Athreya et al. 1998; Pentericci et al. 2000b). The large radio rotation measures are probably caused by dense hot gas that surrounds the radio galaxies, similar to the hot gas in the centers of massive clusters.

At lower redshifts, $0.3 < z < 1.5$, radio galaxies are known to predominantly lie in moderately rich clusters. Yates et al. (1989) discovered that powerful radio galaxies at redshifts $z > 0.3$ occupy environments on average as rich as Abell class 0 clusters of galaxies. In support of this, Hill & Lilly (1991) found that about half of the powerful classical double radio sources at $z \sim 0.5$ resides in rich clusters of galaxies. Galaxy overdensities comparable to that expected for clusters of Abell class 0 richness are found near radio galaxies up to $z = 1.6$ (Best 2000; Best et al. 2003; Stern et al. 2003; Barr et al. 2004; Bornancini et al. 2004). At higher redshifts $z > 2$, targeted searches for companion galaxies near powerful radio sources have been given promising results (Le Fèvre et al. 1996; Pascarelle et al. 1996; Keel et al. 1999), although the number of confirmed companions is small.

Taken together, these properties of HzRGs provide strong *indirect* evidence that luminous distant radio sources pinpoint massive galaxies at the centers of forming clusters of galaxies.

To search for *direct* evidence of the association of forming clusters with distant powerful radio galaxies, companion galaxies near radio galaxies must be selected and spectroscopically confirmed. Therefore, an effective technique is needed to identify distant galaxies.

1.3 Searches for high redshift galaxies

Between the 1950s and the 1990s radio galaxies, because of their large radio luminosities and bright emission lines, were the most distant galaxies known (Spinrad et al. 1981; Djorgovski et al. 1987; Chambers et al. 1988, 1990; Chambers 1990; Spinrad et al. 1995).

Since the 1970s astronomers have been searching for distant *star forming* galaxies ($z \gg 2$). The early attempts were unsuccessful (e.g., Davis & Wilkinson 1974; Partridge 1974), and the only objects that were discovered with redshifts above 1 were active galaxies, such as quasars and radio galaxies (e.g., Schmidt 1974).

In the 1980s and early 1990s several deep, magnitude limited redshift surveys were conducted to search for distant galaxies. It was known from deep optical imaging

that the galaxy number counts in the *B*-band increased rapidly towards fainter magnitudes. These so-called faint blue galaxies were first thought to be at high redshift, but the redshift surveys showed that they lie at redshifts $z < 1$ (Cowie et al. 1991; Colless et al. 1993; Songaila et al. 1994). For example, a faint galaxy redshift survey down to a magnitude of $m_B = 24$ conducted by Glazebrook et al. (1995) found a median redshift of $z = 0.46$ with the survey extending out to $z > 1$. The highest redshift galaxy in the survey has $z = 1.1$. More recent (and deeper) magnitude limited spectroscopic surveys have a median redshift of $z \sim 0.7$ down to *I*-band magnitude of $m_I = 24$ (e.g., Le Fèvre et al. 2004, 2005). Only a small fraction ($< 5\%$) in such redshift surveys has a redshift $z > 2.5$ (Le Fèvre et al. 2005).

Because high redshift galaxies do not dominate the number counts in deep images, a selection must be applied to identify galaxies at $z > 2$. Koo (1985) suggested to use broad-band colors of galaxies to obtain a "poor person's redshift", nowadays called a photometric redshift. The achieved accuracy of this indirect redshift was roughly 10% (Koo 1985). One of the first groups to efficiently apply the photometric redshift method on deep images to search for $z \sim 3$ galaxies was that of Steidel and collaborators (Steidel & Hamilton 1992, 1993; Steidel et al. 1995). They selected galaxies based on two assumptions. First, the UV continuum of distant galaxies is nearly flat ($f_\nu \sim \nu^0$) due to the presence of massive stars. Second, a spectral break is present at 912 Å in the rest-frame caused by H I absorption in the galaxy and in the intergalactic medium (e.g., Madau 1995). While in 1995 the highest redshift "normal" field galaxy was at $z = 1.1$, a year later Steidel et al. (1996) reported the confirmation of >16 normal, star forming galaxies at $z = 3.0 - 3.4$. Because the galaxies are selected on having a spectral break at the Lyman limit at 912 Å, the galaxies are called Lyman Break Galaxies (LBGs). Surveys for LBGs have been extremely successful. Nowadays, thousands of *confirmed* redshift $z \sim 3$ LBGs are found, and the efficiency of selecting the galaxies in deep broad-band optical imaging is high, 70–80% (Steidel et al. 1999, 2003; Cooke et al. 2005). Although very efficient, a disadvantage of this technique is that it selects galaxies over a relatively broad redshift range of $\Delta z = 0.6 - 1.0$ (e.g., Steidel et al. 2003). In contrast, galaxies in a large scale structure near a HzRG are expected to have a velocity range of $\sim 3000 \, \mathrm{km \, s^{-1}}$, or $\Delta z = 0.04$ at $z \sim 3$. Despite the fact that forming clusters of LBGs are found at $z \sim 3$, even in these fields still 75% of the LBGs is either foreground or background to the large scale structure (e.g., Steidel et al. 1999).

An alternative method for detecting distant galaxies is to perform narrow-band imaging searches for galaxies with a strong Lyα emission line. Models of stellar populations predicted that the Lyα emission in star bursting galaxies must be luminous (Meier 1976; Charlot & Fall 1993). However, until a decade ago, searches for Lyα emitting galaxies were fruitless (see Pritchet 1994 for a review).

The situation changed with the advent of the 8–10 m class telescopes, which led to an increase in sensitivity. Using the Keck telescope, Cowie & Hu (1998) and Hu et al. (1998) found a significant population of Lyα emitting galaxies (densities of 15 000 emitters $\mathrm{deg^{-2}}$ per unit z) at $z \simeq 3.4$ in several blank fields. Now, blank field narrow-band imaging is being carried out with great success and high redshift galaxies are found up to $z > 6.5$ (e.g., Kudritzki et al. 2000; Rhoads & Malhotra 2001; Fynbo et al. 2001; Hu et al. 2002; Fynbo et al. 2003; Fujita et al. 2003; Kodaira et al. 2003; Rhoads

et al. 2003; Ouchi et al. 2003; Dawson et al. 2004; Palunas et al. 2004; Hayashino et al. 2004; Hu et al. 2004; Ouchi et al. 2005).

Although only a small fraction of high redshift star forming galaxies has a strong Lyα line ($< 20 - 25\%$, Steidel et al. 2000; Shapley et al. 2003), the advantage of this method is that galaxies can be selected in a relatively small redshift range $\Delta z < 0.1$. This makes the narrow-band imaging technique a promising method for investigating the environment of HzRGs.

1.4   VLT pilot project: a protocluster at *z* = 2.16

Using the Lyα imaging technique, the surroundings of radio galaxies can efficiently be studied to search for *direct* evidence of the association of a cluster or a forming cluster (protocluster) with a radio galaxy. Promising results were obtained by Le Fèvre et al. (1996), who found two bright Lyα emitting galaxies near a radio galaxy at $z = 3.1$. Our group conducted a pilot project at the Very Large Telescope (VLT) aimed at finding an excess of Lyα emitters around the clumpy radio galaxy MRC 1138–262 at $z = 2.16$. Deep observations of a $7' \times 7'$ field surrounding MRC 1138–262 were carried out in a narrow-band filter which encompassed the redshifted Lyα line of the radio galaxy (Kurk et al. 2000, 2004b). The imaging resulted in a list of ~ 40 candidate Lyα emitters near the redshift of the radio galaxy (Kurk et al. 2000, 2004b). The surface density of the candidate emitters is higher than in blank fields, which could be an indication that the radio galaxy resides in a forming cluster (Kurk et al. 2000).

A subset of these candidates was subsequently observed spectroscopically. The multi-object spectroscopy confirmed 14 Lyα emitters and one QSO of which the velocities were within 1000 km s^{-1} of the central radio galaxy (Pentericci et al. 2000a; Kurk et al. 2004b). By comparing the volume density of the confirmed Lyα emitters near MRC 1138–262 to the field density of Lyα emitters at that redshift, Kurk et al. (2004b) found that the region near the radio galaxy is overdense by a factor 4.4 ± 1.2. The velocity distribution of the galaxies suggests that the Lyα emitters reside in two subgroups with velocity dispersions of 300 and 500 km s^{-1} (Pentericci et al. 2000a). If these subgroups are virialized, then the combined mass would be $> 10^{14} M_\odot$ (Pentericci et al. 2000a), which is consistent with a protocluster near the radio galaxy.

Additional evidence for the protocluster near MRC 1138–262 comes from the detection of an overdensity of extremely red objects (EROs) in the same field (Kurk et al. 2004b). The overdensity is most likely caused by dusty star forming galaxies at the redshift of the radio galaxy (Kurk et al. 2004b). Also, using near-infrared narrow-band images, a significant population of Hα emitters was selected at the redshift of the radio galaxy (Kurk et al. 2004b). Spectroscopy of nine candidate Hα emitters confirmed that all nine sources were associated with the radio galaxy (Kurk et al. 2004a). Also, observations with the *Chandra X-ray Observatory (CXC)* revealed an excess of soft X-ray sources in the field of MRC 1138–262 (Pentericci et al. 2002), indicating that several AGNs might be present in the protocluster.

The VLT pilot project provided convincing additional evidence that HzRGs can be used to pinpoint regions of galaxy overdensity at high redshift.

1.5   This Thesis

As shown by the successful study of the overdense region near MRC 1138–262, distant radio galaxies trace high redshift protoclusters, providing ideal laboratories for studying the development of large scale structure and galaxy evolution. To further investigate the formation of large scale structure in the early Universe and the evolution of galaxies in dense environments, a large program at the VLT was initiated to search for Lyα emitting galaxies around luminous radio galaxies with redshifts $2 < z < 5$. The goal of this project was to address (i) what fraction of HzRGs resides in regions of galaxy overdensities, similar to structure near MRC 1138–262, (ii) if and how the macro properties of the protocluster regions, such as the velocity dispersion of the galaxies and size, change with redshift, and whether this change can be reconciled with theories of large scale structure formation, (iii) how characteristics of individual galaxies like size, star formation rate and (luminous) mass, located in the overdense regions depend on redshift and on environment and (iv) what the origin is of the large (> 50 kpc) Lyα halos associated with HzRGs and what role they play in the formation of massive galaxies and the surrounding clusters.

In the large program, we observed the surroundings of eight radio galaxies with redshifts $2 < z < 5.2$ in a total of 25 nights at the VLT and the Keck telescope. Deep narrow-band and broad-band imaging were used to locate galaxies having excess Lyα emission in 3×3 Mpc^2 regions around the radio galaxies. Follow-up spectra have confirmed that the candidate Lyα emitters have redshifts similar to those of the HzRGs.

This thesis describes the results of this VLT large program and supporting observations. A summary of the chapters in the thesis is given below.

Chapter 2

The first radio galaxy that was observed in the VLT large program was TN J1338–1942 at $z = 4.1$. This radio galaxy is among the brightest and most Lyα luminous known. In this chapter we present deep imaging with a custom narrow-band filter of the field surrounding the radio galaxy. In the imaging 28 candidate Lyα emitting galaxies were detected. Follow-up spectroscopy of 23 candidates confirmed 20 Lyα emitters to have redshifts within 600 km s^{-1} of the radio galaxy. Compared to the density of Lyα emitters at $z = 4.5$ in a blank field survey, the overdensity near TN J1338–1942 is 4.0 ± 1.4. The velocity dispersion of the confirmed emitters of 325 km s^{-1} is a factor 4 smaller than that of the narrow-band filter, implying an overdensity of $\sim$ 15. At the time of discovery, this structure of Lyα emitters was the most distant known. The mass of the structure is estimated to be 10^{15} $M_\odot$, suggesting that the structure will evolve into a massive cluster of galaxies.

Chapter 3

This chapter describes the observations of the surroundings of the radio galaxy MRC 0316–257 at $z = 3.13$. This radio source already had two spectroscopically confirmed companions, an indication that the radio galaxy resides in an overdense environment. Besides imaging this field in narrow-band and broad-band filters with the VLT, we observed the radio source and its surroundings with the Advanced Camera for Surveys

on board the *Hubble Space Telescope (HST)*. The high resolution images from the *HST* allows us the study the size and morphologies of the detected galaxies.

To detect Lyα emitting galaxies at the redshift of the radio galaxy, the field of MRC 0316–257 was imaged in a narrow-band filter encompassing the redshifted Lyα emission line, and in broad-band filters to measure the continuum. In this chapter we describe in detail how the data are reduced. Extensive simulations are performed to check the completeness and the reliability of the photometry of the extracted sources. To select the best candidate Lyα emitters, we developed a method to compute the equivalent width and strength of an emission line in objects which had an excess flux in the narrow-band image. To assess both the asymmetric errors in the equivalent width and line strength, and the accuracy of the obtained photometric measurements, detailed Monte Carlo simulations were performed. This resulted in a list of 77 candidate Lyα emitting objects with a rest-frame equivalent width > 15 Å and a signal-to-noise on the equivalent width of > 3.

To confirm whether these candidate Lyα emitting galaxies were at the same redshift as the radio galaxy, some of the candidates were observed spectroscopically using multi-object spectroscopy on the VLT, confirming 31 Lyα emitters to be at $z = 3.1$. The continuum of the emitters is faint, and more than 90% of the emitters have a luminosity fainter than L^*. The colors are on average very blue, and $\sim 67\%$ of the emitters have colors consistent with that of dust free star burst galaxies. By combining the deep Lyα imaging with high resolution images from the *HST*, we find that the Lyα emitters have a range of different morphologies. A comparison with the sizes of LBGs at $z \sim 3$ suggests that the Lyα emitters are on average smaller than LBGs. These properties are in agreement with Lyα emitters being young, star forming galaxies in their first starburst phase.

The volume density of Lyα emitting galaxies near MRC 0316–257 is a factor ~ 3 higher compared to the density of Lyα emitters in blank field surveys. The width of the velocity distribution is a factor of > 2 smaller than the width of the narrow-band filter. We conclude that the confirmed Lyα emitters are members of a protocluster at $z = 3.13$. The estimated mass of the protocluster is $> 3 - 6 \times 10^{14} \, M_\odot$, and the structure could be the progenitor of a present-day cluster of galaxies.

Chapter 4

At the moment, the most distant known radio galaxy is TN J0924–2201 at a redshift of $z = 5.2$. The Universe at this redshift is only ~ 1 Gyr old. To investigate whether large scale structures of galaxies can be found at such a large lookback time, we searched the surroundings of this radio galaxy for companion galaxies. As a result, six Lyα emitters were confirmed to lie near the radio galaxy. The density of emitters is comparable to that in the forming clusters MRC 0316–257 at $z = 3.1$ and TN J1338–1942 at $z = 4.1$ (Chapter 2 and 3). This confirms that substantial clustering of Lyα emitters occurs at $z > 5$.

Chapter 5

Chapter 5 presents the results of the VLT large program. We observed eight radio galaxy fields with redshifts $2.0 < z < 5.2$. Following the procedures outlined in Chapter 3, we selected roughly 300 candidate Lyα emitters from the narrow-band and broadband imaging of $\sim 3 \times 3\,\mathrm{Mpc}^2$ fields surrounding the radio galaxies. Spectroscopy was conducted of 152 candidates in seven of the radio galaxy fields. We achieved a success rate of $> 91\%$ in confirming Lyα emitters. Combined with the data of the pilot project, we have redshifts for 168 Lyα emitters in the surroundings of eight radio galaxies. We present the spatial and velocity distributions of the confirmed emitters in each radio galaxy field.

At least six out of the eight fields are overdense in Lyα emitters by a factor of 3–5 as compared to the field density of Lyα emitting galaxies at similar redshifts. The overdensities combined with significant clustering in velocity space suggest that we have discovered six forming clusters of galaxies. The data are consistent with each luminous distant radio galaxy being associated with protoclusters. We estimate that the density of luminous radio sources at $z > 2$ residing in an overdensity is comparable to the local density of rich clusters of galaxies.

The structures have sizes > 1.75 Mpc, which is consistent with the sizes of protoclusters found by other groups. The velocity dispersion of the Lyα emitters in the protoclusters increase with decreasing redshift, which is in agreement with the trend of the dark matter velocity dispersion seen in numerical simulations of forming massive clusters.

Chapter 6

While in Chapter 5 we investigated the global properties of the Lyα emitters like the velocity dispersions, in Chapter 6 the individual emitters are discussed. We analyse a sample of 153 confirmed Lyα emitters, supplemented by another $\sim$150 candidate Lyα emitters. We show that the population of Lyα emitters is dominated by star forming galaxies. The fraction of QSOs among the emitters is low ($< 10\%$), which is based on the distribution of the line widths.

Similar to the results on the small sample of Lyα emitters near MRC 0316–257 (Chapter 3), the star forming Lyα emitting galaxies are generally fainter than L^* and blue. The star formation rates (SFRs) are below $10\,M_\odot\,\mathrm{yr}^{-1}$, as measured from both the Lyα line and from the UV continuum. The similarity between the UV SFRs and the SFRs calculated from the Lyα emission suggests that the absorption by dust is almost negligible. In 30% of the Lyα emitters the stellar UV continuum is absent. Using models of star forming galaxies we estimate that 16% of the Lyα emitters could be younger than 10 Myr. From the distribution of the equivalent width, no evidence is found for zero metallicity stars or extreme initial mass functions.

Chapter 7

In this final chapter, we compare the observed protoclusters from our large program with high resolution N-body simulations of forming massive clusters of galaxies. The simulations were complemented by semi-analytical models to follow the formation

and evolution of galaxies in the clusters. Stellar population models were employed to calculate spectral energy distributions of the cluster galaxies.

Based on the observed properties of the Lyα emitters and their location in the proto-clusters, we can identify the Lyα emitters with the young population of model galaxies in the simulations. The trend in the velocity dispersions of the emitters, which show an increase with cosmic time, can be reproduced by the model galaxies in the simulations. The agreement between theory and observations provides strong additional evidence that luminous radio galaxies are preferentially located in dense environments.

References

Archibald, E. N., Dunlop, J. S., Hughes, D. H., et al. 2001, MNRAS, 323, 417

Athreya, R. M., Kapahi, V. K., McCarthy, P. J., & van Breugel, W. J. M. 1998, A&A, 329, 809

Bahcall, N. A. & Cen, R. 1992, ApJ, 398, L81

Bahcall, N. A. & Fan, X. 1998, ApJ, 504, 1

Barr, J. M., Baker, J. C., Bremer, M. N., Hunstead, R. W., & Bland-Hawthorn, J. 2004, AJ, 128, 2660

Baugh, C. M., Cole, S., Frenk, C. S., & Lacey, C. G. 1998, ApJ, 498, 504

Baugh, C. M. & Gaztanaga, E. 1996, MNRAS, 280, L37

Best, P. N. 2000, MNRAS, 317, 720

Best, P. N., Lehnert, M. D., Miley, G. K., & Röttgering, H. J. A. 2003, MNRAS, 343, 1

Bornancini, C. G., Martínez, H. J., Lambas, D. G., et al. 2004, AJ, 127, 679

Carilli, C. L., Röttgering, H. J. A., van Ojik, R., Miley, G. K., & van Breugel, W. J. M. 1997, ApJ, 109, 1

Carlstrom, J. E., Holder, G. P., & Reese, E. D. 2002, ARA&A, 40, 643

Chambers, K. C. 1990, Ph.D. Thesis

Chambers, K. C., Miley, G. K., & van Breugel, W. J. M. 1988, ApJ, 327, L47

Chambers, K. C., Miley, G. K., & van Breugel, W. J. M. 1990, ApJ, 363, 21

Charlot, S. & Fall, S. M. 1993, ApJ, 415, 580

Colless, M., Ellis, R. S., Broadhurst, T. J., Taylor, K., & Peterson, B. A. 1993, MNRAS, 261, 19

Cooke, J., Wolfe, A. M., Prochaska, J. X., & Gawiser, E. 2005, AJ accepted, astro-ph/0411681

Cowie, L. L. & Hu, E. M. 1998, AJ, 115, 1319

Cowie, L. L., Songaila, A., & Hu, E. M. 1991, Nature, 354, 460

Davis, M. & Wilkinson, D. T. 1974, ApJ, 192, 251

Dawson, S., Rhoads, J. E., Malhotra, S., et al. 2004, ApJ, 617, 707

De Breuck, C., Bertoldi, F., Carilli, C., et al. 2004, A&A, 424, 1

De Breuck, C., Downes, D., Neri, R., et al. 2005, A&A, 430, L1

De Breuck, C., Neri, R., Morganti, R., et al. 2003a, A&A, 401, 911

De Breuck, C., Neri, R., & Omont, A. 2003b, New Astronomy Review, 47, 285

De Breuck, C., van Breugel, W. J. M., Stanford, S. A., et al. 2002, AJ, 123, 637

Dey, A., van Breugel, W. J. M., Vacca, W. D., & Antonucci, R. 1997, ApJ, 490, 698

Djorgovski, S., Strauss, M. A., Spinrad, H., McCarthy, P., & Perley, R. A. 1987, AJ, 93, 1318

Eggen, O. J., Lynden-Bell, D., & Sandage, A. R. 1962, ApJ, 136, 748

Eke, V. R., Cole, S., & Frenk, C. S. 1996, MNRAS, 282, 263

Ellis, R. S., Smail, I., Dressler, A., et al. 1997, ApJ, 483, 582

Fan, X., Bahcall, N. A., & Cen, R. 1997, ApJ, 490, L123

Fujita, S. S., Ajiki, M., Shioya, Y., et al. 2003, AJ, 125, 13

Fynbo, J. P. U., Ledoux, C., Møller, P., Thomsen, B., & Burud, I. 2003, A&A, 407, 147

Fynbo, J. P. U., Møller, P., & Thomsen, B. 2001, A&A, 374, 443

Giavalisco, M. 2002, ARA&A, 40, 579

Gladders, M. D. 2002, Ph.D. Thesis

Glazebrook, K., Ellis, R., Colless, M., et al. 1995, MNRAS, 273, 157

Goto, T. 2005, MNRAS, 356, L6

Greve, T. R., Ivison, R. J., & Papadopoulos, P. P. 2004, A&A, 419, 99

Hashimoto, Y., Barcons, X., Böhringer, H., et al. 2004, A&A, 417, 819

Hayashino, T., Matsuda, Y., Tamura, H., et al. 2004, AJ, 128, 2073

Hill, G. J. & Lilly, S. J. 1991, ApJ, 367, 1

Holden, B. P., van der Wel, A., Franx, M., et al. 2005, ApJ, 620, L83

Hu, E. M., Cowie, L. L., Capak, P., et al. 2004, AJ, 127, 563

Hu, E. M., Cowie, L. L., & McMahon, R. G. 1998, ApJ, 502, L99

Hu, E. M., Cowie, L. L., McMahon, R. G., et al. 2002, ApJ, 568, L75

Jarvis, M. J., Rawlings, S., Eales, S., et al. 2001, MNRAS, 326, 1585

Keel, W. C., Cohen, S. H., Windhorst, R. A., & Waddington, I. 1999, AJ, 118, 2547

Kodaira, K., Taniguchi, Y., Kashikawa, N., et al. 2003, PASJ, 55, L17

Koo, D. C. 1985, AJ, 90, 418

Kudritzki, R.-P., Méndez, R. H., Feldmeier, J. J., et al. 2000, ApJ, 536, 19

Kurk, J. D., Pentericci, L., Overzier, R. A., Röttgering, H. J. A., & Miley, G. K. 2004a, A&A, 428, 817

Kurk, J. D., Pentericci, L., Röttgering, H. J. A., & Miley, G. K. 2004b, A&A, 428, 793

Kurk, J. D., Röttgering, H. J. A., Pentericci, L., et al. 2000, A&A, 358, L1

Le Fèvre, O., Vettolani, G., Garilli, B., et al. 2005, A&A, submitted (astro-ph/0409133)

Le Fèvre, O., Vettolani, G., Paltani, S., et al. 2004, A&A, 428, 1043

Le Fèvre, O., Deltorn, J. M., Crampton, D., & Dickinson, M. 1996, ApJ, 471, L11

Lilly, S. J. & Longair, M. S. 1982, MNRAS, 199, 1053

Madau, P. 1995, ApJ, 441, 18

Maughan, B. J., Jones, L. R., Ebeling, H., & Scharf, C. 2004, MNRAS, 351, 1193

Meier, D. L. 1976, ApJ, 207, 343

Miles, T. A., Raychaudhury, S., Forbes, D. A., et al. 2004, MNRAS, 355, 785

Miley, G. K., Overzier, R. A., Tsvetanov, Z. I., et al. 2004, Nature, 427, 47

Nakata, F., Bower, R. G., Balogh, M. L., & Wilman, D. J. 2005, MNRAS, 357, 679

Nath, B. B. 2004, MNRAS, 353, 941

Ouchi, M., Shimasaku, K., Akiyama, M., et al. 2005, ApJ, 620, L1

Ouchi, M., Shimasaku, K., Furusawa, H., et al. 2003, ApJ, 582, 60

Overzier, R. A., Zirm, A. W., Miley, G. K., et al. 2005, ApJ, submitted

Palunas, P., Teplitz, H. I., Francis, P. J., Williger, G. M., & Woodgate, B. E. 2004, ApJ, 602, 545

Papadopoulos, P. P., Röttgering, H. J. A., van der Werf, P. P., et al. 2000, ApJ, 528, 626

Partridge, R. B. 1974, ApJ, 192, 241

Pascarelle, S. M., Windhorst, R. A., Driver, S. P., Ostrander, E. J., & Keel, W. C. 1996, ApJ, 456, L21

Pentericci, L., Kurk, J. D., Carilli, C. L., et al. 2002, A&A, 396, 109

Pentericci, L., Kurk, J. D., Röttgering, H. J. A., et al. 2000a, A&A, 361, L25

Pentericci, L., Röttgering, H. J. A., Miley, G. K., et al. 1999, A&A, 341, 329

Pentericci, L., Röttgering, H. J. A., Miley, G. K., et al. 1998, ApJ, 504, 139

Pentericci, L., van Reeven, W., Carilli, C. L., Röttgering, H. J. A., & Miley, G. K. 2000b, A&AS, 145, 121

Pritchet, C. J. 1994, PASP, 106, 1052

Reuland, M., Röttgering, H. J. A., van Breugel, W. J. M., & De Breuck, C. 2004, MNRAS, 353, 377

Rhoads, J. E., Dey, A., Malhotra, S., et al. 2003, AJ, 125, 1006

Rhoads, J. E. & Malhotra, S. 2001, ApJ, 563, L5

Rocca-Volmerange, B., Le Borgne, D., De Breuck, C., Fioc, M., & Moy, E. 2004, A&A, 415, 931

Rosati, P., Tozzi, P., Ettori, S., et al. 2004, AJ, 127, 230

Schmidt, M. 1974, ApJ, 193, 505

Shapley, A. E., Steidel, C. C., Pettini, M., & Adelberger, K. L. 2003, ApJ, 588, 65

Songaila, A., Cowie, L. L., Hu, E. M., & Gardner, J. P. 1994, ApJ, 94, 461

Spinrad, H., Dey, A., & Graham, J. R. 1995, ApJ, 438, L51

Spinrad, H., Stauffer, J., & Butcher, H. 1981, ApJ, 244, 382

Stanford, S. A., Eisenhardt, P. R., & Dickinson, M. 1998, ApJ, 492, 461

Steidel, C. C., Adelberger, K. L., Giavalisco, M., Dickinson, M., & Pettini, M. 1999, ApJ, 519, 1

Steidel, C. C., Adelberger, K. L., Shapley, A. E., et al. 2000, ApJ, 532, 170

Steidel, C. C., Adelberger, K. L., Shapley, A. E., et al. 2003, ApJ, 592, 728

Steidel, C. C., Giavalisco, M., Pettini, M., Dickinson, M., & Adelberger, K. L. 1996, ApJ, 462, L17

Steidel, C. C. & Hamilton, D. 1992, AJ, 104, 941

Steidel, C. C. & Hamilton, D. 1993, AJ, 105, 2017

Steidel, C. C., Pettini, M., & Hamilton, D. 1995, AJ, 110, 2519

Stern, D., Holden, B., Stanford, S. A., & Spinrad, H. 2003, AJ, 125, 2759

Stevens, J. A., Ivison, R. J., Dunlop, J. S., et al. 2003, Nature, 425, 264

Tanaka, M., Goto, T., Okamura, S., Shimasaku, K., & Brinkmann, J. 2004, AJ, 128, 2677

Tozzi, P., Rosati, P., Ettori, S., et al. 2003, ApJ, 593, 705

Tran, K. H., van Dokkum, P. G., Illingworth, G. D., et al. 2005, ApJ, 619, 134

Valageas, P., Schaeffer, R., & Silk, J. 2003, MNRAS, 344, 53

van Dokkum, P. G. & Stanford, S. A. 2003, ApJ, 585, 78

van Zee, L., Barton, E. J., & Skillman, E. D. 2004, AJ, 128, 2797

Vernet, J., Fosbury, R. A. E., Villar-Martín, M., et al. 2001, A&A, 366, 7

White, S. D. M., Efstathiou, G., & Frenk, C. S. 1993, MNRAS, 262, 1023

White, S. D. M. & Rees, M. J. 1978, MNRAS, 183, 341

Yates, M. G., Miller, L., & Peacock, J. A. 1989, MNRAS, 240, 129

Zirm, A. W., Dickinson, M., & Dey, A. 2003, ApJ, 585, 90

Zirm, A. W., Overzier, R. A., Miley, G. K., et al. 2005, ApJ, submitted

Chapter 2

A protocluster at $z = 4.1$

Abstract. Imaging and spectroscopy with the Very Large Telescope have revealed 20 Lyα emitters within a projected distance of 1.3 Mpc and 600 km s^{-1} of the luminous radio galaxy TN J1338–1942 at $z = 4.1$. Compared to the field density of Lyα emitters, this implies an overdensity on the order of 15. The structure has a projected size of at least 2.7 Mpc $\times$ 1.8 Mpc and a velocity dispersion of 325 km s^{-1}, which makes it the most distant structure known. Using the galaxy overdensity and assuming a bias parameter $b = 3 - 5$, the mass is estimated to be $\sim 10^{15}$ $M_\odot$. The radio galaxy itself is surrounded by an uniquely asymmetric Lyα halo. Taken together with our previous data on PKS 1138–262 at $z \sim 2.16$, these results suggest that luminous radio sources are excellent tracers of high density regions in the early Universe, which evolve into present-day clusters. The statistics of bright radio sources and of concentrations in the Lyman break galaxy population are consistent with the picture that each of those concentrations harbours an active or passive luminous radio source.

B. P. Venemans, J. D. Kurk, G. K. Miley, H. J. A. Röttgering,
W. J. M. van Breugel, C. L. Carilli, C. De Breuck, H. Ford,
T. Heckman, P. McCarthy & L. Pentericci,
The Astrophysical Journal Letters, **569**, 11 (2002)

2.1 Introduction

S TUDIES of high redshift (proto)clusters of galaxies ($z > 2$) can directly constrain theories of galaxy evolution and cosmological models (e.g., Bahcall & Fan 1998), but the detection of (proto)clusters at these redshifts using conventional optical and X-ray techniques is difficult. High redshift radio galaxies (HzRGs, $z > 2$) can help: they are among the most evolved and most massive galaxies in the early Universe (De Breuck et al. 2002) and are most likely located in dense (proto)cluster environments (e.g., Le Fèvre et al. 1996; Pascarelle et al. 1996; Röttgering et al. 1996; Carilli et al. 1997; van Ojik et al. 1997; Pentericci et al. 2000b). In addition, HzRGs have properties that would be expected of forming central cluster galaxies. Their extremely clumpy morphologies revealed by *Hubble Space Telescope* images (Pentericci et al. 1999) are strikingly similar to simulations of forming brightest cluster galaxies, based on hierarchical models (e.g., Aragón-Salamanca, Baugh, & Kauffmann 1998).

A pilot project on the Very Large Telescope (VLT) to search for Lyα emitting galaxies around the clumpy radio galaxy PKS 1138–262 resulted in the discovery of 14 galaxies and a QSO at approximately the same redshift as the radio galaxy (Kurk et al. 2000; Pentericci et al. 2000). If the structure found is virialized, the total mass of the protocluster would be 10^{14} $M_\odot$. Motivated by this result, we started a large program at the VLT to search for forming clusters (protoclusters) around HzRGs at redshifts 2 and higher. The first radio galaxy field we observed was TN J1338–1942 at a redshift of 4.1 (De Breuck et al. 1999). This HzRG is one of the brightest and most luminous in Lyα known. Both its Lyα profile and radio structure are very asymmetric (De Breuck et al. 1999), which indicates strong interaction with dense gas, and the rest-frame radio luminosity is comparable to that of the most luminous 3CR sources ($P_{178\mathrm{MHz}} \simeq 4 \times 10^{35}$ erg s^{-1} Hz^{-1} sr^{-1}). Here we report on the discovery of a substantial overdensity of Lyα emitters around this radio galaxy at $z \sim 4.1$. Throughout this chapter, magnitudes are in the AB system and a Λ-dominated cosmology with $H_0 = 65$ km s^{-1} Mpc^{-1}, $\Omega_M = 0.3$, and $\Omega_\Lambda = 0.7$ is assumed.

2.2 Observations and candidate selection

2.2.1 VLT imaging and selection of candidate Lyα emitters

We carried out narrow- and broad-band imaging on 2001 March 25 and 26 with the 8.2 m VLT Kueyen (UT2), using the imaging mode of the FOcal Reducer/low dispersion Spectrograph 2 (FORS2). At $z = 4.10$ the Lyα emission line is redshifted to 6202 Å, which falls in our custom narrow-band filter with a central wavelength of 6195 Å and FWHM of 60 Å. The broad-band R filter had a central wavelength of 6550 Å and FWHM of 1650 Å. The detector was a SiTE CCD with 2048×2048 pixels, with a scale of 0.″2 per pixel and a field of view of 6.′8×6.′8. We took 18 separate 1800 s exposures and one 900 s exposure in the narrow-band and 21 exposures of 300 s in *R*, shifted by $\sim 15''$ with respect to each other to minimize flat-fielding problems and to handle cosmic rays. The nights were photometric and the average seeing in both narrow-band and broad-band images was 0.″65. The 1 σ limiting magnitude per square arcsecond was 28.6 for the narrow-band and 29.2 for the broad-band image. For the flux cali-

bration the spectrophotometric standard star GD 108 (Oke 1990) was used. The final images have sizes of 6.4×6.2 (39.7 arcmin^2). The total volume probed at $z = 4.1$ by our narrow-band filter is 7315 Mpc^3.

NTT imaging data, taken on 1998 April 27 and 29 under nonphotometric conditions with SuSI2, were also used to provide *B*- and *I*-band magnitudes for candidate emitters where possible. The 1 σ limiting magnitude per square arcsecond was about 27.8 in both bands.

For the detection and photometry of objects in the images, we used the object detection and classification program SExtractor (Bertin & Arnouts 1996). Detected objects had at least nine connected pixels with values larger than the rms sky noise on the narrow-band image. A photometric analysis was then carried out on both the narrow-band and the broad-band image. In total 2407 objects were extracted. Based on the statistics of our detection of Lyα emitters around PKS 1138–262, we selected objects with a rest-frame equivalent width (EW$_0$) greater than 15 Å (or $m_{BB} - m_{NB} > 0.84$) and significance $\Sigma > 3$ as candidate Lyα emitting galaxies, with Σ the ratio of continuum-subtracted counts in the narrow-band to the combined noise in the broad-band and narrow-band (Bunker et al. 1995). Of the 2407 objects, 34 objects satisfied these criteria, including the radio galaxy. Of these 34 objects, 31 were detected in the *R*-band image, nine were detected in the NTT *I* image and five in the NTT *B* image. The five objects with a detection in B have a color of $B - R \sim 0$–1, inconsistent with the colors expected for galaxies at $z = 4$ (Steidel et al. 1999). Three of these objects are located in the halo of the radio galaxy, which affects the narrow-band photometry. The other two are likely to be foreground objects with another line falling in the narrow-band filter, e.g. [O III] $\lambda5007$ or [O II] $\lambda3727$. Excluding the radio galaxy, the resulting 28 objects were our Lyα emitting candidates for follow-up spectroscopy.

2.2.2   VLT spectroscopy

On 2001 May 20, 21, and 22 we carried out spectroscopy using FORS2 in the mask multi-object spectroscopy mode with standard resolution. The nights were photometric with an average seeing of 1 ″. The spectra were obtained with the 600RI grism with a dispersion of 1.32 Å pixel^{-1} and a wavelength range from 5300 Å to 8000 Å. This grism was preferred because of its high throughput (peak efficiency is 87%). Two different masks were used to observe 23 of the candidate Lyα emitters and the radio galaxy, with slit sizes of 1 ″, resulting in a resolution of 6 Å, which corresponds to 290 km s^{-1} at $z = 4.1$. The total exposure time was 31,500 s for the first mask and 35,100 s for the second mask. Wavelength calibration was obtained from exposures of He, Ar, Ne, and HgCd arc-lamps. The accuracy of the wavelength calibration was better than 0.05 Å. For the flux calibration, long slit exposures with a 5 ″ slit were used of the spectrophotometric standard stars EG 274 and LTT 7987 (Stone & Baldwin 1983; Baldwin & Stone 1984).
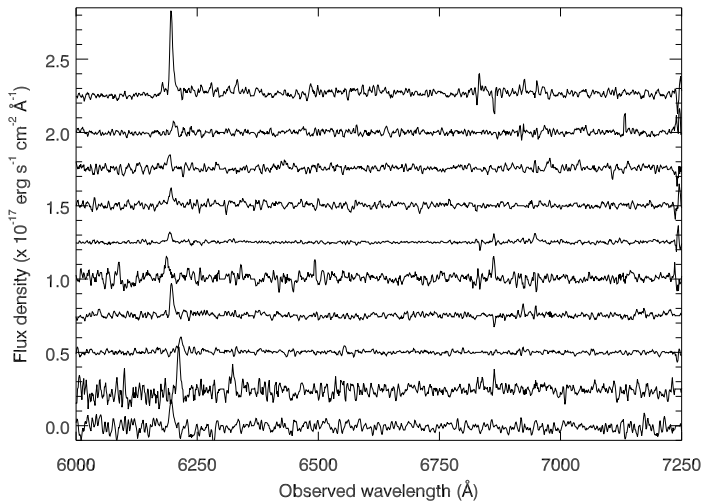
Figure 2.1 — Spectra of ten of the 20 confirmed Lyα emitters. For clarity, each spectrum is offset by multiples of 2.5×10^{-18} erg s^{-1} cm^{-2} Å^{-1}.

2.3   Results

2.3.1   Line emitters in the field

2.3.1.1   Line identifications

Of the 23 candidates observed, 20 show an emission line with a peak between $\lambda = 6187$ Å and $\lambda = 6216$ Å. The signal-to-noise of these lines is at least 10. Ten randomly selected spectra from our sample are shown in Fig. 2.1. Two nondetections were very faint ($m_{NB} = 25.9$ and $m_{NB} = 26.1$ respectively). The third nondetection had a very low surface brightness. The success rate of our selection criteria was therefore 87%.

The first question is whether the detected lines are indeed due to Lyα at the redshift of the radio galaxy. Intervening neutral hydrogen will absorb emission blueward of the Lya line (Steidel et al. 1999). This discontinuity of the continuum over the Lya emission line is observed in one of the spectra, but the continuum emission of the other emitters was too faint to be detected (R ~ 27). Identification of the lines with [O III] $\lambda5007$ at $z \sim 0.24$ can be excluded, because of the lack of confirming lines [O III] $\lambda4959$ and Hβ in the spectra. The position of the emitter within the slit mask determines the wavelength coverage of the resulting spectrum. In nine cases this coverage was suitable to exclude the identification with [O II] $\lambda3727$ at $z \sim 0.66$ on similar grounds. The detected emitters are anyway unlikely to be foreground [O II] galaxies. First of all, if one of the lines would be [O II], then the rest-frame equivalent width would be at least 70 Å. A survey of nearby field galaxies, conducted by Jansen et al. (2000), gives a mean EW$_0$ of the [O II] line of ~ 30 Å for galaxies with $M_B = -16$, which roughly compares to R ≈ 27 at $z = 0.66$. Only two galaxies out of 159 galaxies with [O II] in emission have EW$_0$([O II]) > 70 Å. The number of [O II] emitters expected in our field, using another study (Hogg et al. 1998), is ~ 7. Again, only a few percent of the [O II] emitters observed by Hogg et al. have an EW$_0 > 70$ Å. Therefore, from our sample of 20 emitters, < 1 is expected to be an [O II] emitter.

Additional evidence that the observed lines are predominantly Lyα lines at $z \sim 4.1$ associated with the radio galaxy is provided by their velocity distribution, which has a dispersion of 326 ± 73 km s^{-1} and a FWHM of 768 ± 172 km s^{-1} (Fig. 2.2), which is 4 times smaller than the FWHM of the narrow-band filter. Further, the velocity distri-

Figure 2.2 — Velocity distribution of the Lyα emitters. The bin size is 175 $\mathrm{km\,s^{-1}}$ and the median of the velocities is taken as zero point. The velocity of the radio galaxy, corrected for absorption (De Breuck et al. 1999), is indicated by an arrow. The normalized transmission curve of the narrowband filter is also plotted. Note that the velocity distribution of the detected emitters is substantially narrower than the filter width and centered within 200 $\mathrm{km\,s^{-1}}$ of the redshift of the radio galaxy.
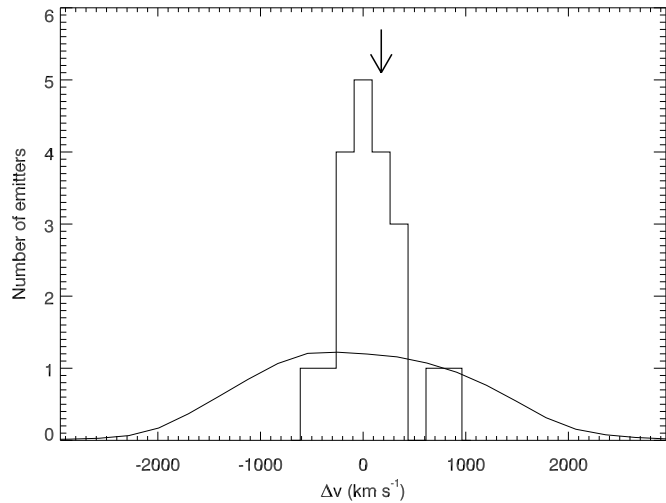
bution peaks within 200 $\mathrm{km\,s^{-1}}$ of the radio galaxy Lyα peak, corrected for absorption (De Breuck et al. 1999).

For all these reasons we interpret the observed emission lines as Lyα. To estimate the redshifts, flux densities, and widths (FWHM) of the lines, a Gaussian function was fitted to each of the one-dimensional spectra. Details are provided in Chapter 5.

2.3.1.2 Significance and properties of the overdensity

The next question to be addressed is to what extent the statistics of our detections represent a significant overdensity of galaxies in the field. A "blank-field" study of Lyα emitters at approximately the same redshift is the Large-Area Lyman Alpha survey (LALA survey, Rhoads et al. 2000). Preliminary results of this survey indicate a number density of $4000 \pm 460 \ \mathrm{deg^{-2}} \ \Delta z^{-1}$ for objects with $EW_0 > 15\text{Å}$ and line + continuum $> 2.6 \times 10^{-17} \ \mathrm{erg\,s^{-1}\,cm^{-2}}$. For our field the second criterion corresponds to $m_{\mathrm{NB}} < 24.55$ and we expect 2.3 ± 0.3 such Lyα emitters within our probed volume. However, nine of the confirmed emitters satisfy the above criteria (including the radio galaxy). In our cosmology the comoving volume density of the LALA survey is $n_{LALA} = (3.1 \pm 0.4) \times 10^{-4} \ \mathrm{Mpc^{-3}}$. The volume density in our field is $n_{1338} = 9/7315 \ \mathrm{Mpc^{-3}} = (12 \pm 4) \times 10^{-4} \ \mathrm{Mpc^{-3}}$. The difference in number density is $n_{1338}/n_{LALA} = 4.0 \pm 1.4$. However, the FWHM of the velocity distribution is approximately 4 times smaller than the FWHM of the filter (see Fig. 2.2). This implies that our radio galaxy field is overdense in Lyα emitters by a factor of 15 compared with a blank field.

The spatial distribution of the emitters is not homogeneous (Fig. 2.3). The structure appears to have a boundary in the northwest but our FOV is not large enough to show such an edge in the south. The size of the structure is therefore at least $6' \times 4'$, which corresponds to greater than 2.7 Mpc $\times$ 1.8 Mpc. Remarkably, the radio galaxy, probably the most massive system in the structure, does not appear to be at the center of the protocluster, in disagreement with models for the formation of dominant cluster galaxies (e.g., West 1994).
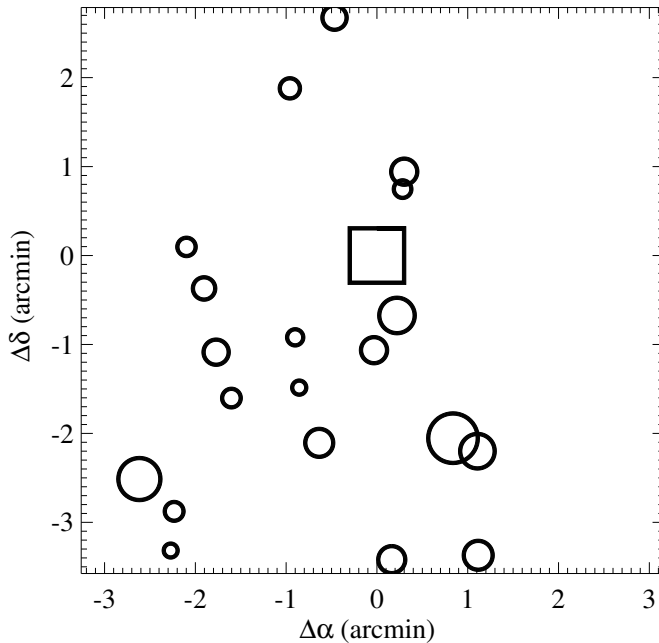
Figure 2.3 — Spatial distribution of the 20 confirmed Lyα emitters at $z \sim 4.1$ (*circles*) and the radio galaxy (*square*). The size of the circles is scaled according to the Lyα flux of the object, ranging between 0.3 and 4.1 $\times 10^{-17}$ erg s^{-1} cm^{-2}. The structure appears to have a boundary only in the north-west of the image and not in the south. Note that the radio galaxy is not centered in the galaxy distribution.

2.3.2 Radio galaxy halo

The radio galaxy is located close to the apparent north-west boundary of the galaxy overdensity structure. The radio emission is dominated by two components, separated by 5.5 (De Breuck et al. 1999). The brightest component coincides with the optical emission, while the other is in the south-east, towards the center of the galaxy overdensity. A spectacular feature of the radio galaxy, visible in the narrow-band image, is the large Lyα halo (Fig. 2.4). Although giant Lyα halos are a common feature of HzRGs, they are usually fairly symmetrically extended around the radio galaxy. In the case of TN J1338–1942, the halo is highly asymmetric and extends for $\sim 15''$ (110 kpc) to the north-west, i.e., away from the center of the overdensity structure. In its narrowness and asymmetry the TN J1338–1942 halo is unique among known distant radio galaxies. Possible mechanisms to produce this structure include cooling flows in colliding sub-structures and buoyancy effects (Gisler 1976) and will be considered in a subsequent paper.

2.4   Discussion

2.4.1   Nature of the overdensity

Could the structure that we have detected be a protocluster at $z \sim 4.1$ that will evolve into a rich cluster of galaxies in the local Universe? At $z = 4.1$ the Universe is ~ 1.6 Gyr old, too short for the structure to have virialized since the mean crossing time for galaxies at the observed velocity dispersion is at least 4 Gyr. Thus the observed velocities are probably infall velocities of the galaxies accreting onto a large overdensity. The total mass of this structure can be estimated by using $M = \overline{\rho} V (1 + \delta_m)$ with $\overline{\rho}$ the mean density of the Universe and δ_m the mass overdensity within our volume V (Steidel et al. 1998). The mass overdensity is related to the galaxy overdensity δ_{gal} through
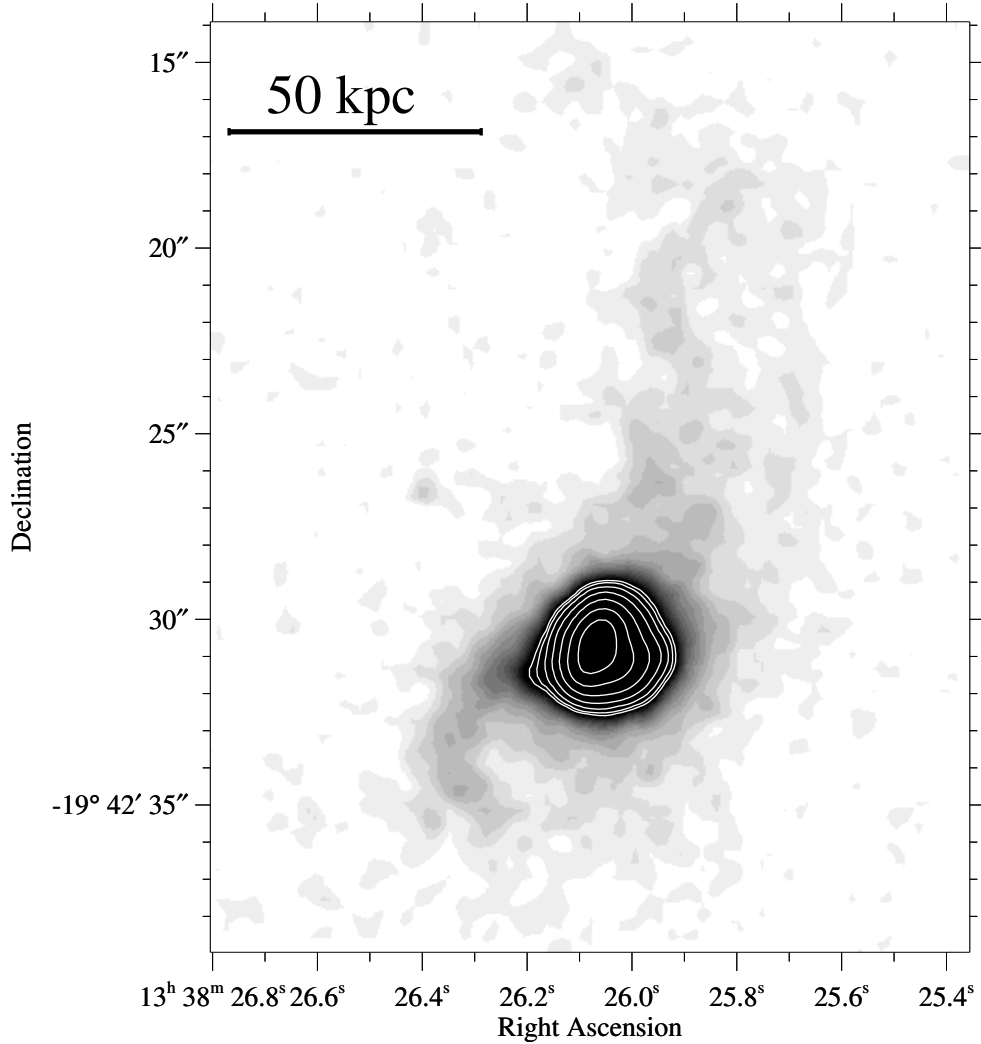
Figure 2.4 — Continuum-subtracted Lyα image of the radio galaxy halo. The contours represent the Lyα flux density in the center of the halo. The surface brightness ranges from ~ 0.07 to 1×10^{-17} erg s^{-1} cm^{-2} arcsec^{-2}. The low-brightness halo is extended to the north-west, pointing away from the overdensity structure. This Lyα halo is the most asymmetric radio galaxy halo known.

$1 + b\delta_m = C(1 + \delta_{\text{gal}})$, where C takes into account the redshift space distortions caused by peculiar velocities (see Chapter 3 for more details) and b is the bias parameter. From the statistics of redshift "spikes", Steidel et al. (1998) argue that $b \gtrsim 4$. Taking b in the range 3–5 and assuming that the structure is just breaking away from the Hubble expansion, δ_m is estimated to be 0.5–2.3, giving a mass of our structure of $(1-2) \times 10^{15} \ M_\odot$. This is comparable to the mass of the Lyman break galaxy overdensity (spike) found by Steidel et al. and to that of the Coma cluster (e.g., Fusco-Femiano & Hughes 1994).

2.4.2   Relation to overdensity spikes

It is instructive to compare the number of luminous radio sources at $z \sim 3$ to the number of redshift spikes. Steidel et al. (1998) estimate that about one velocity spike is detected in each $9' \times 18'$ field in their spectroscopic survey, corresponding to 9×10^5 redshift spikes in the whole sky. Their survey is sensitive to redshifts between 2.7 and 3.4, corresponding to a cosmic evolution time of 0.6 Gyr.

How many luminous radio sources are there at $z \sim 3$? Using the pure luminosity evolution model of Dunlop & Peacock (1990) to describe the steep spectrum radio luminosity function, we estimate that in the redshift range $2.7 < z < 3.4$ there should be $\sim 1.2 \times 10^4$ radio sources with luminosities exceeding 10^{33} $\mathrm{erg\,s^{-1}\,Hz^{-1}\,sr^{-1}}$ at 2.7 GHz ("Cygnus A type" radio sources: $\mathrm{P_{2.7GHz}}$(Cygnus A) $\simeq 2 \times 10^{33}$ $\mathrm{erg\,s^{-1}\,Hz^{-1}\,sr^{-1}}$, Becker, White, & Edwards 1991). Assuming that HzRGs are only once active for 10^7 yr (Blundell & Rawlings 1999), we expect the number of (previously) active radio sources in this redshift range to be $\sim 7 \times 10^5$.

Hence, the luminosity functions and lifetimes of luminous radio sources are consistent with every velocity "spike" in the space densities of Lyman break galaxies being associated with a massive galaxy that has been or will become a luminous radio source once. Note that West (1994) presented similar statistical evidence to argue that distant powerful radio galaxies are the precursors of cD galaxies at the centers of galaxy clusters.

2.5   Conclusion

We have found a structure of 20 Lyα emitting galaxies around the high redshift radio galaxy TN J1338–1942. The overdensity of this protocluster is on the order of 15 compared to field samples. Our results demonstrate that by $z = 4.1$ megaparsec-scale structure had already formed.

Together with our previous data, this implies that the most luminous radio sources are tracers of regions of galaxy overdensity in the early Universe. The estimated masses of $10^{14} - 10^{15}$ $M_\odot$ are consistent with the overdensities being ancestors of rich clusters of galaxies in the local Universe.

Acknowledgments

References

Aragón-Salamanca, A., Baugh, C. M., & Kauffmann, G. 1998, MNRAS, 297, 427

Bahcall, N. A. & Fan, X. 1998, ApJ, 504, 1

Baldwin, J. A. & Stone, R. P. S. 1984, MNRAS, 206, 241

Becker, R. H., White, R. L., & Edwards, A. L. 1991, ApJ, 75, 1

Bertin, E. & Arnouts, S. 1996, A&AS, 117, 393

Blundell, K. M. & Rawlings, S. 1999, Nature, 399, 330

Bunker, A. J., Warren, S. J., Hewett, P. C., & Clements, D. L. 1995, MNRAS, 273, 513

Carilli, C. L., Röttgering, H. J. A., van Ojik, R., Miley, G. K., & van Breugel, W. J. M. 1997, ApJ, 109, 1

De Breuck, C., van Breugel, W., Minniti, D., Miley, G. K., Röttgering, H. J. A., Stanford, S. A., & Carilli, C. 1999, A&A, 352, L51

De Breuck, C., van Breugel, W. J. M., Stanford, S. A., et al. 2002, AJ, 123, 637

Dunlop, J. S. & Peacock, J. A. 1990, MNRAS, 247, 19

Fusco-Femiano, R. & Hughes, J. P. 1994, ApJ, 429, 545

Gisler, G. R. 1976, A&A, 51, 137

Hogg, D. W., Cohen, J. G., Blandford, R., & Pahre, M. A. 1998, ApJ, 504, 622

Jansen, R. A., Fabricant, D., Franx, M., & Caldwell, N. 2000, ApJ, 126, 331

Kurk, J. D., et al. 2000, A&A, 358, L1

Le Fèvre, O., Deltorn, J. M., Crampton, D., & Dickinson, M. 1996, ApJ, 471, L11

Oke, J. B. 1990, AJ, 99, 1621

Pascarelle, S. M., Windhorst, R. A., Driver, S. P., Ostrander, E. J., & Keel, W. C. 1996, ApJ, 456, L21

Pentericci, L., et al. 2000a, A&A, 361, L25

Pentericci, L., Röttgering, H. J. A., Miley, G. K., McCarthy, P., Spinrad, H., van Breugel, W. J. M., & Macchetto, F. 1999, A&A, 341, 329

Pentericci, L., van Reeven, W., Carilli, C. L., Röttgering, H. J. A., & Miley, G. K. 2000b, A&AS, 145, 121

Rhoads, J. E., Malhotra, S., Dey, A., Stern, D., Spinrad, H., & Jannuzi, B. T. 2000, ApJ, 545, L85

Röttgering, H. J. A., West, M. J., Miley, G. K., & Chambers, K. C. 1996, A&A, 307, 376

Steidel, C. C., Adelberger, K. L., Dickinson, M., Giavalisco, M., Pettini, M., & Kellogg, M. 1998, ApJ, 492, 428

Steidel, C. C., Adelberger, K. L., Giavalisco, M., Dickinson, M., & Pettini, M. 1999, ApJ, 519, 1

Stone, R. P. S. & Baldwin, J. A. 1983, MNRAS, 204, 347

van Ojik, R., Röttgering, H. J. A., Miley, G. K., & Hunstead, R. W. 1997, A&A, 317, 358

West, M. J. 1994, MNRAS, 268, 79

Chapter 3

Properties of Lyα emitters around the radio galaxy MRC 0316–257

Abstract. Observations of the radio galaxy MRC 0316–257 at $z = 3.13$ and the surrounding field are presented. Using narrow- and broad-band imaging obtained with the VLT, 77 candidate Lyα emitters with a rest-frame equivalent width of $>$ 15 Å were selected in a $\sim 7' \times 7'$ field around the radio galaxy. Spectroscopy of 40 candidates resulted in the discovery of 33 emission line galaxies of which 31 are Lyα emitters with redshifts similar to that of the radio galaxy, while the remaining two galaxies turned out to be [O II] emitters. The Lyα profiles have widths (*FWHM*) in the range of 120–800 km s^{-1}, with a median of 260 km s^{-1}. Where the signal-to-noise was large enough, the Lyα profiles were found to be asymmetric, with apparent absorption troughs blueward of the profile peaks, indicative of absorption along the line of sight of an H I mass of at least $2 \times 10^2 - 5 \times 10^4\ M_\odot$. The continuum of the emitters is faint, with luminosities ranging from 1.3 L^* to < 0.03 L^*. The colors of the confirmed emitters are, on average, very blue. The median UV continuum slope is $\beta = -1.76$, bluer than the average slope of LBGs with Lyα emission ($\beta \sim -1.09$). Observations with *HST* show that the emitters have a range of different morphologies. Four Lyα emitters ($\sim 25\%$) were unresolved, three objects ($\sim 19\%$) show multiple clumps of emission, as does the radio galaxy, and the rest ($\sim 56\%$) are single, resolved objects with $r_h < 1.5$ kpc. A comparison with the sizes of LBGs at $z \sim 3$ suggests that the Lyα emitters are on average smaller than LBGs. The average star formation rate of the Lyα emitters is 2.6 $M_\odot$ yr^{-1} as measured by the Lyα emission line. The properties of the Lyα galaxies (faint, blue and small) are consistent with young star forming galaxies which are nearly dust free. The volume density of Lyα emitting galaxies near MRC 0316–257 is a factor of $3.3^{+0.5}_{-0.4}$ larger compared with the density of field Lyα emitters at that redshift. The velocity distribution of the spectroscopically confirmed emitters has a dispersion of 640 km s^{-1}, which is substantially smaller than the width of the narrow-band filter (FWHM ~ 3500 km s^{-1}). The peak of the velocity distribution is located within 200 km s^{-1} of the redshift of the radio galaxy. We conclude that the confirmed Lyα emitters are members of a protocluster at $z \sim 3.13$. The size of the protocluster is larger than 3.3×3.3 Mpc^2 and the mass is estimated to be > 3–$6 \times 10^{14}\ M_\odot$. This structure could be the progenitor of a cluster similar to e.g. the Virgo cluster.

B. P. Venemans, H. J. A. Röttgering, G. K. Miley, J. D. Kurk,
C. De Breuck, R. A. Overzier, W. J. M. van Breugel, C. L. Carilli,
H. Ford, T. Heckman, L. Pentericci & P. McCarthy,
Astronomy & Astrophysics, **431**, 793 (2005)

23

3.1   Introduction

WITHIN Cold Dark Matter (CDM) scenarios the first stars and stellar systems form through gravitational infall of primordial gas in large CDM halos (e.g., White & Rees 1978). Numerical simulations suggest that as these halos merge they form vast, web-like networks of young galaxies and ionized gas (e.g., Baugh et al. 1998). The most massive galaxies, and the richest clusters emerge from regions with the largest over-densities. Although clusters of galaxies have been studied extensively out to $z \sim 1.3$ (e.g., Rosati et al. 1999; Della Ceca et al. 2000; Stanford et al. 2002; Blakeslee et al. 2003b; Maughan et al. 2003; Toft et al. 2004), the epoch of cluster formation is still an open question due to the difficulty in identifying their progenitors in the early Universe.

During the last decade, evidence has mounted that the most powerful high redshift radio galaxies (HzRGs; $z > 2$) are progenitors of brightest cluster galaxies and are located in dense environments. HzRGs are amongst the brightest and presumably most massive galaxies (Jarvis et al. 2001; De Breuck et al. 2002; Zirm et al. 2003). They have high star formation rates ($> 100\ M_\odot\ \mathrm{yr}^{-1}$), based on deep spectra of their UV continuum (e.g., Dey et al. 1997) and the detections of dust (e.g., Archibald et al. 2001; Stevens et al. 2003; Reuland et al. 2004) and extended CO emission (Papadopoulos et al. 2000; De Breuck et al. 2003a,b). Furthermore, radio galaxies at redshifts between 0.5 and 1.5 are known to predominantly lie in moderately rich clusters (Hill & Lilly 1991; Best 2000; Best et al. 2003). At higher redshifts ($z > 2$), some radio galaxies were found to possess companion galaxies (Le Fèvre et al. 1996; Pascarelle et al. 1996; Röttgering et al. 1996; Keel et al. 1999). Also, 20% of the HzRGs have extreme radio rotation measures ($> 1000\ \mathrm{rad\,m}^{-2}$), giving an indication that these radio galaxies are surrounded by dense hot gas (Carilli et al. 1997; Athreya et al. 1998; Pentericci et al. 2000b).

To search for direct evidence of the association of a cluster or a forming cluster (protocluster) with a radio galaxy, we conducted a pilot project on the Very Large Telescope (VLT) aimed at finding an excess of Lyα emitters around the clumpy radio galaxy PKS 1138–262 at $z = 2.16$. Narrow-band imaging resulted in a list of ~ 50 candidate Lyα emitters (Kurk et al. 2000, 2004). Subsequent multi-object spectroscopy confirmed 14 Lyα emitting galaxies and one QSO whose velocities were within 1000 $\mathrm{km\,s}^{-1}$ of the central radio galaxy (Pentericci et al. 2000; Kurk et al. 2004). The volume density of Lyα emitters near PKS 1138–262 was found to be a factor 4.4 ± 1.2 times that of Lyα emitters in blank fields (Kurk et al. 2004). Using near-infrared narrow- and broad-band images of the field, significant populations of Hα emitters at the redshift of the radio galaxy and extremely red objects were found. Also, *Chandra* observations revealed an excess of soft X-ray sources in the field of PKS 1138–262 (Pentericci et al. 2002), indicating that several AGN are present in the protocluster.

As shown by the study of the overdense region near PKS 1138–262, distant protoclusters provide ideal laboratories for tracing the development of large scale structure and galaxy evolution. To further study the formation of large scale structure in the early Universe and to investigate the evolution of galaxies in dense environments, we initiated a large program on the VLT to search for Lyα emitting galaxies around luminous radio galaxies with redshifts $2 < z < 5$ (Chapter 5; Venemans et al. 2003). The goals were to find protoclusters of galaxies, determine the fraction of HzRGs associ-

ated with protoclusters and study the properties of protoclusters and their galaxies. The first result was the discovery of a protocluster around the radio galaxy TN J1338–1942 at $z = 4.1$ (Chapter 2). Deep imaging and spectroscopy revealed 20 Lyα emitters within a projected distance of 1.3 Mpc and 600 km s^{-1} of the radio galaxy. By comparing the density of Lyα emitters in the protocluster to the field, the galaxy overdensity was claimed to be 4.0 ± 1.4 and the mass of the structure was estimated to be $\sim 10^{15}$ $M_\odot$ (Chapter 2).

Here we report on observations of the radio galaxy MRC 0316–257. This 1.5 Jy radio source was listed in the 408 MHz Molonglo Reference Catalogue (Large et al. 1981) and optically identified by McCarthy et al. (1990). Its discovery spectrum yielded a redshift of 3.13 (McCarthy et al. 1990). This object was included in our program because the redshift of the radio galaxy shifted the Lyα line into one of the narrow-band imaging filters available at the VLT. Also, it already had two spectroscopically confirmed Lyα emitting companions (Le Fèvre et al. 1996, hereafter LF96), an indication that the radio galaxy is located in a dense environment. Further, the redshift of the radio galaxy of 3.13 allows an efficient search for Lyman Break Galaxies (LBGs) and for [O III] λ5007 Å emitters using a *K*-band narrow-band filter, which is available in the Infrared Spectrometer and Array Camera (ISAAC, Moorwood 1997) at the VLT.

Besides observing MRC 0316–257 with the VLT as part of our large program, we made additional observations of the field with the Advanced Camera for Surveys (ACS; Ford et al. 1998) on the *Hubble Space Telescope (HST)* to study the sizes and morphologies of the detected galaxies.

This paper is organized in the following way. In §3.2 the imaging observations and data reduction are described and §3.3 discusses how candidate Lyα emitters in the field are detected. The spectroscopic observations and the results are presented in §3.4. The properties of the Lyα emitters are analyzed in §3.5, and details of individual emitters are presented in §3.6. Evidence for the presence of a protocluster in the field is discussed in §3.7, and the properties are presented in §3.8. In §3.9 the nature of the Lyα emitters is discussed, followed by a description of the implications of a protocluster at $z = 3.13$ in §3.10.

Throughout this chapter, magnitudes are in the AB system (Oke 1974), using the transformations $V_{\mathrm{AB}} = V_{\mathrm{Vega}} + 0.01$ and $I_{\mathrm{AB}} = I_{\mathrm{Vega}} + 0.39$ (Bessell 1979). A Λ-dominated cosmology with H$_0 = 65$ km s^{-1} Mpc^{-1}, $\Omega_{\mathrm{M}} = 0.3$, and $\Omega_\Lambda = 0.7$ is assumed. In this cosmology, the luminosity distance of MRC 0316–257 is 28.8 Gpc and 1$''$ corresponds to 8.19 kpc at $z = 3.13$.

3.2 Imaging observations and data reduction

3.2.1 VLT imaging

An overview of the observations is shown in Table 3.1. On 2001 September 20 and 21, narrow- and broad-band imaging was carried out with the 8.2 m Yepun (VLT UT4) to search for Lyα emitting galaxies around MRC 0316–257. The instrument used was the FOcal Reducer/low dispersion Spectrograph 2 (FORS2; Appenzeller & Rupprecht 1992) in imaging mode. For the narrow-band imaging the OIII/3000 filter was used with a central wavelength of 5045 Å and full width half maximum (*FWHM*) of 59

Table 3.1 — Summary of the observations of the field around MRC 0316–257.

Date	Telescope	Instrument	Mode	Optical element	Seeing	t_{exp}^a
2001 Sep 20 & 21	VLT UT4	FORS2	Imaging	Bessel V	0.″7	4 860
2001 Sep 20 & 21	VLT UT4	FORS2	Imaging	OIII/3000	0.″7	23 400
2001 Sep 22	VLT UT4	FORS2	MOS[b]	GRIS_1400V	~ 1.″5	12 600
2001 Oct 18	VLT UT4	FORS2	MXU[c], mask I	GRIS_1400V	1.″0	10 800
2001 Oct 18, 19 & 20	VLT UT4	FORS2	MXU[c], mask II	GRIS_1400V	1.″0	29 100
2001 Nov 15 & 16	VLT UT3	FORS1	PMOS[d]	GRIS_300V	0.″8	19 800
2002 Jul 18	*HST*	ACS	Imaging	F814W	–	6300
2002 Sep 6, 7 & 8	VLT UT4	FORS2	Imaging	Bessel I	0.″7	4 680

[a] Total exposure time in seconds.
[b] Multi-object spectroscopy mode, performed with 19 movable slitlets with lengths of 20″–22″.
[c] Multi-object spectroscopy mode with a user-prepared mask.
[d] Spectropolarimetry mode using nine movable slitlets of 20″.

Å, which samples the Lyα line from the radio galaxy, which is redshifted to 5021 Å (McCarthy et al. 1990, LF96). To measure the UV continuum near the Lyα line, the field was imaged with broad-band filter Bessel V with a central wavelength of 5540 Å and *FWHM* of 1115 Å. The detector was a SiTE CCD with 2048×2048 pixels. The pixel scale was 0.″2 per pixel, resulting in a field of view of 6.′8×6.′8. A year later, on 2002 September 6, 7 and 8, broad-band images of the field were taken in the Bessel I filter, with a central wavelength of 7680 Å and a *FWHM* of 1380 Å. The instrument was again FORS2, but the detector was replaced by two MITs CCDs with 2048×2048 pixels each. The gap between the two CCDs was ~ 4 arcsec. The pixel scale of the MIT CCDs was 0.″125 per pixel. To decrease the readout time, the pixels were binned by 2×2, resulting in a spatial scale of 0.″25 pixel^{-1}. The field of view was restricted by the geometry of the Multi-Object Spectroscopy (MOS) unit, and was 6.′8×6.′8.

The observations in the narrow-band were split into 13 separate exposures of 1800 s, in V-band into 27 separate 180 s exposures and in the I-band 26 exposures of 180 s were taken. The individual exposures were shifted by ~ 15″ with respect to each other to facilitate identifying cosmic rays and removing residual flat field errors.

All nights except for 2001 September 20 were photometric, and the average seeing was 0.″65 - 0.″7 in the narrow-band, V-band and I-band images (see Table 3.1). For the flux calibration, the spectrophotometric standard star LTT 1788 (Stone & Baldwin 1983; Baldwin & Stone 1984) was observed in the V-band and the photometric standard stars in the field SA98 (Landolt 1992) were used to calibrate the I-band images.

3.2.2   Data reduction of VLT data

The VLT images were reduced using standard routines within the reduction software package IRAF. The reduction steps included bias subtraction, flat fielding using twilight sky flats and illumination correction using the unregistered science frames.

The magnitude zero-points derived from different standard stars were consistent with each other within 0.02 magnitude. To derive the zero-point of the narrow-band image, the magnitude of the ~ 400 brightest objects in the field were measured in the V- and I-band images. These objects had a signal-to-noise of at least 25 in both V-

and *I*-band images. A magnitude limit of $m_I > 20$ was set to reject saturated stars. Narrow-band magnitudes were derived from the *V*- and *I*-band magnitudes assuming a powerlaw spectral energy distribution for these 400 objects. With these derived narrow-band magnitudes and the associated counts in the narrow-band image, the zero-point of the narrow-band image was computed. The rms of the computed zero-point was 0.006 mag.

All magnitudes were corrected for galactic extinction which was estimated by Schlegel et al. (1998) to have a value of $E(B - V) = 0.014$ mag. The measured $1\,\sigma$ limiting magnitudes per square arcsecond were 28.35, 28.90 and 28.69 for the narrow-band, *V*-band and *I*-band respectively.

Astrometric calibration was performed using the USNO-A2.0 catalog (Monet et al. 1998; Monet 1998) from which 20 stars were identified in the field. This resulted in a fit with a typical error in the right ascension and declination of $0\overset{''}{.}17$. The astrometric accuracy of the images is dominated by the uncertainty of the USNO-A2.0 catalog of $0\overset{''}{.}25$ (Deutsch 1999). The VLT images were registered in the following way. Because the *V*-band and narrow-band images were taken with the same detector, a simple pixel shift was sufficient to align the images, using the positions of a few stars over the field. The *I*-band frames were taken with the MIT CCD, which had a different pixel scale ($0\overset{''}{.}25$ pixel^{-1}) as compared to the SiTE CCD ($0\overset{''}{.}2$ pixel^{-1}). The distortions were also different, and rescaling the *I*-band image to the same pixel scale as the *V*-band image resulted in positional errors up to a few arcseconds in the corners of the *I*-band image. Instead, the position of a few hundred objects detected in both the *I*-band and *V*-band images with a signal-to-noise greater than 15, were used for the alignment. This way the positional error of objects in the *I*-band image dropped to $0\overset{''}{.}04$. Subsequently, the algorithm DRIZZLE (Fruchter & Hook 2002) was used to map the *I*-, *V*- and narrow-band images on new frames with a common pixel scale of $0\overset{''}{.}16$.

The area of the reduced images was 46.7 arcmin^2. Due to the presence of two bright stars in the field, the area that could be used for detecting candidate Lyα emitters was 45.75 arcmin^2. The width of the narrow-band filter in redshift is 0.049 at $z \sim 3.13$ and the volume probed by the filter at $z = 3.13$ is 9331 Mpc^3.

3.2.3 Hubble Space Telescope imaging and reduction

A part of the field imaged by the VLT was observed in 2002 July with the ACS on board the *HST* as part of an imaging program of HzRGs. The $3\overset{'}{.}4 \times 3\overset{'}{.}4$ field of view of the ACS was chosen to include not only the radio galaxy but also as many confirmed Lyα emitters as possible (see Fig. 3.19 for the position of the ACS field within the FORS field). The field was imaged in the F814W filter (hereafter I_{814}) with a central wavelength of 8333 Å and a width of 2511 Å. The total exposure time was 6300 s. The images were reduced using the ACS GTO pipeline (Blakeslee et al. 2003a).

3.3 Detection and selection of candidate emitters

3.3.1 Source detection

For the detection and photometry of objects in the images, the program SExtractor (version 2.2.2, Bertin & Arnouts 1996) was applied. The narrow-band image was used to
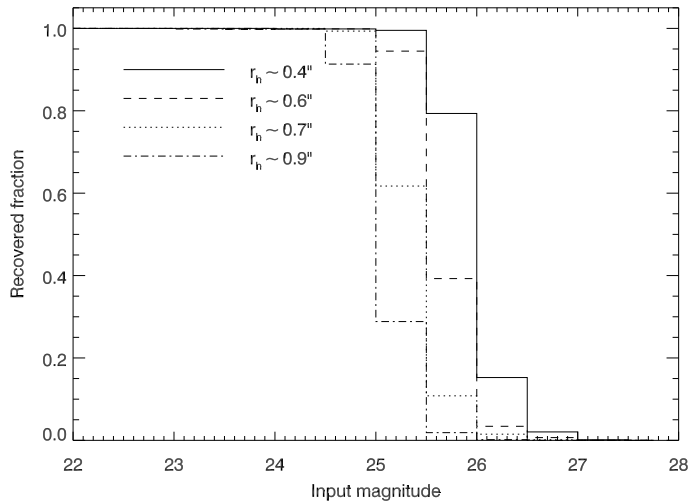
Figure 3.1 — Fraction of galaxies recovered in the narrow-band image versus magnitude for various galaxy sizes.

detect the objects. Because some of the Lyα emitters remained undetected in the broad-band images (see Table 3.3), this was preferred above a combination of the narrow-band and broad-band images as detection image, which is favoured by some other groups (e.g., Fynbo et al. 2002). Detected objects in the narrow-band image were defined to have at least 15 connected pixels with values larger than the rms sky noise. This resulted in a list of 3505 objects, of which 3209 had a signal-to-noise greater than five. To assess the completeness of the catalog, artificial and real galaxies were added to the narrow-band image and recovered. The galaxies had various sizes, the smallest galaxies had a half light radius $r_h \sim 0.4''$, similar to that of stars in the field (unresolved objects), the largest galaxies had a half light radius $r_h \sim 0.9''$, roughly 2.5 times that of stars. We found that the completeness depended on the size of the galaxies that were added to the image as shown in Fig. 3.1. The limit where half of the galaxies were recovered ranged from a magnitude of $m_{\mathrm{nb}} \lesssim 26.25$ for unresolved objects to $m_{\mathrm{nb}} \lesssim 25.25$ for the largest objects. The 90% recovery limit was $m_{\mathrm{nb}} \sim 26.0$ for unresolved and $m_{\mathrm{nb}} \sim 25.0$ for the largest objects.

3.3.2 Photometry

To measure the flux of the detected objects, the double image mode of SExtractor was employed. In this mode, SExtractor detects objects in one image, and carries out the photometry on a second image. In our case, the narrow-band image was used for the detection of the objects and the photometry was done on the narrow-band and broad-band images. Of each detected object in the narrow-band the flux was measured in two apertures: a circular aperture to compute the colors of the object, and an elliptical aperture to estimate the total brightness of the object. The radius of the circular aperture (R_{aper}) depended on the isophotal area of the object (A_{iso}), which is the area of pixels with values above the rms sky noise and is an output parameter of SExtractor: $R_{\mathrm{aper}} = \sqrt{A_{\mathrm{iso}}/\pi}$. A minimum aperture radius of $0\overset{''}{.}525$, 1.5 times the radius of the seeing disc, was set to avoid very small apertures. The maximum radius was set to 4 times the radius of the seeing disc to avoid overlapping apertures due to neighbouring galaxies. The shape and size of the elliptical aperture was derived from the object's light distribution. The ellipticity ε and position angle of the object were computed from the

Figure 3.2 — Difference between measured magnitude and input magnitude as a function of input magnitude for objects with various sizes. The difference is larger for fainter and/or larger objects.
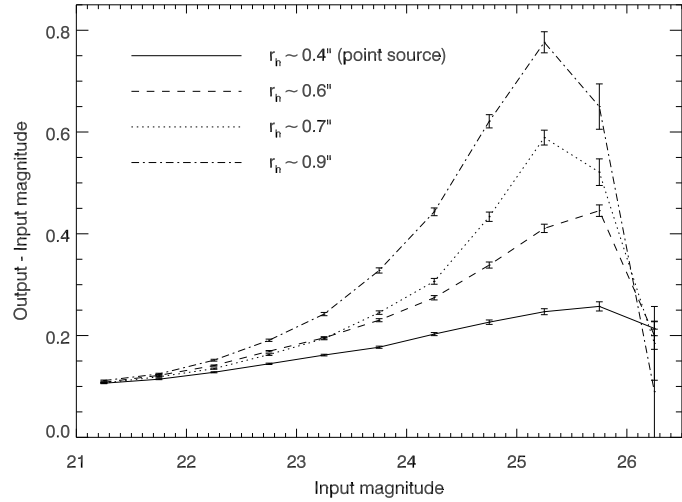
second order moment of the light distribution. Using the first moment r_1, the elliptical aperture had major and minor axes of kr_1/ε and εkr_1 (Bertin & Arnouts 1996). The scaling factor k determines the size of aperture and is a free parameter in SExtractor. We tested SExtractor on a set of images and compared SExtractor's output magnitudes for values of k in the range $1.0 < k < 2.75$. It was found that a scaling factor of $k \approx 1.75$ both optimized the signal-to-noise and minimized the fraction of the flux of the object outside the aperture.

The aperture used to measure the total flux of an object was the elliptical aperture, except when more than 10% of the pixels in the elliptical aperture was significantly effected by bright and close neighbours (SExtractor output parameter FLAGS equals 1) or when the object was originally blended with another one (FLAGS equals 2). In those cases the circular aperture was used to derive the total flux.

To estimate the fraction of the total flux of the object falling outside the (elliptical) aperture, Monte Carlo simulations were performed. Galaxies in the magnitude range $21 < m_{\rm nb} < 28$ with various shapes (Gaussian and elliptical profiles) and sizes (half light radii $0.4'' < r_h < 0.9''$) were added to the narrow-band image and recovered. The number of galaxies added to the image was limited to 40 to avoid overcrowding. This routine was repeated until 8000 galaxies per magnitude bin were simulated. By comparing the measured magnitudes to the input magnitude of the simulated galaxies, the fraction of the flux that was outside the aperture could be estimated to correct the aperture magnitudes. The simulations showed that this fraction depends on both the original size of the object and the magnitude of the object: the fraction of the flux outside the aperture is higher for a large and/or faint object, compared to a compact and/or bright object (see Fig. 3.2). At faint magnitudes the correction becomes smaller again, because these objects have a larger probability to be detected if they coincide with a peak in the noise. For the brightest objects the fraction of the flux outside the aperture is constant at a value of $\sim 11\%$. To avoid an overestimation of the magnitude correction, we decided to use only point sources to measure the correction (see Fig. 3.2). The magnitude correction applied to the sources in our field was $\lesssim 0.1$ for objects with $m_{\rm nb} \lesssim 21$, rising to ~ 0.25 for objects with $m_{\rm nb} \sim 26$.

3.3.3   Selection of candidate Lyα emitters

An efficient method of detecting Lyα emitting galaxies at high redshift is to select objects with a large line equivalent width (e.g., Cowie & Hu 1998) using the narrow- and broad-band photometry. The observed equivalent width EW_{obs} of a Lyα line is defined as:

$$EW_{\mathrm{obs}} = F_{\mathrm{Ly}\alpha}/C_{\mathrm{Ly}\alpha} \tag{3.1}$$

with $F_{\mathrm{Ly}\alpha}$ the flux of the Lyα line and $C_{\mathrm{Ly}\alpha}$ the UV continuum at the wavelength of the Lyα line. Assume that a Lyα line is observed in both a narrow-band filter and a broad-band filter, then the flux density in the narrow-band ($f_{\lambda,\mathrm{nb}}$) and broad-band ($f_{\lambda,\mathrm{bb}}$) can be described as:

$$f_{\lambda,\mathrm{nb}} \;=\; C(\lambda = \lambda_{\mathrm{eff,nb}}) + F_{\mathrm{Ly}\alpha}/\Delta\lambda_{\mathrm{nb}} \tag{3.2}$$

$$f_{\lambda,\mathrm{bb}} \;=\; C(\lambda = \lambda_{\mathrm{eff,bb}}) + F_{\mathrm{Ly}\alpha}/\Delta\lambda_{\mathrm{bb}}, \tag{3.3}$$

where C is the UV continuum and $\Delta\lambda_{\mathrm{bb(nb)}}$ is the width of broad-band (narrow-band) filter (Eq. 3.5) and $\lambda_{\mathrm{eff,bb(nb)}}$ the effective wavelength of broad-band (narrow-band) filter (Eq. 3.4).

The effective wavelength of a filter with transmission curve $T(\lambda)$ is given by:

$$\lambda_{\mathrm{eff}} = \frac{\int \lambda\, T(\lambda)\, d\lambda}{\int T(\lambda)\, d\lambda} \tag{3.4}$$

and the width of the filter $\Delta\lambda$ by:

$$\Delta\lambda = \int T(\lambda)\, d\lambda / T_{\mathrm{max}}, \tag{3.5}$$

with T_{max} the peak transmission of the filter. For a top-hat filter, the effective wavelength is equal to the central wavelength and the width equals the *FWHM*.

If the central wavelengths of the narrow-band and broad-band filters are roughly equal and the Lyα line falls in the centre of the filters, then eliminating either C or $F_{\mathrm{Ly}\alpha}$ by substituting equation (3.2) in equation (3.3) gives:

$$F_{\mathrm{Ly}\alpha} \;=\; \frac{\Delta\lambda_{\mathrm{bb}}\Delta\lambda_{\mathrm{nb}}(f_{\lambda,\mathrm{nb}} - f_{\lambda,\mathrm{bb}})}{\Delta\lambda_{\mathrm{bb}} - \Delta\lambda_{\mathrm{nb}}} \tag{3.6}$$

$$C_{\mathrm{Ly}\alpha} \;=\; \frac{\Delta\lambda_{\mathrm{bb}}f_{\lambda,\mathrm{bb}} - \Delta\lambda_{\mathrm{nb}}f_{\lambda,\mathrm{nb}}}{\Delta\lambda_{\mathrm{bb}} - \Delta\lambda_{\mathrm{nb}}}, \tag{3.7}$$

and using equation (3.1) results in an expression for EW_{obs}:

$$EW_{\mathrm{obs}} = \frac{\Delta\lambda_{\mathrm{bb}}\Delta\lambda_{\mathrm{nb}}(f_{\lambda,\mathrm{nb}} - f_{\lambda,\mathrm{bb}})}{\Delta\lambda_{\mathrm{bb}}f_{\lambda,\mathrm{bb}} - \Delta\lambda_{\mathrm{nb}}f_{\lambda,\mathrm{nb}}} \tag{3.8}$$

(e.g., Bunker et al. 1995; Malhotra & Rhoads 2002). Alternatively, equation (3.8) can be used if it is expected that the fraction of the continuum flux falling in the filters that is absorbed by foreground H I is comparable to the fraction of the Lyα line that is extinguished by intergalactic absorption (as assumed by e.g., Malhotra & Rhoads 2002).

If the central wavelengths of the narrow-band and broad-band filters differ, as is the case with our filters, then the slope of the UV continuum is needed to extrapolate the continuum strength from the central wavelength of the broad-band to the central wavelength of the narrow-band. Including an extra broad-band contribution redward of the Lyα line, the continuum slope can be calculated as well. Below is described how the equivalent width of a $z = 3.13$ Lyα emitter can be computed using our available photometry.

Assuming that a Lyα emitter has a spectral energy distribution that consists of a Lyα line with flux $F_{\mathrm{Ly}\alpha}$ and a UV continuum redward of the Lyα line with strength C and powerlaw slope β ($f_\lambda = C \lambda^\beta$), the flux density in the narrow-band ($f_{\lambda,\mathrm{nb}}$), V-band ($f_{\lambda,\mathrm{V}}$) and I-band ($f_{\lambda,\mathrm{I}}$) can then be characterized as:

$$f_{\lambda,\mathrm{nb}} = Q_{\mathrm{nb}} C \lambda_{\mathrm{eff,nb}}^{\beta} + \epsilon_{\mathrm{nb}} F_{\mathrm{Ly}\alpha}/\Delta\lambda_{\mathrm{nb}} \tag{3.9}$$

$$f_{\lambda,\mathrm{V}} = Q_{\mathrm{V}} C \lambda_{\mathrm{eff,V}}^{\beta} + \epsilon_{\mathrm{V}} F_{\mathrm{Ly}\alpha}/\Delta\lambda_{\mathrm{V}} \tag{3.10}$$

$$f_{\lambda,\mathrm{I}} = C \lambda_{\mathrm{eff,I}}^{\beta} \tag{3.11}$$

with $\lambda_{\mathrm{eff,nb/V/I}}$ the effective wavelength corresponding to the narrow-band, V and I filter respectively (Eq. 3.4), $\Delta\lambda$ the width of the filter (Eq. 3.5), ϵ the efficiency of the filter at the wavelength of the redshifted Lyα line and Q the fraction of the continuum flux falling in the filter that is absorbed by the Lyα forest (Eq. 3.12). It should be mentioned that, in contrast to equation (3.8), no correction factor for foreground absorption of the Lyα line is applied in this calculation. If foreground extinction of the Lyα line is taken into account, then the equivalent width and Lyα line flux will be higher by $\sim 60\%$ (see Eq. 3.13).

For the filters (and instrument) used in this project, the input parameters are: $\lambda_{\mathrm{eff,nb}} = 5040.1$ Å, $\Delta\lambda_{\mathrm{nb}} = 61.1$ Å, $\lambda_{\mathrm{eff,V}} = 5561.9$ Å, $\Delta\lambda_{\mathrm{V}} = 1145.6$ Å and $\lambda_{\mathrm{eff,I}} = 7946.5$ Å. The efficiency ϵ of the filters depends on the redshift of the Lyα line. For all objects a redshift of $z = 3.13$ is assumed, and the efficiencies are $\epsilon_{\mathrm{nb}} = 0.76$ and $\epsilon_{\mathrm{V}} = 0.74$. It should be stressed that the computed equivalent width does not depend strongly on the assumed redshift in the interval $z = 3.13 - 3.17$. Assuming a redshift of $z = 3.12$ will yield equivalent widths that are a factor of ~ 2 higher compared to the equivalent widths computed with $z = 3.13$.

The fraction of the continuum flux that is absorbed by foreground neutral hydrogen averaged over the bandpass is Q:

$$Q = \frac{\int e^{-\tau_{\mathrm{eff}}} T(\lambda)\mathrm{d}\lambda}{\int T(\lambda)\mathrm{d}\lambda} \tag{3.12}$$

where τ_{eff} is the effective opacity of H I. For observed wavelengths between the redshifted Lyα and redshifted Lyβ line ($\lambda_{\mathrm{Ly}\beta}(1+z) < \lambda_{\mathrm{obs}} < \lambda_{\mathrm{Ly}\alpha}(1+z)$), the expression for τ_{eff} is:

$$\tau_{\mathrm{eff}} = 0.0036 \left(\frac{\lambda_{\mathrm{obs}}}{1216\text{Å}} \right)^{3.46} \tag{3.13}$$

(Press et al. 1993; Madau 1995). Because the Lyα line of an object at $z = 3.13$ falls in the blue wing of the *V* filter, the fraction of the continuum flux falling in the *V* filter that is absorbed is small and Q is near unity: $Q_{\mathrm{V}} \sim 0.97$. In the narrow-band, $Q_{\mathrm{nb}} = 0.92$ for a source at $z = 3.13$.

To calculate the equivalent width of an individual Lyα line, equations (3.9) – (3.11) were solved for β, C and $F_{\mathrm{Ly}\alpha}$. This was done in the following way. Equation (3.9) was multiplied by $\Delta\lambda'_{\mathrm{nb}} = \Delta\lambda_{\mathrm{nb}}/\epsilon_{\mathrm{nb}}$ and equation (3.10) by $\Delta\lambda'_{\mathrm{V}} = \Delta\lambda_{\mathrm{V}}/\epsilon_{\mathrm{V}}$. Substituting $C = f_{\lambda,\mathrm{I}}/\lambda^{\beta}_{\mathrm{eff,I}}$ (Eq. 3.11) gave:

$$\Delta\lambda'_{\mathrm{nb}} f_{\lambda,\mathrm{nb}} = f_{\lambda,\mathrm{I}} \Delta\lambda'_{\mathrm{nb}} Q_{\mathrm{nb}} \left(\frac{\lambda_{\mathrm{eff,nb}}}{\lambda_{\mathrm{eff,I}}} \right)^{\beta} + F_{\mathrm{Ly}\alpha} \tag{3.14}$$

$$\Delta\lambda'_{\mathrm{V}} f_{\lambda,\mathrm{V}} = f_{\lambda,\mathrm{I}} \Delta\lambda'_{\mathrm{V}} Q_{\mathrm{V}} \left(\frac{\lambda_{\mathrm{eff,V}}}{\lambda_{\mathrm{eff,I}}} \right)^{\beta} + F_{\mathrm{Ly}\alpha}. \tag{3.15}$$

Subtraction of equation (3.14) from equation (3.15) results in an equation of the form $a^{\beta} - b^{\beta} = constant$. This equation was solved numerically.

When β was computed, the UV continuum flux density C and the Lyα line flux $F_{\mathrm{Ly}\alpha}$ were calculated using equations (3.9) and (3.10):

$$C = \frac{\Delta\lambda'_{\mathrm{V}} f_{\lambda,\mathrm{V}} - \Delta\lambda'_{\mathrm{nb}} f_{\lambda,\mathrm{nb}}}{\Delta\lambda'_{\mathrm{V}} Q_{\mathrm{V}} \lambda^{\beta}_{\mathrm{eff,V}} - \Delta\lambda'_{\mathrm{nb}} Q_{\mathrm{nb}} \lambda^{\beta}_{\mathrm{eff,nb}}} \tag{3.16}$$

and

$$F_{\mathrm{Ly}\alpha} = \frac{f_{\lambda,\mathrm{nb}}/(Q_{\mathrm{nb}} \lambda^{\beta}_{\mathrm{eff,nb}}) - f_{\lambda,\mathrm{V}}/(Q_{\mathrm{V}} \lambda^{\beta}_{\mathrm{eff,V}})}{1/(\Delta\lambda'_{\mathrm{nb}} Q_{\mathrm{nb}} \lambda^{\beta}_{\mathrm{eff,nb}}) - 1/(\Delta\lambda'_{\mathrm{V}} Q_{\mathrm{V}} \lambda^{\beta}_{\mathrm{eff,V}})}. \tag{3.17}$$

With C and $F_{\mathrm{Ly}\alpha}$, the equivalent width (*EW*) for each object was computed:

$$EW_{\mathrm{obs}} = \frac{F_{\mathrm{Ly}\alpha}}{C(\lambda_{\mathrm{Ly}\alpha}(1+z))^{\beta}} \tag{3.18}$$

with $\lambda_{\mathrm{Ly}\alpha}$ the wavelength of the Lyα line. The rest-frame equivalent width (*EW*₀) is given by: $EW_0 = EW_{\mathrm{obs}}/(1+z)$.

Figure 3.3 — Color–color diagram for the 3209 objects detected in the narrow-band image with a signal-to-noise greater than 5. The dashed line shows the color of objects with a rest-frame equivalent width of $EW_0 = 0$ Å. The solid line indicates where $EW_0 = 15$ Å. Objects not detected in the V-band and/or in the I-band are plotted with an arrow.
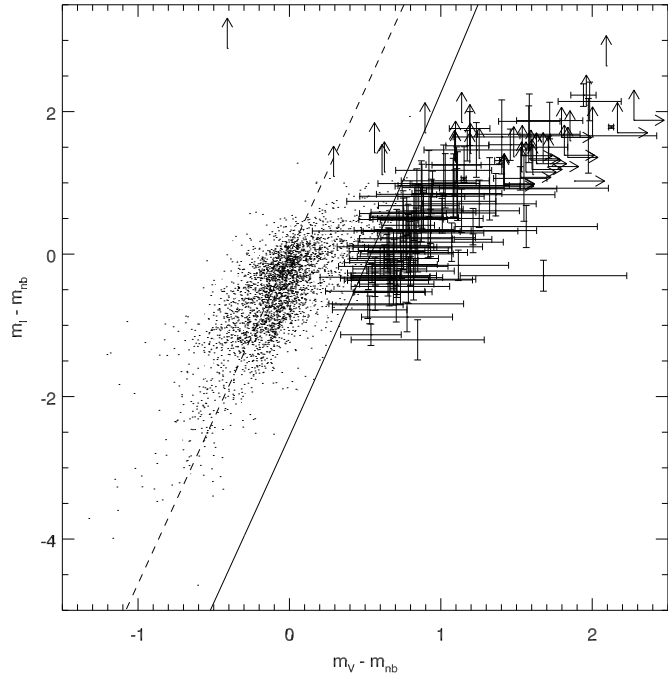
To estimate the uncertainties in the computed parameters, the observed flux densities were randomly varied 50 000 times over a range having a standard deviation equal to the uncertainty. The distributions of β, C, $F_{\text{Ly}\alpha}$ and EW_0 were used to estimate the errors in these quantities. Because the values of the equivalent width were not normally-distributed (Gaussian) around the central value, two errors were calculated, labelled ΔEW_0^- and ΔEW_0^+. These were computed from the values in the distribution that were outside the central 99.73% of all values. The difference between these values and the central value was taken as defining three sigma uncertainties.

For each object detected in the narrow-band image, the line flux, UV continuum and equivalent width and their errors were computed. Because no I-band data had been taken yet at the time that the candidates for the spectroscopy had to be selected, a flat spectrum ($\beta = -2$) was assumed for all sources. In Fig. 3.3, the $m_I - m_{\text{nb}}$ color is plotted against the $m_V - m_{\text{nb}}$ color. Following Chapter 2, objects with $EW_0 > 15$ Å and $EW_0/\Delta EW_0^- > 3$ were selected as candidate Lyα emitters. Each individual Lyα candidate was inspected visually in order to remove spurious candidates, like leftover cosmic rays or objects in the "spikes" of bright stars. This resulted in a list of 77 candidate Lyα emitters with $EW_0 > 15$ Å of which 6 had 15 Å $< EW_0 <$ 20 Å.

The main difference between the usage of equation (3.8) and equations (3.9)–(3.18) to compute the equivalent width can be seen in Fig. 3.4. Using equation (3.8) (and thereby assuming a fixed slope of $\beta = -2$) the line with $EW_0 = 15$ Å would lie at a constant $m_V - m_{\text{nb}} = 0.72$ (the solid line in Fig. 3.4). As a result, the EW_0 of three very blue objects (with $\beta < -2$) would be overpredicted, falsely selecting objects as Lyα emitters (e.g. the three crosses in Fig. 3.4). On the other hand, 11 red Lyα emitters with $\beta > -2$ would not pass the selection criterion $m_V - m_{\text{nb}} > 0.72$, while their EW_0 as calculated with equations (3.9)–(3.18) is greater than 15 Å (diamonds in Fig. 3.4).
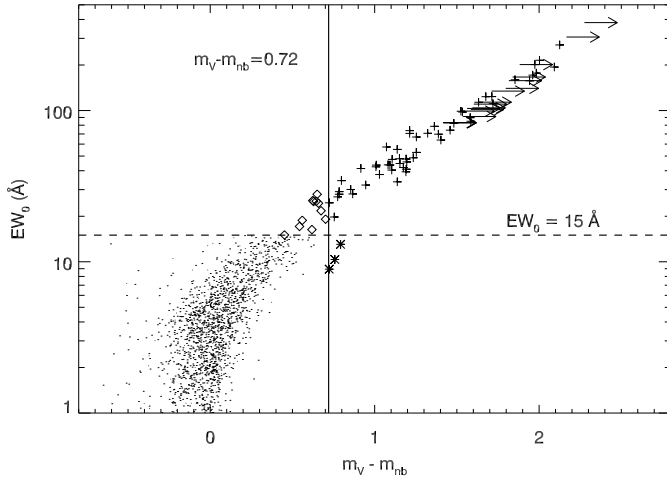
Figure 3.4 — Equivalent width (calculated from Eqs. 3.9–3.18) versus $m_V - m_{nb}$ color. For clarification, only objects with an $EW_0 > 1$ Å are plotted and the error bars are left out. The solid line indicates a color of $m_V - m_{nb} = 0.72$, while the dashed line denotes the division between low ($EW_0 < 15$ Å) and high ($EW_0 > 15$ Å) equivalent width objects.

3.4 Spectroscopy

3.4.1 Spectroscopic observations

Spectra of candidate Lyα emitters were taken during three separate observing sessions (see Table 3.1 for an overview). The first spectroscopy session was carried out on 2001 September 22 with VLT/FORS2 in the multi-object spectroscopy mode with 19 movable slits of a fixed length of $\sim 20 - 22''$. The night was photometric, but because of strong winds (> 12 m s^{-1}) the seeing fluctuated between $1''$ and $2''$. Spectra of 12 candidate Lyα emitters were obtained for 4×2700 s and 1×1800 s through $1''$ slits with the 1400V grism at a dispersion of 0.5 Å pixel^{-1}. This grism was chosen for a number of reasons. First, it has a high peak efficiency of $\sim$85% at wavelengths that correspond to the redshifted Lyα line of the radio galaxy. Second, because observations of high redshift Lyα emitting galaxies have shown that the width of the Lyα line lies predominantly in the range 200–500 km s^{-1} (e.g., Pentericci et al. 2000; Dawson et al. 2002; Hu et al. 2004), the resolution of the grism ($R = 2100$, corresponding to ~ 150 km s^{-1}) ensured that the Lyα emission line is marginally resolved (see §3.5.1), maximizing the signal-to-noise of the observed line. Also, the resolution is large enough to distinguish a high redshift Lyα emitting galaxy from a low redshift contaminant, the [O II] $\lambda\lambda3726, 3729$ emitter. With the 1400V grism the [O II] doublet is resolved (see Fig. 3.5 for two examples). For the wavelength calibration exposures of He, HgCd and Ne arc lamps were obtained. The spectrophotometric standard star LTT 1788 (Stone & Baldwin 1983; Baldwin & Stone 1984) was observed with a $5''$ slit for the flux calibration.

On 2001 October 18, 19 and 20 spectra were obtained with FORS2 in the mask multi-object spectroscopy mode. In this mode objects are observed through a user defined, laser-cut mask with slits which had variable lengths (typically $10 - 12''$) and widths of $1''$. The nights were photometric with an average seeing of $1''$. The 1400V grism was used to observe 37 candidate Lyα emitters in two masks, of which 25 were included in both masks. The first mask was observed for 4×2700 s and the second mask for 10×2700 s and 1×2100 s. The pixels were binned by 2×2 to avoid the noise in the spectra being dominated by read noise. This resulted in a dispersion of 1 Å pixel^{-1} and a spatial scale of $0\overset{''}{.}4$ pixel^{-1}. Spectra of the standard star LTT 1788 were obtained for

Table 3.2 — Characteristics of the Voigt absorption profiles derived from the spectra. For each absorption profile, its centre relative to the peak of the emission line, width (*b*) and H I column density (*N*) is printed.

Object	Centre	b (km s^{-1})	$\log N$ (cm^{-2})
344	-80 ± 10	52 ± 11	14.4 ± 0.1
995	-150 ± 20	74 ± 59	16.0 ± 2.5
1147	-70 ± 20	101 ± 24	14.6 ± 0.1
1203	-90 ± 10	104 ± 11	14.9 ± 0.1
1518	80 ± 50	38 ± 16	13.8 ± 0.2
	-210 ± 60	155 ± 52	15.0 ± 0.2
1612	-150 ± 10	79 ± 16	14.4 ± 0.1
1710	-130 ± 20	80 ± 30	14.1 ± 0.2
1867	-60 ± 20	30 ± 16	13.1 ± 0.3
2487	250 ± 170	108 ± 14	14.6 ± 0.1
	-1150 ± 200	629 ± 93	16.0 ± 0.2
3101	-40 ± 110	193 ± 131	14.4 ± 0.4
	-240 ± 20	79 ± 38	14.3 ± 0.3
3388	-130 ± 10	59 ± 13	14.3 ± 0.1
HzRG	200 ± 10	151 ± 9	14.9 ± 0.1
	-270 ± 10	245 ± 25	14.9 ± 0.1
	-660 ± 10	144 ± 20	14.8 ± 0.1
	-970 ± 20	131 ± 27	14.2 ± 0.1

the flux calibration.

During the last observing session (2001 November 15 and 16), the instrument used was FORS1 on Melipal (VLT UT3). The main goal of this run was to measure the polarization of the radio galaxy (C. De Breuck et al., in preparation). Due to constraints on the positioning and orientation of the mask, only three candidate Lyα emitters could be observed. The width of the slits was 1$''$. The total exposure time was 19 800 s. The average seeing of these photometric nights was 0$\overset{''}{.}$8. The grism used for the observations was the "300V" with a resolution of 440, a dispersion of 2.64 Å pixel^{-1} and a spatial scale of 0$\overset{''}{.}$2 pixel^{-1}. The spectrophotometric standard stars Feige 110 and LTT 377 (Stone & Baldwin 1983; Baldwin & Stone 1984) were observed for the flux calibration.

3.4.2 Data reduction

The spectra were reduced in the following way. Individual frames were flat fielded using lamp flats, cosmic rays were identified and removed and the background was subtracted. The next step was the extraction of the one-dimensional (1D) spectra. Typical aperture sizes were 1$''$–1$\overset{''}{.}$5. If the spectrum of the object could be seen in the individual frames, then a spectrum was extracted from each frame and these spectra were combined. If the object was undetected in the individual frames, then the background subtracted two-dimensional frames were combined and a 1D spectrum was extracted from this image. All 1D spectra were wavelength calibrated using the arc lamp spectra. For spectra taken with the 1400V grism the rms of the wavelength calibration was always better than 0.05 Å, which translates to $\Delta z = 0.00004$ at $z \sim 3.13$. The wavelength calibration with the 300V grism had an rms of 0.8 Å ($\Delta z = 0.0007$ at $z \sim 3.13$). A heliocentric correction was applied on measured redshifts to correct for the radial velocity of the Earth in the direction of the observations. Finally, the spectra were flux
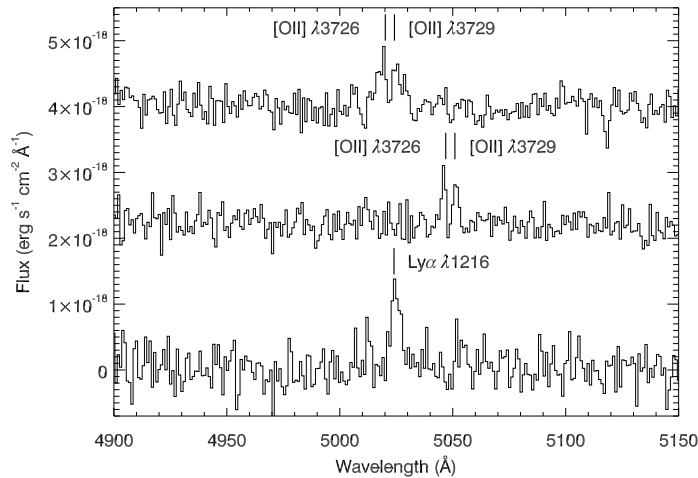
Figure 3.5 — Spectra of two [O II] emitters observed in the field (top two spectra). For comparison, the spectrum of one of the confirmed Lyα emitters is shown at the bottom. The spectra are offset from each other by 1.5×10^{-18} erg s^{-1} cm^{-2} Å^{-1}.

calibrated. The fluxes of the photometric standard stars in the individual images were consistent with each other to within 5%, so we estimate that the flux calibration of the spectra is accurate to $\sim 5\%$.

3.4.3   Results

Spectra were obtained for a total of 40 candidate Lyα emitters, of which 11 were observed during two separate observing sessions, and the central radio galaxy. Of the 40 candidate emitters, only seven failed to show an emission line. Six of these unconfirmed emitters had predicted line fluxes below 10^{-17} erg s^{-1} cm^{-2} and were probably too faint to be detected. Two of the 33 emission line objects showed two lines with almost equal strength, separated by ~ 4 Å (Fig. 3.5). These objects were identified to be [O II] $\lambda\lambda 3726, 3729$ emitters at a redshift of ~ 0.35. One of the [O II] emitters was re-observed in 2001 November and a nearly flat continuum was revealed with no break around the emission line, confirming that the object could not be a Lyα emitter at $z \sim 3.13$. None of the other emitters had more than one emission line in the spectrum. This excluded identification of the emission line with [O III] $\lambda 5007$, because then the confirming [O III] $\lambda 4959$ would have been visible. Furthermore, a number of emitters showed an asymmetric line profile (Figs. 3.6–3.11), a feature often seen in spectra of high redshift Lyα emitters (e.g., Ajiki et al. 2002; Dawson et al. 2002). Therefore, the 31 remaining emitters were identified with being Lyα emitters. The fraction of contaminants in our sample is 2/33 = 6.1%, similar to the fraction of low redshift interlopers of 6.5% in the study of Lyα emitters at $z \sim 3.09$ of Steidel et al. (2000).

3.5   Properties of the Lyα emitting galaxies

The one-dimensional Lyα emission lines were fitted by a Gaussian function and – if absorption was clearly present – in combination with Voigt absorption profiles. The best fit Gaussian was used to calculate the redshift, line flux and *FWHM* of each emitter. In Table 3.3 the properties of the confirmed Lyα emitters are summarized. The IDs correspond to the object's number in the SExtractor catalog. The rest-frame equivalent width EW_0 was taken from the imaging. The star formation rate (*SFR*) was calculated

Table 3.3 — Position and properties of the Lyα emission line of the 31 confirmed Lyα emitters and the radio galaxy.

Object	Position		z	Flux	EW_0	$FWHM$	$SFR_{\mathrm{Ly}\alpha}$
	α_{J2000}	δ_{J2000}		$10^{-17}\,\mathrm{erg\,s^{-1}\,cm^{-2}}$	Å	$\mathrm{km\,s^{-1}}$	$M_\odot\,\mathrm{yr^{-1}}$
344	03 18 05.83	−25 37 55.7	3.1332 ± 0.0001	4.2 ± 0.3	144^{+339}_{-30}	260 ± 20	2.8 ± 0.2
695	03 18 13.26	−25 37 18.9	3.1712 ± 0.0001	2.3 ± 0.2	246^{+553}_{-51}	180 ± 20	4.0 ± 0.4
748	03 18 21.51	−25 37 13.9	3.1359 ± 0.0003	0.4 ± 0.1	70^{+949}_{-20}	260 ± 50	1.1 ± 0.2
995	03 18 09.67	−25 36 47.5	3.1239 ± 0.0003	4.3 ± 0.6	65^{+36}_{-14}	450 ± 30	2.6 ± 0.4
1029	03 18 00.07	−25 36 43.6	3.1301 ± 0.0007	0.3 ± 0.1	39^{+17}_{-8}	< 590	1.7 ± 0.2
1099	03 18 02.79	−25 36 35.8	3.1313 ± 0.0004	1.1 ± 0.3	42^{+65}_{-11}	240 ± 70	1.4 ± 0.3
1147	03 18 03.99	−25 36 31.9	3.1666 ± 0.0003	6.0 ± 2.2	318^{+1000}_{-90}	290 ± 40	1.4 ± 0.2
1203	03 18 12.55	−25 36 23.0	3.1234 ± 0.0002	10.3 ± 1.8	78^{+24}_{-12}	220 ± 10	3.3 ± 0.3
1361	03 18 01.57	−25 36 07.8	3.1306 ± 0.0002	1.5 ± 0.2	106^{+234}_{-24}	210 ± 40	2.6 ± 0.3
1395	03 18 24.78	−25 36 05.7	3.1442 ± 0.0011	1.8 ± 0.6	$\lesssim 30$	790 ± 190	0.4 ± 0.1
1446	03 18 04.89	−25 35 57.7	3.1316 ± 0.0002	0.5 ± 0.1	12^{+8}_{-4}	210 ± 50	0.6 ± 0.2
1498	03 18 14.14	−25 35 54.3	3.1319 ± 0.0003	1.0 ± 0.1	58^{+435}_{-18}	460 ± 60	0.6 ± 0.1
1518	03 18 16.78	−25 35 46.2	3.1311 ± 0.0007	3.2 ± 0.8	23^{+2}_{-2}	570 ± 70	4.8 ± 0.2
1612	03 18 03.49	−25 35 39.2	3.1222 ± 0.0003	3.1 ± 0.3	> 370	500 ± 40	1.8 ± 0.3
1710	03 18 15.17	−25 35 28.9	3.1462 ± 0.0004	1.9 ± 0.3	61^{+61}_{-14}	420 ± 50	1.0 ± 0.1
1724	03 18 06.92	−25 35 26.2	3.1426 ± 0.0002	0.4 ± 0.1	> 150	160 ± 50	0.9 ± 0.1
1753	03 18 01.22	−25 35 22.3	3.1301 ± 0.0001	1.5 ± 0.2	32^{+16}_{-7}	130 ± 40	2.1 ± 0.4
1759	03 18 25 50	−25 35 20.4	3.1271 ± 0.0002	0.6 ± 0.1	48^{+29}_{-11}	120 ± 50	2.5 ± 0.4
1829	03 18 15.12	−25 35 13.1	3.1313 ± 0.0002	0.7 ± 0.1	24^{+19}_{-7}	200 ± 40	1.3 ± 0.3
1867	03 18 09.00	−25 34 59.6	3.1358 ± 0.0002	5.8 ± 0.4	56^{+3}_{-3}	650 ± 40	11.6 ± 0.2
1891	03 18 04.29	−25 35 04.9	3.1454 ± 0.0002	0.6 ± 0.1	$\lesssim 31$	130 ± 40	0.8 ± 0.2
1946	03 18 20.29	−25 34 59.4	3.1335 ± 0.0003	0.7 ± 0.1	$\lesssim 19$	260 ± 50	0.7 ± 0.3
1955	03 18 07.58	−25 34 55.5	3.1391 ± 0.0003	0.7 ± 0.1	> 139	330 ± 60	1.1 ± 0.2
1962	03 18 12.03	−25 34 52.8	3.1407 ± 0.0007	1.7 ± 0.4	33^{+12}_{-6}	600 ± 130	0.9 ± 0.1
1968	03 18 05.14	−25 34 51.2	3.1564 ± 0.0004	0.4 ± 0.1	$\lesssim 66$	300 ± 80	1.7 ± 0.3
2413	03 18 20.40	−25 33 00.3	3.1339 ± 0.0002	0.7 ± 0.2	62^{+28}_{-11}	200 ± 50	2.7 ± 0.3
2487	03 17 59.63	−25 34 01.3	3.1175 ± 0.0024	19.3 ± 2.6	202^{+9}_{-8}	2510 ± 190	$-^a$
2637	03 18 22.52	−25 34 10.1	3.1224 ± 0.0002	1.3 ± 0.3	79^{+43}_{-16}	200 ± 50	3.2 ± 0.5
2871	03 18 25.71	−25 33 40.5	3.1334 ± 0.0003	0.4 ± 0.1	> 75	250 ± 70	0.7 ± 0.1
3101	03 18 24.09	−25 32 12.2	3.1313 ± 0.0003	4.3 ± 1.2	114^{+47}_{-18}	800 ± 100	5.2 ± 0.3
3388	03 18 26.09	−25 32 53.1	3.1379 ± 0.0002	2.1 ± 0.1	112^{+26}_{-13}	370 ± 20	8.6 ± 0.3
HzRG	03 18 12.01	−25 35 10.8	3.1307 ± 0.0001	155.1 ± 4.2	257^{+9}_{-8}	1320 ± 10	76.1 ± 0.4^a

^{a} Object contains an AGN, therefore the estimated *SFR* is unreliable.

using the Lyα line flux derived from the images, and assuming Case B recombination and using the Hα luminosity to *SFR* conversion from Madau et al. (1998, see §3.5.4).

3.5.1   Line profiles

As mentioned in the previous paragraph, emitters which clearly showed an emission line with an absorbed blue wing (see Figs. 3.6–3.11) were fitted by a Gaussian emission line with one or more Voigt absorption profiles. The characteristics of the absorption profiles are listed in Table 3.2. The other emitters were fitted by a single Gaussian. The observed width of the line was deconvolved with the instrumental width, which was $150\,\mathrm{km\,s^{-1}}$ (see §3.4.1).

The radio galaxy has an emission line that can be fitted by a Gaussian with a *FWHM* of $\sim 1300\,\mathrm{km\,s^{-1}}$. The line width is very similar to that of other HzRGs (e.g., De Breuck et al. 2001; Willott et al. 2002). Only one of the confirmed emitters has a broad Lyα line. Emitter #2487 has a line *FWHM* of $\sim 2500\,\mathrm{km\,s^{-1}}$, and is therefore likely to also harbour an AGN. The *FWHM* of the Lyα emission line of the rest of the emitters ranges from

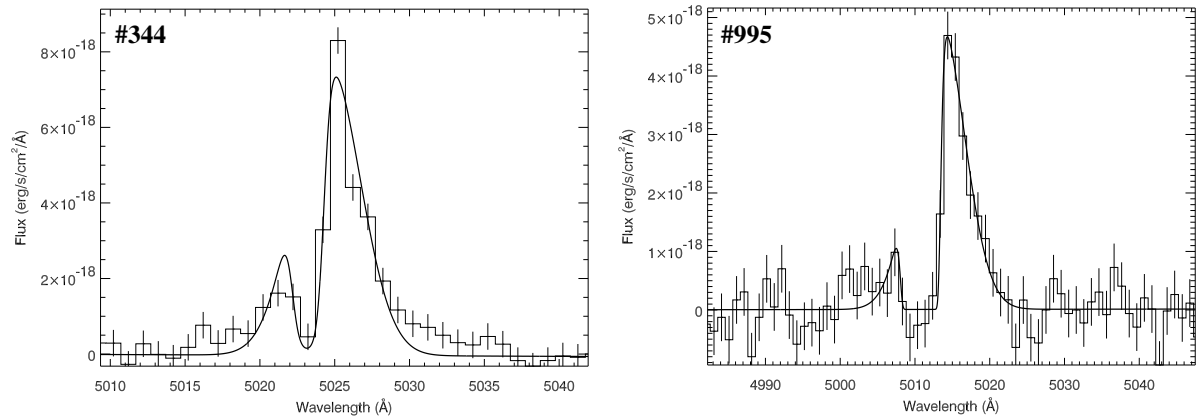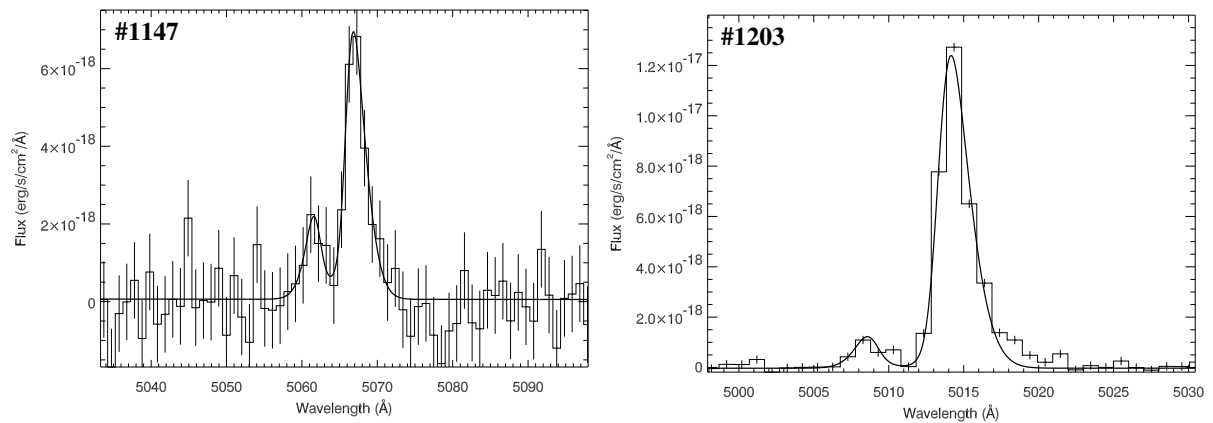**Figure 3.6 —** Spectra of emitter #344 (left) and #995 (right).

Figure 3.7 — Spectra of emitter #1147 (left) and #1203 (right).
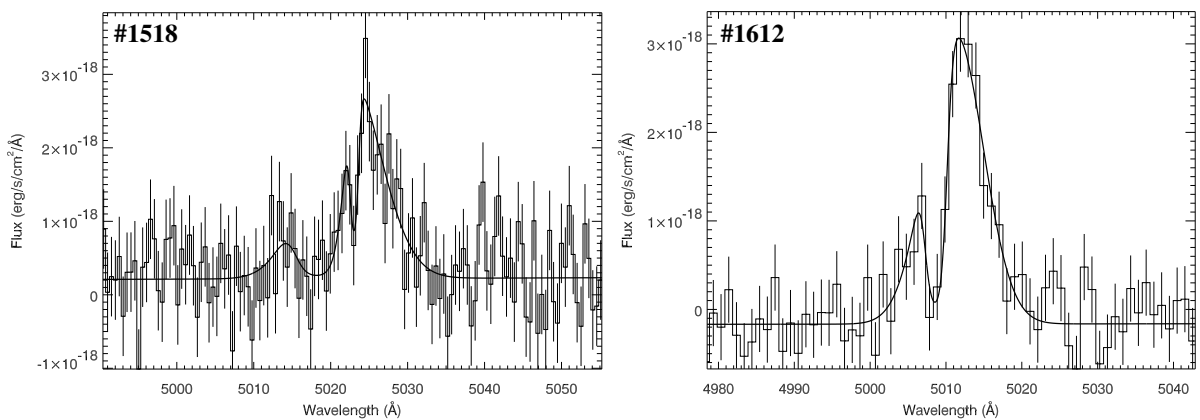
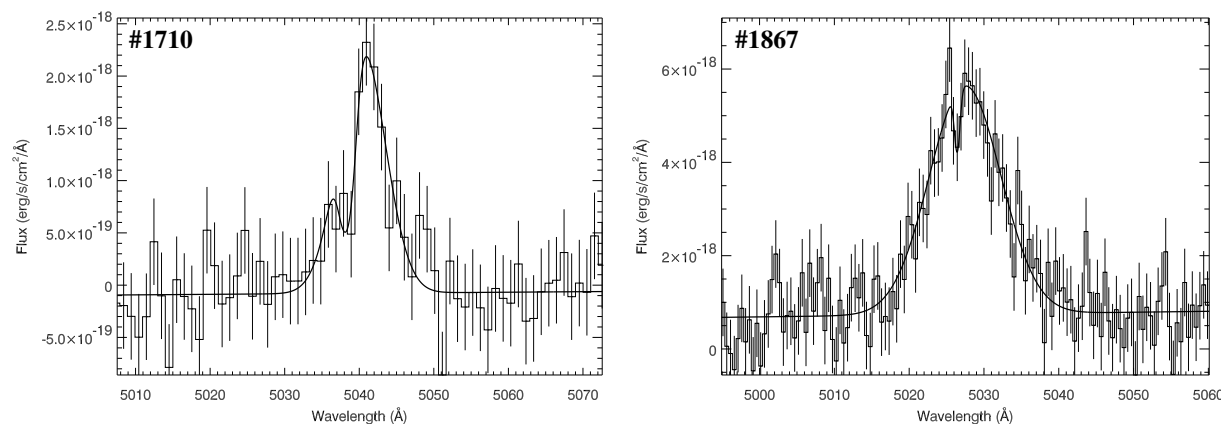**Figure 3.8 —** Spectra of emitter #1518 (left) and #1612 (right).

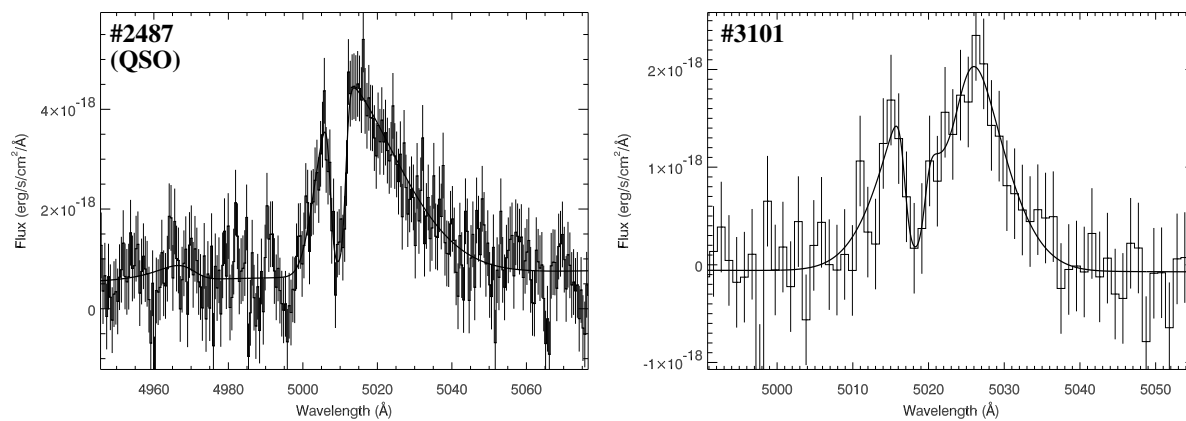**Figure 3.9 —** Spectra of emitter #1710 (left) and #1867 (right).

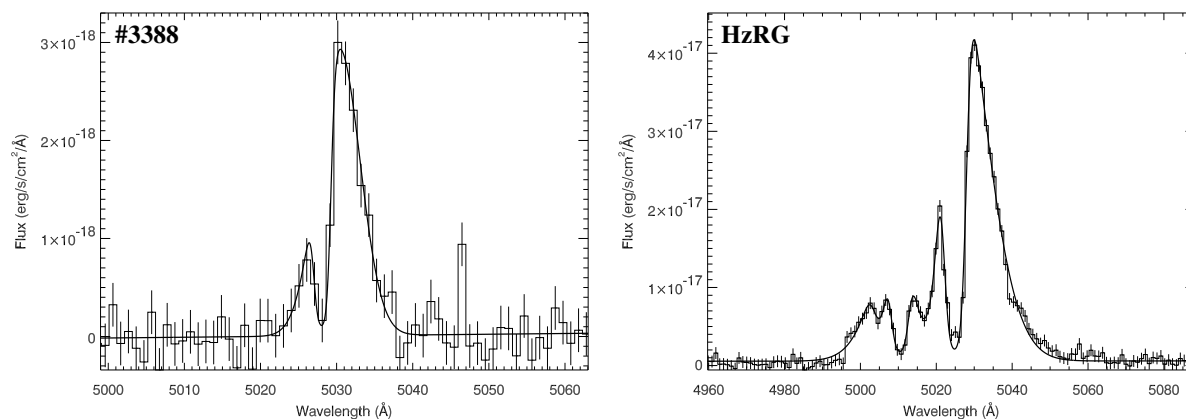**Figure 3.10 —** Spectra of emitter #2487 (left) and #3101 (right).

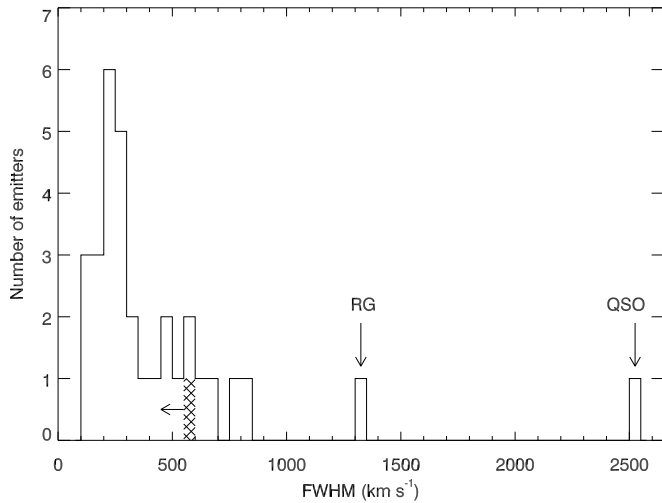**Figure 3.11 —** Spectra of emitter #3388 (left) and HzRG (right).

Figure 3.12 — Histogram of the line widths of the emitters.

120 km s^{-1} to 800 km s^{-1} (Fig. 3.12), with a median of 260 km s^{-1} and a mean of 340 km s^{-1}.

The inferred column densities of the absorbers are in the range of 10^{13}–10^{16} cm^{-2} (see §3.6). Using the spatial extend in the 2D spectra as an estimate of the size of the H I absorber, the amount of projected neutral H I near the emitters is in the range of $> 2 \times 10^2 - 5 \times 10^4 \ M_\odot$ (see §3.6 for the details of the individual emitters). For the fainter Lyα emitters, it cannot be excluded that the troughs are due to substructure in the Lyα emitting regions, rather than H I absorption.

3.5.2   Continuum colors

In Table 3.4, the magnitudes and UV continuum slopes of the confirmed emitters are listed (for a description on how the slope was calculated, see §3.3.3). For objects detected in the ACS image which were not resolved into several components, the I_{814} magnitude and the continuum slope β_{ACS} calculated using this magnitude is given. In Fig. 3.13 the *I* magnitude is plotted against the continuum slope. Excluding the radio galaxy and emitter #2487, which contains an AGN (§3.5.1), the UV continuum slope of the confirmed emitters ranges from $\beta = 0.62$ to $\beta = -4.88$ with a median of $\beta = -1.76$.

The blue median color of the Lyα emitters may be due to a selection effect. The candidate emitters for spectroscopy were selected when only one broad-band flux was available and a slope of $\beta = -2$ was assumed for all objects to compute the equivalent width (see §3.3.3 and Fig. 3.4). Because the narrow-band is on the blue side of the broad-band filter that was used, the equivalent width and line flux of bluer objects with $\beta < -2$ tend to have been overestimated, while "red" objects ($\beta > -2$) have an equivalent width and Lyα flux that are likely to be underestimated (see §3.3.3). This effect could have biased the spectroscopic sample towards blue objects. For example, the emitter with the bluest color, #1446, has an equivalent width of $EW_0 = 12$ Å, which falls below the selection criteria ($EW_0 > 15$ Å), but the object was selected for spectroscopy because it had $m_V - m_{\mathrm{nb}} > 0.72$ (see discussion at the end of §3.3.3). To determine the effect of this bias, the color of a flux limited sample was determined. There are 31 (candidate) Lyα emitting objects with a Lyα flux $> 1.5 \times 10^{-17}$ erg s^{-1} cm^{-2} in the field, of which 25 are confirmed. Again excluding the radio galaxy and the AGN, the median

Table 3.4 — Narrow-band, *V*, *I* and ACS I_{814} magnitudes and UV continuum slopes β of the confirmed emitters. Colors were measured in a circular aperture, while elliptical apertures were used to determine the total magnitudes (see §3.3.2). For objects with a signal-to-noise less than two a 2σ upper limit is given.

Object	$m_{\rm nb}$	m_V	m_I	I_{814} mag.	β	$\beta_{\rm ACS}$
344	24.63 ± 0.06	26.62 ± 0.22	26.78 ± 0.28	27.76 ± 0.23	-1.43 ± 1.21	-3.91 ± 1.06
695	24.89 ± 0.09	26.42 ± 0.20	25.96 ± 0.19	26.53 ± 0.10	0.62 ± 1.05	-0.92 ± 1.09
748	25.45 ± 0.14	27.03 ± 0.37	27.13 ± 0.42	$-$	-1.75 ± 1.85	$-$
995	24.97 ± 0.08	26.14 ± 0.16	26.49 ± 0.23	26.59 ± 0.11	-2.40 ± 0.72	-2.65 ± 0.63
1029	25.00 ± 0.07	26.19 ± 0.12	26.76 ± 0.23	$-$	-3.18 ± 0.74	$-$
1099	25.23 ± 0.13	26.39 ± 0.28	26.49 ± 0.28	$-$	-1.98 ± 0.96	$-$
1147	25.74 ± 0.12	27.83 ± 0.44	> 28.38	$-^b$	< -1.40	$-$
1203	24.79 ± 0.06	26.00 ± 0.11	$-^a$	27.30 ± 0.15	$-$	-4.77 ± 0.55
1361	24.76 ± 0.10	26.47 ± 0.24	26.63 ± 0.27	$-$	-1.65 ± 1.14	$-$
1395	26.40 ± 0.21	27.50 ± 0.47	> 27.69	$-$	< -2.30	$-$
1446	25.53 ± 0.10	26.32 ± 0.12	27.46 ± 0.29	26.55 ± 0.12	-4.88 ± 0.96	-2.46 ± 0.46
1498	26.14 ± 0.14	27.55 ± 0.29	27.79 ± 0.50	27.12 ± 0.18	-2.20 ± 2.09	-0.49 ± 1.06
1518	23.65 ± 0.02	24.47 ± 0.03	24.54 ± 0.04	24.57 ± 0.03	-2.20 ± 0.11	-2.12 ± 0.12
1612	25.79 ± 0.16	27.65 ± 0.54	> 27.38	27.84 ± 0.28	$-$	> -0.65
1710	25.51 ± 0.08	27.09 ± 0.19	27.37 ± 0.38	27.34 ± 0.19	-2.26 ± 1.40	-2.18 ± 0.78
1724	25.74 ± 0.15	> 27.91	> 27.44	$-^b$	$-$	$-$
1753	24.72 ± 0.09	25.67 ± 0.18	25.71 ± 0.20	$-^c$	-1.90 ± 0.60	$-$
1759	24.77 ± 0.09	25.87 ± 0.19	26.02 ± 0.27	$-$	-2.03 ± 0.83	$-$
1829	25.11 ± 0.13	25.73 ± 0.26	25.02 ± 0.25	$-^c$	-0.07 ± 0.60	$-$
1867	22.86 ± 0.01	24.25 ± 0.03	24.17 ± 0.04	$-^c$	-1.42 ± 0.15	$-$
1891	25.56 ± 0.13	26.76 ± 0.29	> 27.24	27.45 ± 0.20	< -3.02	-3.50 ± 1.01
1946	25.58 ± 0.18	26.40 ± 0.36	> 26.76	$-$	< -2.93	$-$
1955	25.59 ± 0.13	27.56 ± 0.47	27.25 ± 0.54	27.50 ± 0.18	> -0.32	> -1.03
1962	25.44 ± 0.08	26.44 ± 0.11	26.07 ± 0.13	26.10 ± 0.08	-0.85 ± 0.48	-0.99 ± 0.38
1968	25.00 ± 0.14	26.48 ± 0.45	> 26.37	26.61 ± 0.12	< -1.23	-1.89 ± 1.63
2413	24.51 ± 0.07	25.97 ± 0.16	26.04 ± 0.23	$-$	-1.76 ± 0.73	$-$
2487	22.25 ± 0.01	23.40 ± 0.02	23.30 ± 0.02	$-$	-0.57 ± 0.09	$-$
2637	24.88 ± 0.09	25.97 ± 0.17	25.88 ± 0.20	$-$	-1.23 ± 0.64	$-$
2871	26.04 ± 0.18	> 27.64	> 27.22	$-$	$-$	$-$
3101	23.99 ± 0.04	25.70 ± 0.12	25.49 ± 0.15	$-$	-0.71 ± 0.60	$-$
3388	23.31 ± 0.03	25.25 ± 0.09	25.54 ± 0.16	$-$	-1.92 ± 0.52	$-$
HzRG	$21.19^d \pm 0.01$	$23.31^d \pm 0.02$	$22.97^d \pm 0.02$	$-^c$	0.27 ± 0.09	$-$

^{a} Photometry unreliable due to nearby bright star.
^{b} Undetected in the ACS image, $I_{814} > 27.1$ mag arcsec^{-2}
^{c} Resolved by *HST* into several components.
^{d} Photometry influenced by nearby objects.

color of the remaining 29 emitters is $\beta = -1.70$. This is bluer than the average color of Lyα emitting Lyman Break Galaxies (LBGs), which have a slope of $\beta = -1.09 \pm 0.05$ (Shapley et al. 2003).

Models of galaxies with active star formation predict UV continuum slopes in the range $\beta = -2.6$ to $\beta = -2.1$ for an unobscured, continuously star forming galaxy with ages between a few Myr and more than a Gyr (Leitherer et al. 1999). 18 out of the 27 (67%) confirmed Lyα emitters for which β could be measured, have colors within 1 σ
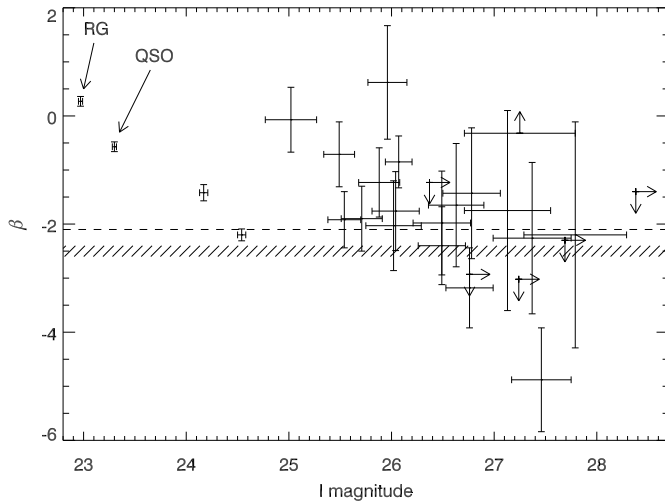
Figure 3.13 — *I* magnitude versus UV continuum slope β. The dashed line corresponds to $\beta = -2.1$, the color of an unobscured continuously star forming galaxy with an age of $\sim 10^8 - 10^9$ yr. The hashed area indicates the color of a young ($\sim 10^6$ yr), star forming galaxy.

consistent with being an unobscured starburst galaxy. Of those, 15 (56% of the sample) have such blue colors with 1 σ that they could be star forming galaxies with ages of order 10^6 yr, which have $\beta \sim -2.5$.

3.5.3 Morphologies

Of the 32 confirmed Lyα emitting sources, 19 (including the radio galaxy) were located in the area that was imaged by the ACS (Fig. 3.19). Two of these emitters remained undetected to a depth of $I_{814} > 27.1$ mag arcsec^{-2} (3 σ). On the position of the radio galaxy, the ACS image shows several objects within 3″ ($\sim$25 kpc), surrounded by low surface brightness emission ($\gtrsim 24.8$ mag arcsec^{-2}, see Fig. 3.14). Such a clumpy structure is often seen at the position of HzRGs (e.g., Pentericci et al. 1999). Interestingly, there are three other Lyα emitters with morphologies that resemble the radio galaxy (Fig. 3.14). Each of these three objects consists of at least three clumps of emission, which are less than one kpc separated from each other. The remainder of the confirmed emitters can be identified with single objects in the ACS image (Fig. 3.15).

To quantify the size of these objects, the half light radius (r_h) of each emitter was measured using the program SExtractor. The half light radius is defined as the radius of a circular aperture in which the flux is 50% of the total flux. However, as already discussed in §3.3.2 and shown in Fig. 3.2, the fraction of the total flux of an object that is missed by SExtractor increases when the object is fainter. As a consequence, the half light radius that is measured by SExtractor would underestimate the size of the object. To determine how much the half light radius was underestimated, galaxies with a range of sizes were varied in brightness and added to the ACS image, and the half light radii of those objects was measured by SExtractor. It was found, as mentioned above, that the fainter the object, the smaller its measured r_h, an effect that was stronger for larger galaxies, see Fig. 3.16. Using the results of these simulations, an attempt could be made to correct the measured sizes of the confirmed Lyα emitters. Unfortunately, this correction could overestimate the true size of compact objects (i.e. objects with a half light radius similar to that of stars). However, this only strengthens our conclusions (see below). In Table 3.5 the sizes of the emitters in the I_{814}-band are printed. The half light radii of the emitters range from 0″.06 to 0″.18. The error in the half light radius is
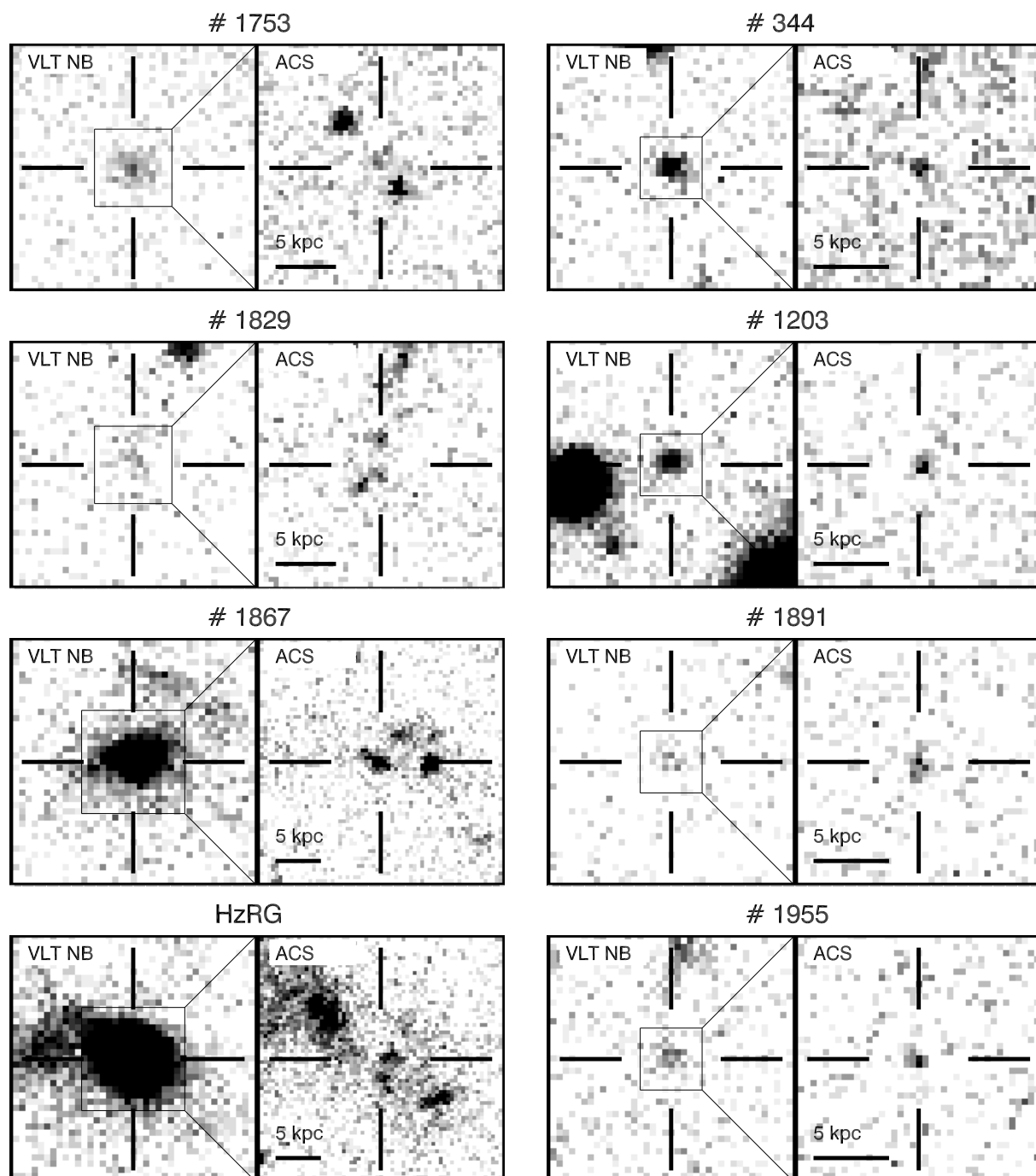
Figure 3.14 — VLT narrow-band and ACS images of Lyα emitters with a clumpy counterpart (*left*) and of emitters that remained unresolved in the ACS image (*right*). The cutouts of the narrow-band image are ∼ 8″ on the side. The ACS images are zoomed in on the centre of the narrow-band image. The grayscale ranges from 0.5 to 5 times the rms background noise. The emission to the left of the radio galaxy in the VLT image (and in the top-left corner of the ACS image) are from a foreground galaxy at z ∼ 0.87 (see also §3.6).

Figure 3.15 — VLT narrow-band and ACS images of Lyα emitters, which are resolved by the *HST*. The cutouts of the narrow-band image are ~ 8″ on the side. The grayscale ranges from 0.5 to 5 times the rms background noise.

Figure 3.16 — The ratio of recovered size over input size as a function of magnitude in the ACS image. The fainter and/or larger the objects, the more the size is underestimated.

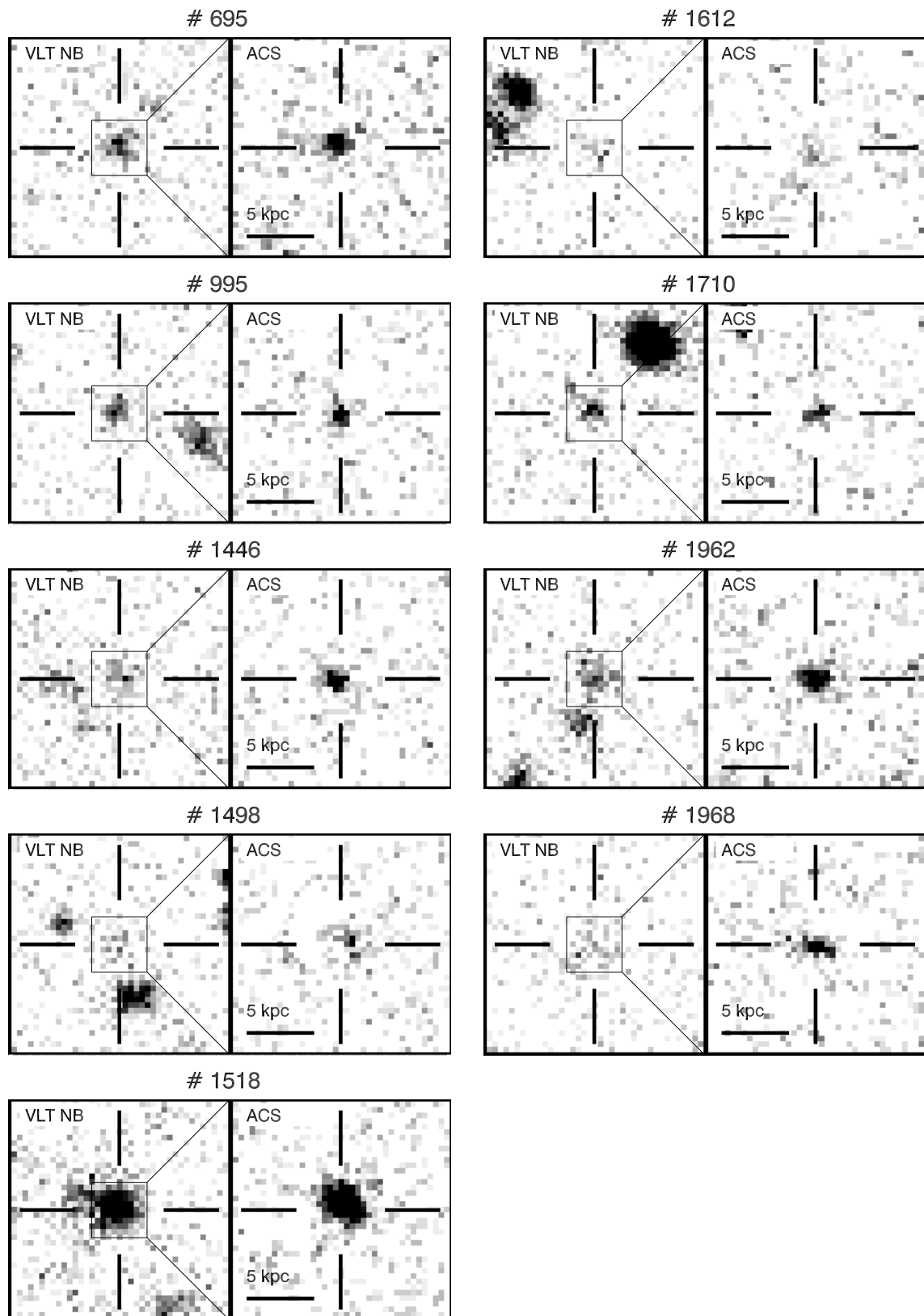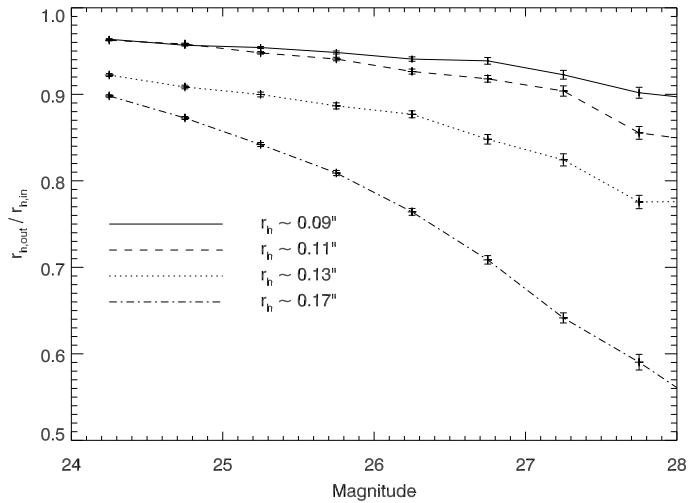defined as the half light radius divided by the signal-to-noise of the object. Translating the sizes directly to physical sizes, the measured half light radii correspond to 0.5–1.5 kpc. The median size is ∼1 kpc.

The mean half light radius of isolated, unsaturated stars in the field was found to be ∼0''06. Four of the emitters in the ACS field have a r_h that is within 1 σ equal to the half light radii of the stars in the field. These four emitters are classified as unresolved (Fig. 3.14).

The sizes of the confirmed Lyα emitters can be compared to other high redshift galaxies, e.g. LBGs. Recently, sizes were measured of galaxies at various redshifts in the Great Observatories Origins Deep Survey (GOODS, Ferguson et al. 2004). For their analysis, they used SExtractor with circular apertures having a radius that is 10 times larger than the first radial moment of the light distribution to ensure that all the flux was inside the aperture. The survey was restricted to rest-frame luminosities between $0.7\,L^*$ and $5\,L^*$. Using the luminosity function of LBGs derived by Steidel et al. (1999), this corresponds to a magnitude range of $22.78 < m_R < 24.92$. Only two confirmed emitters located in the ACS field (#1518 and #1867) satisfy the luminosity criterion used in the GOODS analysis. Emitter #1867 is resolved into several clumps of emission. The size of emitter #1518 measured with the same input parameter as Ferguson et al. (2004), is $0''106 \pm 0''006$, consistent with the $0''102 \pm 0''003$ derived using our own input parameters. The half light radius of emitter #1518 is among the smallest Ferguson et al. are finding. The average size of LBGs at $z \sim 3$ is $0''28$ (~ 2.3 kpc). Thus, the Lyα emitters are small compared to LBGs at the same redshift, provided that the method we used to measure the sizes of the Lyα emitting galaxies gives comparable half light radii as the approach of Ferguson et al. (as was the case for emitter # 1518).

3.5.4 Star formation rate

The average star formation rate (SFR) of the confirmed emitters, as derived from the Lyα flux (see Table 3.3), is $2.5\,M_\odot\,\mathrm{yr}^{-1}$ (excluding the radio galaxy and the QSO, emitter #2487). This calculation assumed a Lyα/Hα ratio of 8.7 (Case B recombination, Brocklehurst 1971) and a Hα luminosity to SFR conversion for a Salpeter initial mass function (IMF) from Madau et al. (1998):

Object	r_h ($''$)	r_h (kpc)	s/n
344	$0\farcs07 \pm 0\farcs03$	< 0.8	4.8
695	$0\farcs10 \pm 0\farcs02$	0.6 ± 0.2	10.5
995	$0\farcs09 \pm 0\farcs01$	0.5 ± 0.2	10.2
1203	$0\farcs06 \pm 0\farcs01$	< 0.6	7.1
1446	$0\farcs14 \pm 0\farcs02$	1.0 ± 0.2	9.4
1498	$0\farcs18 \pm 0\farcs06$	1.4 ± 0.5	6.0
1518	$0\farcs10 \pm 0\farcs01$	0.7 ± 0.1	43.1
1612	$0\farcs14 \pm 0\farcs05$	1.0 ± 0.5	3.8
1710	$0\farcs10 \pm 0\farcs03$	0.6 ± 0.4	5.8
1753	Clumpy	–	~ 12
1829	Clumpy	–	~ 7
1867	Clumpy	–	~ 20
1891	$0\farcs10 \pm 0\farcs03$	< 1.3	5.5
1955	$0\farcs08 \pm 0\farcs03$	< 1.0	6.1
1962	$0\farcs13 \pm 0\farcs01$	1.0 ± 0.1	12.8
1968	$0\farcs14 \pm 0\farcs02$	1.1 ± 0.2	9.0
HzRG	Clumpy	–	~ 35

Table 3.5 — Half light radii of the confirmed emitters located within the field of the ACS.

$$SFR_{\mathrm{H}\alpha} = \frac{L_{\mathrm{H}\alpha}}{1.6 \times 10^{41} \ \mathrm{erg\,s^{-1}}}. \tag{3.19}$$

Because of Lyα absorption (see e.g. Fig. 3.6–3.11), this SFR calculation gives a lower limit.

An alternative way to estimate the SFR is to use the level of the UV continuum. The flux density at a wavelength of $\lambda_{\mathrm{rest}} = 1500$ Å can be converted to a SFR following the relation

$$SFR_{\mathrm{UV}} = \frac{L_{\mathrm{UV}}(\lambda_{\mathrm{rest}} = 1500 \ \text{Å})}{8.0 \times 10^{27} \ \mathrm{erg\,s^{-1}\,Hz^{-1}}} \tag{3.20}$$

for a Salpeter IMF (Madau et al. 1998). In Fig. 3.17 the SFR as calculated from the Lyα emission is plotted against the UV continuum SFR. On average, the two methods to calculate the SFR give the same result, with the SFR measured from the UV continuum a factor 1–1.5 higher than the Lyα inferred SFR. The average SFR of the emitters as measured by the UV continuum is $\lesssim 3.8 \, M_\odot \, \mathrm{yr}^{-1}$. This is much lower than the average SFR of LBGs, which is somewhere between 10 and 100 $M_\odot \, \mathrm{yr}^{-1}$ (e.g., Giavalisco 2002).

Recent measurements of the polarization of the UV continuum of the radio galaxy indicate that the UV continuum is dominated by emission from stars. The contribution from a scattered AGN is small, which is implied by the upper limit on the polarization of the continuum of $P < 4\%$ (C. De Breuck et al., in preparation). If all the light at a rest-frame wavelength of 1500 Å is due to young stars, then the SFR of the radio galaxy is $40.5 \pm 0.8 \, M_\odot \, \mathrm{yr}^{-1}$. No correction is made for dust absorption. This is similar to the uncorrected SFR (as calculated from the rest-frame UV continuum) in radio galaxies

Figure 3.17 — SFR calculated from the UV continuum plotted against the SFR computed using the Lyα flux for the confirmed Lyα emitters.
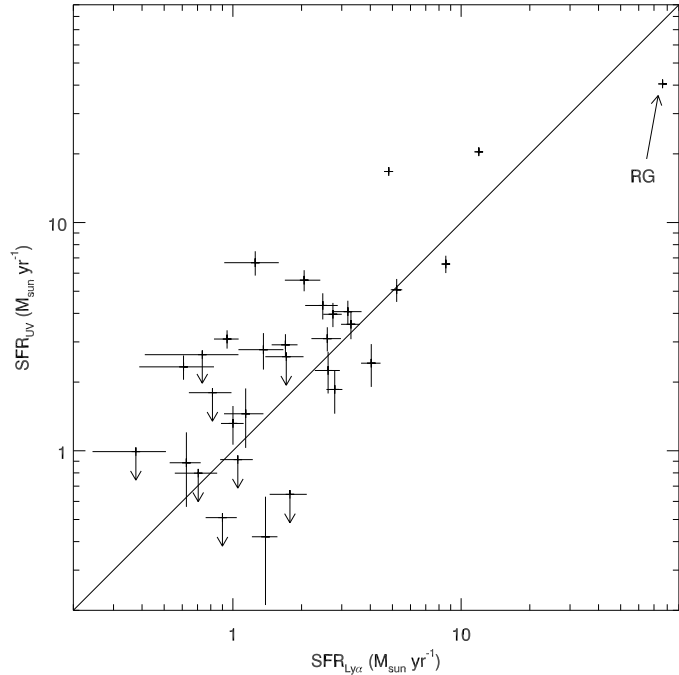
at $z \sim 2.5$ (e.g., Vernet et al. 2001) and a factor of ~ 5 lower than the SFR of the radio galaxy 4C41.17 at $z = 3.8$ (Chambers et al. 1990; Dey et al. 1997).

3.6   Notes on individual objects

- **#344**: The spectrum of this emitter is shown in Fig. 3.6. The Lyα line can be fitted by a combination of a Gaussian and a Voigt absorption profile which is located 80 ± 10 km s^{-1} blueward of the peak of the Gaussian. The fit is shown as the solid line in Fig. 3.6. From the 2D spectrum a lower limit of $2''$ (~ 16 kpc) on the linear size of the absorber could be derived, giving a lower limit on the H I mass of $M(\text{H I}) > 550\ M_\odot$.
- **#995**: The spectrum of this object can be fitted by a Gaussian with a narrow Voigt profile centred 150 ± 20 km s^{-1} blueward of the emission peak (solid line in Fig. 3.6). The column density of the absorbing neutral hydrogen is nearly unconstraint by our spectrum and lies in the range $N(\text{H I}) \sim 10^{13.5-18.5}$. The absorber has a size of $> 2''$ in the 2D spectrum and taking a column density of 10^{16} cm^{-2}, the inferred mass of neutral hydrogen is at least $2 \times 10^4\ M_\odot$.
- **#1147**: This object is one of the two emitters that were not detected in the ACS image down to a 3σ magnitude limit of 27.1 mag arcsec^{-2}. Its redshift is ~ 2400 km s^{-1} redder than the median redshift of the emitters, and is therefore unlikely to be associated with the protocluster (see §3.7.2). The spectrum shows absorption which is located 70 ± 20 km s^{-1} blueward of the peak of the unabsorbed emission (Fig. 3.7). A lower limit of $550\ M_\odot$ can be given for the H I mass.
- **#1203**: This emitter is unresolved in both the VLT and ACS images (Fig. 3.14). The spectrum is shown in Fig. 3.7. The absorption is located 90 ± 10 km s^{-1} to the blue of the peak of the Gaussian. We obtain a lower limit for the mass of neutral

hydrogen responsible for the absorption of $> 1700\ M_\odot$.

- **#1446**: The emitter has a very blue continuum slope ($\beta = -4.88 \pm 0.96$). The computed equivalent width of $EW_0 = 12$ Å is below the selection criterion ($EW_0 > 15$ Å). The VLT *I*-band magnitude and the I_{814} magnitude derived from the ACS image are different at the 2.8 σ level, taking the differences in effective wavelength of the filters into account. Using the ACS magnitude the continuum slope becomes -2.61 and the $EW_0 \sim 20$ Å. The object is resolved in the ACS image and has a half light radius of 1.0 ± 0.2 kpc (Fig. 3.15).

- **#1498**: In the ACS image, an object with $r_h = 1.4 \pm 0.5$ kpc is located $\sim 0\rlap{.}{''}5$ from the position of the weak emitter in the VLT image.

- **#1518**: This is the fourth brightest Lyα emitter in the field. The object is extended in both the Lyα image and the ACS image (see §3.5.3 and Fig. 3.15). The emission line can be fitted by a Gaussian with two Voigt profiles superimposed, one 80 ± 50 km s^{-1} to the red and the other 210 ± 60 km s^{-1} to the blue of the Gaussian (Fig. 3.8). This results in a lower limit of the mass of H I of $2300\ M_\odot$.

- **#1612**: This emitter has a faint continuum ($I_{814} = 27.84 \pm 0.28$) and is barely detected in ACS image (signal-to-noise of ~ 4), and is marginally resolved (Table 3.5, Fig. 3.15). The spectrum shows absorption of $10^{14.4 \pm 0.1}$ cm^{-2} H I, located 150 ± 10 km s^{-1} to the blue of the redshift of this galaxy (Fig. 3.8).

- **#1710**: This is a blue emitter ($\beta = -2.26 \pm 1.40$) with an absorption trough on the blue wing of the emission line (see Fig. 3.9), the result of at least $200\ M_\odot$ of H I.

- **#1753**: At the position of this Lyα emitter, the ACS image shows three separate objects located within ~ 8 kpc (Fig. 3.14).

- **#1829**: This object is resolved by the ACS into an elongated structure consisting of several objects (Fig. 3.14).

- **#1867**: Denoted as galaxy "A" by LF96, a spectrum of this object taken under bad seeing conditions confirms the redshift measured by LF96 (Table 3.3). The Lyα line is asymmetric and can be fitted by a Gaussian and one Voigt absorber, which is 60 ± 20 km s^{-1} blueward of the Lyα peak (Fig. 3.9). The VLT narrow-band image shows an extended Lyα halo of ~ 25 kpc (Fig. 3.14), while in ACS image the object is very clumpy.

- **#1968**: This emitter was undetected in the VLT *I*-band, but in the ACS image an object with a half light radius of 1.1 ± 0.2 kpc is visible.

- **#2487**: This emitter has the brightest Lyα line in the field after the radio galaxy, and is called galaxy "B" in LF96. As mentioned in §3.5.1, the Lyα line is broad ($FWHM \sim 2500$ km s^{-1}) which is most likely caused by an AGN. The spectrum is characterized by a large absorption trough with a column density of $N($H I$) \sim 10^{14.6}$ cm^{-2}. Furthermore, the red wing of the Lyα line is much broader than the blue wing. The spectrum can be fitted with two absorbers, located 250 ± 170 km s^{-1} to the red and 1150 ± 200 km s^{-1} to the blue of the centre of the emission line. The inferred mass of H I is $> 5 \times 10^4\ M_\odot$.

- **#2719**: This is galaxy "C" from LF96. Galaxy "C" was not selected as a candidate Lyα emitter in our images. It has colors comparable to those quoted in LF96, but an EW_0 of $1.0^{+1.2}_{-1.1}$. LF96 measured an $EW_0 > 12$ Å and a line flux of $\sim 5 \times 10^{-17}$ erg s^{-1} cm^{-2}, although no spectrum was taken of this object to confirm the

existence of the line. An explanation for the fact that this galaxy is not selected by us as an emission line candidate could be the large width of the narrow-band filter used by LF96, making it sensitive to a wider redshift range than our filter. Their filter was sensitive to Lyα emitters having redshifts in the range $z = 3.08 - 3.16$, while our filter is sensitive to the redshift range $z = 3.12 - 3.17$. Galaxy "C" could be a Lyα emitter with a redshift between $z = 3.08$ and $z = 3.12$, and it would therefore be part of the protocluster, but not be included as one of our candidates (see §3.7.2).

- **#3101**: The Lyα line of this emitter is broad (*FWHM* $= 800 \pm 100$ km s^{-1}, see Fig. 3.10), as compared to the median line width of the emitters (260 km s^{-1}). The spectrum can be fitted by a Gaussian, superimposed by two Voigt absorbers located 40 ± 110 and 240 ± 20 km s^{-1} to the blue of the emission, the result of at least $\sim 1000 \, M_\odot$ of H I.
- **#3388**: This blue Lyα emitter ($\beta = -1.92 \pm 0.52$) shows an absorption trough 130 ± 10 km s^{-1} blueward of the emission redshift (Fig. 3.11), implying a neutral Hydrogen mass of $> 625 \, M_\odot$.
- **Radio galaxy MRC 0316–257**: The absorption structure of the radio galaxy is complicated. Only a Gaussian emission line profile with four separate absorbers gives a reasonable fit (solid line in Fig. 3.11 and Table 3.2). The absorbers are 200 ± 10 km s^{-1} to the red of the peak of the Gaussian and 270 ± 10 km s^{-1}, 660 ± 10 km s^{-1} and 970 ± 20 km s^{-1} to the blue. Approximately $2''$ to the north-east of the radio galaxy is a foreground galaxy, with a clear spiral structure in the ACS image. An emission line was detected in a spectrum of this object, with a wavelength around 6965 Å, most likely [O II] at $z \sim 0.87$ (C. De Breuck, private communications).

3.7 A protocluster at $z = 3.13$?

3.7.1 Volume density

Several surveys have been carried out to estimate the (field) volume density of Lyα emitters at $z \sim 3$ (e.g., Cowie & Hu 1998; Hu et al. 1998; Kudritzki et al. 2000; Ciardullo et al. 2002; Fynbo et al. 2003). To estimate the (over)density of Lyα emitters in our field, we will compare our numbers with those found in the survey of Ciardullo et al. (2002), since it covers the largest area of all the surveys, and of Fynbo et al. (2003), because they present the deepest and spectroscopically most complete comparison sample of blank field $z \sim 3$ Lyα emitters.

Ciardullo et al. (2002) made a blank field survey to estimate the density of emission line sources and to calculate the contamination of intra-cluster planetary nebulae searches. They searched for faint emission line sources in a 0.13 deg^2 field at a wavelength of 5019 Å. They found 21 objects with an observed equivalent width greater than 82 Å and a $m_{\rm nb} < 24.3$. Assuming all their sources are Lyα emitters at $z \sim 3.13$, the volume density of field emitters is $n_{\rm field} = 2.4^{+0.6}_{-0.5} \times 10^{-4}$ Mpc^{-3}. Applying the same selection criteria to our data, five emission line objects (excluding the radio galaxy) are found in the field around 0316–257, all confirmed to be Lyα emitters at $z \sim 3.13$. This gives a density of $n_{0316} = 5.4^{+3.7}_{-2.3} \times 10^{-4}$ Mpc^{-3}. The density in the 0316 field is therefore
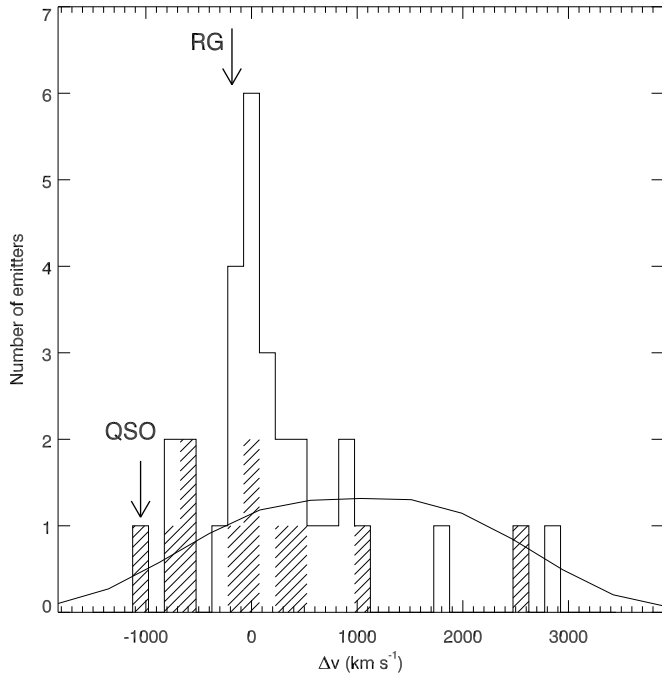
Figure 3.18 — Velocity distribution of the confirmed Lyα emitters. The bin size is 150 km s^{-1}. The median redshift of the confirmed emitters $z = 3.1313$ is taken as the zero-point. The velocities of the radio galaxy and the QSO are indicated with arrows. The solid line represents the selection function of the narrow-band filter, normalized to the total number of emitters found. The hashed histogram represents the velocities of emitters with absorption in their line profile. The three objects in the red part of the filter (with a velocity greater than 1500 km s^{-1}) might not be part of the protocluster.

a factor $2.2^{+1.8}_{-1.0}$ higher than the field density. The large errors on this number are due to small number statistics.

More recently, Fynbo et al. (2003) presented the first results of a program to detect faint Lyα emitters at $z \sim 3$. They used the same VLT narrow-band filter as described in §3.2.1 to image a field that contained a damped Lyα absorber. The 5σ detection limit for point sources in their narrow-band image is $m_{\mathrm{nb}} < 26.5$ as measured in a circular aperture with a size twice the seeing *FWHM*, is very similar to our 5σ detection limit ($m_{\mathrm{nb}} < 26.4$). They found 27 candidate Lyα emitters with an equivalent width greater than 12.5–25 Å, the limit depending on the predicted line flux. Subsequent spectroscopy confirmed that 18 of the 22 candidate emitters observed are Lyα emitters and two were foreground [O II] emitters. Assuming that the seven unconfirmed candidate emitters are all Lyα emitters at $z \sim 3$, the number of Lyα emitters down to a flux limit of 6×10^{-18} erg s^{-1} cm^{-2} in their field is 25. Our number of emitters selected with the same equivalent width limits is ~ 75 after correction for foreground contaminants. This implies a density of $3.0^{+0.9}_{-0.7}$ times the field density. Roughly, we find three times the number of Lyα emitters as might be expected from field surveys.

Maier et al. (2003) gathered measured abundances of Lyα emitters from the literature, shifted them to $z = 3.5$ and fitted a model function through the points (a description of the model can be found in Thommes & Meisenheimer 2005). They predict approximately 2325 Lyα emitters per deg^2 in a volume with $\Delta z = 0.1$ with line fluxes exceeding 5×10^{-18} erg s^{-1} cm^{-2}. If their model is correct, then ~ 15 Lyα emitting galaxies at $z = 3.13$ are expected within our volume brighter than 7×10^{-18} erg s^{-1} cm^{-2}. Applying this limit, we find 63 galaxies or 59 galaxies if we correct for possible foreground contaminants. Of these, 29 are spectroscopically confirmed. The density is a factor $4.0^{+0.6}_{-0.5}$ higher than the model prediction, in agreement with the above estimates.

To summarize, the density of Lyα emitters near the radio galaxy is a factor 2–4

Figure 3.19 — Spatial distribution of Lyα emitters around the radio galaxy MRC 0316–257 (denoted by a square). The confirmed emitters in the protocluster are represented by circles (emitters with a redshift smaller than the median, $z < 3.1313$) and diamonds (emitters with $z > 3.1313$). The triangles show the position of the three Lyα emitting galaxies with a velocity > 1500 km s^{-1} from the median velocity of the emitters. The sizes of the symbols are scaled according to the velocity offset from the median, with larger symbols representing emitters with a redshift closer to the median redshift. The pluses are objects satisfying the selection criteria (see §3.3.3), but are not (yet) confirmed. The quadrangle represents the outline of the ACS image.
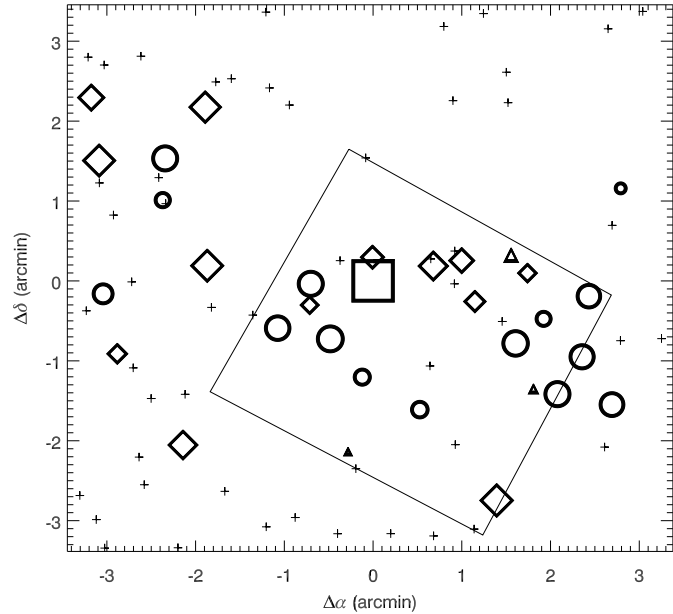
higher than the field density, indicating that the radio galaxy might reside in an overdense region.

3.7.2 Velocity distribution

The velocity distribution of the emitters is plotted in Fig. 3.18. The response of the narrow-band filter used to select the candidate emitters for spectroscopy is also shown. Interestingly, the emitters are not distributed homogeneously over the filter, but most of them appear to cluster on the blue side of the filter. The emitters which show absorption in their emission line profiles seem to be distributed more homogeneously, but this could be due to the small number of objects.

To test whether the clustering of emitters in redshift space is significant, Monte Carlo simulations of the redshift distribution were performed. 10000 realizations with 31 emitters were reproduced, with the narrow-band filter curve as the redshift probability function for each emitter. The mean of the observed redshift distribution ($z = 3.136$) differs 2.6 σ compared to the simulated distribution ($z = 3.146 \pm 0.004$) and the width of the observed redshift distribution differs by 1.7 σ (0.012 compared to 0.022 $\pm$ 0.006). In total, the measured redshift distribution deviates from the simulated one by 3.07 σ. This means that a redshift distribution as observed was reproduced in only 0.2% of the cases. The peak of velocity distribution of the Lyα emitters lies within 200 km s^{-1} of the redshift of the radio galaxy (Fig. 3.18), providing evidence that most of the Lyα emitters are physically associated with the radio galaxy. All together, the observed overdensity of Lyα emitters in our field (§3.7.1), combined with the peak in the redshift distribution provide compelling evidence that the Lyα emitters reside in a protocluster at $z \sim 3.13$.

3.8 Properties of the protocluster

In this section, we discuss the macro properties of the Lyα emitters in the protocluster.

3.8.1 Velocity dispersion

To determine the velocity dispersion of the emitters, the biweight scale estimator was used (Beers et al. 1990). This is the most appropriate scale estimator for samples of 20–50 objects (Beers et al. 1990). The velocity dispersion is 640 ± 195 km s^{-1}, corresponding to a *FWHM* of 1510 ± 460 km s^{-1}. This is significantly smaller than the width of the narrow-band filter, which has a *FWHM* of ~ 3500 km s^{-1}. Although most Lyα emitters are likely to be members of the protocluster, the three emitters with velocities > 1500 km s^{-1} from the peak of the distribution (Fig. 3.18) are probably field galaxies. Ignoring these three field galaxies, the velocity dispersion drops to 535 ± 100 km s^{-1}. On the lower redshift side (negative velocities), no clear edge is visible in the distribution. This could be due to the decrease in sensitivity of the narrow-band filter on this side of the redshift distribution. If the protocluster extends to much lower redshifts, our estimate of the velocity dispersion is a lower limit.

3.8.2 Spatial distribution

The spatial distribution of the emitters is shown in Fig. 3.19, where the circles, diamonds and triangles represent the spectroscopically confirmed emitters, and with the sizes of the symbols scaled according to the velocity offset from the median of the emitters. The pluses are unconfirmed candidate Lyα emitters satisfying our selection criteria (see §3.3.3). The majority of these candidates (96%) has not yet been observed spectroscopically, while the remaining 4% were too faint to be confirmed. The imaging field of view (3.3×3.3 Mpc^2 at $z = 3.13$) is not large enough to show clear boundaries of the structure.

3.8.3 Mass

At a redshift of $z = 3.13$, the age of the Universe is only 2.2 Gyr. Taking the velocity dispersion as a typical velocity for a galaxy in the protocluster, it would take at least 5 Gyr to cross the structure, making it highly unlikely that the protocluster is near virialization. Therefore, the virial theorem cannot be used to calculate the mass of the protocluster.

Another way to compute the mass is to use the (comoving) volume V occupied by the overdensity, the (current) mean density of the Universe $\bar{\rho}$ and the mass overdensity of the protocluster δ_m:

$$M = \bar{\rho}\,V\,(1 + \delta_m) = \bar{\rho}\,V\,(1 + \delta_{\text{gal}}/b). \qquad (3.21)$$

where b is the bias parameter ($b \equiv \delta_{\text{gal}}/\delta_m$), relating the observed galaxy overdensity ($\delta_{\text{gal}} = n_{0316}/n_{\text{field}} - 1$) to the mass overdensity, and $\bar{\rho} = 3.5 \times 10^{10}\ M_\odot\,\text{Mpc}^{-3}$ for the cosmological parameters used in this paper.

The weighted mean of the three density estimates in §3.7.1 is $n_{0316}/n_{\text{field}} = 3.3^{+0.5}_{-0.4}$, giving an overdensity of $\delta_{\text{gal}} = 2.3^{+0.5}_{-0.4}$. Taking $V = 9.3 \times 10^3$ Mpc^3 (§3.2.2) and $b =$

$3 - 6$ (Steidel et al. 1998; Shimasaku et al. 2003) results in a mass for the protocluster within the observed volume of $4 - 6 \times 10^{14} \, M_\odot$. Because the size of the protocluster is unconstrained (e.g. Fig. 3.19), this mass estimate is a lower limit.

However, the redshift range of protocluster galaxies is likely to be smaller than the redshifts for which the narrow-band filter is sensitive (see Fig. 3.18). Assuming that the three outlying galaxies on the red side of the filter as field galaxies, the redshift range of the protocluster galaxies is 0.029 and the volume occupied by these emitters is 5.4×10^3 Mpc^3. This estimate of the volume does not take into account the redshift space distortions caused by peculiar velocities (Steidel et al. 1998, see below). Assuming that in total $\sim 10\%$ of the (candidate) emitters are field galaxies (see §3.7.2), the density of emitters within this volume with respect to the field density is $1 + \delta_{\mathrm{gal}} = 3.3^{+0.5}_{-0.4} \times 0.9 \times \frac{9331}{5400} = 5.1^{+0.8}_{-0.6}$. In this approach, the relation between the mass overdensity δ_m and the observed galaxy overdensity δ_{gal} is (Steidel et al. 1998):

$$1 + b\delta_m = C(1 + \delta_{\mathrm{gal}}), \tag{3.22}$$

where C takes into account the redshift space distortions (Steidel et al. 1998). Assuming that the structure is just breaking away from the Hubble flow, C can be approximated by

$$C = 1 + f - f(1 + \delta_m)^{1/3} \tag{3.23}$$

(Steidel et al. 1998), with f the rate of growth of linear velocity perturbations at the redshift of the protocluster (Peebles 1980; Lahav et al. 1991). f not only depends on z, but also on Ω_m and Ω_Λ. In the cosmology adopted in this paper ($\Omega_m = 0.3$ and $\Omega_\Lambda = 0.7$), f is close to 1 at high redshift ($z > 2$, Lahav et al. 1991).

Again assuming that $b = 3 - 6$, the computed mass of the protocluster is $> 3 - 5 \times 10^{14} \, M_\odot$. As both the redshift range of the galaxies and the size of the protocluster could be larger than is observed (see §3.8.1 and §3.8.2), this estimate is again a lower limit. The computed mass roughly corresponds to the virial mass of the Virgo cluster (e.g., Fouqué et al. 2001).

3.9 Nature of the Lyα emitters

What can we deduce about the nature of the Lyα emitters in our field? Four of the 16 emitters (25%) detected in the ACS image are unresolved and may be narrow-line (*FWHM* $\lesssim$ 1000–2000 km s^{-1}, e.g., Bennert et al. 2002) QSOs. The number density of faint ($21 < m_R < 25.5$) QSOs near $z = 3$ in the LBG survey of Steidel and collaborators (Steidel et al. 2003) is 250 QSO deg^{-2} in a redshift interval $\Delta z \simeq 0.6$ (Steidel et al. 2002). They observe a ratio of narrow-line to broad-line QSOs of N(narrow)$/N$(broad) $= 1.2 \pm 0.4$ (Steidel et al. 2002). Assuming an overdensity of galaxies in our field of $n_{0316}/n_{\mathrm{field}} = 4.0$ (§3.7.1), the predicted number of QSOs in field is ~ 1. Indeed, one (broad-line) QSO is found (emitter #2487). Extrapolating the faint end of the QSO luminosity function given by Hunt et al. (2004) to $m_R > 25.5$, the number of QSOs near

MRC 0316–257 with $25.5 < m_R < 28.5$ is calculated to be < 1, making the identification of the Lyα emitters with QSO unlikely. Another reason against the classification of the Lyα emitters as QSOs is the continuum slope of narrow-line QSOs in the LBG survey of $\beta = -0.4$ (Steidel et al. 2002). This is much redder than the median of the unresolved emitters ($\beta \sim -1.43$). We therefore conclude that all the Lyα emitters are star forming galaxies[1].

The next question is how the properties of the Lyα emitters compare to those of the LBG population as a whole.

- *Continuum luminosity:* Besides that of the radio galaxy and the broad-line QSO, the continuum of the emitters is faint, the brightest emitter having $m_R = 24.24$ (using $m_R = -2.5^{10}\log(f_\nu(\lambda_{\rm rest} = 1700\text{Å})) - 48.59$) and the faintest $m_R > 28.45$. Using $m_* = 24.53$ at $z = 3.13$ (Steidel et al. 1999), this corresponds to luminosities ranging from $1.3\ L^*$ to $< 0.03\ L^*$. Roughly 90% of the emitters are fainter than $m_R = 25.5$, the spectroscopic limit for LBGs. A similar percentage was found by Fynbo et al. (2003).
- *Size:* A comparison of the sizes of Lyα emitters with those of LBGs at $z \sim 3$ suggests that Lyα emitters are generally smaller (with $r_h < 1.5$ kpc) than LBGs which have an average size of $r_h \sim 2.3$ kpc.
- *Color:* The colors of the confirmed emitters are, on average, very blue. The median UV continuum slope is $\beta = -1.76$, bluer than the average slope of LBGs with Lyα emission ($\beta \sim -1.09$; Shapley et al. 2003). A large fraction of the confirmed emitters ($\sim 2/3$) have colors consistent with negligible absorption and could be dust-free starburst galaxies.

Summarizing these properties, the Lyα emitters are on average fainter, bluer and smaller than $z \sim 3$ LBGs.

Various models have been proposed to explain the properties of Lyα emitters. Based on rest-frame optical photometry of LBGs, Shapley et al. (2001) concluded that LBGs with Lyα in emission are "old" (age $>$ few $\times 10^8$ yr), while "young" (age $< 10^8$ yr) LBGs have Lyα in absorption. This could be explained by the young galaxies being dusty which caused the absorption of Lyα photons, while the older galaxies are more quiescent with less dust, and superwinds which allow Lyα photons to escape. Other groups have suggested that strong Lyα emitters are young star forming galaxies which was derived from the blue colors and high equivalent widths of the Lyα emitters (e.g. LF96, Rhoads & Malhotra 2001; Keel et al. 2002; Malhotra & Rhoads 2002; Tapken et al. 2004). Trying to connect these observations, various authors (e.g., Friaça & Terlevich 1999; Thommes & Meisenheimer 2005) discuss a model in which a forming galaxy has two Lyα bright phases: an initial phase when the galaxy has started the very first period of star formation and is still nearly dust free. Due to supernova explosions, the interstellar medium will be enriched with metals, and dust will form in the galaxy. This dust will absorb the Lyα photons, extinguishing the Lyα emission line. A second Lyα bright phase occurs at a later time when strong galactic winds facilitate the escape of Lyα emission.

---

[1]We can not entirely exclude that some of the emitters harbour a (concealed) AGN. A 40 ks exposure by the *Chandra* X-ray observatory is scheduled for early 2005, which should help to estimate the fraction of the Lyα emitters that contains an AGN.

The observations of Lyα emitters in our field support this second picture, and the Lyα emitting galaxies might be young star forming galaxies in their first starburst phase. This should be confirmed by deep infrared observations. Modelling the spectral energy distribution of the Lyα emitters from the UV to the rest-frame optical should allow the discrimination of Lyα emitters being either young dust free galaxies or more evolved star forming galaxies with an underlying old stellar population.

3.10 Implications of a protocluster at $z = 3.13$

3.10.1 Star formation rate density

The total UV star formation rate density (SFRD) of the confirmed emitters (excluding the radio galaxy) within the volume of the narrow-band filter is $\lesssim 0.0127 \pm 0.0003$ $M_\odot\,\mathrm{yr}^{-1}\,\mathrm{Mpc}^{-3}$. The SFRD derived from observations of LBGs at $z \sim 3$ with $m_R \lesssim 27$ is $0.0184 \pm 0.0034\ M_\odot\,\mathrm{yr}^{-1}\,\mathrm{Mpc}^{-3}$ (Steidel et al. 1999). Using the same magnitude limit, we find a SFRD of $0.0109 \pm 0.0002\ M_\odot\,\mathrm{yr}^{-1}\,\mathrm{Mpc}^{-3}$. This is a lower limit, because it does not include a contribution from the radio galaxy, the emitters with only a limit on their UV SFR are ignored and no correction has been made for incompleteness. Assuming that only 20–25% of the star forming, UV bright galaxies at $z \sim 3$ have a Lyα line satisfying our selection criteria (Steidel et al. 2000; Shapley et al. 2003), then the SFRD around MRC 0316–257 is roughly > 2.4–3.0 times higher than in the field, in accordance with the number density of the Lyα emitters.

It should be noted that the total SFRD in the protocluster might be much higher. From rest-frame UV and optical colors, Steidel et al. (1999) and Shapley et al. (2001) found that the UV continuum is on average attenuated by a factor of ~ 5. Also, very dusty, obscured galaxies could be missed. For example, De Breuck et al. (2004) found an overdensity of bright sources at 1.2 mm wavelength in the field of the protocluster near the radio galaxy TN J1338–1942 at $z = 4.1$. These objects could contribute substantially to the total SFR within the protocluster.

3.10.2 Enrichment of the intracluster medium

It is interesting to estimate the metal production in the protocluster surrounding MRC 0316–257. At redshift $z \sim 0.3$, the intracluster medium (ICM) in clusters has a metallicity of 0.2–0.3 $Z_\odot$ (e.g., Mushotzky & Loewenstein 1997), showing little evolution up to $z \sim 1.2$ (Tozzi et al. 2003; Hashimoto et al. 2004; Maughan et al. 2004; Rosati et al. 2004).

The extinction corrected total star formation rate density of UV bright star forming galaxies at $z \sim 3.1$ is $\sim 0.13\ M_\odot\,\mathrm{yr}^{-1}\,\mathrm{Mpc}^{-3}$ (Steidel et al. 1999; Giavalisco et al. 2004). The protocluster has a volume of 5.4×10^3 Mpc^3 and a galaxy overdensity of $n_{0316}/n_{\mathrm{field}} = 5.1$ (§3.8.3). This gives a total SFR in the protocluster of $\sim 3580\ M_\odot\,\mathrm{yr}^{-1}$. This value includes correction for dust absorption, but it ignores any contribution to the SFR from very dusty, obscured star forming galaxies. Taking an average yield of 0.02 (Lia et al. 2002), this means that $\sim 72\ M_\odot$ of metals are produced every year. Taking $4 \times 10^{14}\ M_\odot$ as the mass of the protocluster (§3.8.3) and assuming a baryon fraction of $\Omega_b/\Omega_m = 0.17$ (e.g., Spergel et al. 2003) and assuming that the star formation rate in the protocluster is constant with time, then enough metals can be produced to enrich the baryons in the protocluster to 0.2 $Z_\odot$ at $z \sim 1$. However, a large fraction ($> 90\%$)

of the produced metals must escape the galaxies in which they are formed. A possible mechanism to inject the metals into the ICM are supernova-driven outflows (e.g., Heckman et al. 1995; Aguirre et al. 2001), which are frequently seen in $z \sim 3$ LBGs (e.g., Pettini et al. 2001; Adelberger et al. 2003). This simple calculation shows that the star formation rate in the protocluster is high enough to enrich the ICM to the observed value at lower redshifts.

3.10.3 High redshift protoclusters near radio galaxies

Based on the high volume density of Lyα emitters near MRC 0316–257, which is a factor of $3.3^{+0.5}_{-0.4}$ higher as compared to blank fields, and the small velocity distribution of the confirmed emitters (*FWHM* of 1510 km s^{-1}) compared to the width of the narrow-band filter (*FWHM* $\sim$ 3500 km s^{-1}), we conclude that the Lyα emitters are located in a protocluster of galaxies with an estimated mass of > 3–6 $\times 10^{14}$ $M_\odot$. A likely scenario is that this protocluster will evolve and form a massive cluster of galaxies. The radio galaxy at the centre of the protocluster has the properties expected of the progenitor of a massive cD elliptical. The clumpy appearance of the radio galaxy in the ACS image could be explained as a merger of smaller subunits, and is very similar to *HST* observations of other $z \sim 2-3$ radio galaxies (e.g., Pentericci et al. 1999).

Based on the observations obtained in our VLT large program, the protocluster around MRC 0316–257 is not unique. We have found galaxy overdensities around all five radio galaxies (with redshifts between $z = 2.16$ and $z = 4.1$) that were studied to a similar depth as the 0316 field (Chapter 2; Chapter 5; Kurk et al. 2000; Pentericci et al. 2000; Venemans et al. 2003; Kurk et al. 2004). Each of these radio galaxy fields has at least 20 confirmed protocluster members, the velocity dispersions of the protoclusters range from 300 km s^{-1} to 1000 km s^{-1} and the associated masses are $> 10^{14}$ $M_\odot$ (Chapter 5; Venemans et al. 2003). At an even higher redshift, $z = 5.2$, we found a similar overdensity of Lyα emitters near the radio galaxy TN J0924–2201 (Chapter 4). In Chapter 5, the properties of these radio galaxy protoclusters are described and compared.

Acknowledgments

References

Adelberger, K. L., Steidel, C. C., Shapley, A. E., & Pettini, M. 2003, ApJ, 584, 45

Aguirre, A., Hernquist, L., Schaye, J., et al. 2001, ApJ, 561, 521

Ajiki, M., Taniguchi, Y., Murayama, T., et al. 2002, ApJ, 576, L25

Appenzeller, I. & Rupprecht, G. 1992, The Messenger, 67, 18

Archibald, E. N., Dunlop, J. S., Hughes, D. H., et al. 2001, MNRAS, 323, 417

Athreya, R. M., Kapahi, V. K., McCarthy, P. J., & van Breugel, W. J. M. 1998, A&A, 329, 809

Baldwin, J. A. & Stone, R. P. S. 1984, MNRAS, 206, 241

Baugh, C. M., Cole, S., Frenk, C. S., & Lacey, C. G. 1998, ApJ, 498, 504

Beers, T. C., Flynn, K., & Gebhardt, K. 1990, AJ, 100, 32

Bennert, N., Falcke, H., Schulz, H., Wilson, A. S., & Wills, B. J. 2002, ApJ, 574, L105

Bertin, E. & Arnouts, S. 1996, A&AS, 117, 393

Bessell, M. S. 1979, PASP, 91, 589

Best, P. N. 2000, MNRAS, 317, 720

Best, P. N., Lehnert, M. D., Miley, G. K., & Röttgering, H. J. A. 2003, MNRAS, 343, 1

Blakeslee, J. P., Anderson, K. R., Meurer, G. R., Benítez, N., & Magee, D. 2003a, in ASP Conf. Ser. 295: Astronomical Data Analysis Software and Systems XII, 257

Blakeslee, J. P., Franx, M., Postman, M., et al. 2003b, ApJ, 596, L143

Brocklehurst, M. 1971, MNRAS, 153, 471

Bunker, A. J., Warren, S. J., Hewett, P. C., & Clements, D. L. 1995, MNRAS, 273, 513

Carilli, C. L., Röttgering, H. J. A., van Ojik, R., Miley, G. K., & van Breugel, W. J. M. 1997, ApJ, 109, 1

Chambers, K. C., Miley, G. K., & van Breugel, W. J. M. 1990, ApJ, 363, 21

Ciardullo, R., Feldmeier, J. J., Krelove, K., Jacoby, G. H., & Gronwall, C. 2002, ApJ, 566, 784

Cowie, L. L. & Hu, E. M. 1998, AJ, 115, 1319

Dawson, S., Spinrad, H., Stern, D., et al. 2002, ApJ, 570, 92

De Breuck, C., Bertoldi, F., Carilli, C. L., et al. 2004, A&A, 424, 1

De Breuck, C., Neri, R., Morganti, R., et al. 2003a, A&A, 401, 911

De Breuck, C., Neri, R., & Omont, A. 2003b, New Astronomy Review, 47, 285

De Breuck, C., van Breugel, W. J. M., Röttgering, H. J. A., et al. 2001, AJ, 121, 1241

De Breuck, C., van Breugel, W. J. M., Stanford, S. A., et al. 2002, AJ, 123, 637

Della Ceca, R., Scaramella, R., Gioia, I. M., et al. 2000, A&A, 353, 498

Deutsch, E. W. 1999, AJ, 118, 1882

Dey, A., van Breugel, W. J. M., Vacca, W. D., & Antonucci, R. 1997, ApJ, 490, 698

Ferguson, H. C., Dickinson, M., Giavalisco, M., et al. 2004, ApJ, 600, L107

Ford, H. C., Bartko, F., Bely, P. Y., et al. 1998, in Proc. SPIE Vol. 3356, Space Telescopes and Instruments V, Pierre Y. Bely; James B. Breckinridge; Eds., 234

Fouqué, P., Solanes, J. M., Sanchis, T., & Balkowski, C. 2001, A&A, 375, 770

Friaça, A. C. S. & Terlevich, R. J. 1999, MNRAS, 305, 90

Fruchter, A. S. & Hook, R. N. 2002, PASP, 114, 144

Fynbo, J. P. U., Ledoux, C., Møller, P., Thomsen, B., & Burud, I. 2003, A&A, 407, 147

Fynbo, J. P. U., Møller, P., Thomsen, B., et al. 2002, A&A, 388, 425

Giavalisco, M. 2002, ARA&A, 40, 579

Giavalisco, M., Dickinson, M., Ferguson, H. C., et al. 2004, ApJ, 600, L103

Hashimoto, Y., Barcons, X., Böhringer, H., et al. 2004, A&A, 417, 819

Heckman, T. M., Dahlem, M., Lehnert, M. D., et al. 1995, ApJ, 448, 98

Hill, G. J. & Lilly, S. J. 1991, ApJ, 367, 1

Hu, E. M., Cowie, L. L., Capak, P., et al. 2004, AJ, 127, 563

Hu, E. M., Cowie, L. L., & McMahon, R. G. 1998, ApJ, 502, L99

Hunt, M. P., Steidel, C. C., Adelberger, K. L., & Shapley, A. E. 2004, ApJ, 605, 625

Jarvis, M. J., Rawlings, S., Eales, S., et al. 2001, MNRAS, 326, 1585

Keel, W. C., Cohen, S. H., Windhorst, R. A., & Waddington, I. 1999, AJ, 118, 2547

Keel, W. C., Wu, W., Waddington, I., Windhorst, R. A., & Pascarelle, S. M. 2002, AJ, 123, 3041

Kudritzki, R.-P., Méndez, R. H., Feldmeier, J. J., et al. 2000, ApJ, 536, 19

Kurk, J. D., Pentericci, L., Röttgering, H. J. A., & Miley, G. K. 2004, A&A, 428, 793

Kurk, J. D., Röttgering, H. J. A., Pentericci, L., et al. 2000, A&A, 358, L1

Lahav, O., Rees, M. J., Lilje, P. B., & Primack, J. R. 1991, MNRAS, 251, 128

Landolt, A. U. 1992, AJ, 104, 340

Large, M. I., Mills, B. Y., Little, A. G., Crawford, D. F., & Sutton, J. M. 1981, MNRAS, 194, 693

Le Fèvre, O., Deltorn, J. M., Crampton, D., & Dickinson, M. 1996, ApJ, 471, L11

Leitherer, C., Schaerer, D., Goldader, J. D., et al. 1999, ApJ, 123, 3

Lia, C., Portinari, L., & Carraro, G. 2002, MNRAS, 330, 821

Madau, P. 1995, ApJ, 441, 18

Madau, P., Pozzetti, L., & Dickinson, M. 1998, ApJ, 498, 106

Maier, C., Meisenheimer, K., Thommes, E., et al. 2003, A&A, 402, 79

Malhotra, S. & Rhoads, J. E. 2002, ApJ, 565, L71

Maughan, B. J., Jones, L. R., Ebeling, H., et al. 2003, ApJ, 587, 589

Maughan, B. J., Jones, L. R., Ebeling, H., & Scharf, C. 2004, MNRAS, 351, 1193

McCarthy, P. J., Kapahi, V. K., van Breugel, W. J. M., & Subrahmanya, C. R. 1990, AJ, 100, 1014

Monet, D. B. A., Canzian, B., Dahn, C., et al. 1998, VizieR Online Data Catalog, 1252, 0

Monet, D. G. 1998, Bulletin of the American Astronomical Society, 30, 1427

Moorwood, A. F. 1997, in Proc. SPIE Vol. 2871, p. 1146-1151, Optical Telescopes of Today and Tomorrow,
        Arne L. Ardeberg; Ed., 1146–1151

Mushotzky, R. F. & Loewenstein, M. 1997, ApJ, 481, L63

Oke, J. B. 1974, ApJ, 27, 21

Papadopoulos, P. P., Röttgering, H. J. A., van der Werf, P. P., et al. 2000, ApJ, 528, 626

Pascarelle, S. M., Windhorst, R. A., Driver, S. P., Ostrander, E. J., & Keel, W. C. 1996, ApJ, 456, L21

Peebles, P. J. E. 1980, The Large Scale Structure of the Universe (Princeton Univ. Press, NJ)

Pentericci, L., Kurk, J. D., Carilli, C. L., et al. 2002, A&A, 396, 109

Pentericci, L., Kurk, J. D., Röttgering, H. J. A., et al. 2000a, A&A, 361, L25

Pentericci, L., Röttgering, H. J. A., Miley, G. K., et al. 1999, A&A, 341, 329

Pentericci, L., van Reeven, W., Carilli, C. L., Röttgering, H. J. A., & Miley, G. K. 2000b, A&AS, 145, 121

Pettini, M., Shapley, A. E., Steidel, C. C., et al. 2001, ApJ, 554, 981

Press, W. H., Rybicki, G. B., & Schneider, D. P. 1993, ApJ, 414, 64

Reuland, M., Röttgering, H. J. A., van Breugel, W. J. M., & De Breuck, C. 2004, MNRAS, 353, 377

Rhoads, J. E. & Malhotra, S. 2001, ApJ, 563, L5

Rosati, P., Stanford, S. A., Eisenhardt, P. R., et al. 1999, AJ, 118, 76

Rosati, P., Tozzi, P., Ettori, S., et al. 2004, AJ, 127, 230

Röttgering, H. J. A., West, M. J., Miley, G. K., & Chambers, K. C. 1996, A&A, 307, 376

Schlegel, D. J., Finkbeiner, D. P., & Davis, M. 1998, ApJ, 500, 525

Shapley, A. E., Steidel, C. C., Adelberger, K. L., et al. 2001, ApJ, 562, 95

Shapley, A. E., Steidel, C. C., Pettini, M., & Adelberger, K. L. 2003, ApJ, 588, 65

Shimasaku, K., Ouchi, M., Okamura, S., et al. 2003, ApJ, 586, L111

Spergel, D. N., Verde, L., Peiris, H. V., et al. 2003, ApJ, 148, 175

Stanford, S. A., Holden, B., Rosati, P., et al. 2002, AJ, 123, 619

Steidel, C. C., Adelberger, K. L., Dickinson, M., et al. 1998, ApJ, 492, 428

Steidel, C. C., Adelberger, K. L., Giavalisco, M., Dickinson, M., & Pettini, M. 1999, ApJ, 519, 1

Steidel, C. C., Adelberger, K. L., Shapley, A. E., et al. 2000, ApJ, 532, 170

Steidel, C. C., Adelberger, K. L., Shapley, A. E., et al. 2003, ApJ, 592, 728

Steidel, C. C., Hunt, M. P., Shapley, A. E., et al. 2002, ApJ, 576, 653

Stevens, J. A., Ivison, R. J., Dunlop, J. S., et al. 2003, Nature, 425, 264

Stone, R. P. S. & Baldwin, J. A. 1983, MNRAS, 204, 347

Tapken, C., Appenzeller, I., Mehlert, D., Noll, S., & Richling, S. 2004, A&A, 416, L1

Thommes, E. & Meisenheimer, K. 2005, A&A, 430, 877

Toft, S., Mainieri, V., Rosati, P., et al. 2004, A&A, 422, 29

Tozzi, P., Rosati, P., Ettori, S., et al. 2003, ApJ, 593, 705

Venemans, B. P., Miley, G. K., Kurk, J. D., Rottgering, H. J. A., & Pentericci, L. 2003, The Messenger, 111, 36

Vernet, J., Fosbury, R. A. E., Villar-Martín, M., et al. 2001, A&A, 366, 7

White, S. D. M. & Rees, M. J. 1978, MNRAS, 183, 341

Willott, C. J., Rawlings, S., Blundell, K. M., et al. 2002, MNRAS, 335, 1120

Zirm, A. W., Dickinson, M., & Dey, A. 2003, ApJ, 585, 90

Chapter 4

Discovery of six Lyα emitters near a radio galaxy at $z \sim 5.2$

Abstract. We present the results of narrow-band and broad-band imaging with the Very Large Telescope of the field surrounding the radio galaxy TN J0924–2201 at $z = 5.2$. Fourteen candidate Lyα emitters with a rest-frame equivalent width of > 20 Å were detected. Spectroscopy of eight of these objects showed that six have redshifts similar to that of the radio galaxy. The density of emitters at the redshift of the radio galaxy is estimated to be a factor 1.5–6.2 higher than in the field, and comparable to the density of Lyα emitters in radio galaxy protoclusters at $z = 4.1, 3.1$ and 2.2. The Lyα emitters near TN J0924–2201 could therefore be part of a structure that will evolve into a massive cluster. These observations confirm that substantial clustering of Lyα emitters occurs at $z > 5$ and support the idea that radio galaxies pinpoint high density regions in the early Universe.

4.1 Introduction

ONE of the most intriguing questions in modern astrophysics concerns the formation of structure in the early Universe (e.g., Bahcall et al. 1997). The narrow-band imaging technique can efficiently select objects with a strong Lyα line in a narrow redshift range, and is therefore ideal for finding and investigating overdense regions at high redshift (Steidel et al. 2000; Møller & Fynbo 2001; Shimasaku et al. 2003; Palunas et al. 2004). For example, Steidel et al. (2000) used narrow-band imaging to map the extent of a large scale structure at $z \sim 3.09$, discovered in a survey for continuum-selected Lyman-break galaxies. Shimasaku et al. (2003) serendipitously found a large scale structure at $z \sim 4.9$ while searching for Lyα emitters in the Subaru Deep Field. Their results demonstrate that Mpc-scaled structures have already formed by $z \sim 4.9$ and that Lyα emitters must be very biased tracers of mass in the early Universe.

Narrow-band imaging of distant powerful radio galaxies at $z = 2 - 4$ has shown that these objects are often located in rich environments, possibly the early stages in the formation of massive clusters (Chapter 2; Chapter 3; Pascarelle et al. 1996; Le Fèvre et al. 1996; Pentericci et al. 2000; Venemans et al. 2003; Kurk et al. 2004). An interesting question is out to which redshift such large scale structures (protoclusters) can be detected. The most distant known radio galaxy is TN J0924–2201, with a redshift of $z = 5.2$ (van Breugel et al. 1999). In this chapter, we describe broad- and narrow-band observations of this radio galaxy, and report the discovery of six Lyα emitters in the field whose redshifts are close to that of the radio galaxy. Throughout this chapter, magnitudes are in the AB system and a Λ-dominated cosmology with $H_0 = 65$ $\mathrm{km\,s^{-1}\,Mpc^{-1}}$, $\Omega_M = 0.3$, and $\Omega_\Lambda = 0.7$ is assumed.

4.2 Observations and candidate selection

4.2.1 Imaging observations and candidate selection

To search for candidate Lyα emitters near TN J0924–2201, narrow-band and broad-band (*I*- and *V*-band) imaging of the field was carried out during two separate observing sessions in 2002 March and April with the VLT Yepun (UT4), using the FOcal Reducer/ low dispersion Spectrograph 2 (FORS2). The custom made narrow-band filter had a *FWHM* of 89 Å and a central wavelength of 7528 Å, which encompasses the wavelength of the Lyα emission line at $z \sim 5.2$. The effective exposure times are 36860 s (narrow-band), 9750 s (*I*-band) and 3600 s (*V*-band). The seeing in the narrow-band, *I*-band and *V*-band images is 0."8, 0."8 and 1."05 respectively. The 3 σ limiting magnitudes in an aperture with a 2."0 diameter are 26.29, 26.65 and 26.80 for the narrow-band, *I*- and *V*-band respectively. For a Lyα emitter at $z \sim 5.2$ with negligible continuum, the 5 σ limiting line luminosity is $L_{\mathrm{lim}}(\mathrm{Ly}\alpha) = 3 \times 10^{42}$ erg s^{-1}. The images have an area useful for detecting Lyα emitters of 46.8 □′.

A total of 3471 objects were detected in the narrow-band image with a signal-to-noise greater than 5 using the program SExtractor (Bertin & Arnouts 1996). For each object, the observed equivalent width was calculated using a method that is described in Chapter 3. Lyα emitters at $z \sim 5.2$ with a rest-frame equivalent width of $EW_0 > 20$ Å would have an observed equivalent width (EW_λ) of 124 Å. We find 24 such objects

in the field. The *V*-band image was used to identify low redshift interlopers with an emission line falling in the narrow-band filter. Ten of the 24 objects with $EW_\lambda > 124$ Å were also detected in the *V*-band with a signal-to-noise greater than 2, and had $V - I$ colors that were much bluer ($V - I < 1.2$) than a $V - I$ color of ~ 2.75 as expected for a galaxy at $z \sim 5.2$ (e.g., Songaila 2004). The remaining 14 candidates were our high priority candidates for follow-up spectroscopy.

4.2.2 Spectroscopy

For the spectroscopy, a mask was constructed which included the radio galaxy and eight of the 14 high priority candidate Lyα emitters. This was the maximum number that could be fitted on the mask. The rest of the mask was filled with objects having an excess flux in the narrow-band, but with a lower equivalent width than our selection criterion and/or with a blue $V - I$ color. The observations were carried out on 2003 March 3 and 4 using FORS2 on the VLT Yepun. The mask was observed through the 600RI grism (with a peak efficiency of 87%) with 1.4 slits. The pixels were 2×2 binned to decrease the readout time and noise, giving a spatial scale of 0.25 pixel^{-1} and a dispersion of 1.66 Å pixel^{-1}. The total exposure time was 20676 s. The mean airmass was 1.23 and the seeing in the individual frames varied between 0.7 and 1.0, giving a spectral resolution of 185–265 km s^{-1} for point sources. For the wavelength calibration, exposures were taken of He, HgCd, Ar and Ne lamps. The rms of the wavelength calibration was always better than 0.25 Å (~ 10 km s^{-1}).

4.3 Results

The radio galaxy and all of the eight observed candidate Lyα emitters showed an emission line near 7500 Å. The redshift of the radio galaxy of $z = 5.1989 \pm 0.0006$ is consistent with the redshift of $z = 5.2$, reported by van Breugel et al. (1999).

Two of the eight candidate Lyα objects (emitters # 463 and # 559) are identified with [O III] $\lambda 5007$ at $z \sim 0.5$, confirmed by the accompanying lines [O III] $\lambda 4959$ and Hβ (Fig. 4.1 and Table 4.1). The other six spectra (Fig. 4.1) did not show any other emission line in a wavelength range covering more than 3300 Å (see Table 4.1).

To distinguish high redshift Lyα emitters from low redshift interlopers various tests can be applied (see Stern et al. 2000, for a review).

Emission line ratios As mentioned above, no other emission lines were found in the spectra of the emitters. To estimate the likelihood that the emitters are [O II] emitters, we can derive an upper limit on the flux of the [Ne III] $\lambda 3869$ line and compare that to local emission line galaxies (Fynbo et al. 2001). Stacking the six spectra to increase the signal-to-noise, we find an upper limit on the ratio of [Ne III] line flux over the [O II] flux of flux([Ne III])/flux([O II]) < 0.07 (2 σ). Using the spectrophotometric catalogue of local emission line galaxies of Terlevich et al. (1991), we found that only five out of a sample of 151 of the galaxies with both [O II] and [Ne III] lines detected ($5/151 \approx 3\%$) have such a weak Neon line. The total number of $z \sim 1$ [O II] emitters expected in our field, derived from Teplitz et al. (2003), is ~ 1. We therefore expect that < 1 of our six emission line galaxies is an [O II] emitter.
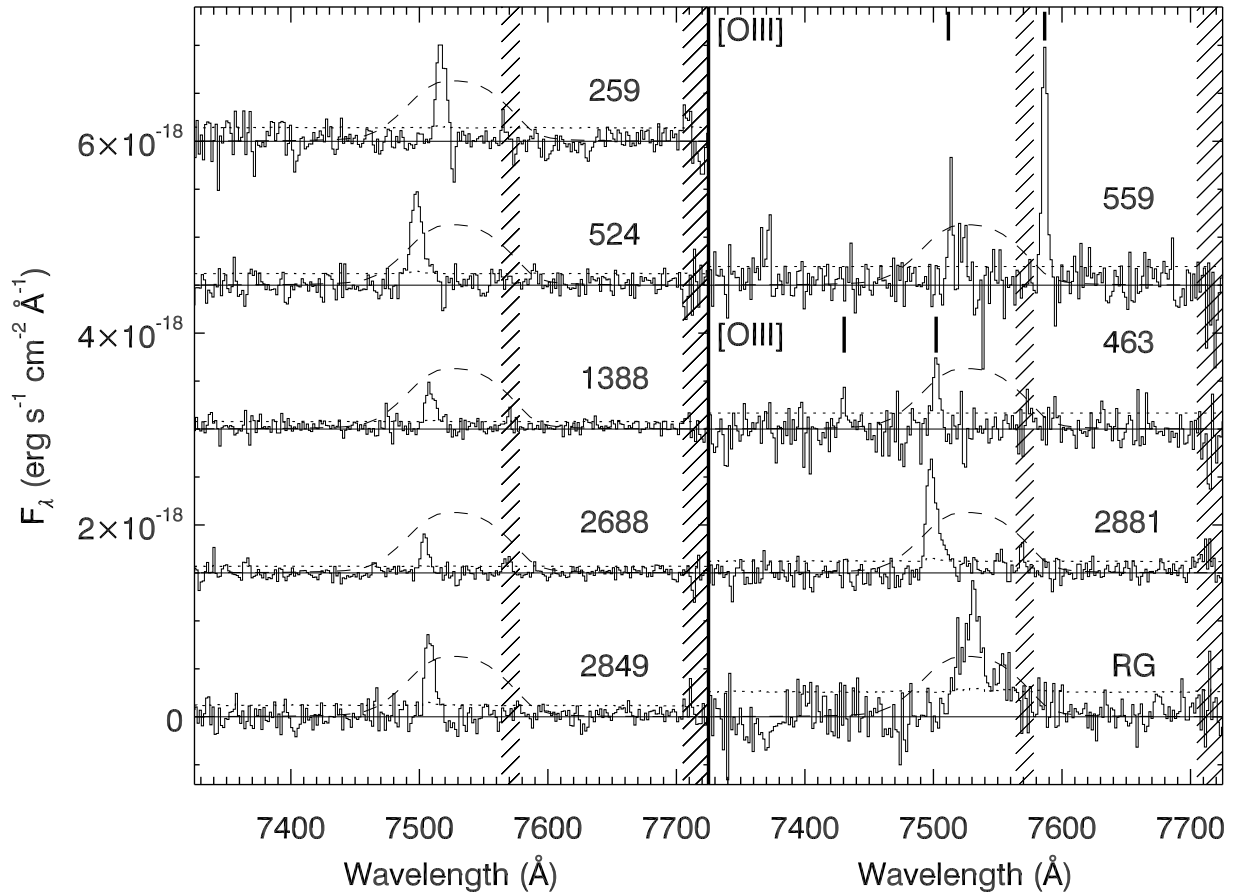
Figure 4.1 — Part of the spectra of the eight spectroscopically observed high priority emitters and the radio galaxy. For clarity the spectra are offset by 1.5×10^{-18} erg s^{-1} cm^{-2}. The solid lines indicate the zero point of the spectra, the dotted lines the 1σ uncertainty in the data, and the dashed lines are the scaled transmission curves of the narrow-band filter. The regions in the spectrum where strong telluric skylines dominate are indicated with hashed lines.

Asymmetric line profile A characteristic feature of a high redshift Lyα line is the flux decrement on the blue wing of the Lyα emission (e.g., Dawson et al. 2002). Following Rhoads et al. (2003), the asymmetry of an emission line can be described by the parameters a_λ and a_f. These parameters measure the ratio of the line width and line flux redward and blueward of the line peak and depend both on the characteristics of the line (line width, amount of absorption, merged doublet) and on the resolution of the spectrum (Rhoads et al. 2003, and reference therein). Simulations of observed spectra indicate that Gaussian Lyα lines with a *FWHM* of 150–800 km s^{-1} and with the blue side fully absorbed have $a_\lambda = 1.0 - 1.6$ and $a_f = 1.0 - 1.4$, while [O II] $\lambda 3727$ emitters have $a_\lambda \approx 0.9$ and $a_f = 0.8 - 0.9$. This is consistent with values found by Rhoads et al. (2003), who measure typical values of $0.9 < a_f < 1.9$ and $0.9 < a_\lambda < 3.1$ for a sample of high redshift Lyα emitters and for [O II] emitters at $z \sim 1$ $a_f \approx 0.8$ and $a_\lambda \approx 0.9$. Only two of the emission lines (of emitters # 1388 and # 2881) have a signal-to-noise that is high enough to measure the asymmetry. These two lines are (marginally) asymmetric (with $a_\lambda = 2.0 \pm 0.9$ (2.2 ± 0.6) and $a_f = 1.7 \pm 0.8$ (1.4 ± 0.6) for emitter # 1388 (2881)), an indication that emitters # 1388 and # 2881 are Lyα emitters at $z \sim 5.2$.

Continuum break A high redshift Lyα emitter must have a continuum break across the Lyα line, caused by the Lyα forest between the galaxy and the observer. Madau (1995) predicts a break of a factor ~ 5 across the Lyα line at $z \sim 5$. To measure continuum in our spectra, regions that were not effected by strong telluric lines were chosen redward and blueward of the emission line. Four spectra had a significant ($> 3\sigma$) detection of continuum emission redward of the emission line, resulting in 2σ lower limits on their flux decrements of $3.6 - 5.3$. Such large breaks in the optical are exclusively found in high redshift objects (e.g., Stern et al. 2000). Hammer et al. (1997) showed that observed [O II] emitters at $0.5 < z < 1.0$ have a total 4000 Å and Balmer break of factor < 3. Therefore, the continuum break measured in four of the emitters is most likely caused by neutral H I absorption, and hence these emitters can be identified with Lyα emitters at $z \sim 5.2$.

Equivalent width The emission line objects have observed equivalent widths in excess of ~ 250 Å. The two emitters which do not show a convincing line asymmetry and do not show continuum both redward and blueward of the emission line, have observed equivalent widths of $EW_\lambda > 540$ Å. This would correspond to a rest-frame equivalent width of > 269 Å if the emission line is [O II] $\lambda 3727$ at $z \sim 1.0$. Such high [O II] equivalent width emitters are rare. The fraction of [O II] emitters with a rest-frame $EW > 200$ Å is $< 2.5\%$ (Teplitz et al. 2003). With the estimated number of [O II] emitters (see above), this fraction suggests that these two emission line objects are probably not [O II] emitters at $z \sim 1$, but Lyα emitters at $z = 5.2$.

On the basis of these four lines of arguments, we conclude that these six line emitters are almost certainly Lyα emitters at $z = 5.2$.

The extracted Lyα lines were fitted with a Gaussian function to estimate the redshift, line flux and widths (*FWHMs*). In Table 4.1 the properties of the Lyα emitters are summarized. The IDs correspond to the object's number in the catalogue. To correct for the instrumental broadening, the observed *FWHM* was deconvolved with the resolution. The star formation rates ($SFR_{\rm UV}$ and $SFR_{\rm Ly\alpha}$) were calculated from the measured UV continuum fluxes and line fluxes in the images assuming a flat f_ν spectrum and UV flux density to SFR conversion of Madau et al. (1998).

The velocities of the six confirmed Lyα emitters cluster within a range of 900 km s^{-1} in the rest-frame, while the narrow-band filter is ~ 3500 km s^{-1} wide. The peak of the Lyα emission of the radio galaxy is roughly 1000 km s^{-1} away from the central velocity of the emitters. This is different from other $z > 2$ radio galaxy protoclusters, where the radio galaxy has a velocity close to the average velocity of the Lyα emitters (Chapter 3; Pentericci et al. 2000; Kurk et al. 2004). This could be due to H I absorption on the Lyα emission line of the radio galaxy. It has been shown that in radio galaxies this absorption can cause a velocity shift of the Lyα line up to 1000 km s^{-1} as compared to other UV emission lines (e.g., Röttgering et al. 1997).

Of the remaining objects covered by the mask, one is identified as a [O II] $\lambda 3727$ emitter, also showing [Ne III] $\lambda 3869$ emission and nine were identified as [O III] $\lambda 5007$ emitters, confirmed by various lines such as [O III] $\lambda 4959$, Hβ, Hγ, Hδ, [Ne III] $\lambda 3869$ and [O II] $\lambda 3727$. In total 11 [O III] emitters were confirmed in the field, all having a redshift of $z \sim 0.5$.

Table 4.1 — Properties of the eight spectroscopically observed high priority candidates and the radio galaxy.

Object	Position		z	Flux	EW_0	$FWHM$	SFR_{UV}	$SFR_{Ly\alpha}$
	α_{J2000}	δ_{J2000}		erg s^{-1} cm^{-2}	Å	km s^{-1}	M$_\odot$ yr^{-1}	M$_\odot$ yr^{-1}
259	09 24 07.07	-22 02 09.2	5.1834 ± 0.0002	$8.8 \pm 0.8 \times10^{-18}$	> 103	208 ± 39	< 3.2	3.9 ± 0.7
524	09 24 09.41	-22 02 00.5	5.1683 ± 0.0003	$1.2 \pm 0.1 \times10^{-17}$	97^{+866}_{-21}	392 ± 25	9.1 ± 3.6	10.4 ± 1.2
1388	09 24 16.68	-22 01 16.9	5.1772 ± 0.0003	$4.1 \pm 0.5 \times10^{-18}$	59^{+476}_{-14}	295 ± 38	5.1 ± 2.0	3.5 ± 0.5
2688	09 24 25.67	-22 03 01.1	5.1731 ± 0.0003	$3.1 \pm 0.4 \times10^{-18}$	> 88	167 ± 63	< 2.9	3.0 ± 0.6
2849	09 24 24.30	-22 02 30.9	5.1765 ± 0.0003	$8.0 \pm 0.9 \times10^{-18}$	47^{+785}_{-13}	249 ± 32	6.1 ± 2.7	3.3 ± 0.7
2881	09 24 23.88	-22 03 44.8	5.1683 ± 0.0005	$1.4 \pm 0.2 \times10^{-17}$	42^{+45}_{-9}	479 ± 28	13.7 ± 3.4	6.8 ± 1.1
463[a]	09 24 08.48	-22 00 04.0	0.4983 ± 0.0001	$4.7 \pm 0.7 \times10^{-18}$	339^{+1966}_{-91}	< 200	–	–
559[a]	09 24 09.51	-22 00 18.3	0.51515 ± 0.00003	$1.3 \pm 0.1 \times10^{-17}$	207^{+160}_{-47}	< 70	–	–
RG	09 24 19.90	-22 01 42.0	5.1989 ± 0.0006	$2.1 \pm 0.2 \times10^{-17}$	83^{+148}_{-14}	1161 ± 55	11.6 ± 3.5	11.4 ± 0.7

[a] [O III] λ5007 emitter

4.4 Discussion and conclusions

The fraction of foreground contaminants in our sample is estimated to be $2/8 \sim 25\%$. There are six additional unconfirmed high priority candidate Lyα emitters in the field. Based on the fraction of contaminants in our sample, roughly four of those are expected to be $z \sim 5.2$ Lyα emitters.

Is there an overdensity of Lyα emitters near TN J0924–2201? To investigate this question, we have to compare the density of Lyα emitters in our field with the density in blank fields. The largest survey near $z \sim 5$ for Lyα emitters is the search for Lyα emitters at $z \sim 4.79$ in the Subaru Deep Field (SDF, Shimasaku et al. 2004). This survey is comparable in depth to our observations ($L_{\lim}(Ly\alpha) = 3 \times 10^{42}$ erg s^{-1} for an emitter at $z = 4.79$ with no continuum) and the selection criteria applied to identify Lyα emitters are very similar to ours ($EW_\lambda > 80$ Å, Shimasaku et al. 2004). In the SDF, Shimasaku et al. find 51 candidate Lyα emitters in an area of $25' \times 45'$. However, there is no spectroscopic confirmation of these candidates. We therefore conservatively assume that all their candidates are Lyα emitters at $z \sim 4.8$, resulting in a number density of Lyα emitters in the SDF of $2.1 \pm 0.3 \times 10^{-4}$ Mpc^{-3} (Shimasaku et al. 2004). Excluding the radio galaxy, the density of confirmed Lyα emitters in our field is $5.3^{+3.2}_{-2.1} \times 10^{-4}$ Mpc^{-3}, which is a factor $2.5^{+1.6}_{-1.0}$ higher than in the SDF. If the four unconfirmed candidate Lyα emitters are included, this factor rises to $4.2^{+2.0}_{-1.4}$. We used the data from the SDF to estimate the chance of finding six or more Lyα emitters in within a single 6.8×6.8 FORS2 field by counting the number of emitters in randomly placed 6.8×6.8 apertures. In only 7% of the cases, more than six Lyα emitters were found. This further indicates that the TN J0924–2201 field is overdense in Lyα emitters.

Lyα emitters at high redshift show large cosmic variance in their clustering properties (e.g., Shimasaku et al. 2004). Various authors have found that the distribution of Lyα emitters on the sky and/or in redshift space can be very inhomogeneous (e.g., Ouchi et al. 2003; Fynbo et al. 2003; Shimasaku et al. 2003; Palunas et al. 2004; Hu et al. 2004). For example, most of the Lyα emitters found at $z = 4.86$ in the SDF are concentrated within a large scale structure with a radius of $\sim 6'$ (~ 2.5 Mpc, Shimasaku et al. 2003). It is therefore possible that the Lyα emitters around TN J0924–2201 in the $\sim 6.8 \times 6.8$ field of view of FORS2 are located inside such a large scale structure.

It is interesting to compare the (over)density in this field with the protoclusters that were found around radio galaxies at $z = 4.1, 3.1$ and 2.2, each with at least 20 confirmed protocluster members and estimated masses of $\sim 10^{14} - 10^{15}$ M$_\odot$ (Chapter 2; Chapter 3; Pentericci et al. 2000; Kurk et al. 2004). In the TN 0924–2201 field objects were selected with a (Lyα) line luminosity of $> 3 \times 10^{42}$ erg s^{-1}. At $z = 4.1, 3.1$ and 2.2, this luminosity limit corresponds with a limit of $> 1.5, 3.1$ and 7.0×10^{-17} erg s^{-1} cm^{-2}. The number of candidate (confirmed) emitters with a line brighter than the luminosity limit in the $z = 4.1, 3.1$ and 2.2 protoclusters is 10 (10), 12 (12) and 8 (6) respectively. This is roughly the same number of Lyα emitters as in the TN J0924–2201 field, which contains six confirmed and four possible Lyα emitters. The Lyα emitters at $z = 5.2$ might therefore be the bright end of a population of star forming galaxies in a protocluster at $z = 5.2$, making it the most distant known protocluster. Deep multi-color observations should confirm this by detecting other populations of galaxies (e.g. Lyman break galaxies) in the protocluster.

Acknowledgments

References

Bahcall, N. A., Fan, X., & Cen, R. 1997, ApJ, 485, L53
Bertin, E. & Arnouts, S. 1996, A&AS, 117, 393
Dawson, S., Spinrad, H., Stern, D., et al. 2002, ApJ, 570, 92
Fynbo, J. P. U., Ledoux, C., Møller, P., Thomsen, B., & Burud, I. 2003, A&A, 407, 147
Fynbo, J. P. U., Møller, P., & Thomsen, B. 2001, A&A, 374, 443
Hammer, F., Flores, H., Lilly, S. J., et al. 1997, ApJ, 481, 49
Hu, E. M., Cowie, L. L., Capak, P., et al. 2004, AJ, 127, 563
Kurk, J. D., Pentericci, L., Röttgering, H. J. A., & Miley, G. K. 2004, A&A, 428, 793
Le Fèvre, O., Deltorn, J. M., Crampton, D., & Dickinson, M. 1996, ApJ, 471, L11
Madau, P. 1995, ApJ, 441, 18
Madau, P., Pozzetti, L., & Dickinson, M. 1998, ApJ, 498, 106
Møller, P. & Fynbo, J. P. U. 2001, A&A, 372, L57
Ouchi, M., Shimasaku, K., Furusawa, H., et al. 2003, ApJ, 582, 60
Palunas, P., Teplitz, H. I., Francis, P. J., Williger, G. M., & Woodgate, B. E. 2004, ApJ, 602, 545
Pascarelle, S. M., Windhorst, R. A., Driver, S. P., Ostrander, E. J., & Keel, W. C. 1996, ApJ, 456, L21
Pentericci, L., Kurk, J. D., Röttgering, H. J. A., et al. 2000, A&A, 361, L25

Rhoads, J. E., Dey, A., Malhotra, S., et al. 2003, AJ, 125, 1006

Röttgering, H. J. A., van Ojik, R., Miley, G. K., et al. 1997, A&A, 326, 505

Shimasaku, K., Hayashino, T., Matsuda, Y., et al. 2004, ApJ, 605, L93

Shimasaku, K., Ouchi, M., Okamura, S., et al. 2003, ApJ, 586, L111

Songaila, A. 2004, AJ, 127, 2598

Steidel, C. C., Adelberger, K. L., Shapley, A. E., et al. 2000, ApJ, 532, 170

Stern, D., Bunker, A., Spinrad, H., & Dey, A. 2000, ApJ, 537, 73

Teplitz, H. I., Collins, N. R., Gardner, J. P., et al. 2003, ApJ, 146, 209

Terlevich, R., Melnick, J., Masegosa, J., Moles, M., & Copetti, M. V. F. 1991, A&AS, 91, 285

van Breugel, W., De Breuck, C., Stanford, S. A., et al. 1999, ApJ, 518, L61

Venemans, B. P., Kurk, J. D., Miley, G. K., & Röttgering, H. J. A. 2003, New Astronomy Review, 47, 353

Chapter 5

Characteristics of high redshift protoclusters

Abstract. We present the results of a large program conducted with the Very Large Telescope and the Keck telescope to search for forming clusters of galaxies near powerful radio galaxies at $2.0 < z < 5.2$. Besides MRC 1138–262 at $z = 2.16$, the radio galaxy observed in our pilot program, we obtained narrow- and broad-band images of eight radio galaxies and their surroundings. The imaging was used to select candidate Lyα emitting galaxies in $\sim 3 \times 3$ Mpc^2 areas near the radio galaxies. A total of 300 candidate emitters were found with a rest-frame Lyα equivalent width of $EW_0 > 15$ Å and significance $\Sigma \equiv EW_0/\Delta EW_0^- > 3$. Follow-up spectroscopy was performed on 152 candidates in seven radio galaxy fields. Of these, 139 were confirmed to be Lyα emitters, four were low redshift interlopers and nine were non-detections. With the adopted criteria the success rate is $139/152 = 91\%$. Also, 14 objects with $EW_0 < 15$ and/or $\Sigma < 3$ were confirmed to be Lyα emitters. Combined with the 15 Lyα emitters near MRC 1138–262, we have determined Lyα redshifts for 168 objects near eight radio galaxies.

At least six of our eight fields are overdense in Lyα emitters by a factor 3–5 as compared to the field density of Lyα emitters at similar redshifts, although the statistics in our highest redshift field ($z = 5.2$) are poor. Also, the emitters show significant clustering in velocity space. In the overdense fields, the width of the velocity distributions of the emitters is a factor 2–5 smaller than the width of the narrow-band filters. Taken together, we conclude that we have discovered six forming clusters of galaxies (protoclusters). We estimate that roughly 75% of powerful ($L_{2.7\mathrm{GHz}} > 10^{33}$ erg s^{-1} Hz^{-1} sr^{-1}) high redshift radio galaxies reside in a protocluster. The protoclusters have sizes of $> 1.75 - 2.0$ Mpc, which is consistent with the structure sizes found by other groups. The velocity dispersion of the emitters increases with cosmic time, in agreement with the dark matter velocity dispersion in numerical simulations of forming massive clusters. By using the volume occupied by the overdensities and assuming a bias parameter of $b = 3 - 6$, we estimate that the protoclusters have masses in the range $2 - 9 \times 10^{14}$ $M_\odot$. These protoclusters are likely to be progenitors of present-day (massive) clusters of galaxies.

B. P. Venemans, H. J. A. Röttgering, G. K. Miley, W. J. M. van Breugel,
S. A. Stanford, C. De Breuck, S. Croft, R. A. Overzier, J. D. Kurk,
C. L. Carilli, H. Ford, T. Heckman, P. McCarthy, L. Pentericci

5.1   Introduction

Cⁱᴸᵁˢᵀᴱᴿˢ of galaxies are the largest and most massive discrete structures in the Universe. They are interesting objects to study for many reasons.

First, clusters contain large numbers of galaxies at specific redshifts, making them excellent laboratories with which to investigate the formation and evolution of galaxies. For example, the analysis of galaxies in $z \sim 1$ clusters showed that the stars in massive, early-type galaxies formed at $z > 2$ (e.g., Ellis et al. 1997; Stanford et al. 1998; van Dokkum & Stanford 2003; Holden et al. 2005). Investigating the galaxy population of (forming) clusters at $z > 2$ could provide knowledge of the formation process of such massive galaxies (e.g., Eggen et al. 1962; Baugh & Gaztanaga 1996). Also because clusters are the most extreme overdense regions in the Universe, they allow an efficient investigation of the interaction between galaxies and their environment (e.g., Miles et al. 2004; Tanaka et al. 2004; van Zee et al. 2004; Goto 2005; Nakata et al. 2005; Tran et al. 2005).

A second reason to study clusters is that they can place constraints on cosmology. The number density of massive clusters is a strong function of the fundamental cosmological parameters Ω_M and σ_8, and the evolution of cluster abundances with redshift depends primarily on Ω_M (e.g., Eke et al. 1996). The number density of rich clusters at $z > 0.5$ has already been successfully used to constrain the values of cosmological parameters (e.g., Bahcall et al. 1997; Bahcall & Fan 1998; Ettori et al. 2003).

Several studies of massive clusters with redshifts up to $z = 1.3$ have found little evolution in the cluster properties (e.g., Tozzi et al. 2003; Hashimoto et al. 2004; Maughan et al. 2004; Rosati et al. 2004). Despite the large lookback times, clusters at $z \sim 1$ appear to be very similar to local clusters. For example, the $z = 1.3$ cluster RDCS 1252.9-2927 has thermodynamical properties and metallicity that are very similar to those of lower redshift clusters (Rosati et al. 2004). To study when and how clusters and their galaxies formed, a sample of clusters at $z \gg 1$ is needed.

Unfortunately, conventional methods for finding distant clusters become impractical at $z > 1$. Searches for extended X-ray sources are difficult because the surface brightness of the X-ray emission fades as $(1 + z)^4$. Although large optical surveys have been successful in finding galaxy clusters at $z \lesssim 1$ by searching for concentrations of red galaxies (e.g., Gladders 2002), the detection of $z > 1$ clusters with the same method requires sensitive, wide field near-infrared cameras which are not yet available. In the future, surveys exploiting the Sunyaev-Zeldovich (SZ) effect (e.g., Carlstrom et al. 2002) will be able to detect clusters of galaxies at $z \gg 1$. However, at this moment the sensitivity of SZ surveys is not sufficient to detect any known clusters at $z > 1$.

A different approach is to search for a galaxy concentration near a presumed tracer of high-density regions. There is considerable evidence that powerful high redshift radio galaxies are forming massive galaxies in dense environments (e.g., Carilli et al. 1997; Dey et al. 1997; Athreya et al. 1998; Pentericci et al. 1998; Papadopoulos et al. 2000; Pentericci et al. 2000b; Archibald et al. 2001; Jarvis et al. 2001; De Breuck et al. 2002, 2003a,b; Stevens et al. 2003; Zirm et al. 2003; Reuland et al. 2004, see e.g. Carilli et al. 2001 for a review). Targeted searches for companion galaxies near powerful radio sources at $z > 1$ have long yielded promising results (Le Fèvre et al. 1996; Pascarelle

et al. 1996; Keel et al. 1999; Best 2000; Best et al. 2003; Barr et al. 2004).

We therefore started a large program with the Very Large Telescope (VLT) to systematically search for forming clusters near radio galaxies in the redshift range $2 < z < 5.2$. This program was initiated after a successful pilot project in which the environment of the radio galaxy MRC 1138–262 at $z = 2.16$ was investigated. Deep narrowband images of the radio galaxy and the surrounding field were obtained to search for an excess of Lyα emitting galaxies (Kurk et al. 2000). The imaging and follow-up spectroscopy resulted in ~ 40 candidate Lyα emitters (Kurk et al. 2000, 2004b) of which 15 were confirmed at $z = 2.16 \pm 0.02$ (Pentericci et al. 2000). The presence of a forming cluster that can be associated with MRC 1138–262 was firmly established by the subsequent discovery of significant populations of (spectroscopically confirmed) Hα emitters (Kurk et al. 2004a,b), QSOs (Pentericci et al. 2002) and extremely red objects (Kurk et al. 2004b). The VLT large program was augmented by observations with the Keck telescope.

In this paper, we present the results of our program to search for forming clusters near radio galaxies up to $z = 5.2$. Early results of the program, the discovery of galaxy overdensities at $z = 4.1$ and $z = 5.2$, are presented in Chapter 2 and in Chapter 4. A detailed analysis of the data obtained of the area surrounding the radio galaxy MRC 0316–257 at $z = 3.13$ is given in Chapter 3. In Chapter 3 the data reduction steps, selection procedure of candidate Lyα emitters and the assessment of the data quality are described in detail. Here we will follow the same steps as in Chapter 3 to reduce and analyse the data.

The structure of the paper is as follows: in §5.2.1 we present the targets of our program, and in §5.2.2–5.2.4 we give the details of the imaging observations, the selection of candidate Lyα emitters and follow-up spectroscopy. In §5.3, the results of the imaging and spectroscopy are described for each individual field. A summary of the results and the evidence for the presence of protoclusters near the radio galaxies are given in §5.4. The properties of the protoclusters are presented in §5.5, followed by a discussion of our results in §5.6.

In this article, we adopt a Λ-dominated cosmology with $H_0 = 70$ km s^{-1} Mpc^{-1}, $\Omega_M = 0.3$, and $\Omega_\Lambda = 0.7$. Magnitudes are given in the AB system (Oke 1974).

5.2 Observations

5.2.1 Sample selection

The targets for our program were selected from a list of approximately 150 radio galaxies that are known to have redshifts $z > 2$. We applied several selection criteria to maximize the probability that the selected radio sources are associated with forming massive galaxies. Our targets were chosen to have large radio luminosities ($L_{2.7\text{GHz}} > 10^{33}$ erg s^{-1} Hz^{-1} sr^{-1}) and they were required to be luminous in the optical and infrared. Because our goal was to search for companion Lyα emitting galaxies near the radio sources, a third selection criterion was that the radio galaxies had to have redshifts optimum for imaging with the narrow-band filters that were available at the VLT. Finally, the radio sources need to lie in the southern hemisphere ($\delta \lesssim 0°$) to allow deep imaging of the source with the VLT. Applying these criteria to the list of ~ 150 $z > 2$ radio

Name	α_{J2000}	δ_{J2000}	z	$L^a_{2.7\text{GHz}}$
BRL 1602–174	16 05 01.7	−17 34 18.4	2.04	2.0×10^{34}
MRC 2048–272	20 51 03.5	−27 03 04.1	2.06	6.3×10^{33}
MRC 1138–262	11 40 48.2	−26 29 09.5	2.16	1.3×10^{34}
MRC 0052–241	00 54 29.8	−23 51 31.1	2.86	8.6×10^{33}
MRC 0943–242	09 45 32.7	−24 28 49.7	2.92	7.2×10^{33}
MRC 0316–257	03 18 12.0	−25 35 10.8	3.13	1.4×10^{34}
TN J2009–3040	20 09 48.1	−30 40 07.4	3.16	2.8×10^{33}
TN J1338–1942	13 38 26.1	−19 42 30.8	4.10	9.6×10^{33}
TN J0924–2201	09 24 19.9	−22 01 42.0	5.20	1.5×10^{34}

^{a} Radio luminosity at a rest-frame frequency of 2.7 GHz
in $\text{erg s}^{-1}\,\text{Hz}^{-1}\,\text{sr}^{-1}$

Table 5.1 — Details of the radio galaxies observed in our program.

sources reduced the number of possible targets for our program to 16 of which nine are at $z \sim 2.1$ (this includes the target of our pilot project, MRC 1138–262 at $z = 2.16$), three are at $z \sim 2.9$ and four are at $z \sim 3.1$. To extend the redshift range, we purchased narrow-band filters that were centred on the wavelength of the Lyα line at a redshift of $z = 4.1$ and $z = 5.2$. The following nine radio sources were chosen as targets for our program: BRL 1602–174 (hereafter 1602), MRC 2048–272 (2048) and MRC 1138–262 (1138, all three at $z = 2.1$), MRC 0052–241 (0052) and MRC 0943–242 (0943, at $z = 2.9$), MRC 0316–257 (0316) and TN J2009–3040 (2009, both at $z = 3.1$), TN J1338–1942 (1338, $z = 4.1$) and TN J0924–2201 (0924, $z = 5.2$). The position, redshift and radio power of the targets are given in Table 5.1. Individual radio galaxies are briefly described in §5.3.

5.2.2 Imaging observations

To search for structures of Lyα emitting galaxies near the radio galaxies, the fields surrounding the radio galaxies were observed in a narrow-band filter and at least one broad-band filter. The narrow-band filters were chosen to encompass the Lyα line at the redshift of the radio galaxy, and the broad-band filters were selected to measure the UV continuum redward of the Lyα line.

All the narrow-band imaging and most of the broad-band imaging obtained in the large program were performed with the FOcal Reducer/ low dispersion Spectrograph 2 (FORS2; Appenzeller & Rupprecht 1992) in imaging mode. Before 2002 April, the detector in FORS2 was a SiTE CCD with 2048×2048 pixel^2 and a pixel scale of $0\overset{''}{.}2\,\text{pixel}^{-1}$. In 2002 April, the SiTE CCD was replaced by two MIT CCDs each with 2048×2048 pixel^2 with a scale of $0\overset{''}{.}125\,\text{pixel}^{-1}$. The pixels were binned by 2×2, which decreases the readout time by a factor of 2 and gives a pixels scale of $0\overset{''}{.}25\,\text{pixel}^{-1}$. The field of view, which is restricted by the geometry of the Multi-Object Spectroscopy unit, is $6\overset{'}{.}8 \times 6\overset{'}{.}8$.

Additional (broad-band) imaging was obtained using the Low Resolution Imaging Spectrometer (LRIS, Oke et al. 1995) on the Keck I telescope. LRIS has two arms: a blue channel which is optimised for observations in the blue part of the optical spectrum (LRIS-B, see McCarthy et al. 1998; Steidel et al. 2004, for more information) and a red channel for observing in the red (LRIS-R, Oke et al. 1995). The red arm is equipped with a Tektronix CCD with 2048×2048 pixel^2. The pixel scale is $0\overset{''}{.}21\,\text{pixel}^{-1}$, resulting

Table 5.2 — Overview of the imaging observations of the radio galaxy fields.

Date	Telescope	Instrument	Field	Filter	λ_c[a] (Å)	$\Delta\lambda$[b] (Å)	Seeing	t_{exp}[c]	Depth[d]
2001 Mar 24 & 25	VLT UT2	FORS2	1338-1[e]	FILT_621_5	6199	59	0."6	33 300	28.2
2001 Mar 24 & 25	VLT UT2	FORS2	1338-1[e]	Special *R*	6550	1650	0."6	6 300	28.9
2001 Mar 24–26	VLT UT2	FORS2	0943	HeII/6500	4781	68	0."7	22 500	28.6
2001 Mar 25 & 26	VLT UT2	FORS2	0943	Bessel *B*	4290	880	0."9	4 500	28.7
2001 Mar 25 & 26	VLT UT2	FORS2	1602	OII	3717	73	0."8	15 000	26.6
2001 Mar 26	VLT UT2	FORS2	1602	Bessel *B*	4290	880	0."65	2 700	27.6
2001 May 21–23	VLT UT2	FORS2	2048	OII	3717	73	0."95	25 200	27.9
2001 May 22 & 23	VLT UT2	FORS2	2048	Bessel *B*	4290	880	1."05	3 600	28.8
2001 Sep 20–22	VLT UT4	FORS2	2048	OII	3717	73	0."95	25 200	27.9
2001 Sep 20 & 21	VLT UT4	FORS2	2048	Bessel *B*	4290	880	1."05	3 000	28.8
2001 Sep 20 & 21	VLT UT4	FORS2	0316	OIII/3000	5045	59	0."7	23 400	28.4
2001 Sep 20 & 21	VLT UT4	FORS2	0316	Bessel *V*	5540	1115	0."7	4 860	28.9
2001 Sep 22	VLT UT4	FORS2	0052	HeII	4684	66	0."75	5 400	28.3
2001 Oct 20	VLT UT4	FORS2	0052	HeII	4684	66	0."75	18 000	28.3
2001 Oct 20	VLT UT4	FORS2	0052	Bessel *B*	4290	880	0."8	4 800	29.0
2002 Mar 8	VLT UT4	FORS2	0924	FILT_753_8	7528	89	0."8	14 400	28.1
2002 Mar 8	VLT UT4	FORS2	0924	Bessel *I*	7680	1380	0."8	2 700	28.5
2002 Apr 17–19	VLT UT4	FORS2	0924	FILT_753_8	7528	89	0."8	28 800	28.1
2002 Apr 17–19	VLT UT4	FORS2	0924	Bessel *I*	7680	1380	0."8	8 640	28.5
2002 Apr 17–19	VLT UT4	FORS2	1338-2[e]	FILT_621_5	6199	59	0."75	25 200	28.2
2002 Apr 17–19	VLT UT4	FORS2	1338-2[e]	Special *R*	6550	1650	0."75	4 500	28.9
2002 Apr 17–19	VLT UT4	FORS2	2009	OIII/3000	5045	59	0."9	21 600	28.0
2002 Apr 17–19	VLT UT4	FORS2	2009	Bessel *V*	5540	1115	0."85	4 800	28.6
2002 Apr 19	VLT UT4	FORS2	0924	Bessel *V*	5540	1115	1."05	3 600	28.6
2002 Sep 6–8	VLT UT4	FORS2	0316	Bessel *I*	7680	1380	0."7	4 680	28.7
2002 Sep 8	VLT UT4	FORS2	2009	OIII/3000	5045	59	0."9	7 200	28.0
2002 Sep 8	VLT UT4	FORS2	2009	Bessel *V*	5540	1115	0."85	2 400	28.6
2002 Sep 8	VLT UT4	FORS2	0052	Bessel *V*	5540	1115	0."75	5 400	29.2
2002 Sep 8	VLT UT4	FORS2	0052	Bessel *I*	7680	1380	0."55	4 800	28.5
2003 Jan 31	Keck I	LRIS-B	0316	*u'*	3550	600	1."25	4 050	29.8
2003 Feb 1 & 4	Keck I	LRIS-B	0316	*u'*	3550	600	1."25	9 000	29.8
2003 Feb 4	Keck I	LRIS-B	0943	*u'*	3550	600	1."2	9 600	29.8
2003 Feb 4	Keck I	LRIS-R	0943	*V*	5473	948	1."25	5 600	29.4
2004 Jan 19	Keck I	LRIS-B	0943	*u'*	3550	600	1."2	7 000	29.8
2004 Jan 19	Keck I	LRIS-R	0943	*I*	8331	3131	0."90	6 000	28.4

[a] Central wavelength of the filter in angstrom.
[b] Full width at half maximum (FWHM) of the filter in angstrom.
[c] Total exposure time in seconds.
[d] 1 σ depth of the resulting image in mag per $\square$".
[e] The field near TN J1338–1942 was observed at two different pointings, see §5.3.

in a field of view of $7'.3 \times 7'.3$. The blue channel has two 2k×4k Marconi CCDs with a pixel scale of $0''.135\,\mathrm{pixel}^{-1}$. There is a small gap between the CCDs of roughly $13''.5$. The field of view is $\sim 8' \times 8'$[1].

Observations were split into separate exposures of typically 1200–1800 s in the narrow-band and 240–800 s in the broad-band. Individual exposures were shifted $10''$–$15''$ with respect to each other to facilitate identifying cosmic rays and removing residual flat field errors. The data were reduced using standard reduction routines within the reduction software package IRAF[2]. These routines included bias subtraction

---

[1]The specifications for the blue channel detectors given here apply for data taken after 2002 June.

[2]IRAF is distributed by the National Optical Astronomy Observatories, which are operated by the Association of Universities for Research in Astronomy, Inc., under cooperative agreement with the Na-

Field	$m_{\rm lim}^a$	$F_{5\sigma}^b$ $\mathrm{erg\,s^{-1}\,cm^{-2}}$	$L_{5\sigma}^c$ $\mathrm{erg\,s^{-1}}$	N^d	Area^e arcmin^2
1602	24.4	9.7×10^{-17}	3.4×10^{42}	2	42.3
2048	25.4	3.3×10^{-17}	1.2×10^{42}	10	43.6
1138	25.2^f	3.5×10^{-17f}	1.4×10^{42f}	37^f	46.6^f
0052	26.1	1.1×10^{-17}	8.4×10^{41}	57	44.9
0943	26.1	7.4×10^{-18}	6.2×10^{41}	65	46.5
0316	26.3	6.9×10^{-18}	6.9×10^{41}	77	45.8
2009	25.7	1.3×10^{-17}	1.3×10^{42}	21	46.7
1338-1	26.0	4.7×10^{-18}	8.9×10^{41}	31^g	40.1
1338-2	26.2	5.8×10^{-18}	1.1×10^{42}	33^g	48.9
0924	25.5	7.0×10^{-18}	2.3×10^{42}	14	46.8

Table 5.3 — Depth, sensitivity and size of the imaging of the radio galaxies fields, and the number of candidates that is selected from the images.

^{a} Magnitude at which 50% of artificial and real point sources that were added to the narrow-band image, were recovered.

^{b} Flux of an emitter with no continuum that is detected at the 5σ level in an aperture with a diameter twice that of the seeing disc.

^{c} Luminosity of an emitter with no continuum that is detected at the 5σ level in an aperture with a diameter twice that of the seeing disc.

^{d} Number of candidate Lyα emitters that fulfils the selection criteria $EW_0 > 15$ Å and $EW_0/\Delta EW_0^- > 3$.

^{e} Imaging area useful for the selection of Lyα emitters.

^{f} Values taken from Kurk et al. (2004b).

^{g} The 1338-1 and 1338-2 fields overlap. The total number of unique candidate emitters in the two fields is 54.

using either bias frames or the overscan region of the CCD, flat fielding with twilight sky flats and illumination correction using the unregistered science frames.

All science images were registered on the ICRF astrometric frame of reference (Ma & Feissel 1998), using the USNO-A2.0 catalogue (Monet et al. 1998; Monet 1998). The relative positions of objects in the fields are accurate to 0.″1–0.″2. The absolute accuracy is dominated by the uncertainty in the USNO-A2.0 catalogue of 0.″25 (Deutsch 1999).

The photometric calibration was performed using several photometric and spectrophotometric standard stars from the catalogues of Stone & Baldwin (1983), Baldwin & Stone (1984), Oke (1990) and Landolt (1992). The magnitude zero points derived from these standard stars are consistent with each other within 2–3%. Zero points in the Vega system are converted to the AB system using the transformations of Bessell (1979) and Smith et al. (2002). The zero points were corrected for galactic extinction as estimated by Schlegel et al. (1998).

Table 5.2 summarizes the imaging observations of our Large Program targets and gives the properties of the narrow- and broad-band filters that were used. Also, the image quality (seeing) and depth (in 1 σ limiting magnitudes per square arcsecond) are given in Table 5.2.

5.2.3 Candidate selection

Objects in the images were detected using the program SExtractor (Bertin & Arnouts 1996). The narrow-band images were taken to detect objects, and aperture photometry was subsequently performed on both the narrow-band and the broad-band images.

To assess the completeness of the source detection, artificial and real point sources were added to narrow-band image and recovered. The completeness limit was defined as the narrow-band magnitude at which 50% of the added sources was recovered.

Detected objects were required to have a signal-to-noise of > 5 in the narrow-band image. The colors of the detected objects were measured in circular apertures, while the "total" flux was measured in an elliptical aperture. A correction was made to the "total" flux to account for the flux outside the elliptical aperture. More details on the object detection, completeness assessment, aperture sizes for the photometry and "total" flux correction can be found in Chapter 3.

Following Chapter 3 and 4, we selected objects with a rest-frame equivalent width $EW_0 > 15$ Å and a significance $\Sigma \equiv EW_0 / \Delta EW_0^- > 3$ as good candidate Lyα emitters. In Chapter 3 a detailed description is presented on how EW_0 and Σ are computed from the available photometry. For two fields that are imaged in at least two broad-band filters, the 0316 and 0052 fields, the UV continuum slope β ($f_\lambda \propto \lambda^\beta$) of candidate emitters was also computed. For the other fields, a "flat" continuum slope $\beta = -2$ was used to select the candidates, which is close to the median β of confirmed Lyα emitters in the 0316 field ($\beta = -1.76$, Chapter 3). In each field the candidate emission line galaxies were visually inspected and spurious sources (like spikes of bright, saturated stars) were removed from the catalogues. The resulting lists should have a very low fraction of contaminants ($\sim 5\%$ as esimated in Chapter 3).

In Table 5.3 the 50% completeness limit, number of candidate emitters and area of each observed field is printed. We also calculated the 5σ limiting line flux and luminosity of an emitter with a negligible continuum. The number of candidates in the 1138 field is taken from Kurk et al. (2004b).

5.2.4 Spectroscopic observations

To confirm whether the candidate emission line objects are located at the redshift of the radio galaxy, spectra were taken of good candidate emitters. When taking spectra priority was given to the most luminous line emitters. In Table 5.4 a summary is given of the spectroscopic observations of candidate emitters in the radio galaxy fields.

Most of the spectroscopic observations were performed using user-defined masks (the multi-object spectroscopy (MXU) mode of FORS2 and multi-slit spectroscopy (MSS) modes of LRIS in Table 5.4). This mode allowed us to observe between ~ 20 and 40 objects per slitmask. The slits typically had a length of 10–12 $''$ and a width of $1\rlap{.}''0$–$1\rlap{.}''4$. The grisms used were selected to have the highest throughput at the wavelength of the Lyα line of the radio galaxy and a resolution that matches the width of the Lyα lines (~ 300 km s^{-1}, Chapter 3) to maximize the confirmation rate.

Individual exposures were typically 1800–2700 s, which ensured that the spectra were limited by the sky noise. Between the exposures the pointing of the telescope was shifted 2$''$–5$''$ along the slits to enable more accurate sky subtraction. For the flux

Table 5.4 — Overview of the spectroscopic observations of the radio galaxy fields.

Date	Telescope	Instrument	Field	Mode[a]	Grism name	Dispersion[b]	Resolution[c]	t_{exp}^d
2001 May 20 & 22	VLT UT2	FORS2	1338-1	MXU, mask A	GRIS_600RI	1.32	$260 \times 1{.}''0$	31 500
2001 May 21 & 22	VLT UT2	FORS2	1338-1	MXU, mask B	GRIS_600RI	1.32	$265 \times 1{.}''0$	35 100
2001 Sep 22	VLT UT4	FORS2	0316	MOS	GRIS_1400V	0.50	$130 \times 1{.}''5$	12 600
2001 Oct 18 & 19	VLT UT4	FORS2	2048	MXU	GRIS_600B	2.40	$410 \times 1{.}''0$	16 200
2001 Oct 18	VLT UT4	FORS2	0316	MXU, mask A	GRIS_1400V	1.00	$140 \times 1{.}''0$	10 800
2001 Oct 18–20	VLT UT4	FORS2	0316	MXU, mask B	GRIS_1400V	1.00	$140 \times 1{.}''0$	29 100
2001 Nov 15 & 16	VLT UT3	FORS1	0316	PMOS	GRIS_300V	2.64	$630 \times 0{.}''8$	19 800
2002 Jan 14	Keck I	LRIS	0943	MSS, mask A	600/4000	1.01	$310 \times 0{.}''85$	10 800
2002 Jan 15	Keck I	LRIS	0943	MSS, mask B	600/4000	1.01	$325 \times 0{.}''9$	9 000
2002 Sep 6 & 7	VLT UT4	FORS2	2009	MXU	GRIS_1400V	0.62	$109 \times 0{.}''75$	19 800
2002 Sep 6	VLT UT4	FORS2	0052	MXU, mask A	GRIS_1400V	0.62	$102 \times 0{.}''65$	8 400
2002 Sep 6 & 7	VLT UT4	FORS2	0052	MXU, mask B	GRIS_1400V	0.62	$102 \times 0{.}''65$	17 550
2002 Sep 7	VLT UT4	FORS2	0052	MXU, mask C	GRIS_1400V	0.62	$94 \times 0{.}''6$	10 800
2002 Sep 8	VLT UT4	FORS2	0052	MOS	GRIS_1400V	0.62	$94 \times 0{.}''6$	9 600
2003 Jan 31	Keck I	LRIS	0943	MSS, mask C	600/4000	0.61	$205 \times 0{.}''7$	7 200
2003 Feb 1	Keck I	LRIS	0943	MSS, mask D	600/4000	0.61	$215 \times 0{.}''75$	7 200
2003 Feb 1 & 4	Keck I	LRIS	1338-2	MSS	400/8500	1.85	$319 \times 0{.}''75$	9 000
2003 Mar 3 & 4	VLT UT4	FORS2	0924	MXU	GRIS_600RI	1.66	$223 \times 0{.}''85$	20 676
2003 Mar 4	VLT UT4	FORS2	1338-2	MXU	GRIS_1200R	0.76	$124 \times 0{.}''85$	18 600

[a] Explanation of the different observing modes:
MOS: Multi-object spectroscopy mode of FORS2, performed with 19 movable slitlets with lengths of 20″–22″.
MXU: Multi-object spectroscopy mode of FORS2 with a user-prepared mask.
PMOS: Spectropolarimetry mode of FORS1 using 9 movable slitlets of 20″.
MSS: Multi-slit spectroscopy mode of LRIS, which uses a custom laser-cut mask.
[b] Dispersion in Å pixel^{-1}.
[c] The resolution is given for both the dispersion and spatial axis. The units are [km s^{-1}] × [″].
[d] Total exposure time in seconds.

calibration long slit exposures of (at least) one of the following spectroscopic standard stars EG 274, Feige 67, Feige 110, GD 108, LTT 377, LTT 1020, LTT 1788, LTT 6248 and LTT 7987 (Stone & Baldwin 1983; Baldwin & Stone 1984; Oke 1990) were used. The flux calibration is accurate to about $\sim 5\%$. This does not take into account the uncertainties due to slit losses. Because we are more interested in the redshift of the galaxies than in the total strength of the emission line, we did not attempt to correct the spectra for flux falling outside the slit.

The details of the reduction of the spectroscopic data is given in Chapter 3. In the next section, we will describe the results in the individual fields.

5.3　Results

In this section we describe the results of the imaging, candidate selections and follow-up spectroscopy of the Lyα emitters in each of the radio galaxy fields. For the details of the results in the 1138, 0316 and 0924 fields we refer to Chapter 3, Chapter 4, Kurk et al. (2000), Pentericci et al. (2000)and Kurk et al. (2004b). Below a brief summary of the results in these fields is given.

The redshift and the properties of the Lyα lines were measured by fitting a Gaussian function to the emission line. If absorption was clearly present, a combination of a Gaussian and a Voigt absorption profile was fitted. The properties of the confirmed Lyα emitters in the various fields are summarized in Tables 5.6–5.10. In the Tables, the
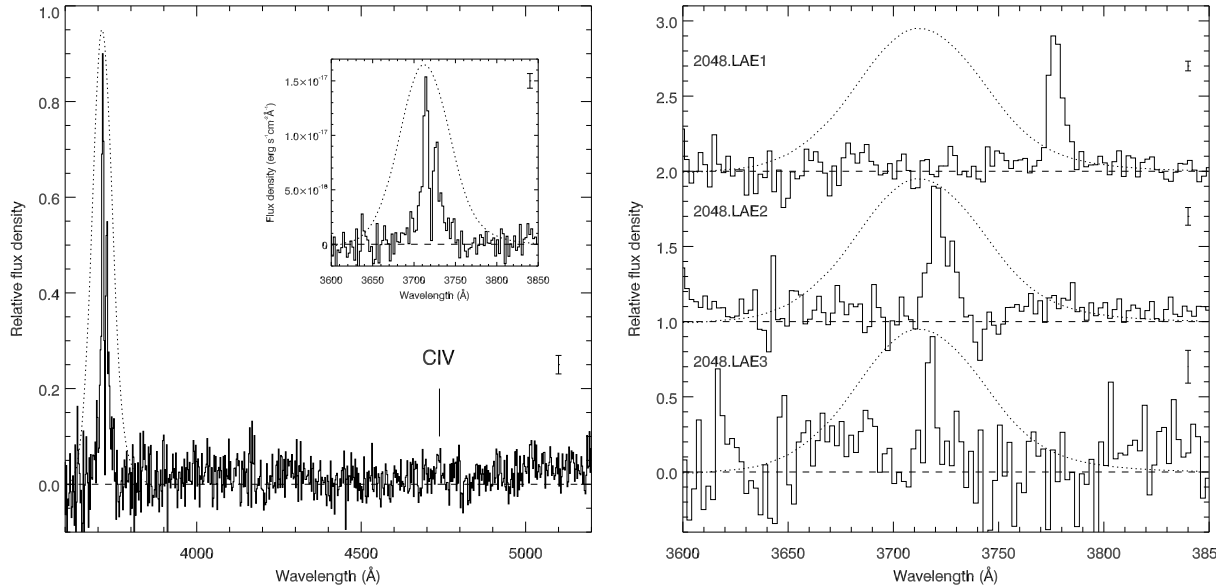
Figure 5.1 — Spectra of the radio galaxy MRC 2048–272 (*left*) and the three confirmed Lyα emitters near the radio galaxy (*right*). The dashed curve represents the transmission of the narrow-band filter that was used to select the candidate Lyα emitters. The error bars in the left corners of the spectra show the uncertainty in the flux density.

objects are ordered on increasing right ascension.

5.3.1 BRL 1602–174, $z = 2.04$

The radio source BRL 1602–174 was optically identified with a galaxy with $m_R = 21.4$ aligned along the radio axis by Best et al. (1999). A spectrum of this galaxy yielded a redshift of 2.043 ± 0.002 based on four emission lines (Best et al. 1999). This places the Lyα line of the radio galaxy in the lowest wavelength narrow-band filter available for FORS2, the O II filter. The field was imaged for 250 minutes in the narrow-band and for 45 minutes in the *B*-band. Due to the high extinction towards this field ($A_B \approx 1$, Schlegel et al. 1998) and the low quantum efficiency at wavelength < 4000 Å of the FORS2 detector, only two candidate Lyα emitters were found. No spectra were taken in this field.

5.3.2 MRC 2048–272, $z = 2.06$

MRC 2048–272 was listed in the 408 MHz Molonglo Reference Catalogue (Large et al. 1981) and identified with a $z = 2.06$ object by McCarthy et al. (1996). High resolution imaging in the infrared with the *HST* revealed three separate components within $3''$ (Pentericci et al. 2001), of which the central object was identified as the radio galaxy. The surface brightness of the central object could be well fit by a de Vaucouleurs profile, indicating that a dynamically relaxed stellar population was already in place in this radio galaxy (Pentericci et al. 2001).

Imaging observations

We observed the field in 2001 May under moderate seeing conditions ($\sim 1''$) for 7 hours in the O II narrow-band filter and for 1 hour in the *B*-band. Because of the low efficiency of the detector at $\lambda < 4000$ Å, the field was imaged again in 2001 September. The combined 14 hours of narrow-band observations of this field have a depth comparable to that of the field surrounding MRC 1138–262 (Kurk et al. 2000, Table 5.3). In total 10 candidate Lyα emitters were found in this field. The number of contaminants is expected to be low in this field, because the only strong line that falls in the filter is [O II] $\lambda 3727$ at a redshift of $z < 0.007$.

Spectroscopic observations

Due to geometrical constraints only three of the candidate emitters could be observed at the same time. Additional targets were included on the slitmask, including objects with a low equivalent width ($EW_0 < 15$ Å. Two of the three good candidates and the radio galaxy show a line in a 4 hr spectrum (see Table 5.6 and Fig. 5.1). The third emitter has most likely an emission line that is too faint to be confirmed in a 4 hr spectroscopic observation. The two confirmed emitters have a redshift very close to that of the radio galaxy with relative velocities of 100 and 10 km s^{-1}. A third Lyα emitter was found among the candidate emitters with a lower equivalent width. This galaxy is a bright Lyα emitter located ~ 4600 km s^{-1} away from the radio galaxy, with the emission line at the edge of the narrow-band filter (Fig. 5.1).

Volume density

Comparing the volume density of Lyα emitters near MRC 2048–272 to that of emitters near MRC 1138–262 (Kurk et al. 2004b), the density in the 2048 field is a factor $3.4^{+1.8}_{-1.2}$ smaller. The large errors are due to small number statistics. Kurk et al. (2004b) found that the 1138 field is overdense in Lyα emitters by a factor of 4 ± 2 compared to the field density of Lyα emitters as derived by Stiavelli et al. (2001). Using this factor, the volume density of emitters near 2048 is $1.2^{+0.8}_{-0.7}$ times the field density of emitters. A direct comparison with Stiavelli et al. (2001) gives a density in the 2048 field of $n_{2048}/n_{\text{field}} = 0.7^{+1.8}_{-0.6}$, consistent with no overdensity of emitters near the radio galaxy.

5.3.3   MRC 1138–262, *z* = 2.16

This radio galaxy was the target of our pilot project. Narrow- and broad-band imaging with FORS1 on the VLT resulted in the detection of 37 candidate Lyα emitters (Kurk et al. 2000, 2004b). Subsequent spectroscopy confirmed 15 Lyα emitters to be near the radio galaxy at $z = 2.16$ (Pentericci et al. 2000). The density of Lyα emitters in this field is roughly a factor 4 higher as compared to field studies (Pentericci et al. 2000; Kurk et al. 2004b). This field is also overdense in X-ray sources (Pentericci et al. 2002) and extremely red objects (EROs, Kurk et al. 2004b). More recently, nine Hα emitters were spectroscopically confirmed to be associated with the radio galaxy (Kurk et al. 2004a,b), increasing the number of confirmed protocluster members to 25.

Figure 5.2 — Spectra of low redshift emission line galaxies which could contaminate our sample. These spectra were observed through the 1400V grism that was used for the spectroscopy sessions of the 0052, 0316 and 2009 fields. Due to the resolution of $R = 2100$, the low redshift interloping galaxies can be distinguished from Lyα emitters.
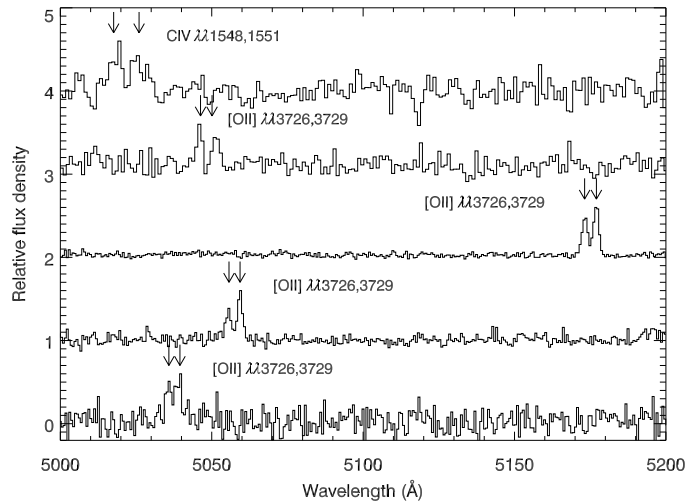
5.3.4 MRC 0052–241, $z = 2.86$

Imaging and spectroscopic observations

The optical counterpart of the radio source 0052–241 from the Molonglo Reference Catalogue (Large et al. 1981) was found by McCarthy et al. (1996) to be a $m_R = 23.2$ object. A spectrum of this object showed strong Lyα emission at a redshift of $z = 2.86$ (McCarthy et al. 1996). At this redshift the Lyα line is shifted into the FORS2 narrowband He II filter. The field was imaged for 390 minutes in this narrow-band and for 80, 90 and 80 minutes in the *B*-band, *V*-band and *I*-band respectively (Table 5.2). Analysis of these data resulted in a list of 57 candidate Lyα emitters with $EW_0 > 15$ Å and $EW_0/\Delta EW_0^- > 3$.

Follow-up spectroscopy of candidate emitters was carried out in 2002 September at the VLT. 36 candidates were observed in four masks with individual exposure times between 140 and 292.5 minutes under good seeing conditions (0″.6–0″.65, see Table 5.4). The resolution of the grism that we used (the 1400V grism) is $R = 2100$, which is high enough to resolve the [O II] $\lambda\lambda3726, 3729$ and C IV $\lambda\lambda1548, 1551$ doublets (see Fig. 5.2 for a few examples). Objects with these emission lines in their spectrum are the main contaminants in searches for $z \sim 3$ Lyα emitters (e.g., Fynbo et al. 2003). The high resolution of the 1400V grism allows us to discriminate high redshift Lyα emitters from low redshift interlopers.

Results

Of the 36 objects observed 35 were confirmed to be Lyα emitters at a redshift $z \sim 2.86$. The 36th candidate was most likely too faint to be confirmed. The candidate had the smallest line flux of the emitters in the mask. In addition to the 36 good candidates, four objects from a list with 20 candidate line emitters with 8 Å $< EW_0 < 15$ Å were observed. Two of them were confirmed to be Lyα emitters at $z \sim 2.86$. One of these, emitter 0052.LAE36, has a Lyα line that falls at the red edge of the filter. Using the measured redshift (instead of $z = 2.86$) the calculated equivalent width is $EW_0 \sim 24$ Å. The spectra of the 37 confirmed Lyα emitters and that of the radio galaxy are shown in Fig. 5.3.
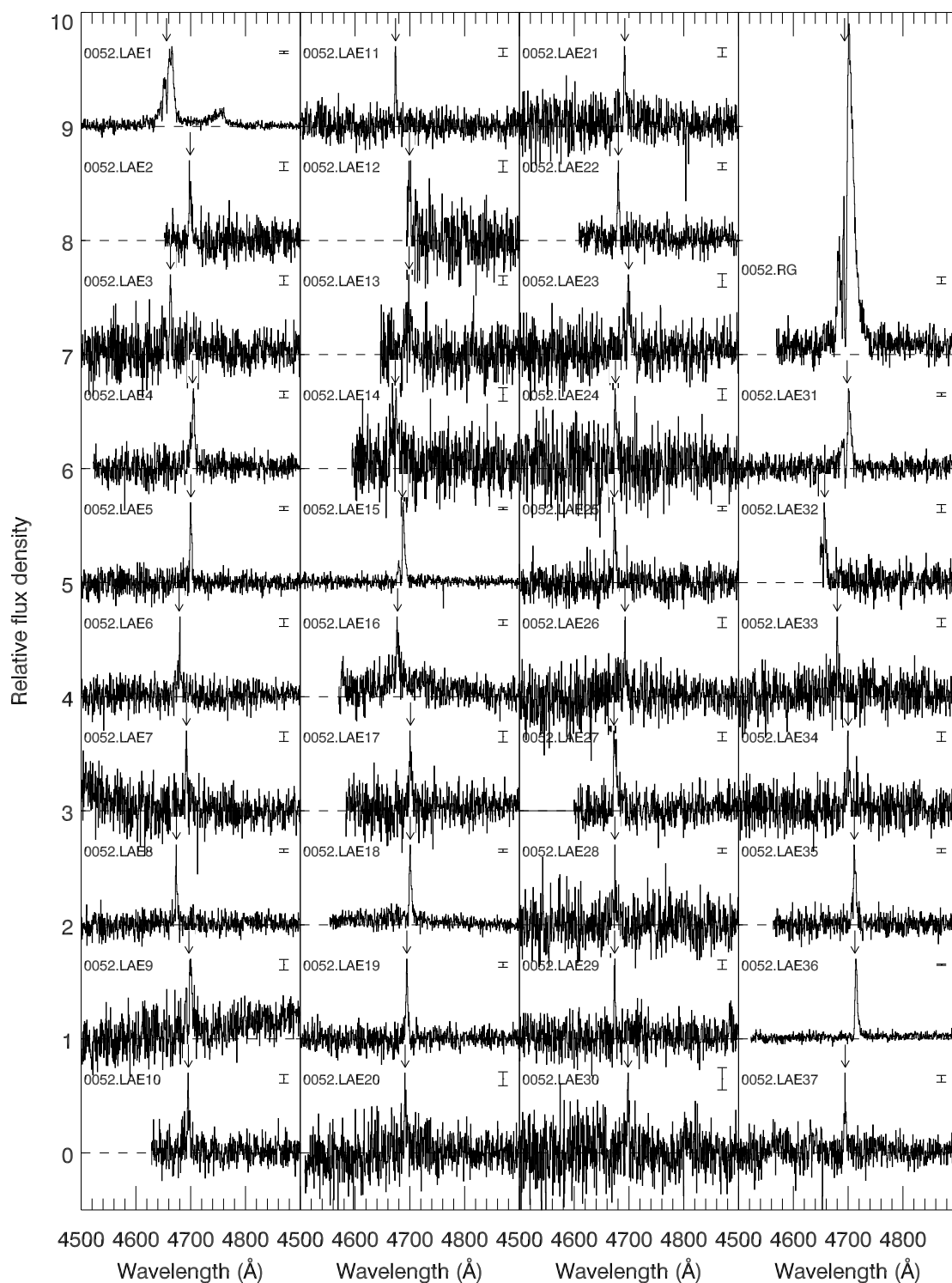
Figure 5.3 — Spectra of the confirmed emitters near the radio galaxy MRC 0052–241. The spectrum of the radio galaxy is shown in the top-right corner of the Figure. Error bars are shown on the right of each spectrum. All spectra are normalized to the peak of the Lyα line at a relative flux of 0.7. The offset between the spectra is 1.0. The arrow indicates the redshift of each emitter. The redshift, flux and width of the emission lines can be found in Table 5.7.
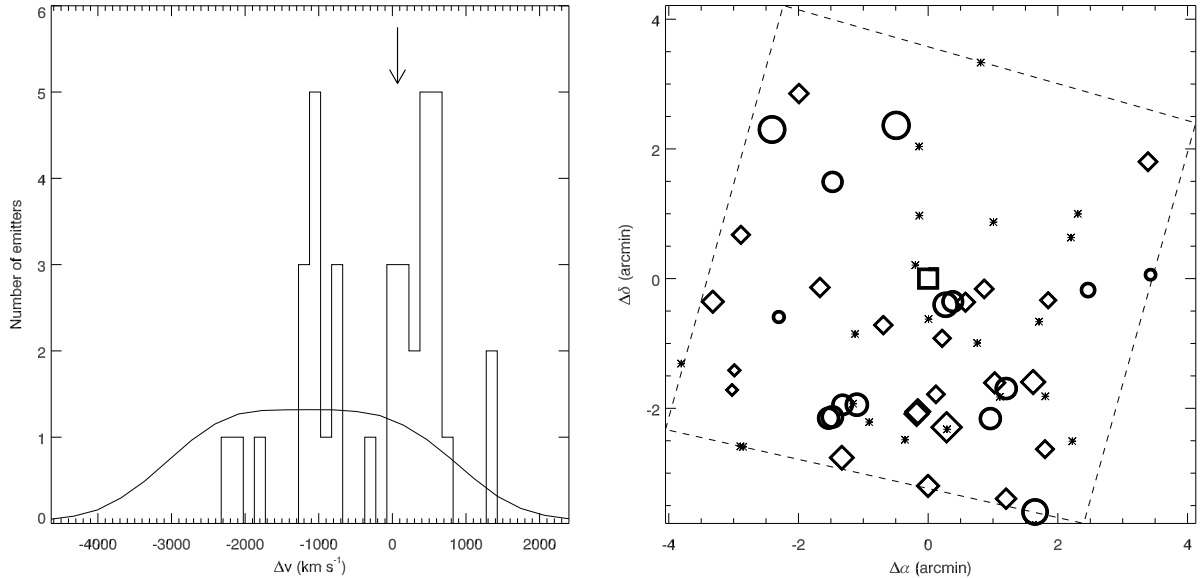
Figure 5.4 — *Left:* Velocity distribution of the confirmed emitters near MRC 0052–241. The median of the emitters is taken as zero point. The bin size is 150 km s^{-1}. The velocity of the radio galaxy is indicated by an arrow. The solid line represents the selection function of the narrow-band filter, normalized to the total number of confirmed emitters. *Right:* Spatial distribution of the confirmed (circles and diamonds) and candidate (stars) Lyα emitters. The dashed quadrangle represents the outline of the imaging area. The radio galaxy is denoted by a square. The circles represent the emitters with a redshift smaller than the median redshift ($z < 2.8600$) and the diamonds the ones with $z > 2.8600$. The size of the symbols are scaled according to the velocity offset from the median, with smaller symbols standing for emitters with a redshift farther from the median.

Volume density

The density of Lyα emitters can be compared directly to the field density of emitters. Fynbo et al. (2003) used the same narrow-band filter at the VLT to observe a field which contains a damped Lyα absorber. The depth they reach in their images is approximately 0.7 mag deeper compared to our narrow-band image, making their observations suitable for comparison. Fynbo et al. (2003) find 14 emitters (of which 13 are spectroscopically confirmed) with a Lyα flux $> 8 \times 10^{-18}$ erg s^{-1} cm^{-2} and a rest-frame equivalent width > 15 Å. To the same limit, we find 48 emitters. This implies that the overdensity in the 0052 field is $3.4^{+1.5}_{-1.0}$.

Due to cosmic variance, the uncertainty in the number density of Lyα emitters in a small field of view like that of the VLT images is generally higher than the uncertainty derived assuming Poisson statistics (e.g., Somerville et al. 2004). To overcome this, a comparison can be made with the density of Lyα emitters at $z \sim 3.1$ in a 0.13 deg^2 field as found by Ciardullo et al. (2002). This comparison gives a density of $2.5^{+1.8}_{-1.1}$. The large errors are due to the small number statistics. More recently, Hayashino et al. (2004) measured the blank field space density of Lyα emitters at $z \sim 3.1$ using the Suprime-Cam on the Subaru telescope. In a 0.17 deg^2 field, they find 55 candidate Lyα emitters with an observed equivalent width > 154 Å down to a narrow-band magnitude of 25.3. Applying the same equivalent width and magnitude criteria to our field

and taking into account the difference in luminosity distance gives 11 sources. The resulting density of emitters near MRC 0052-241 is a factor $3.1^{+1.4}_{-1.0}$ higher than the field density. The weighted average of the three estimates of the overdensity is $3.0^{+0.9}_{-0.6}$.

It is interesting to compare the density of Lyα emitters in the 0052 field with the density of emitters near the radio galaxy MRC 0316–257 at $z = 3.13$ (Chapter 3). The depth and sensitivity of the imaging of the two fields are very similar (see Tables 5.2 and 5.3). There are 52 candidate emitters in the 0052 field with a narrow-band magnitude brighter than 26.1, against 59 in the 0316 field. Taking into account the difference in the volume probed by the narrow-band images, the ratio of the number density is $n_{0052}/n_{0316} = 0.8^{+0.2}_{-0.2}$. Because the 0316 field is overdense in Lyα emitters by a factor $3.3^{+0.5}_{-0.4}$ (Chapter 3), this means that the 0052 field has an overdensity of Lyα emitting galaxies of $2.7^{+0.8}_{-0.6}$, which is consistent with the other estimates.

Velocity and spatial distributions

The velocity histogram and the spatial distribution of the candidate and confirmed emitters are shown in Fig. 5.4. The redshifts of the confirmed emitters are not uniformly distributed throughout the narrow-band filter (solid curve in Fig. 5.4). Instead, the majority of the emitters (31 out of the 37) appear to be clustered in two groups with velocity dispersions of 180 and 230 km s^{-1}. Using Monte-Carlo simulations, we estimate that the chance that such a clumpy redshift distribution is drawn from a random sample is only 0.04%. Interestingly, a similar redshift distribution was found near the radio galaxy MRC 1138–262 (Pentericci et al. 2000). The velocity of the radio galaxy lies $\sim$70 km s^{-1} from the median redshift of the emitters and falls inside one of the two groups. The combination of the observed overdensity of Lyα emitters with the clumpy redshift distribution provides evidence that the Lyα emitters near MRC 0052-241 are part of a forming cluster of galaxies at $z = 2.86$.

In contrast to the velocity distribution, the emitters do not have a preferred location on the sky. The structure of emitters appears not to be bounded by the image, indicating that the overdensity seen in this field extends beyond the edges of our field of view.

5.3.5 MRC 0943–242, $z = 2.92$

This powerful radio source with a flux density of 1.1 Jy at 408 MHz has a redshift of $z = 2.923$ (Röttgering et al. 1995; Röttgering et al. 1997). The radio galaxy is surrounded by a metal-enriched, low surface brightness gas halo extending for at least 8 $''$ (67 kpc, Villar-Martín et al. 2003). The estimated dynamical mass of the gas halo is $7 - 44 \times 10^{11}$ $M_\odot$ (Villar-Martín et al. 2003; Jarvis et al. 2003). This could be an indication that we are witnessing the formation of a massive galaxy.

Imaging and spectroscopic observations

The field surrounding the radio galaxy was observed with the VLT in 2001 March. Images were taken in the narrow-band for 375 min and 75 min in the *B*-band (Table 5.2). A part of the field (1.1 arcmin^2) was not usable to search for Lyα emitters due to the presence of a bright star (*R* magnitude of 8.7) located $2''.5$ to the north-west of the radio galaxy. A total of 65 emission line candidates with $EW_0 > 15$ Å and $\Sigma > 3$ is
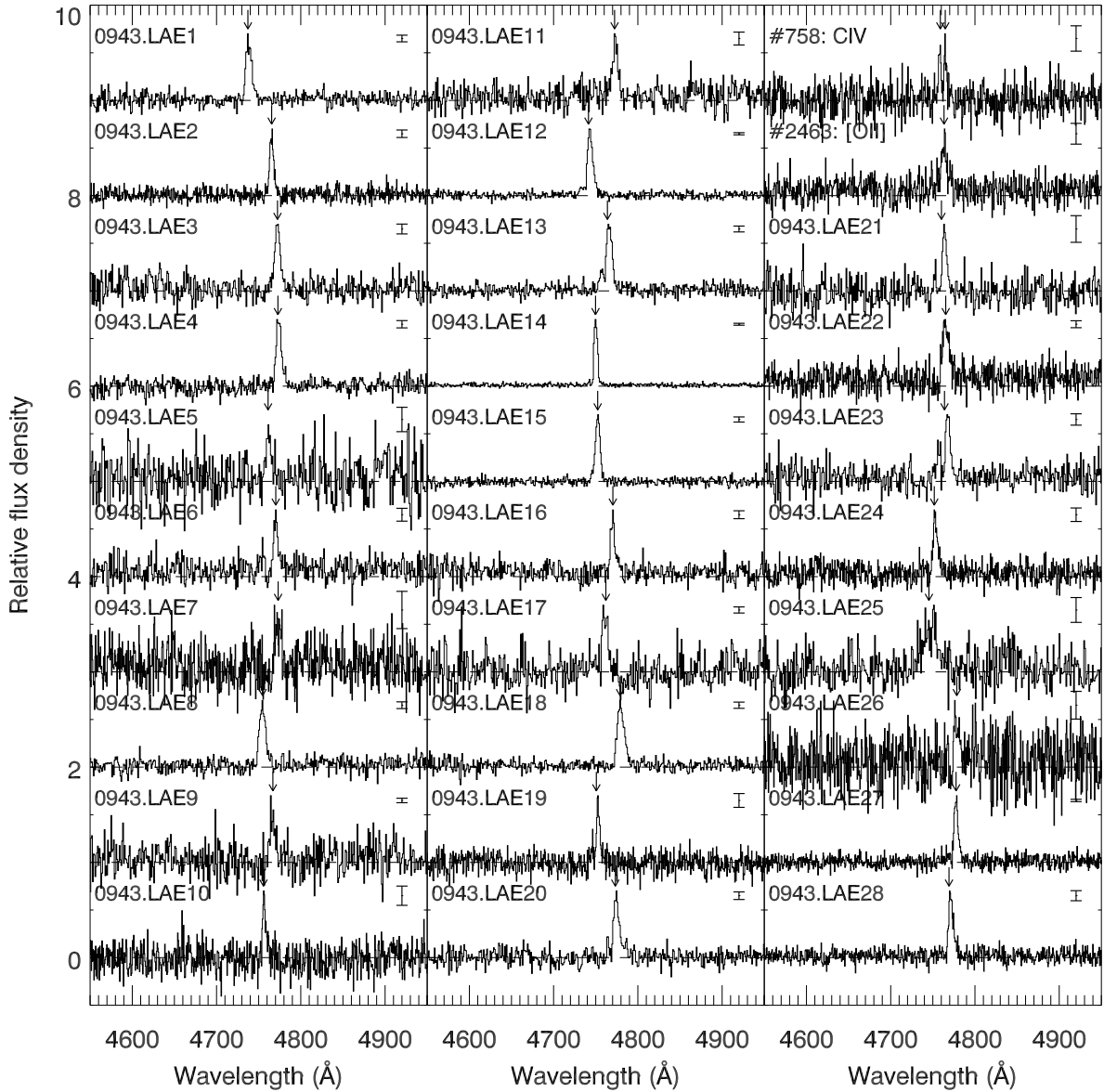
Figure 5.5 — Spectra of the confirmed emitters near the radio galaxy MRC 0943–242. Error bars are shown on the right of each spectrum. All spectra are normalized to the peak of the Lyα line at a relative flux of 0.7. The offset between the spectra is 1.0. The arrow indicates the redshift of the emitters. The redshift, flux and width of the emission lines can be found in Table 5.8.

found in the images.

Additional images of the field were taken in 2003 February and 2004 January with the LRIS instrument on the Keck I telescope. Observations were done in the u'-band (for 277 min), V-band (93 min) and I-band (100 min). The main purpose to take these images is to search for Lyman-break galaxies in the field. In this paper we use the images only to separate possible Lyα emitters at $z \sim 2.9$ from low redshift line emitters.

Follow-up spectroscopy was carried out during two observing sessions with LRIS on Keck I. In total, four user-defined slitmasks were observed with exposure times be-

tween 120 and 180 min (Table 5.4). In the four masks, 30 of the 65 candidate Lyα emitters were observed. Of these 30 objects, 26 showed an emission line at a wavelength expected for Lyα at $z = 2.9$, the remaining four did not show a line (or continuum) in their spectrum. These four unconfirmed emitters were among the five faintest emitters observed. Most likely, the emission lines of the four objects are too faint to be confirmed. In addition to the 26 confirmed emission line galaxies, four objects which had a predicted Lyα equivalent width < 15 Å also showed an emission line in their spectrum. The spectra of these 30 emission line objects are shown in Fig. 5.5.

Line identification

The next question is whether these 30 line emitters are due to Lyα at $z \simeq 2.9$. In contrast to the observations of the 0052 field, the resolution of the spectra was not high enough to resolve the [O II] doublet.

For three galaxies the redshift could be securely derived. One of these objects (# 758 in Fig. 5.5) is identified as a C IV $\lambda\lambda1548, 1551$ emitter at $z = 2.07$ as its emission line is resolved into two lines separated by ~ 8 Å. The redshifts of two other objects are confirmed by the presence of other emission lines in their spectrum. In the spectrum of emitter 0943.LAE25 N V $\lambda1240$ is detected, confirming that the object is a Lyα emitter at $z \sim 2.90$. The redshift of emitter 0943.LAE18 ($z \sim 2.93$) is confirmed by the detection of C IV $\lambda1549$ (and a very weak detection of He II $\lambda1640$). The relatively small *FWHM* of the Lyα line (*FWHM* $= 700$ km s^{-1}) suggests that this object is a type-II QSO (e.g., Norman et al. 2002).

The remaining 27 sources merely show a single emission line in their spectra, which typically cover a wavelength range over 5500 Å. The most numerous and brightest low redshift emission line galaxies that contaminates searches of $z \sim 3$ Lyα emitters are [O II] $\lambda\lambda3726, 3729$ emitters (e.g., Fynbo et al. 2003). To distinguish high redshift Lyα emitters from low redshift emission line galaxies, various tests can be applied (see Stern et al. 2000, for a detailed review). Below we will briefly describe and apply three tests (the asymmetry of the emission line, the presence of a continuum break and the limits on accompanying emission lines) that are frequently used in the literature to discriminate Lyα emitters from low redshift galaxies (e.g., Stern et al. 2000; Fynbo et al. 2001; Rhoads et al. 2003; Dawson et al. 2004, Chapter 4).

• *Emission line asymmetry.* This test, which makes use of the characteristic blue wing absorption profile of the Lyα emission line, has been successfully applied to confirm $z > 4.5$ Lyα emitters (e.g., Kodaira et al. 2003; Rhoads et al. 2003; Dawson et al. 2004; Hu et al. 2004). What makes this test extra useful is that a blended [O II] doublet would appear as a single line with *excess* emission on the blue side. To quantify the asymmetry of an emission line, Rhoads et al. (2003) introduced the two asymmetry parameters a_λ ("wavelength ratio") and a_f ("flux ratio"). These parameters depend on the wavelength where the flux peaks (λ_p), and where the flux is at 10% of the peak value on the red side ($\lambda_{10,r}$) and the blue side ($\lambda_{10,b}$) of the emission line. Using these wavelengths, the "wavelength ratio" is defined as $a_\lambda = (\lambda_{10,r} - \lambda_p)/(\lambda_p - \lambda_{10,b})$ and the "flux ratio" as $a_f = \int_{\lambda_p}^{\lambda_{10,r}} f_\lambda d\lambda / \int_{\lambda_{10,b}}^{\lambda_p} f_\lambda d\lambda$ (Rhoads et al. 2003, 2004; Dawson et al. 2004). Dawson et al. (2004) found that $z = 4.5$ Lyα emitters have $a_\lambda > 1.0$ and/or $a_f > 1.0$, while [O II]

emitters at $z \sim 1$ have $a_\lambda \approx 0.8$ and $a_f \approx 0.8$.

However, this line asymmetry test critically depends on the assumption that a large fraction of the blue part of the Lyα emission line is absorbed. Although absorption is often present, there can still be a significant amount of flux on the blue wing (see the emission lines in e.g. Fig. 5.3, Tapken et al. 2004,Chapter 3). Also, the peak of the Lyα line could move to the red, reducing the red wing flux (see e.g. the spectra on the left side of Fig. 5.9 and the spectra in Chapter 3). As a consequence, the asymmetry parameters for a Lyα line can be smaller than 1.0. For example, if the spectrum of the radio galaxy MRC 0943–242 would be convolved with a Gaussian with a *FWHM* $\approx$ 250 km s^{-1} (or would be observed with slightly lower resolution), then the asymmetry parameters would give $a_l = 0.67$ and $a_f = 0.92$. Also, the asymmetry parameters of emitter 0052.LAE1, which is a QSO at $z = 2.86$ with confirming N V, are $a_l = 0.48$ and $a_f = 0.38$ and those of emitter 0052.LAE31 measure $a_\lambda = 1.0$ and $a_f = 0.41$. Thus, while lines with $a_\lambda > 1.0$ or $a_f > 1.0$ are most likely Lyα lines, a profile with low values of a_λ and a_f can be either an [O II] or a Lyα line.

With this caveat in mind, we measured the asymmetry of our single emission line sources. 21 have $a_\lambda > 1.0$ and/or $a_f > 1.0$, and these emission lines are most likely Lyα lines at $z \simeq 2.8$. The identification of the remaining six lines remains unclear and we have to rely on others tests to secure the redshift.

• *Continuum break*. A prominent feature of high redshift galaxies is the absorption of the continuum blueward of the Lyα line, caused by neutral Hydrogen located in the galaxy between the galaxy and the observer (e.g., Madau 1995). To measure whether the continuum of the line emitters has a discontinuity, we looked at the u'- and V-band images. For a galaxy at $z = 2.9$ the central wavelength of the u' filter lies below the 912 Å Lyman limit, while the V-band begins just redward of the Lyα line. Based on a large imaging and spectroscopic survey of high redshift galaxies, Cooke et al. (2004) estimate that the vast majority of galaxies at $z \sim 3$ have a break of $u' - V > 1.2 - 1.6$. In contrast, low redshift objects with the Balmer/4000 Å break that falls between the u'- and V-band have a color of $u' - V \ll 1.5$ (e.g., Hammer et al. 1997).

Of the 27 single emission line sources, 26 were inside the field of view of the u'-band image. Two objects were too close to a bright foreground object to reliably measure the magnitude. Of the remaining 24 sources two are detected in the u'-band, the others are not detected. The undetected emitters have typically 2σ limits of $m_{u'} > 27.6$ within an aperture radius of 1″.2, which is twice the radius of the seeing disc. One of the two detected objects in the u'-band has a signal-to-noise of ~ 2.0 and a $u' - V \simeq 2.5$ is measured for this object. The second detection, of emitter # 2463 in Fig. 5.5, has a signal-to-noise of 8 and a $u' - V = 1.0$. Combined with a measured line asymmetry of $a_\lambda = 0.7$ and $a_f = 0.7$, we conclude that this emitter is a foreground galaxy. The emission line can be most likely identified with [O II] at a redshift of $z \sim 0.28$. It should be noted that this source had a predicted equivalent width of 9 Å, and was therefore not in our list of good candidate Lyα emitters.

Five out of 24 emission line objects have large breaks with a 2σ limit of $u' - V > 2.0$. These objects can securely be identified with high redshift Lyα emitting galaxies. For the remaining 18 emission line galaxies, either the continuum was too faint to detect a large $u' - V$ break in our images or the photometry in the V-band was unreliable due
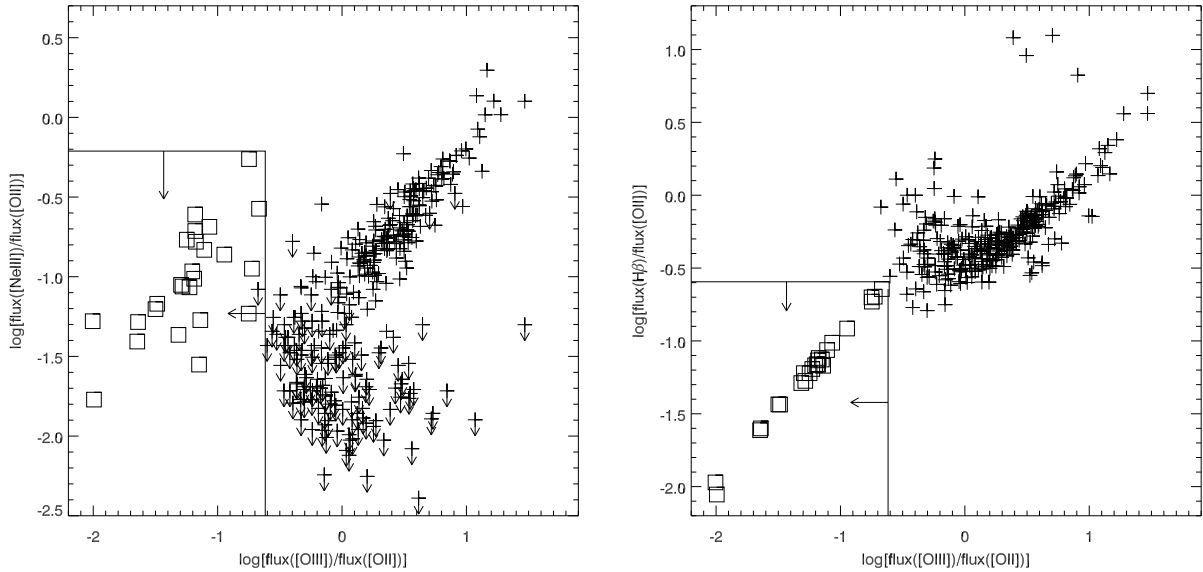
Figure 5.6 — Limits on the observed flux ratios for the single emission line sources near MRC 0943–242 (squares). All limits are 2σ upper limits. Line ratios of low redshift [O II] emitters from Terlevich et al. (1991) are plotted as pluses. The measured limits on the line ratios prefer the identification of the emission lines with Lyα (see text).

to the presence of a nearby bright object.

• *Emission line intensity ratios.* Although no other emission lines were found in the spectra of the 27 emission line sources, we can derive upper limits on various line ratios. This is very useful because several emission lines are expected in a spectrum of an [O II] emitter, such as [Ne III]λ3869, Hβ and [O III]λ5007.

What makes this test very useful for us, is the large wavelength range of the spectra of the emission line sources. If the emission line in the spectrum is [O II], then we are able to place limits on the flux of the [Ne III]λ3869, Hβ and [O III]λ5007 lines. Although Hα is also within the probed wavelength range, it falls in a region where bright skylines dominate the spectrum, and the Hα upper limits are not useful. Instead, we measured the limits on the expected positions of [Ne III], Hβ and [O III]. Two sigma limits were computed in a region which is twice the *FWHM* of the emission line. The limits on various emission line ratios are presented in Fig. 5.6. To compare our limits with low redshift [O II] emitters, we also plotted line ratios as found by Terlevich et al. (1991) for local H II galaxies. In all cases, our observed ratios lie in a region outside the values found for local galaxies with [O II] in emission. We therefore conclude that the emission line objects are Lyα emitters.

To summarize, after applying three tests that can discriminate Lyα emitters from low redshift emission line galaxies on our sample of 27 single emission line sources, we identify one [O II] emitter (object #2487 in Fig. 5.5) and confirm that the remaining 26 Lyα emitters are at $z \sim 2.9$. Combined with the two emitters with C IV in their spectrum, the total number of Lyα emitters near the radio galaxy MRC 0943-242 is 28. The properties of the Lyα emission lines of these $z = 2.9$ galaxies are printed in Table 5.8.
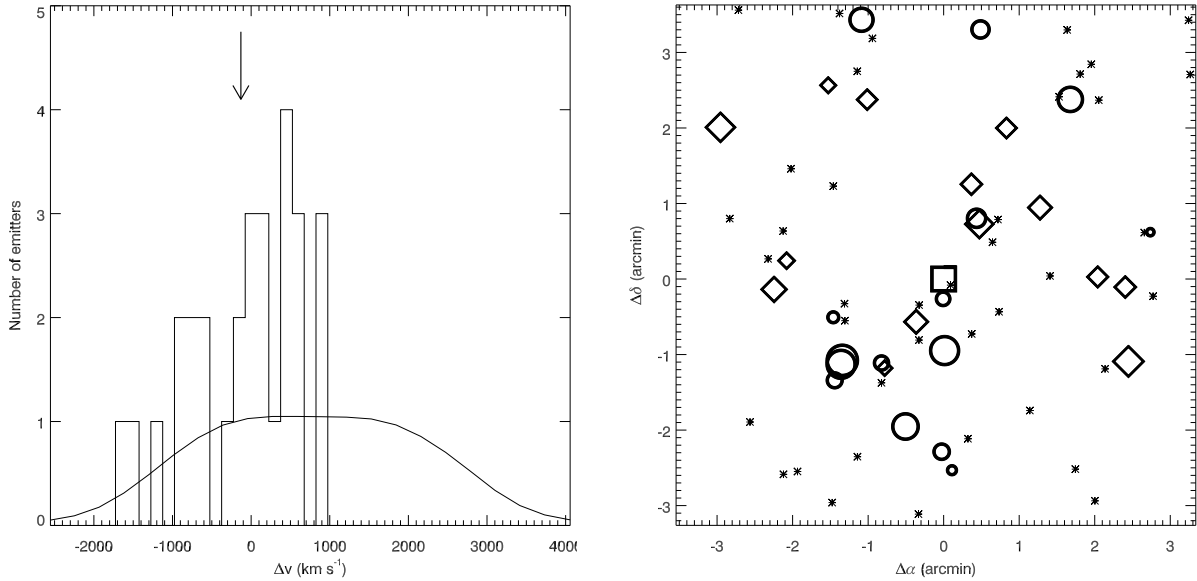
Figure 5.7 — Same as Fig. 5.4, but for the velocity distribution (*left*) and spatial distribution (*right*) of the emitters near MRC 0943–242.

A large scale structure of Lyα emitters

The density of emitters near MRC 0943–242 and of those near the radio galaxy MRC 0316–257 (Chapter 3) is very similar. Down to a narrow-band magnitude of $m_{\rm nb} = 26.1$ there are 63 emitters in the 0943 field compared to 59 in the 0316 field. Correcting for the difference in observed comoving volume, the density ratio is $n_{0943}/n_{0316} = 1.0^{+0.2}_{-0.2}$. This translates to a density of $n_{0943} = 3.2^{+0.9}_{-0.7}$ times the field density. Comparing to blank field surveys for $z \sim 3$ Lyα emitters gives similar results (see also §5.3.4). For example, the field density of Lyα emitters at $z \simeq 3.1$ was measured by Hayashino et al. (2004) in the 0.17 deg^2 Subaru Deep Field. They estimate a space density of $n_{\rm field} = 3.5 \times 10^{-4}$ Mpc^{-3} for Lyα emitters with a rest-frame equivalent width > 37 Å down to a narrow-band magnitude of 25.3. Applying the same selection criteria (taking into account the difference in luminosity distance), gives a space density of emitters in the field of MRC 0943–242 of $n_{0943} = 9.6 \times 10^{-4}$ Mpc^{-3}. The density ratio is $n_{0943}/n_{\rm field} = 2.7^{+1.3}_{-0.9}$. When compared to the space density of Lyα emitters found by Ciardullo et al. (2002), the overdensity in the 0943 field is $n_{0943}/n_{\rm field} = 5.2^{+2.7}_{-1.8}$. All three estimates of the density presented here are consistent with each other.

In Fig. 5.7 the velocity and spatial distribution of the emitters is shown. Although the emitters have no preferred position on the sky, they are clustered in velocity space. We can estimate the significance of the clustering by performing Monte Carlo simulations of the redshift distribution. We reproduced 10 000 realizations of 28 emitters using the narrow-band filter curve as redshift probability function for each emitter. We find that both the mean velocity and the dispersion of the emitters deviate from the simulated redshift distributions by $\sim 3.3\sigma$ (Fig. 5.8). This is a strong indication that the grouping of Lyα emitters is physical.
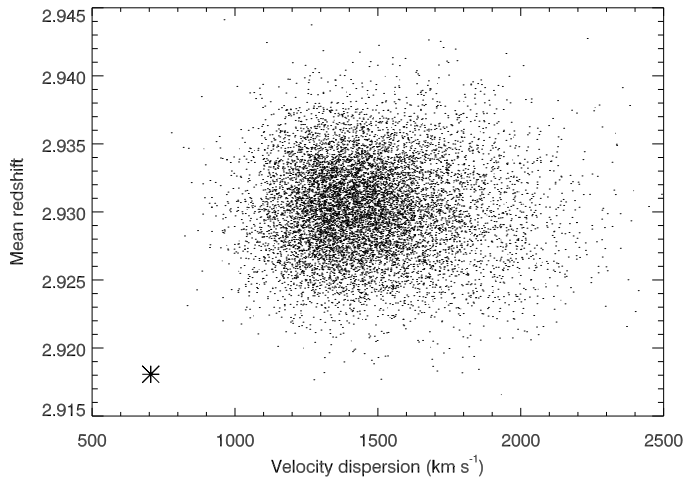
Figure 5.8 — Velocity dispersion and mean redshift of 10 000 simulated redshift distributions of 28 emitters. The observed velocity dispersion and mean redshift of the emitters near MRC 0943–242 is $\sigma_v = 715$ km s^{-1} and $\bar{z} = 2.918$ (indicated with a cross), which is significantly different (at the 4.7σ level) compared with the $\sigma_v = 1475 \pm 235$ km s^{-1} and $\bar{z} = 2.930 \pm 0.004$ of the simulated distributions.

5.3.6   MRC 0316–257, $z = 3.13$

This 1.5 Jy radio source from the Molonglo Reference Catalogue (Large et al. 1981) was discovered to be at a redshift of 3.13 by McCarthy et al. (1990). This target was especially interesting, because Le Fèvre et al. (1996) found two bright Lyα emitters close to the radio galaxy, which indicated that this radio galaxy is in an overdense environment. Narrow- and broad-band imaging of this field with the VLT resulted in the discovery of 77 candidate Lyα emitters. Follow-up spectroscopy revealed 33 emission line galaxies of which 31 are Lyα emitters near the radio galaxy, while the remaining two are foreground galaxies. By comparing the number density of Lyα emitters near the radio galaxy to that of the field, the overdensity of emitters near 0316 is estimated to be a factor $3.3^{+0.5}_{-0.4}$ times the field density (Chapter 3). The velocity distribution of the emitters has a width of *FWHM* = 1510 km s^{-1}, which is smaller than the width of the narrow-band filter (*FWHM* $\sim$ 3500 km s^{-1}), and the peak of the distribution located within 200 km s^{-1} of the redshift of the radio galaxy. In Chapter 3 we conclude that the confirmed emitters are members of a protocluster at $z \sim 3.13$ with an estimated mass of $> 3 \times 10^{14} M_\odot$.

5.3.7   TN J2009-3040, $z = 3.15$

This radio source was selected by De Breuck et al. (2000) as an ultra steep spectrum radio source ($\alpha = -1.36$, with $f_\nu \propto \nu^\alpha$) and was identified with a $m_K = 18.05 \pm 0.05$ object which has a strong unresolved component (De Breuck et al. 2002). Spectroscopy of this object showed three emission lines, including Lyα with a FWHM of ~ 2000 km s^{-1} at a redshift of 3.156 (C. De Breuck, private communications).

Imaging observations

Obtaining deep images of this field was challenging for two reasons. First, the field is located close to the galactic centre ($l = 11°$ and $b = -30°$) and the extinction towards the radio source is high, with an $E(B - V) = 0.181$ (Schlegel et al. 1998). Secondly, due to emission from inside our galaxy the background towards the quasar is not flat, but varies up to 10% over scales of roughly 10$''$. We removed this variable background
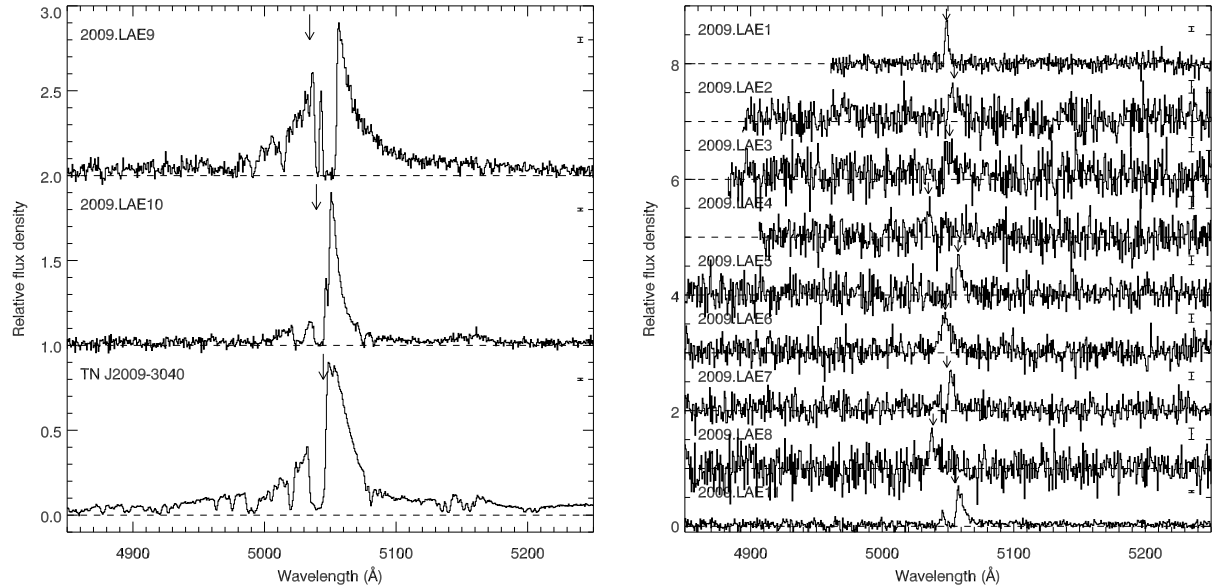
Figure 5.9 — Spectra of the confirmed emitters near the radio source TN J2009–3040. The spectra of the radio source and two quasars are shown on the right, and on the left the confirmed Lyα emitters are plotted. Error bars are shown on the right of each spectrum. The arrow indicates the redshift of the emitters. The redshift, flux and width of the emission lines can be found in Table 5.9.

by subtracting the median pixel value calculated in $10''\times10''$ boxes surrounding each pixel.

Spectroscopic observations and results

Analysis of the narrow-band and *V*-band images resulted in a list of 21 candidate Lyα emitters. In 2002 September spectra were taken of nine of these candidates for 330 min with FORS2. The use of the same 1400V grism (with a resolution of $R = 2100$) that was also used to observe the 0052 field, allowed us to identify low redshift interlopers like [O II] emitters (see Fig. 5.2). We confirmed that all nine candidates were Lyα emitters at $z \sim 3.15$ (Fig. 5.9). Two objects with predicted $EW_0 \simeq 10$ Å and $\Sigma \simeq 2.5$ (2009.LAE2 and 2009.LAE5 in Fig. 5.9 and Table 5.9) were also confirmed to be Lyα emitters near the radio source. Two galaxies with a predicted $EW_0 \simeq 6$ and 9 Å were confirmed to be [O II] emitters at $z \sim 0.35$ (bottom two spectra in Fig. 5.2). In total, 11 Lyα emitters are found near the radio source. Two of these emitters are broad-line QSOs with a *FWHM* of 1600 and 3200 km s^{-1}.

In Fig. 5.10 the velocity histogram and the spatial distribution of the confirmed Lyα emitters are shown. The median redshift of the emitters is located 170 km s^{-1} away from the radio source. The velocity dispersion of the emitters as calculated with the Gapper scale estimator (Beers et al. 1990) is 515 ± 85 km s^{-1}. This is a factor ~ 3 smaller than that of the narrow-band filter, which has a $\sigma = FWHM/2\sqrt{2\ln(2)} = 1490$ km s^{-1}. Using Monte Carlo simulations of the distribution of 11 emitters through the narrow-band filter, we found that there is an 8% chance that the velocities of the emitters are drawn from a random distribution. On the sky, the emitters appear to be concentrated on the southern half of the field. The position of the radio source is on the edge of the
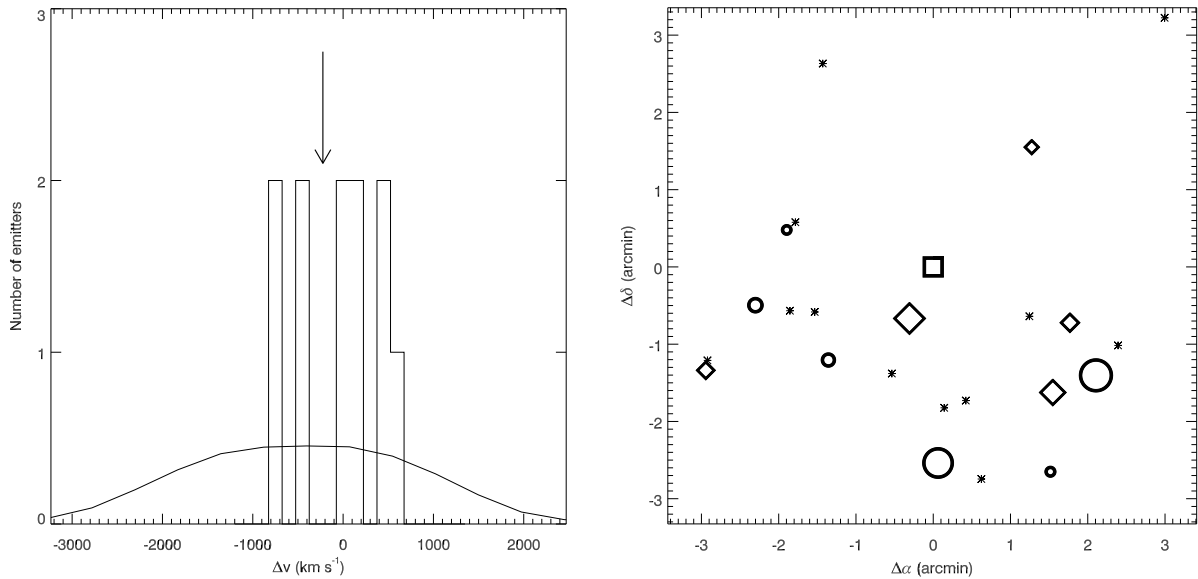
Figure 5.10 — Same as Fig. 5.4, but for the velocity distribution (*left*) and spatial distribution (*right*) of the emitters near TN J2009–3040.

distribution of Lyα emitters, very similar to the situation in the field of TN J1338–1942 at $z = 4.1$ (§5.3.8, Chapter 2).

Volume density

We can compare the number density of Lyα emitters in this field directly to that of the 0316 field, because the same narrow-band filter was used for the observations. The number of (candidate) emitters down to the same luminosity limit is in the 2009 field a factor $2.0^{+0.7}_{-0.5}$ smaller than that in the 0316 field. The 0316 field is overdense by a factor $3.3^{+0.5}_{-0.4}$ (Chapter 3), which implies that the number density of Lyα emitters near TN J2009–3040 is a factor $1.7^{+0.8}_{-0.6}$ times the field density, consistent with no overdensity. However, the redshift distribution of the confirmed emitters in the 2009 field ($\Delta z = 0.019$) is much narrower than that of the emitters in the 0316 field ($\Delta z = 0.0537$, and 90% of the confirmed emitters are within a redshift range of $\Delta z = 0.0287$). This could indicate that the number density of Lyα emitters near the radio source TN J2009–3040 is much higher (up to a factor 2.9–4.8) than the field density. Thus although the volume density of Lyα emitters near TN J2009–3040 is consistent with the field density at that redshift, the clustering both on the sky and in velocity space of the emitters points to a structure of galaxies. More observations are needed to determine the reality of this clustering.

5.3.8   TN J1338-1942, $z = 4.10$

This radio galaxy has a redshift of 4.1 (De Breuck et al. 1999, 2001) and is one of the brightest known in Lyα (De Breuck et al. 1999, 2001). The radio source has a rest-frame radio luminosity comparable to that of the most luminous 3CR sources. Because no narrow-band filter is available at the VLT that is centred on the wavelength of a Lyα line at $z = 4.1$, we used a custom narrow-band filter with an effective wavelength of

6199 Å and a FWHM of 59 Å. Narrow-band and *R*-band imaging and follow-up spectroscopy with the VLT of the surroundings of TN J1338–1942 revealed 20 Lyα emitters within a projected distance of 1.3 Mpc and 600 km s^{-1} of the radio galaxy (Chapter 2). The structure is overdense in Lyα emitters by a factor of 4–15 and could be the ancestor of a rich cluster of galaxies. Multi-color imaging with the Advanced Camera for Surveys (ACS) on board the *Hubble Space Telescope (HST)* revealed an anomalously large number of Lyman Break Galaxies (LBGs) near the radio galaxy, confirming the presence of a protocluster at $z = 4.1$ (Miley et al. 2004, Overzier et al. in prep).

New observations

The VLT observations presented in Chapter 2 showed that the emitters are not distributed homogeneously over the field, but appear to have a boundary in the northwest. To further determine the extent and shape of the protocluster region, the field near TN J1338–1942 was imaged at a second position. The second pointing is located towards the south-east of the radio galaxy and overlaps the first field (hereafter the 1338-1 field) at the position where the concentration of Lyα emitters seemed to be the highest (see Fig. 5.12 for the outline of the imaging areas). The second field (hereafter called the 1338-2 field) was observed for 420 min in the narrow-band and for 75 min in the *R*-band. Analysis of data in the second field resulted in the discovery of 35 candidate emitters. Ten candidate emitters were also selected as candidates in the 1338-1 field and eight of them were confirmed in Chapter 2. One candidate emitter in the second field catalogue has a $EW_0 = 19^{+14}_{-5}$ Å, but a computed equivalent width of 8.5 Å in the first field catalogue. The (weighted) average of these two measurements is $EW_0 = 14.5$ Å. Because this is below our selection criterion of $EW_0 = 15$ Å, we removed the object from our candidate list. Follow-up spectroscopy showed that the object is an [O II] emitter at $z \sim 0.66$ (see the spectrum of #2672 in Fig. 5.11). Another candidate was removed from the list, because it had a *R*-band magnitude of $m_R = 22.2$, making it brighter than the radio galaxy. The total number of good candidate emitters in the two fields combined is 54.

Spectroscopic observations of candidate emitters in the second field were carried out in 2003 February with Keck/LRIS (150 min) and in 2003 March with VLT/FORS2 (310 min, see Table 5.4). In the two observing sessions combined, spectra were taken of 15 good candidate emitters. In addition, objects were observed that were lower on our priority list. These additional objects included four emitters that were already confirmed in Chapter 2, six candidate emitters with 9 Å$< EW_0 < 15$ Å and five galaxies with an $EW_0 > 15$ Å, but with a signal-to-noise in the narrow-band image of ~ 4.

Of the 15 good candidate emitters, 13 were confirmed to be Lyα emitters at $z \sim 4.1$. The two unconfirmed emitters were among the faintest candidates that were observed in that mask. From the additional objects that were observed, the four emitters that were confirmed in Chapter 2 were all reconfirmed. Among the low equivalent width sources was one Lyα emitter at $z = 4.1$ and five [O II] emitters at a redshift $z = 0.66$. The low signal-to-noise sources added another two Lyα emitters at $z = 4.1$ to the list of confirmed emitters. Combined with the data described in Chapter 2, the total number of confirmed Lyα emitters at $z \sim 4.1$ is 37. In Fig. 5.11 the spectra of the confirmed emitters and of the radio galaxy are shown. In Table 5.10 the properties of the emission

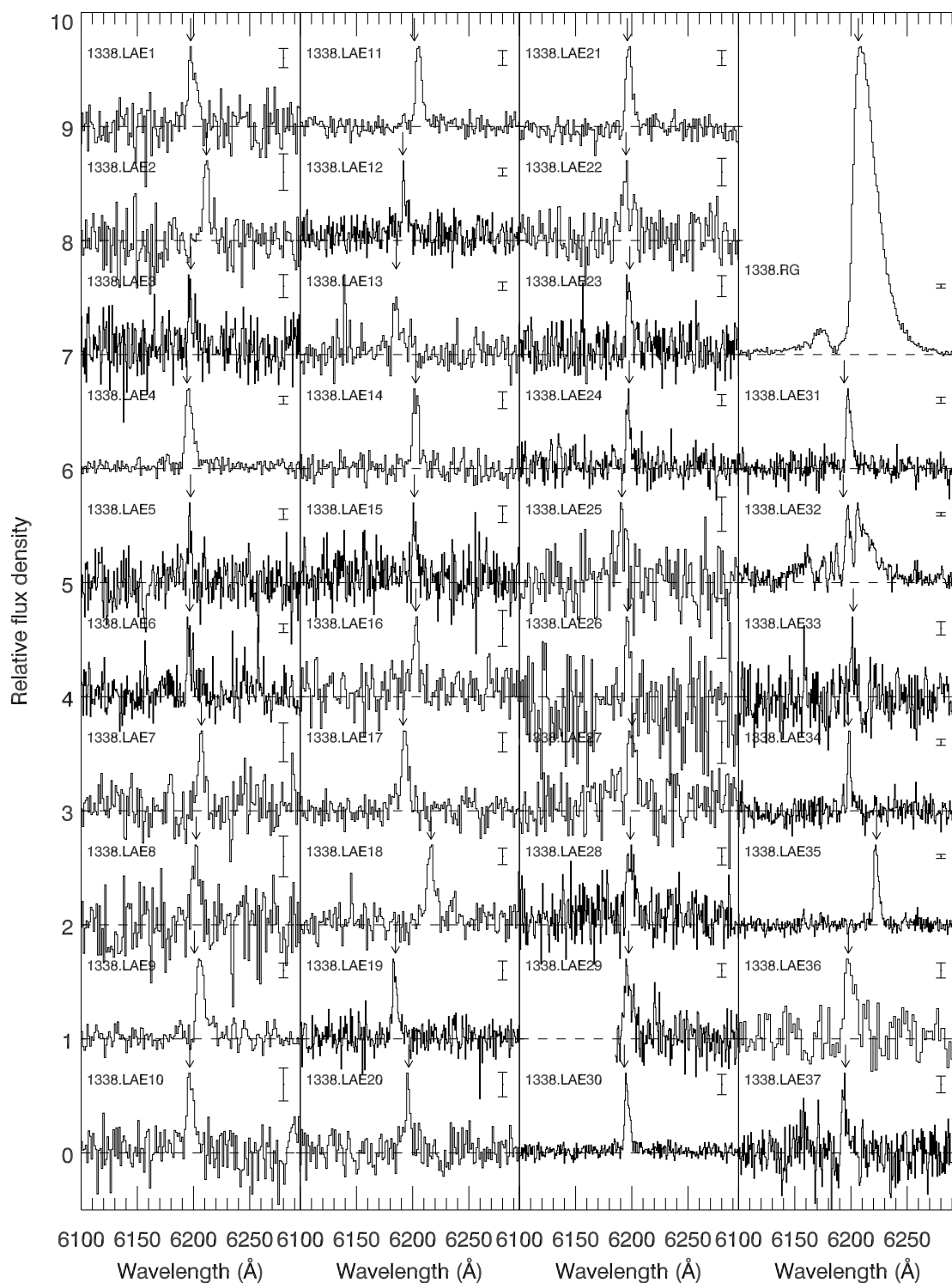**Figure 5.11** — Spectra of the confirmed emitters near the radio galaxy TN J1338–1942. Error bars are shown on the right of each spectrum. All spectra are normalized to the peak of the Lyα line, which has a relative flux of 0.7. The offset between the spectra is 1.0. The arrow indicates the redshift of the emitters. The redshift, flux and width of the emission lines can be found in Table 5.10.

Figure 5.12 — Spatial distribution of the confirmed and candidate Lyα emitters near TN J1338–1942. Symbols and their sizes are the same as in Fig. 5.4. The filled circle at (-1.5,-2.8) represents the centre of all the emitters. The dashed lines outline the area of the VLT images.
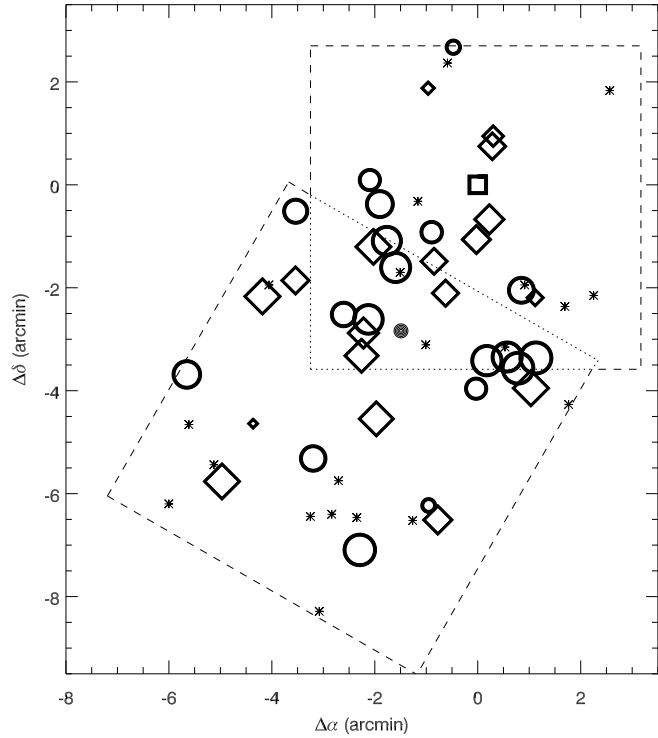
lines are printed.

Volume density

Several blank field surveys for Lyα emitters at redshifts between $z = 4$ and $z = 5$ have been conducted in recent years. The two surveys covering the largest area are the LALA survey, aimed at finding Lyα emitters at $z = 4.5$ (Rhoads et al. 2000; Dawson et al. 2004), and the Subaru Deep Field (SDF) survey, in which was searched for Lyα emitters at $z = 4.8$ (Ouchi et al. 2003; Shimasaku et al. 2003, 2004).

To estimate the (over)density of Lyα emitters near TN J1338–1942, we compare our density to that found in the LALA and SDF surveys. In the LALA survey the volume searched was 1.5×10^6 comoving Mpc³ and ~ 350 candidate Lyα emitters were discovered in this volume with an observed equivalent width > 80 Å and a 5σ line flux $> 2 \times 10^{-17}$ erg s⁻¹ cm⁻² (Rhoads et al. 2000; Dawson et al. 2004). Follow-up spectroscopy confirmed 72% of the targeted sources (Dawson et al. 2004), but we will conservatively assume that all 350 LALA candidates are real Lyα emitters. Applying the same luminosity and equivalent width criteria used in the LALA survey to our data selects 14 candidate Lyα emitters in our fields of which 13 are confirmed (one has not been observed spectroscopically yet). Compared to the LALA survey, the density of Lyα emitters near TN J1338–1942 is a factor $5.2^{+1.8}_{-1.4}$ higher. The large errors are due to small number statistics.

The SDF survey covers an area of $25' \times 45'$, which is observed in two 1% narrowband filters, one centred on Lyα at $z \approx 4.79$ and one at $z \approx 4.86$. The volume density of emitters with magnitudes $m_{\mathrm{nb}} < 25.5$ at these two redshifts is very similar
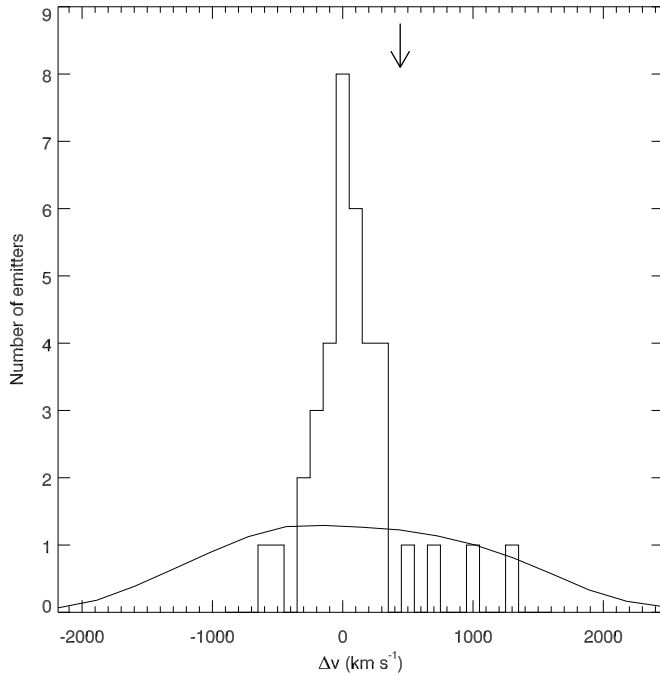
Figure 5.13 — Velocity distribution of the confirmed emitters near TN J1338–1942. The median of the emitters is taken as zero point. The velocity of the radio galaxy is indicated by an arrow. The solid line represents the selection function of the narrow-band filter, normalized to the total number of confirmed emitters.

$(2.7 \pm 0.4 \times 10^{-4}$ at $z \sim 4.79$ and $3.1 \pm 0.5 \times 10^{-4}$ at $z \sim 4.86$, Shimasaku et al. 2004). Selecting Lyα emitters in our field in the same way as was done in the SDF by Shimasaku et al. (2003), and comparing our numbers to those at $z = 4.79$ and $z = 4.86$ gives a density of $4.5^{+1.8}_{-1.3}$. The weighted average of these density measurements is $4.7^{+1.0}_{-0.8}$, consistent with the overdensity found in Chapter 2.

Structure properties

As mentioned in Chapter 2, the spatial distribution of emitters near 1338 is not homogeneous through the field. In Fig. 5.12 the spatial distribution is plotted of all the confirmed and candidate emitters in the two fields. The centre of the emitters (filled circle in Fig. 5.12) lies approximately 1.5 east and 2.8 south of the radio galaxy. The radio galaxy appears to be at the edge of the galaxy distribution. Even more interesting than the spatial distribution is the redshift distribution of the emitters (Fig. 5.13). The velocity distribution is very narrow, with a dispersion of only 260 ± 65 km s^{-1} (*FWHM* $= 625 \pm 150$ km s^{-1}). This is much narrower than the width of the narrow-band filter, which has a *FWHM* of 2860 km s^{-1}. Monte-Carlo simulations indicate that the chance that such a narrow redshift distribution is drawn from a random sample is only 0.05%. Although the number of confirmed emitters has almost doubled since the discovery of this protocluster, the velocity dispersion has not changed. This indicates that the confirmed emitters in both the southern and northern field are members of one single structure. The properties of this protocluster at $z = 4.1$ will be described in §5.5.

5.3.9 TN J0924–2201, z = 5.20

TN J0924–2201 is currently the highest redshift radio galaxy known with a redshift of $z = 5.2$ (van Breugel et al. 1999). To select Lyα emitters in this field, a custom narrow-band filter encompassing the wavelength of the Lyα line of the radio galaxy at 7537 Å

Table 5.5 — Summary of the results of the imaging and spectroscopic observations of the radio galaxy targets. For completeness, the target of the pilot project, MRC 1138–262 is included.

Field	z	$N_{\rm img}^a$	$N_{\rm spec}^b$	$N_{\rm conf}^c$	$N_{\rm none}^d$	$N_{\rm low\,z}^e$	$N_{\rm extra}^f$	$N_{\rm tot}^g$	$n_{\rm rg}/n_{\rm field}^h$	σ_v^i km s^{-1}	$M_{\rm pcl}^j$ $10^{14}\,M_\odot$
2048	2.06	10	3	2	1	0	1	3	$1.2^{+0.8}_{-0.7}$	–	–
1138	2.16	37	11?	11	0?	0	4	15	4 ± 2	900 ± 240	3–4
0052	2.86	57	36	35	1	0	2	37	$3.0^{+0.5}_{-0.4}$	980 ± 120	3–4
0943	2.92	65	30	25	4	1	3	28	$3.2^{+0.9}_{-0.7}$	715 ± 105	4–5
0316	3.13	77	30	28	1	1	3	31	$3.3^{+0.5}_{-0.4}$	640 ± 195	3–5
2009	3.16	21	9	9	0	0	2	11	$1.7^{+0.8}_{-0.6}$	515 ± 90	–
1338	4.10	54	36	34	2	0	3	37	$4.7^{+1.0}_{-0.8}$	265 ± 65	6–9
0924	5.20	14	8	6	0	2	0	6	$2.5^{+1.6}_{-1.0}$	305 ± 110	4–9

[a] Number of candidate Lyα emitters with $EW_0 > 15$ Å and $EW_0/EW_0^- > 3$.
[b] Number of spectroscopically observed candidates.
[c] Number of spectroscopically confirmed Lyα emitters.
[d] Number of candidates not detected spectroscopically.
[e] Number of low redshift emission line galaxies among the observed candidates.
[f] Number of confirmed Lyα emitters not satisfying the imaging selection criteria.
[g] Total number of confirmed Lyα emitters near the radio galaxy.
[h] Density of the emitters as compared to the field density on the basis of the imaging candidates. Note that the redshift range of the confirmed emitters is generally smaller than the width of the filter (see §5.3 and §5.5.2).
[i] Velocity dispersion of the confirmed emitters.
[j] Estimated mass of the protocluster (§5.5.2).

was purchased. The details of the observations and candidate selection in this field are presented in Chapter 4. Follow-up spectroscopy of eight of 14 high priority candidate Lyα emitters resulted in six Lyα emitters near the radio galaxy (Chapter 4). The field is overdense in Lyα emitters by a factor of 1.5–6.2 times the field density at that redshift and comparable in density to the radio galaxy fields 1138, 0316 and 1338 at $z = 2.2, 3.1$ and 4.1.

5.4 The environment of high redshift radio galaxies

Besides the target of our pilot project, MRC 1138-262 at $z = 2.16$, we imaged areas surrounding eight radio galaxies with $2.0 < z < 5.2$. A total of 300 candidate Lyα emitters was selected fulfilling the selection criteria $EW_0 > 15$ Å and $\Sigma \equiv EW_0/EW_0^- > 3$ (Table 5.3). One field (near BRL 1602–174 at $z = 2.04$) suffered from high galactic extinction and a low response of the CCD. We will discard this field in the following discussion. In the remaining seven radio galaxy fields spectra were taken of 152 candidates. These observations confirmed 139 Lyα emitters. The success rate of our selection procedure is $> 91\%$. Only nine candidates could not be confirmed spectroscopically. These candidates had a faint predicted line flux ($F_{\rm Ly\alpha} < 10^{-17}$ erg s^{-1} cm^{-2}) and the non-detections are most likely caused by a lack of signal-to-noise. An overview of the number of candidates, spectroscopically observed and confirmed Lyα emitters per field is given in Table 5.5.

Four candidate emitters were identified with low redshift objects. We estimate that the contamination of our sample is roughly 3%, although this percentage varies strongly from field to field. For example, the fraction of contaminants in the field surrounding TN J0924–2201 at $z = 5.2$ is 25% (Chapter 4), while in four fields near $z \sim 3$, the contamination fraction is $\sim 2\%$ (see Table 5.5).

Fourteen objects that fell outside our selection criteria were also confirmed to be Lyα emitters, increasing the number of confirmed Lyα emitters to 153. Adding the 15 confirmed emitters in the 1138 field (Pentericci et al. 2000), a total of 168 Lyα emitters are confirmed near eight high radio galaxies.

Based on the overdensity and the clustering of emitters in redshift space, we argue that at least five of the radio galaxies (MRC 1138-262, MRC 0052–241, MRC 0943–242, MRC 0316–257 and TN J1338–1942) are associated with a forming cluster of galaxies (protocluster). We are not able to make a definite statement about the environment of TN J0924–2201 at $z = 5.2$, due to the small number of confirmed galaxies (Chapter 4). Recent multi-color observations with the *Hubble Space Telescope* indicate that this field is rich in *V*-band dropouts (Overzier et al. 2005), and these dropouts could represent an additional galaxy population in the protocluster. Although follow-up spectroscopy is needed to confirm that the dropouts are at $z = 5.2$, the richness of Lyman break galaxies in the field strengthens our idea that a large scale structure is present at $z = 5.2$. The two remaining radio galaxy fields, the 2048 and 2009 fields, have Lyα volume densities consistent with the field density. In the 2009 field, clustering can be seen in the position of the emitters on the sky and in velocity space. More observations in the field are needed to confirm the clustering and to identify a possible structure of galaxies. Based on the results in the eight radio galaxy fields, 75% of radio galaxies at $z > 2$ are associated with a forming cluster of galaxies. Further, our results are consistent with all $z > 2$ luminous radio galaxies being associated with protoclusters.

In the next section, we will describe the properties of the radio galaxy protoclusters. The properties of the high redshift Lyα emitters are or will be discussed elsewhere (Kurk et al. 2004b; Chapter 3; Chapter 6).

5.5 Properties of high redshift protoclusters

5.5.1 Structure size

As can be seen in Figs. 5.4, 5.7, 5.10 and 5.12, the sizes of the protoclusters are generally larger than the field of view of the FORS2 camera ($>3.2\times3.2$ Mpc^2). Only in the 1138 field a clear boundary can be seen to the north-west of the radio galaxy. Kurk et al. (2004b) found that the surface density of Lyα emitters decreased with increasing distance to the radio galaxy in their field. Within the limitations of the relatively small number of objects, we tested each of our fields to see whether there is a concentration of emitters near the radio galaxy. In two fields, the 0052 and 0316 fields, we found that density did not change with distance to the radio galaxy, and that the distribution of emitters was homogeneous over the imaged area. Most likely, the extent of the protocluster in these fields is larger than the area covered by our imaging. In the 0943 field at $z = 2.9$, the surface density of Lyα emitters did decline further away from the radio galaxy, as is shown in Fig. 5.14. At a distance of ~1.75 Mpc from the radio galaxy, the

Figure 5.14 — Surface density of emitters as a function of distance from the radio galaxy MRC 0943–242. The horizontal dashed line is the surface density of Lyα emitters in blank fields. The vertical dotted line represents the maximum distance allowed in the image.
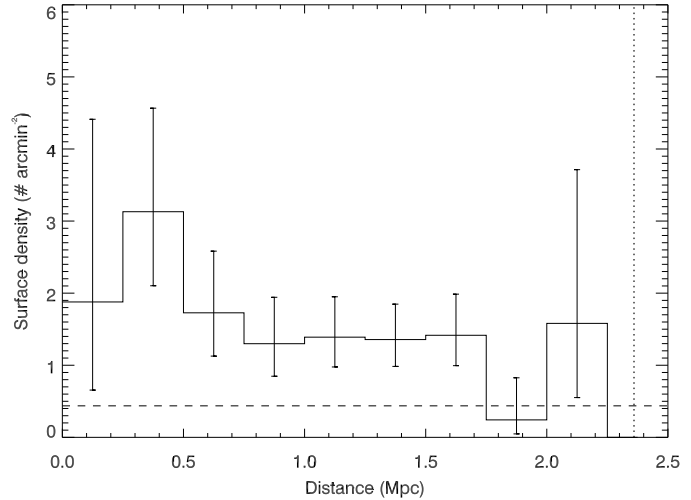
surface density of Lyα emitters has declined and is consistent with the field density of emitters. We regard this radius as the size of the protocluster. A similar distribution was found in the 1338 field, but only if the average position of the emitters was taken as centre (see Fig. 5.15). As mentioned in §5.3.8, the radio galaxy is located at a distance of 1.3 Mpc from the centre of the emitters. We estimate that the size of this protocluster is 2.0 Mpc (Fig. 5.15).

Our size estimates of >1.75–2.0 Mpc are consistent with the determination by other groups. For example, Keel et al. (1999) estimate that the large scale structure around the radio galaxy 53W002 at $z = 2.4$ has a diameter of ~ 3.3 Mpc. Hayashino et al. (2004) imaged a protocluster at $z \sim 3.1$, that was serendipitously discovered by Steidel et al. (1998). They found that the overdensity of Lyα emitters in this field has a size of approximately 5×5 Mpc^2. At a higher redshift, an overdensity of Lyα emitters at $z = 4.9$ was discovered by Shimasaku et al. (2003) in the Subaru Deep Field. This overdensity has a shape of roughly a circle with a radius of ~ 2.0 Mpc (Shimasaku et al. 2003), which is very similar to the size of the 1338 protocluster.

To summarize, we find that the sizes of the protoclusters at $z = 2.9$ and $z = 4.1$ are roughly 1.75–2.0 Mpc. The other protoclusters do not show a boundary and are most likely larger than this. Wide field imaging is needed for these protoclusters to see a boundary of the galaxy distribution.

5.5.2 Mass

The age of the Universe at $z = 3$ is only $\sim 15\%$ of its current age, which corresponds to ~ 2 Gyr in our adopted cosmology. A protocluster galaxy with a relative velocity of $500 \, \text{km} \, \text{s}^{-1}$ would take at least 4 Gyr to cross a structure with a size of 2 Mpc. Therefore, the protoclusters are most likely still in the process of formation. They are still far from virialization and we cannot use the virial theorem to calculate the mass of the galaxy structures.

An alternative approach to calculate the mass of the structures is to assume that the mass that is located within the volume that is occupied by the protocluster galaxies will collapse into a single structure (see e.g., Steidel et al. 1998). To use this method we need to know the mass overdensity δ_m within the volume. The mass overdensity is
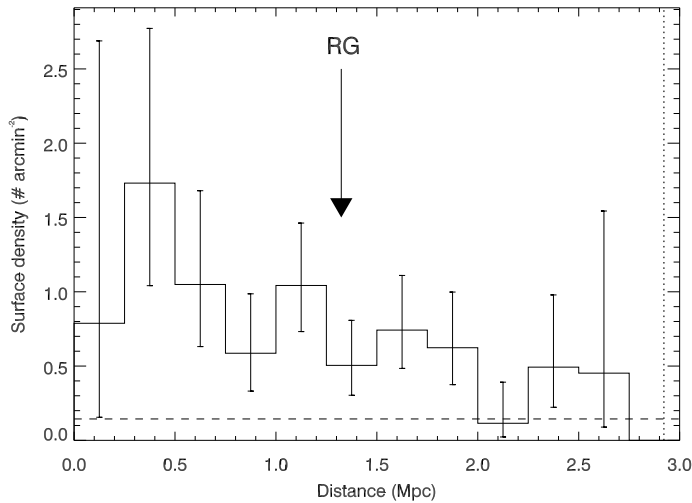
Figure 5.15 — Surface density of emitters as a function of distance from the average position of the emitters in the field near TN J1338–1942 at $z = 4.1$. The position of the radio galaxy is indicated by the arrow. The dashed line is the surface density of field Lyα emitters (Dawson et al. 2004; Shimasaku et al. 2004, see §5.3.8). The dotted line is the maximum distance allowed by our imaging.

related to the galaxy overdensity δ_{gal} by the bias parameter $b \equiv \delta_{\text{gal}}/\delta_m$.

To compute the volume of the protocluster, we estimate the redshift range of the confirmed Lyα emitters after removing outliers (galaxies more than $\sim 1500\,\text{km\,s}^{-1}$ away from the median redshift). Because redshift space distortions modify the occupied volume, we corrected for peculiar velocities by assuming the structure is just breaking away from the Hubble flow (see Steidel et al. 1998; Chapter 3 for more details). If outliers are included, the volume occupied by the protoclusters increases and the estimated masses are higher.

Using this method, in Chapter 3 we estimate that the mass of the 0316 protocluster is $\sim 5 \times 10^{14}\,M_{\odot}$. Below we will estimate the mass of the protoclusters in the 1138, 0052, 0943, 1338 and 0924 fields. A bias parameter of $b = 3 - 6$ will be assumed, as suggested by e.g. Steidel et al. (1998) and Shimasaku et al. (2003).

• *1138:* Near the radio galaxy MRC 1138–262, the overdensity of emitters in a comoving volume of 4490 Mpc^3 is $\delta_{\text{gal}} > 3.4$ (Pentericci et al. 2000; Kurk et al. 2004b). The computed mass in this volume is at least $3 - 4 \times 10^{14}\,M_{\odot}$.

Interestingly, the redshift distribution of the Lyα emitters in this field appears to be bimodal (Pentericci et al. 2000). The emitters are located in two subgroups with velocity dispersions of 520 and 280 km s^{-1} (Pentericci et al. 2000). Calculating the mass of the individual groups gives $\sim 2 \times 10^{14}$ and $1 - 2 \times 10^{14}\,M_{\odot}$. If the galaxies in these two groups are close to virialization, we can apply the virial theorem. Kurk et al. (2004b) estimated that the virial radii of the two groups is ~ 1 Mpc. Using the velocity dispersions as given by Pentericci et al. (2000), the virial masses of the groups are 4.0×10^{14} and $1.0 \times 10^{14}\,M_{\odot}$, comparable to the other estimates.

• *0052:* To estimate the volume that most likely will collapse into a single structure, we removed the three lowest and the two highest redshift galaxies. These galaxies are on the edges of the redshift distribution (Fig. 5.4), and we regard them as outliers. The remaining 32 emitters have redshifts in the range $2.8437 \leq z \leq 2.8673$. The range of $\Delta z = 0.0236$ is a factor 0.44 smaller than the redshift range probed by the narrow-band filter ($\Delta z = 0.0541$). The volume occupied by the emitters is 3510 comoving Mpc^3 (uncorrected for peculiar velocities). The overdensity within the volume is $0.0541/0.0236 \times 32/37 \times 3.0 = 5.95$. Using these values, the estimated mass is

$3 - 4 \times 10^{14} M_\odot$. Because the field of view of our imaging is not large enough to show a boundary of the structure (Fig. 5.4), this mass is a lower limit.

As is the case in the 1138 field, the emitters appear to be concentrated in two groups (see Fig. 5.4). The groups consist of 12 and 19 members and have velocity dispersions of 185 and 230 km s^{-1} respectively. Assuming that the virial theorem can be applied for the two groups, this gives masses of 1.1×10^{14} and $7 \times 10^{13} M_\odot$ for the groups. Most likely, the mass of the protocluster lies in the range $2 - 4 \times 10^{14} M_\odot$.

- *0943:* The redshift range of the confirmed emitters is 0.034, and, as described in §5.5.1, the size of the structure is roughly 1.75 Mpc in radius. This gives a comoving volume of 4570 Mpc^3. Within this volume 61 of the 65 emitters (94%) are located. The overdensity of emitters in this volume is 5.5, giving a protocluster mass of $4 - 5 \times 10^{14} M_\odot$. Because the protocluster might extend towards lower redshifts (see Fig. 5.7), this mass must be regarded as a lower limit.

- *1338:* The $z = 4.1$ protocluster has a size of 2 Mpc in radius (§5.5.1), giving an area that is 78% of the total area observed (Fig. 5.12). The fraction of (candidate) emitters in this area is 91%. The volume occupied by these emitters is 5815 Mpc^3. The density of emitters in this volume is ~ 8.5, resulting in a mass of $6 - 9 \times 10^{14} M_\odot$.

- *0924:* The redshifts of the confirmed emitters near TN J0924–2201 only span a narrow redshift range of $\Delta z = 0.0151$ (Chapter 4). The corresponding volume is 1870 Mpc^3 and the density of emitters as compared to the field density in this volume is 20.3. The structure mass is estimated to be $4 - 6 \times 10^{14} M_\odot$, although the small number of confirmed emitters makes this mass quite uncertain.

To summarize, the mass estimates of the protoclusters are in the range $2 - 9 \times 10^{14} M_\odot$. Locally, such masses correspond to clusters with richness class 0 and higher (e.g., Bahcall & Cen 1993). This indicates that the protoclusters are the progenitors of present-day massive clusters.

5.5.3 Velocity dispersions

In Fig. 5.16, the velocity dispersion of the Lyα emitters in the radio galaxy fields are plotted as a function of redshift. Although the number of data points is very limited, the dispersion appears to increase with decreasing redshift. While at $z > 4$ the velocity dispersion is ~ 300 km s^{-1}, the dispersion increases to 500–700 km s^{-1} at $z \sim 3$. In our two lowest redshift fields ($z = 2.86$ and $z = 2.16$), the velocity dispersion of the emitters is 1000 km s^{-1}. However, it should be noted that the velocity distribution of emitters at $z = 2.86$ and $z = 2.16$ is bimodal (§5.5.2), and the velocity dispersion of the individual subgroups is much lower (200–500 km s^{-1}). Numerical simulations of the evolution of massive clusters predict that the velocity dispersion of the dark matter increases with cosmic time (e.g., Eke et al. 1998). Our observations are consistent with these predictions. Our data approximately follow the evolution of a massive cluster of galaxies, with a velocity dispersion of 1000 km s^{-1} at $z = 0$ (Fig. 5.16). Additional observations of high redshift protoclusters are needed to confirm this.
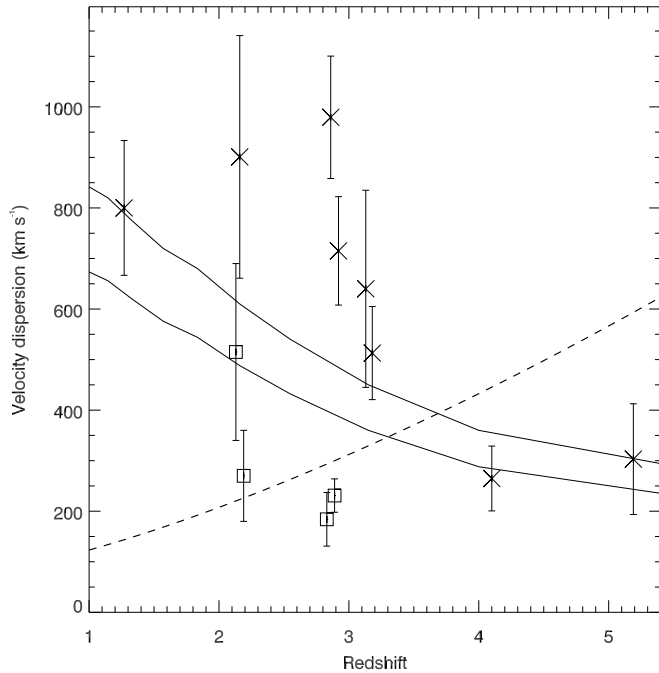
Figure 5.16 — Velocity dispersion of Lyα emitters in our radio galaxy fields (*crosses*) as a function of redshift. The squares represent the velocity dispersions of the subgroups in the 1138 and 0052 fields (see §5.5.2). The data point near $z = 1$ represents the velocity dispersion in the X-ray cluster RDCS 1252.9-2927 at $z = 1.24$ (Rosati et al. 2004). The dashed line is the Hubble flow $H(z)$ over 1 Mpc. The solid lines show the evolution of the dark matter velocity dispersions σ_{dm} of simulated massive clusters (Eke et al. 1998). The top line is scaled to 1000 km s^{-1} at $z = 0$, the bottom line to 800 km s^{-1} at $z = 0$.

5.6 Discussion

A question is whether the radio galaxy selected protoclusters presented in this paper are biased. To answer this question, we have to assess the number density of powerful radio galaxies at $z > 2$.

The radio galaxies in our program have luminosities $L_{2.7\mathrm{GHz}} \gtrsim 10^{33}$ erg s^{-1} Hz^{-1} sr^{-1} (Table 5.1). The number density of radio sources with this luminosity limit in the redshift range $2 < z < 5$ is 4×10^{-8} Mpc^{-3} (Dunlop & Peacock 1990). Using the more recent radio luminosity function at 151 MHz as derived by Willott et al. (2001) and assuming a spectral slope of $\alpha \simeq -0.8$ gives a number density that is similar within a factor of 2. It should be noted that the number density depends strongly on the lower luminosity limit that is assumed, since the density varies approximately with $n \propto L^{-2}$ (Dunlop & Peacock 1990).

The association of 75% of $z > 2$ radio galaxies with a protocluster (§5.4) implies that there are roughly 3×10^{-8} forming clusters at $2.0 < z < 5.2$ per comoving Mpc^3 with an active radio source. However, it is likely that there will be many more forming clusters in this redshift range without an active radio source. Blundell & Rawlings (1999) argue that high redshift radio galaxies are visible only when they are younger than 10^7 yr. This means that between $z = 5.2$ and $z = 2$, there must be two orders of magnitude more forming clusters *without* a radio source. Therefore, most high redshift protoclusters will not have a powerful radio source.

Based on these calculations, we estimate that the number density of protoclusters such as the ones presented in this paper is $\sim 6 \times 10^{-6}$ Mpc^{-3}. It is instructive to compare this number with the density of protoclusters as derived by other groups. Steidel et al. (1998) estimate that they find one galaxy overdensity in a $9' \times 18'$ field in a redshift range $2.7 < z < 3.4$ in their Lyman break galaxy survey. In our cosmology, this trans-

lates to a number density of protoclusters of 3×10^{-6} Mpc^{-3}. High redshift blank field Lyα searches also found several galaxy overdensities. Shimasaku et al. (2003) reports the discovery of a structure of Lyα emitters at $z = 4.9$ in the Subaru Deep Field with a mass of 3×10^{14} $M_\odot$. The implied volume density of such structures is 7×10^{-6} Mpc^{-3}. At even higher redshifts, Ouchi et al. (2005) find two overdensities of Lyα emitters at $z = 5.7$ in a 1 deg^2 region of the sky. They estimate a density of $> 2 \times 10^{-6}$ Mpc^{-3} for such structures. These blank field density estimates are very similar to our calculated density of $\sim 6 \times 10^{-6}$ Mpc^{-3}. This indicates that the overdensities discovered in blank field surveys and our protoclusters near radio galaxies are the same type of object. It is likely that we see the protocluster at the time that the brightest cluster galaxy undergoes a burst of nuclear activity. When the protoclusters evolve to $z \sim 1$, the central radio source will be extinguished, following the evolution in the space density of active galactic nuclei (AGNs) (e.g., Wall et al. 1980; Dunlop & Peacock 1990; Miyaji et al. 2000). It is therefore not expected that rich clusters at $z < 1$ harbour active luminous radio sources, which is indeed observed.

Interestingly, in the local Universe objects with a similar volume density as the protoclusters are clusters with masses $\gtrsim 2 \times 10^{14}$ $M_\odot$ (Girardi et al. 1998; Reiprich & Böhringer 2002). This supports the idea that the protoclusters are the ancestors of clusters of galaxies.

Acknowledgments

References

Appenzeller, I. & Rupprecht, G. 1992, The Messenger, 67, 18
Archibald, E. N., Dunlop, J. S., Hughes, D. H., et al. 2001, MNRAS, 323, 417

Athreya, R. M., Kapahi, V. K., McCarthy, P. J., & van Breugel, W. J. M. 1998, A&A, 329, 809

Bahcall, N. A. & Cen, R. 1993, ApJ, 407, L49

Bahcall, N. A. & Fan, X. 1998, ApJ, 504, 1

Bahcall, N. A., Fan, X., & Cen, R. 1997, ApJ, 485, L53

Baldwin, J. A. & Stone, R. P. S. 1984, MNRAS, 206, 241

Barr, J. M., Baker, J. C., Bremer, M. N., Hunstead, R. W., & Bland-Hawthorn, J. 2004, AJ, 128, 2660

Baugh, C. M. & Gaztanaga, E. 1996, MNRAS, 280, L37

Beers, T. C., Flynn, K., & Gebhardt, K. 1990, AJ, 100, 32

Bertin, E. & Arnouts, S. 1996, A&AS, 117, 393

Bessell, M. S. 1979, PASP, 91, 589

Best, P. N. 2000, MNRAS, 317, 720

Best, P. N., Lehnert, M. D., Miley, G. K., & Röttgering, H. J. A. 2003, MNRAS, 343, 1

Best, P. N., Röttgering, H. J. A., & Lehnert, M. D. 1999, MNRAS, 310, 223

Blundell, K. M. & Rawlings, S. 1999, Nature, 399, 330

Carilli, C. L., Miley, G., Röttgering, H. J. A., et al. 2001, in Astronomical Society of the Pacific Conference Series, 101

Carilli, C. L., Röttgering, H. J. A., van Ojik, R., Miley, G. K., & van Breugel, W. J. M. 1997, ApJ, 109, 1

Carlstrom, J. E., Holder, G. P., & Reese, E. D. 2002, ARA&A, 40, 643

Ciardullo, R., Feldmeier, J. J., Krelove, K., Jacoby, G. H., & Gronwall, C. 2002, ApJ, 566, 784

Cooke, J., Wolfe, A. M., Prochaska, J. X., & Gawiser, E. 2004, AJ accepted, astro-ph/0411681

Dawson, S., Rhoads, J. E., Malhotra, S., et al. 2004, ApJ, 617, 707

De Breuck, C., Neri, R., Morganti, R., et al. 2003a, A&A, 401, 911

De Breuck, C., Neri, R., & Omont, A. 2003b, New Astronomy Review, 47, 285

De Breuck, C., van Breugel, W. J. M., Röttgering, H. J. A., & Miley, G. 2000, A&AS, 143, 303

De Breuck, C., van Breugel, W. J. M., Minniti, D., et al. 1999, A&A, 352, L51

De Breuck, C., van Breugel, W. J. M., Röttgering, H. J. A., et al. 2001, AJ, 121, 1241

De Breuck, C., van Breugel, W. J. M., Stanford, S. A., et al. 2002, AJ, 123, 637

Deutsch, E. W. 1999, AJ, 118, 1882

Dey, A., van Breugel, W. J. M., Vacca, W. D., & Antonucci, R. 1997, ApJ, 490, 698

Dunlop, J. S. & Peacock, J. A. 1990, MNRAS, 247, 19

Eggen, O. J., Lynden-Bell, D., & Sandage, A. R. 1962, ApJ, 136, 748

Eke, V. R., Cole, S., & Frenk, C. S. 1996, MNRAS, 282, 263

Eke, V. R., Navarro, J. F., & Frenk, C. S. 1998, ApJ, 503, 569

Ellis, R. S., Smail, I., Dressler, A., et al. 1997, ApJ, 483, 582

Ettori, S., Tozzi, P., & Rosati, P. 2003, A&A, 398, 879

Fynbo, J. P. U., Ledoux, C., Møller, P., Thomsen, B., & Burud, I. 2003, A&A, 407, 147

Fynbo, J. P. U., Møller, P., & Thomsen, B. 2001, A&A, 374, 443

Girardi, M., Borgani, S., Giuricin, G., Mardirossian, F., & Mezzetti, M. 1998, ApJ, 506, 45

Gladders, M. D. 2002, Ph.D. Thesis

Goto, T. 2005, MNRAS, 356, L6

Hammer, F., Flores, H., Lilly, S. J., et al. 1997, ApJ, 481, 49

Hashimoto, Y., Barcons, X., Böhringer, H., et al. 2004, A&A, 417, 819

Hayashino, T., Matsuda, Y., Tamura, H., et al. 2004, AJ, 128, 2073

Holden, B. P., van der Wel, A., Franx, M., et al. 2005, ApJ, 620, L83

Hu, E. M., Cowie, L. L., Capak, P., et al. 2004, AJ, 127, 563

Jarvis, M. J., Rawlings, S., Eales, S., et al. 2001, MNRAS, 326, 1585

Jarvis, M. J., Wilman, R. J., Röttgering, H. J. A., & Binette, L. 2003, MNRAS, 338, 263

Keel, W. C., Cohen, S. H., Windhorst, R. A., & Waddington, I. 1999, AJ, 118, 2547

Kodaira, K., Taniguchi, Y., Kashikawa, N., et al. 2003, PASJ, 55, L17

Kurk, J. D., Pentericci, L., Overzier, R. A., Röttgering, H. J. A., & Miley, G. K. 2004a, A&A, 428, 817

Kurk, J. D., Pentericci, L., Röttgering, H. J. A., & Miley, G. K. 2004b, A&A, 428, 793

Kurk, J. D., Röttgering, H. J. A., Pentericci, L., et al. 2000, A&A, 358, L1

Landolt, A. U. 1992, AJ, 104, 340

Large, M. I., Mills, B. Y., Little, A. G., Crawford, D. F., & Sutton, J. M. 1981, MNRAS, 194, 693

Le Fèvre, O., Deltorn, J. M., Crampton, D., & Dickinson, M. 1996, ApJ, 471, L11

Ma, C. & Feissel, M. 1998, VizieR Online Data Catalog, 1251, 0

Madau, P. 1995, ApJ, 441, 18

Maughan, B. J., Jones, L. R., Ebeling, H., & Scharf, C. 2004, MNRAS, 351, 1193

McCarthy, J. K., Cohen, J. G., Butcher, B., et al. 1998, in Proc. SPIE Vol. 3355, p. 81-92, Optical Astronomical Instrumentation, Sandro D'Odorico; Ed., 81

McCarthy, P. J., Kapahi, V. K., van Breugel, W. J. M., et al. 1996, ApJ, 107, 19

McCarthy, P. J., Kapahi, V. K., van Breugel, W. J. M., & Subrahmanya, C. R. 1990, AJ, 100, 1014

Miles, T. A., Raychaudhury, S., Forbes, D. A., et al. 2004, MNRAS, 355, 785

Miley, G. K., Overzier, R. A., Tsvetanov, Z. I., et al. 2004, Nature, 427, 47

Miyaji, T., Hasinger, G., & Schmidt, M. 2000, A&A, 353, 25

Monet, D. B. A., Canzian, B., Dahn, C., et al. 1998, VizieR Online Data Catalog, 1252, 0

Monet, D. G. 1998, Bulletin of the American Astronomical Society, 30, 1427

Nakata, F., Bower, R. G., Balogh, M. L., & Wilman, D. J. 2005, MNRAS, 357, 679

Norman, C., Hasinger, G., Giacconi, R., et al. 2002, ApJ, 571, 218

Oke, J. B. 1974, ApJ, 27, 21

Oke, J. B. 1990, AJ, 99, 1621

Oke, J. B., Cohen, J. G., Carr, M., et al. 1995, PASP, 107, 375

Ouchi, M., Shimasaku, K., Akiyama, M., et al. 2005, ApJ, 620, L1

Ouchi, M., Shimasaku, K., Furusawa, H., et al. 2003, ApJ, 582, 60

Overzier, R. A., Zirm, A. W., Miley, G. K., et al. 2005, ApJ, submitted

Papadopoulos, P. P., Röttgering, H. J. A., van der Werf, P. P., et al. 2000, ApJ, 528, 626

Pascarelle, S. M., Windhorst, R. A., Driver, S. P., Ostrander, E. J., & Keel, W. C. 1996, ApJ, 456, L21

Pentericci, L., Kurk, J. D., Carilli, C. L., et al. 2002, A&A, 396, 109

Pentericci, L., Kurk, J. D., Röttgering, H. J. A., et al. 2000a, A&A, 361, L25

Pentericci, L., McCarthy, P. J., Röttgering, H. J. A., et al. 2001, ApJ, 135, 63

Pentericci, L., Röttgering, H. J. A., Miley, G. K., et al. 1998, ApJ, 504, 139

Pentericci, L., van Reeven, W., Carilli, C. L., Röttgering, H. J. A., & Miley, G. K. 2000b, A&AS, 145, 121

Reiprich, T. H. & Böhringer, H. 2002, ApJ, 567, 716

Reuland, M., Röttgering, H. J. A., van Breugel, W. J. M., & De Breuck, C. 2004, MNRAS, 353, 377

Rhoads, J. E., Dey, A., Malhotra, S., et al. 2003, AJ, 125, 1006

Rhoads, J. E., Malhotra, S., Dey, A., et al. 2000, ApJ, 545, L85

Rhoads, J. E., Xu, C., Dawson, S., et al. 2004, ApJ, 611, 59

Rosati, P., Tozzi, P., Ettori, S., et al. 2004, AJ, 127, 230

Röttgering, H. J. A., Hunstead, R. W., Miley, G. K., van Ojik, R., & Wieringa, M. H. 1995, MNRAS, 277, 389

Röttgering, H. J. A., van Ojik, R., Miley, G. K., et al. 1997, A&A, 326, 505

Schlegel, D. J., Finkbeiner, D. P., & Davis, M. 1998, ApJ, 500, 525

Shimasaku, K., Hayashino, T., Matsuda, Y., et al. 2004, ApJ, 605, L93

Shimasaku, K., Ouchi, M., Okamura, S., et al. 2003, ApJ, 586, L111

Smith, J. A., Tucker, D. L., Kent, S., et al. 2002, AJ, 123, 2121

Somerville, R. S., Lee, K., Ferguson, H. C., et al. 2004, ApJ, 600, L171

Stanford, S. A., Eisenhardt, P. R., & Dickinson, M. 1998, ApJ, 492, 461

Steidel, C. C., Adelberger, K. L., Dickinson, M., et al. 1998, ApJ, 492, 428

Steidel, C. C., Shapley, A. E., Pettini, M., et al. 2004, ApJ, 604, 534

Stern, D., Bunker, A., Spinrad, H., & Dey, A. 2000, ApJ, 537, 73

Stevens, J. A., Ivison, R. J., Dunlop, J. S., et al. 2003, Nature, 425, 264

Stiavelli, M., Scarlata, C., Panagia, N., et al. 2001, ApJ, 561, L37

Stone, R. P. S. & Baldwin, J. A. 1983, MNRAS, 204, 347

Tanaka, M., Goto, T., Okamura, S., Shimasaku, K., & Brinkmann, J. 2004, AJ, 128, 2677

Tapken, C., Appenzeller, I., Mehlert, D., Noll, S., & Richling, S. 2004, A&A, 416, L1

Terlevich, R., Melnick, J., Masegosa, J., Moles, M., & Copetti, M. V. F. 1991, A&AS, 91, 285

Tozzi, P., Rosati, P., Ettori, S., et al. 2003, ApJ, 593, 705

Tran, K. H., van Dokkum, P. G., Illingworth, G. D., et al. 2005, ApJ, 619, 134

van Breugel, W. J. M., De Breuck, C., Stanford, S. A., et al. 1999, ApJ, 518, L61

van Dokkum, P. G. & Stanford, S. A. 2003, ApJ, 585, 78

van Zee, L., Barton, E. J., & Skillman, E. D. 2004, AJ, 128, 2797

Villar-Martín, M., Vernet, J., di Serego Alighieri, S., et al. 2003, MNRAS, 346, 273

Wall, J. V., Pearson, T. J., & Longair, M. S. 1980, MNRAS, 193, 683

Willott, C. J., Rawlings, S., Blundell, K. M., Lacy, M., & Eales, S. A. 2001, MNRAS, 322, 536

Zirm, A. W., Dickinson, M., & Dey, A. 2003, ApJ, 585, 90

5.A   Appendix: Object lists

Table 5.6 — Position and properties of the Lyα emission line of the confirmed Lyα emitters and the radio galaxy in the 2048 field.

Object	Position		z	Flux	EW$_0$	FWHM
	α_{J2000}	δ_{J2000}		erg s^{-1} cm^{-2}	Å	km s^{-1}
2048.LAE1	20 51 02.05	-27 04 52.7	2.1058 ± 0.0004	$(1.5 \pm 0.2) \times 10^{-16}$	145^{+56}_{-35}	720 ± 70
2048.LAE2	20 51 07.53	-27 04 46.1	2.0591 ± 0.0005	$(1.1 \pm 0.1) \times 10^{-16}$	37^{+4}_{-3}	1015 ± 115
2048.LAE3	20 51 13.26	-27 00 57.8	2.0580 ± 0.0005	$(1.5 \pm 0.8) \times 10^{-17}$	23^{+6}_{-5}	<415
2048.RG	20 51 03.45	-27 03 04.1	2.0590 ± 0.0004	$(2.9 \pm 0.3) \times 10^{-16}$	309^{+50}_{-27}	1580 ± 110

Table 5.7 — Position and properties of the Lyα emission line of the confirmed Lyα emitters and the radio galaxy in the 0052 field.

Object	Position		z	Flux	EW$_0$	FWHM
	α_{J2000}	δ_{J2000}		$\mathrm{erg\,s^{-1}\,cm^{-2}}$	Å	$\mathrm{km\,s^{-1}}$
0052.LAE1	00 54 14.83	−23 51 27.4	2.8301 ± 0.0010	$(4.8 \pm 0.5) \times 10^{-16}$	104^{+6}_{-5}	1075 ± 85
0052.LAE2	00 54 15.01	−23 49 42.9	2.8655 ± 0.0003	$(1.1 \pm 0.2) \times 10^{-17}$	76^{+1000}_{-21}	305 ± 50
0052.LAE3	00 54 19.05	−23 51 41.7	2.8359 ± 0.0002	$(1.0 \pm 0.3) \times 10^{-17}$	9^{+4}_{-3}	155 ± 40
0052.LAE4	00 54 21.74	−23 51 51.1	2.8691 ± 0.0004	$(4.4 \pm 1.6) \times 10^{-17}$	123^{+488}_{-25}	430 ± 50
0052.LAE5	00 54 21.95	−23 54 08.9	2.8666 ± 0.0002	$(1.2 \pm 0.2) \times 10^{-16}$	443^{+156}_{-62}	220 ± 30
0052.LAE6	00 54 22.62	−23 55 07.0	2.8489 ± 0.0002	$(1.8 \pm 0.5) \times 10^{-17}$	52^{+492}_{-13}	255 ± 40
0052.LAE7	00 54 22.75	−23 53 06.7	2.8599 ± 0.0002	$(1.0 \pm 0.3) \times 10^{-17}$	94^{+24}_{-18}	205 ± 50
0052.LAE8	00 54 24.57	−23 53 12.8	2.8449 ± 0.0002	$(2.0 \pm 0.4) \times 10^{-17}$	218^{+42}_{-28}	220 ± 40
0052.LAE9	00 54 24.58	−23 54 54.7	2.8636 ± 0.0004	$(5.2 \pm 2.3) \times 10^{-17}$	49^{+27}_{-9}	525 ± 85
0052.LAE10	00 54 25.35	−23 53 07.5	2.8628 ± 0.0003	$(4.2 \pm 1.0) \times 10^{-18}$	54^{+495}_{-14}	305 ± 50
0052.LAE11	00 54 25.64	−23 53 40.6	2.8448 ± 0.0001	$(6.1 \pm 1.1) \times 10^{-18}$	105^{+24}_{-18}	130 ± 25
0052.LAE12	00 54 26.05	−23 51 40.6	2.8656 ± 0.0004	$(2.7 \pm 0.9) \times 10^{-18}$	68^{+365}_{-16}	280 ± 80
0052.LAE13	00 54 27.31	−23 51 52.9	2.8651 ± 0.0008	$(2.3 \pm 0.6) \times 10^{-17}$	114^{+33}_{-24}	765 ± 150
0052.LAE14	00 54 28.17	−23 51 52.3	2.8444 ± 0.0012	$(1.0 \pm 0.3) \times 10^{-17}$	56^{+199}_{-12}	950 ± 235
0052.LAE15	00 54 28.59	−23 53 48.6	2.8550 ± 0.0002	$(1.2 \pm 0.1) \times 10^{-16}$	108^{+26}_{-11}	585 ± 25
0052.LAE16	00 54 28.65	−23 51 55.3	2.8479 ± 0.0003	$(2.1 \pm 0.4) \times 10^{-17}$	45^{+26}_{-8}	325 ± 50
0052.LAE17	00 54 28.89	−23 52 26.3	2.8673 ± 0.0004	$(1.0 \pm 0.2) \times 10^{-17}$	26^{+9}_{-5}	395 ± 70
0052.LAE18	00 54 29.31	−23 53 18.1	2.8669 ± 0.0002	$(5.2 \pm 0.5) \times 10^{-17}$	132^{+78}_{-19}	425 ± 30
0052.LAE19	00 54 29.84	−23 54 42.8	2.8618 ± 0.0001	$(2.3 \pm 0.3) \times 10^{-17}$	168^{+1000}_{-39}	285 ± 30
0052.LAE20	00 54 30.53	−23 53 34.1	2.8592 ± 0.0003	$(6.9 \pm 2.6) \times 10^{-18}$	78^{+22}_{-17}	150 ± 60
0052.LAE21	00 54 30.61	−23 53 36.2	2.8600 ± 0.0003	$(7.2 \pm 1.6) \times 10^{-18}$	27^{+11}_{-5}	260 ± 50
0052.LAE22	00 54 31.99	−23 49 09.3	2.8503 ± 0.0002	$(4.8 \pm 0.8) \times 10^{-18}$	118^{+26}_{-20}	225 ± 30
0052.LAE23	00 54 32.86	−23 52 14.1	2.8660 ± 0.0003	$(1.1 \pm 0.3) \times 10^{-17}$	74^{+211}_{-16}	365 ± 65
0052.LAE24	00 54 34.64	−23 53 27.7	2.8460 ± 0.0004	$(1.0 \pm 0.3) \times 10^{-17}$	76^{+21}_{-16}	275 ± 75
0052.LAE25	00 54 35.61	−23 53 27.9	2.8441 ± 0.0003	$(1.7 \pm 0.3) \times 10^{-16}$	468^{+165}_{-65}	430 ± 50
0052.LAE26	00 54 35.66	−23 54 16.7	2.8602 ± 0.0002	$(6.6 \pm 2.3) \times 10^{-18}$	34^{+34}_{-8}	90 ± 55
0052.LAE27	00 54 36.28	−23 50 01.6	2.8437 ± 0.0003	$(2.0 \pm 0.2) \times 10^{-17}$	27^{+14}_{-6}	670 ± 60
0052.LAE28	00 54 36.30	−23 53 39.1	2.8451 ± 0.0010	$(6.2 \pm 2.6) \times 10^{-18}$	115^{+46}_{-19}	610 ± 200
0052.LAE29	00 54 36.55	−23 53 40.2	2.8447 ± 0.0002	$(4.8 \pm 1.3) \times 10^{-18}$	146^{+33}_{-23}	120 ± 40
0052.LAE30	00 54 37.13	−23 51 39.2	2.8647 ± 0.0003	$(1.5 \pm 0.6) \times 10^{-17}$	102^{+31}_{-22}	145 ± 55
0052.LAE31	00 54 38.54	−23 48 39.8	2.8647 ± 0.0003	$(6.4 \pm 0.9) \times 10^{-17}$	105^{+21}_{-10}	860 ± 50
0052.LAE32	00 54 39.91	−23 52 06.6	2.8311 ± 0.0003	$(1.3 \pm 0.3) \times 10^{-17}$	410^{+130}_{-82}	495 ± 70
0052.LAE33	00 54 40.36	−23 49 13.1	2.8499 ± 0.0001	$(4.8 \pm 1.4) \times 10^{-18}$	136^{+28}_{-21}	65 ± 40
0052.LAE34	00 54 42.46	−23 50 50.5	2.8663 ± 0.0004	$(5.4 \pm 1.3) \times 10^{-18}$	101^{+1000}_{-25}	410 ± 75
0052.LAE35	00 54 42.90	−23 52 55.9	2.8756 ± 0.0003	$(4.2 \pm 0.5) \times 10^{-17}$	165^{+1000}_{-39}	440 ± 35
0052.LAE36	00 54 43.06	−23 53 14.1	2.8764 ± 0.0004	$(1.7 \pm 0.3) \times 10^{-16}$	28^{+3}_{-2}	590 ± 30
0052.LAE37	00 54 44.36	−23 51 52.4	2.8619 ± 0.0002	$(1.1 \pm 0.2) \times 10^{-17}$	38^{+24}_{-8}	265 ± 45
0052.RG	00 54 29.83	−23 51 31.1	2.8609 ± 0.0011	$(1.11 \pm 0.09) \times 10^{-15}$	133^{+6}_{-5}	2040 ± 85

Table 5.8 — Position and properties of the Lyα emission line of the confirmed Lyα emitters and the radio galaxy in the 0943 field.

Object	Position		z	Flux	EW$_0$	FWHM
	α_{J2000}	δ_{J2000}		erg s^{-1} cm^{-2}	Å	km s^{-1}
0943.LAE1	09 45 20.70	-24 28 12.5	2.8970 ± 0.0002	$(3.1 \pm 0.2)\times10^{-17}$	131^{+1000}_{-44}	600 ± 35
0943.LAE2	09 45 21.99	-24 29 55.1	2.9202 ± 0.0001	$(2.2 \pm 0.2)\times10^{-17}$	88^{+231}_{-16}	290 ± 25
0943.LAE3	09 45 22.17	-24 28 56.2	2.9259 ± 0.0002	$(2.2 \pm 0.2)\times10^{-17}$	144^{+11}_{-10}	425 ± 45
0943.LAE4	09 45 23.77	-24 28 48.0	2.9263 ± 0.0007	$(6.7 \pm 1.0)\times10^{-17}$	38^{+26}_{-6}	555 ± 75
0943.LAE5	09 45 27.14	-24 27 52.6	2.9167 ± 0.0005	$(1.1 \pm 0.3)\times10^{-17}$	61^{+9}_{-8}	360 ± 115
0943.LAE6	09 45 29.09	-24 26 49.7	2.9242 ± 0.0003	$(1.3 \pm 0.2)\times10^{-17}$	70^{+9}_{-8}	225 ± 75
0943.LAE7	09 45 30.60	-24 25 31.4	2.9265 ± 0.0005	$(7.4 \pm 1.8)\times10^{-18}$	9^{+6}_{-2}	455 ± 100
0943.LAE8	09 45 30.66	-24 28 06.2	2.9113 ± 0.0002	$(4.7 \pm 0.4)\times10^{-17}$	35^{+14}_{-5}	455 ± 35
0943.LAE9	09 45 30.83	-24 28 01.4	2.9214 ± 0.0006	$(6.1 \pm 2.1)\times10^{-18}$	8^{+14}_{-3}	410 ± 140
0943.LAE10	09 45 31.13	-24 27 34.4	2.9122 ± 0.0006	$(1.0 \pm 0.2)\times10^{-17}$	71^{+11}_{-10}	440 ± 65
0943.LAE11	09 45 32.26	-24 31 21.6	2.9259 ± 0.0003	$(9.8 \pm 1.4)\times10^{-18}$	49^{+319}_{-11}	445 ± 60
0943.LAE12	09 45 32.68	-24 29 46.5	2.9004 ± 0.0003	$(2.1 \pm 0.2)\times10^{-16}$	67^{+18}_{-10}	625 ± 30
0943.LAE13	09 45 32.77	-24 29 05.4	2.9189 ± 0.0003	$(7.7 \pm 0.8)\times10^{-17}$	103^{+569}_{-20}	630 ± 35
0943.LAE14	09 45 32.86	-24 31 06.9	2.9073 ± 0.0000	$(4.1 \pm 0.1)\times10^{-17}$	177^{+23}_{-19}	180 ± 10
0943.LAE15	09 45 34.34	-24 29 23.7	2.9094 ± 0.0001	$(3.2 \pm 0.2)\times10^{-17}$	111^{+1000}_{-26}	330 ± 20
0943.LAE16	09 45 34.96	-24 30 46.9	2.9242 ± 0.0002	$(1.7 \pm 0.2)\times10^{-17}$	28^{+9}_{-4}	275 ± 50
0943.LAE17	09 45 36.18	-24 30 00.5	2.9174 ± 0.0005	$(1.7 \pm 0.5)\times10^{-17}$	20^{+36}_{-5}	305 ± 90
0943.LAE18	09 45 36.36	-24 29 56.4	2.9313 ± 0.0002	$(5.4 \pm 0.3)\times10^{-17}$	133^{+418}_{-24}	695 ± 35
0943.LAE19	09 45 37.19	-24 26 27.2	2.9081 ± 0.0003	$(2.8 \pm 0.6)\times10^{-17}$	103^{+17}_{-14}	430 ± 45
0943.LAE20	09 45 37.52	-24 25 23.7	2.9266 ± 0.0005	$(5.1 \pm 0.6)\times10^{-17}$	165^{+12}_{-11}	720 ± 60
0943.LAE21	09 45 38.64	-24 29 54.3	2.9159 ± 0.0006	$(2.2 \pm 0.8)\times10^{-17}$	136^{+14}_{-12}	595 ± 80
0943.LAE22	09 45 38.71	-24 29 57.5	2.9201 ± 0.0003	$(1.6 \pm 0.2)\times10^{-17}$	20^{+6}_{-3}	510 ± 55
0943.LAE23	09 45 39.08	-24 30 10.2	2.9189 ± 0.0004	$(5.6 \pm 1.3)\times10^{-17}$	33^{+20}_{-6}	680 ± 65
0943.LAE24	09 45 39.17	-24 29 20.1	2.9089 ± 0.0002	$(2.1 \pm 0.2)\times10^{-17}$	26^{+19}_{-6}	515 ± 40
0943.LAE25	09 45 39.46	-24 26 15.9	2.9037 ± 0.0010	$(2.0 \pm 0.4)\times10^{-17}$	221^{+42}_{-30}	1185 ± 195
0943.LAE26	09 45 41.88	-24 28 35.1	2.9309 ± 0.0008	$(4.3 \pm 1.9)\times10^{-18}$	7^{+5}_{-2}	360 ± 165
0943.LAE27	09 45 42.61	-24 28 57.9	2.9302 ± 0.0001	$(2.1 \pm 0.2)\times10^{-17}$	150^{+1000}_{-32}	285 ± 25
0943.LAE28	09 45 45.72	-24 26 49.1	2.9233 ± 0.0007	$(3.1 \pm 0.7)\times10^{-17}$	86^{+477}_{-17}	630 ± 60
0943.RG	09 45 32.74	-24 28 49.7	2.9209 ± 0.0003	$(3.6 \pm 0.1)\times10^{-15}$	173^{+3}_{-3}	1755 ± 20

Table 5.9 — Position and properties of the Lyα emission line of the confirmed Lyα emitters and the radio galaxy in the 2009 field.

Object	Position		z	Flux	EW$_0$	FWHM
	α_{J2000}	δ_{J2000}		erg s^{-1} cm^{-2}	Å	km s^{-1}
2009.LAE1	20 09 38.32	-30 41 31.6	3.1528 ± 0.0001	$(7.2 \pm 0.7)\times10^{-18}$	75^{+10}_{-8}	175 ± 20
2009.LAE2	20 09 39.89	-30 40 50.7	3.1577 ± 0.0007	$(2.6 \pm 0.8)\times10^{-18}$	12^{+20}_{-4}	530 ± 135
2009.LAE3	20 09 40.92	-30 41 44.9	3.1548 ± 0.0006	$(1.6 \pm 0.6)\times10^{-18}$	25^{+206}_{-6}	385 ± 115
2009.LAE4	20 09 41.06	-30 42 46.4	3.1415 ± 0.0005	$(1.9 \pm 0.7)\times10^{-18}$	73^{+11}_{-9}	320 ± 95
2009.LAE5	20 09 42.19	-30 38 34.3	3.1601 ± 0.0003	$(4.2 \pm 0.7)\times10^{-18}$	16^{+52}_{-6}	370 ± 50
2009.LAE6	20 09 47.83	-30 42 39.6	3.1521 ± 0.0004	$(1.4 \pm 0.2)\times10^{-17}$	27^{+50}_{-6}	720 ± 75
2009.LAE7	20 09 49.55	-30 40 47.4	3.1531 ± 0.0003	$(1.7 \pm 0.4)\times10^{-17}$	23^{+37}_{-5}	485 ± 55
2009.LAE8	20 09 54.43	-30 41 19.7	3.1445 ± 0.0006	$(1.4 \pm 0.4)\times10^{-16}$	38^{+699}_{-10}	505 ± 120
2009.LAE9	20 09 56.94	-30 39 38.6	3.1412 ± 0.0006	$(6.5 \pm 0.3)\times10^{-16}$	49^{+4}_{-3}	3170 ± 50
2009.LAE10	20 09 58.82	-30 40 37.1	3.1454 ± 0.0004	$(7.3 \pm 0.3)\times10^{-16}$	84^{+14}_{-8}	1565 ± 25
2009.LAE11	20 10 01.81	-30 41 27.7	3.1581 ± 0.0003	$(5.8 \pm 0.5)\times10^{-17}$	23^{+6}_{-3}	750 ± 30
2009.RG	20 09 48.12	-30 40 07.4	3.1497 ± 0.0002	$(2.41 \pm 0.04)\times10^{-15}$	68^{+1}_{-1}	2300 ± 25

Table 5.10 — Position and properties of the Lyα emission line of the confirmed Lyα emitters and the radio galaxy in the two 1338 fields.

Object	Position		z	Flux	EW$_0$	FWHM
	α_{J2000}	δ_{J2000}		erg s^{-1} cm^{-2}	Å	km s^{-1}
1338.LAE1	13 38 21.27	-19 45 52.7	4.0977 ± 0.0010	$(1.5 \pm 0.4)\times10^{-17}$	55^{+38}_{-7}	495 ± 105
1338.LAE2	13 38 21.32	-19 44 42.5	4.1092 ± 0.0003	$(8.1 \pm 2.2)\times10^{-18}$	33^{+17}_{-6}	<255
1338.LAE3	13 38 21.68	-19 46 27.9	4.0978 ± 0.0003	$(1.0 \pm 0.4)\times10^{-18}$	14^{+7}_{-3}	75 ± 75
1338.LAE4	13 38 22.47	-19 44 33.8	4.0950 ± 0.0002	$(2.7 \pm 0.3)\times10^{-17}$	51^{+7}_{-4}	230 ± 40
1338.LAE5	13 38 22.78	-19 46 04.8	4.0976 ± 0.0003	$(3.0 \pm 1.1)\times10^{-18}$	49^{+16}_{-13}	120 ± 65
1338.LAE6	13 38 23.65	-19 45 51.7	4.0969 ± 0.0003	$(2.2 \pm 0.7)\times10^{-18}$	24^{+5}_{-3}	95 ± 55
1338.LAE7	13 38 24.79	-19 41 34.2	4.1055 ± 0.0004	$(5.9 \pm 1.4)\times10^{-18}$	29^{+51}_{-7}	<260
1338.LAE8	13 38 24.87	-19 41 46.0	4.1017 ± 0.0007	$(9.2 \pm 2.9)\times10^{-18}$	31^{+23}_{-6}	270 ± 140
1338.LAE9	13 38 25.11	-19 43 11.2	4.1004 ± 0.0007	$(7.0 \pm 1.3)\times10^{-17}$	63^{+15}_{-7}	720 ± 55
1338.LAE10	13 38 25.32	-19 45 55.9	4.0970 ± 0.0002	$(1.6 \pm 0.3)\times10^{-17}$	167^{+25}_{-17}	420 ± 90
1338.LAE11	13 38 26.18	-19 43 34.7	4.1010 ± 0.0006	$(6.0 \pm 1.5)\times10^{-17}$	70^{+23}_{-9}	445 ± 45
1338.LAE12	13 38 26.20	-19 46 28.5	4.0925 ± 0.0005	$(9.0 \pm 1.7)\times10^{-18}$	152^{+32}_{-22}	460 ± 55
1338.LAE13	13 38 28.08	-19 39 50.5	4.0877 ± 0.0004	$(1.4 \pm 0.4)\times10^{-17}$	278^{+1000}_{-62}	<170
1338.LAE14	13 38 28.73	-19 44 37.2	4.1020 ± 0.0002	$(4.5 \pm 0.6)\times10^{-17}$	123^{+1000}_{-18}	<200
1338.LAE15	13 38 29.41	-19 49 01.7	4.1010 ± 0.0005	$(2.5 \pm 0.6)\times10^{-18}$	80^{+22}_{-15}	405 ± 75
1338.LAE16	13 38 29.68	-19 44 00.0	4.1021 ± 0.0003	$(4.6 \pm 1.2)\times10^{-18}$	31^{+9}_{-4}	<165
1338.LAE17	13 38 29.88	-19 43 26.1	4.0927 ± 0.0004	$(7.0 \pm 1.3)\times10^{-18}$	267^{+1000}_{-71}	350 ± 80
1338.LAE18	13 38 30.16	-19 40 38.3	4.1132 ± 0.0005	$(1.6 \pm 0.4)\times10^{-17}$	98^{+391}_{-19}	275 ± 105
1338.LAE19	13 38 30.17	-19 48 44.9	4.0872 ± 0.0003	$(7.1 \pm 1.2)\times10^{-18}$	144^{+1000}_{-37}	240 ± 35
1338.LAE20	13 38 32.85	-19 44 07.2	4.0969 ± 0.0003	$(7.6 \pm 1.8)\times10^{-18}$	45^{+30}_{-6}	<170
1338.LAE21	13 38 33.58	-19 43 36.3	4.0965 ± 0.0009	$(4.6 \pm 0.9)\times10^{-17}$	31^{+3}_{-2}	380 ± 80
1338.LAE22	13 38 34.15	-19 42 53.4	4.0955 ± 0.0009	$(2.6 \pm 0.8)\times10^{-17}$	42^{+105}_{-9}	505 ± 150
1338.LAE23	13 38 34.44	-19 47 03.7	4.0983 ± 0.0003	$(3.7 \pm 0.8)\times10^{-18}$	66^{+348}_{-13}	215 ± 45
1338.LAE24	13 38 34.69	-19 43 43.2	4.0979 ± 0.0002	$(3.3 \pm 0.6)\times10^{-18}$	35^{+301}_{-6}	135 ± 30
1338.LAE25	13 38 34.98	-19 42 25.4	4.0925 ± 0.0008	$(7.4 \pm 2.6)\times10^{-18}$	19^{+7}_{-4}	275 ± 160
1338.LAE26	13 38 35.10	-19 45 07.8	4.0967 ± 0.0005	$(5.4 \pm 2.3)\times10^{-18}$	53^{+18}_{-13}	<150
1338.LAE27	13 38 35.52	-19 45 23.7	4.0999 ± 0.0005	$(9.4 \pm 2.3)\times10^{-18}$	90^{+420}_{-15}	230 ± 110
1338.LAE28	13 38 35.67	-19 45 50.1	4.0987 ± 0.0003	$(3.1 \pm 0.7)\times10^{-18}$	54^{+14}_{-9}	395 ± 70
1338.LAE29	13 38 35.82	-19 49 36.5	4.0975 ± 0.0004	$(3.5 \pm 0.9)\times10^{-18}$	27^{+5}_{-3}	335 ± 70
1338.LAE30	13 38 37.15	-19 45 02.0	4.0943 ± 0.0003	$(6.0 \pm 1.0)\times10^{-17}$	103^{+141}_{-12}	440 ± 35
1338.LAE31	13 38 39.69	-19 47 50.1	4.0948 ± 0.0007	$(3.6 \pm 1.0)\times10^{-17}$	72^{+32}_{-10}	575 ± 45
1338.LAE32	13 38 41.10	-19 43 01.7	4.0941 ± 0.0007	$(2.3 \pm 0.2)\times10^{-16}$	16^{+1}_{-1}	2110 ± 85
1338.LAE33	13 38 41.11	-19 44 22.4	4.1015 ± 0.0005	$(1.9 \pm 0.6)\times10^{-17}$	49^{+17}_{-13}	235 ± 75
1338.LAE34	13 38 43.85	-19 44 41.0	4.0978 ± 0.0003	$(2.4 \pm 0.6)\times10^{-17}$	101^{+1000}_{-26}	220 ± 30
1338.LAE35	13 38 44.65	-19 47 09.4	4.1185 ± 0.0002	$(3.2 \pm 0.3)\times10^{-17}$	313^{+1000}_{-53}	300 ± 40
1338.LAE36	13 38 47.19	-19 48 16.7	4.0979 ± 0.0008	$(1.8 \pm 0.4)\times10^{-17}$	119^{+25}_{-18}	655 ± 125
1338.LAE37	13 38 50.12	-19 46 12.2	4.0958 ± 0.0004	$(1.2 \pm 0.4)\times10^{-18}$	37^{+52}_{-8}	165 ± 55
1338.RG	13 38 26.06	-19 42 30.8	4.1052 ± 0.0006	$(4.4 \pm 0.2)\times10^{-15}$	578^{+16}_{-14}	1810 ± 40

Chapter 6

Properties of distant Lyα emitters in overdense regions

Abstract. Deep narrow-band imaging of high redshift ($z > 2$) radio galaxy fields has resulted in the discovery of ~ 300 Lyα emitters. Follow-up spectroscopy confirmed ~ 150 of the emitters, with a spectroscopic success rate of $> 90\%$. Here we discuss the properties of the candidate and confirmed Lyα emitters. Based on the width of the emission line, the fraction of active galactic nuclei among the emitters is low, and $> 90\%$ of the emitters are star forming galaxies. These star forming galaxies have $L_{\mathrm{Ly}\alpha} < 10^{43}$ erg s^{-1} and are generally fainter than L^* in the continuum. The continuum colors of the emitters are blue, with a mean $\beta = -1.7$. The star formation rates (SFRs) of the Lyα emitting galaxies generally lie in the range $1 < SFR < 10\ M_\odot\,\mathrm{yr}^{-1}$, as measured by both the UV continuum and the Lyα line luminosity. The blue colors and the close relation between the UV and Lyα SFRs suggest that the amount of dust in the galaxies is small. The absence of stellar continuum in $\sim 30\%$ of the sources allows us to derive upper limits on the age of the galaxies. We find that 16% of the Lyα emitters could be younger than 10 Myr, which suggests that the population of Lyα emitters are galaxies with ages < 100 Myr. However, we cannot find evidence that the Lyα emitters are primitive, zero metallicity objects.

B. P. Venemans, H. J. A. Röttgering & G. K. Miley

6.1   Introduction

ALREADY in the 1970s blank field surveys with a narrow-band filter were proposed to be an efficient method to find high redshift galaxies (Meier 1976). Models of stellar population synthesis to compute the Lyα emission from galaxies predicted high Lyα luminosities $L_{\mathrm{Ly}\alpha} > 10^{44}$ erg s^{-1} (e.g., Charlot & Fall 1993). Despite the efforts of many research groups, for twenty years all searches for high redshift Lyα emitters failed (e.g., Koo & Kron 1980; Pritchet & Hartwick 1987; Smith et al. 1989; Lowenthal et al. 1990; de Propris et al. 1993; Thompson et al. 1995; Thompson & Djorgovski 1995). A review of the unsuccessful surveys and the implications thereof can be found in Pritchet (1994).

The situation changed with the advent of the 8–10 m class telescopes, which led to an increase in sensitivity. Using the Keck telescope, Cowie & Hu (1998) and Hu et al. (1998) found a significant population of Lyα emitting galaxies (densities of 15 000 emitters deg^{-2} per unit z) at $z \simeq 3.4$ in several blank fields. Now, blank field narrow-band imaging is being carried out with great success and high redshift galaxies are found up to $z > 6.5$ (e.g., Kudritzki et al. 2000; Rhoads & Malhotra 2001; Fynbo et al. 2001; Hu et al. 2002; Fynbo et al. 2003; Fujita et al. 2003; Kodaira et al. 2003; Rhoads et al. 2003; Ouchi et al. 2003; Dawson et al. 2004; Palunas et al. 2004; Hayashino et al. 2004; Hu et al. 2004; Ouchi et al. 2005).

Because narrow-band imaging can efficiently select Lyα galaxies in a narrow red-shift range, this technique is ideal for finding and studying large scale structures of galaxies (e.g., Steidel et al. 2000; Møller & Fynbo 2001; Shimasaku et al. 2003; Palunas et al. 2004; Ouchi et al. 2005). Our program of deep narrow-band imaging of the surroundings of high redshift ($z > 2$) radio galaxies has resulted in the discovery of overdensities of Lyα emitters that are associated with the radio galaxies. The large scale structures of Lyα emitters are likely to be the progenitors of present-day massive clusters (Chapter 5). Analysis of the properties of 31 confirmed Lyα emitters in a pro-tocluster at $z = 3.13$ showed that the emitters can be characterized as faint, blue and small galaxies compared to UV bright star forming galaxies at $z \simeq 3$ (Chapter 3), and that they might be young, dust free star burst galaxies. To further study the nature of the Lyα emitters, we extend in this chapter the study of protocluster Lyα emitters by investigating the properties of the Lyα emitting galaxies in all our observed radio galaxy fields. In §6.2 we shall discuss whether the Lyα emitters have dominant active galactic nuclei or not, and in §6.3, the observed properties of the emitters are presented. §6.4 discusses the star formation rates of the Lyα emitters, and the implications of our results are considered in §6.5. Throughout this chapter, the cosmology used has $\Omega_M = 0.3$, $\Omega_\Lambda = 0.7$ and $H_0 = 70$ km s^{-1} Mpc^{-1}. Magnitudes are in the AB system (Oke 1974).

6.2   Active galactic nuclei or star forming galaxies?

The first question that we shall address is whether the observed Lyα emission is produced by gas excited by active galactic nuclei (AGNs) or by star forming. A clear indication for an AGN in a galaxy is the presence of a broad emission line in the spectrum. In Fig. 6.1 we show the distribution of the full width at half maximum (FWHM) of the

Figure 6.1 — Distribution of the FWHM of 153 confirmed galaxies with a Lyα emission line. For lines that remained unresolved, 2σ upper limits are given.
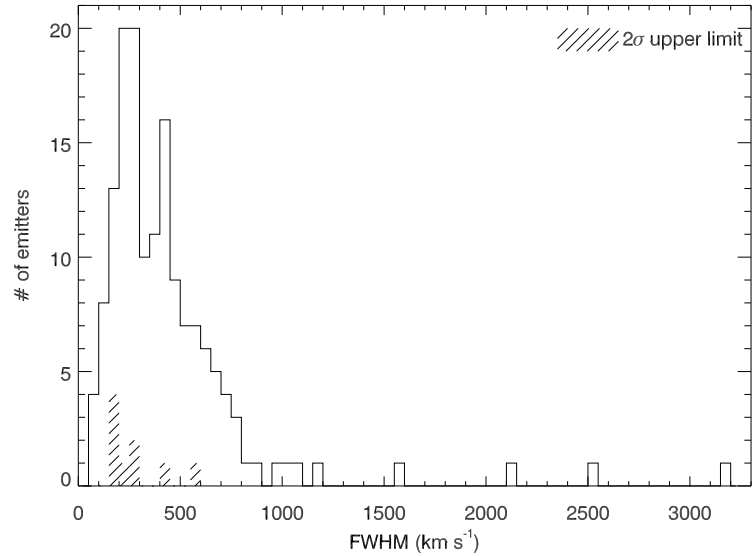
Lyα lines of all 153 confirmed emitters discovered in our large program (Chapter 5). Four emitters have a line with a width of $> 1500 \, \mathrm{km \, s^{-1}}$, which we classify as broad line QSOs (e.g., Della Ceca et al. 2003). Two emitters with a *FWHM* $\simeq 1000 - 1100 \, \mathrm{km \, s^{-1}}$ line show accompanying N vλ1240. Because N V is non existent (or at least extreme faint) in star forming galaxies at $z \sim 3$ (Shapley et al. 2003; Cooke et al. 2004), the detection of N V argues for the presence of an AGN in these galaxies. The rest of the sample, which comprises roughly 95% of the confirmed emitters, has a line width smaller than $1000 \, \mathrm{km \, s^{-1}}$. These emitters are either star forming galaxies or narrow line, obscured QSOs (often called type-II QSOs, e.g., Norman et al. 2002). Based on the detection of emission lines such as C IV λ1549, we identified one type-II QSO in the protocluster near MRC 0943-242 (see Chapter 5). However, for most of our Lyα emitters either the wavelength range of the spectra does not include the C IV line, or the sensitivity is not high enough to establish the presence (or absence) of the C IV line.

In a large survey to detect $z \simeq 3$ star forming galaxies, Steidel et al. (2003) report the detection of 29 QSOs, of which 13 had broad (*FWHM* $> 2000 \, \mathrm{km \, s^{-1}}$) emission lines and 16 narrow lines. The implied ratio of narrow line to broad line QSOs is 1.2 ± 0.4 (Steidel et al. 2003). A similar ratio, although with less statistical significance, was found by Jarvis et al. (2005) in a survey for high redshift Lyα emitters. These optical observations are consistent with early results from deep X-ray observations (Stern et al. 2002). With our detection of four broad line QSOs, we expect only four to five type-II QSOs among the Lyα emitters. Also, as computed in Chapter 3, we expect roughly one AGN (either with broad or narrow emission lines) in each of our seven fields. A more robust limit on the fraction of QSOs among the Lyα emitters can be obtained by X-ray observations. Three of the 37 Lyα emitters (8%) in the protocluster near the radio galaxy MRC 1138–262 at $z = 2.16$ were detected in a 40 ks exposure with the *Chandra* telescope (Pentericci et al. 2002). In contrast, none of the 101 Lyα emitters at $z = 4.5$ in the Large Area Lyman Alpha (LALA) survey were found to show any X-ray emission (Malhotra et al. 2003; Wang et al. 2004).

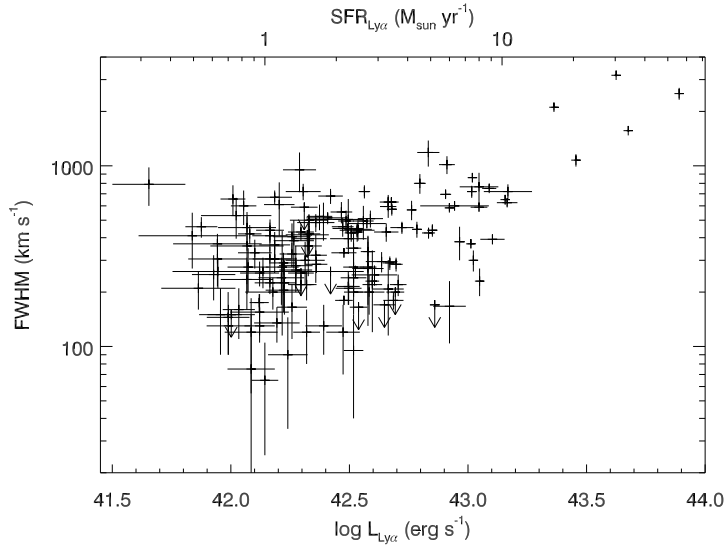We conclude that the majority of the observed Lyα emitters (90–95%) must be star

Figure 6.2 — Lyα luminosity versus FWHM of 153 confirmed Lyα emitters. Five of the seven known QSOs in the protocluster fields occupy the region $L_{\mathrm{Ly}\alpha} > 10^{43}$ erg s^{-1} and *FWHM* > 1000 km s^{-1}.

forming galaxies.

6.3   Nature of the protocluster Lyα emitters

Lyα emitters are by definition characterized by a strong Lyα emission line and, because of the equivalent width selection criterion (§6.1; Chapter 3; Chapter 5), by a relatively faint UV continuum. In this section, we will describe the properties of the Lyα emitters.

6.3.1   Lyα line luminosity

In Fig. 6.2 we show the distribution of the Lyα luminosity of the 153 confirmed emitters versus the width of the emission line. The Lyα luminosity is computed from the narrow- and broad-band imaging (see Chapter 3 for the details on the calculations). At Lyα luminosities $L_{\mathrm{Ly}\alpha} > 2 \times 10^{43}$ erg s^{-1}, the emitters have lines with a *FWHM* > 1000 km s^{-1} and are classified as QSOs (§6.2). Although we reach the sensitivity, we do not find a broad line QSO with $L_{\mathrm{Ly}\alpha} < 10^{43}$ erg s^{-1}. Such objects must therefore be rare. Also all Lyα emitters with a *FWHM* < 1000 km s^{-1} have $L_{\mathrm{Ly}\alpha} \lesssim 2 \times 10^{43}$ erg s^{-1}. The apparent dearth of emitters with $L_{\mathrm{Ly}\alpha} < 10^{42}$ erg s^{-1} is caused by the flux limit of the spectroscopic observations. The faintest lines that were spectroscopically confirmed had a Lyα flux of $f_{\mathrm{Ly}\alpha} \sim 10^{-17}$ erg s^{-1} cm^{-2}, which, for an emitter at $z = 3$, corresponds to $L_{\mathrm{Ly}\alpha} = 8 \times 10^{41}$ erg s^{-1}.

Because the majority of the confirmed emitters are probably star forming galaxies, we can convert the Lyα luminosity to a star formation rate (SFR). The SFR of the Lyα emitters are in the range $0.2 < SFR_{\mathrm{Ly}\alpha} \lesssim 11\ M_\odot$ yr^{-1}. A discussion of the SFRs is given in §6.4.

6.3.2   UV continuum luminosity

In Fig. 6.3 the *I*-band magnitude distribution is shown of confirmed and candidate Lyα emitters in the 0052 ($z = 2.86$) and 0316 ($z = 3.13$) protoclusters. The *I*-band at these redshifts probes the rest-frame continuum near 2000 Å, which is almost free of

Figure 6.3 — *I* magnitudes of 134 candidate and confirmed emitters in the 0052 ($z = 2.86$) and 0316 ($z = 3.13$) fields. For objects that are not detected, a 2σ lower limit on the magnitude is given.
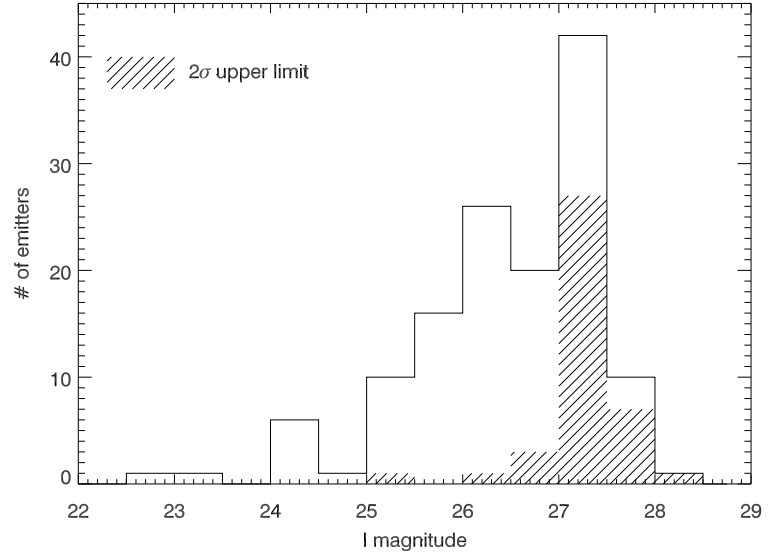
emission lines. The only emission line near 2000 Å is C III] $\lambda 1909$. In $z \sim 3$ Lyman Break Galaxies (LBGs) this emission line has a rest-frame equivalent width of $\lesssim 6$ Å (Shapley et al. 2003), implying a contribution to the *I*-band magnitude of less than 2%. The *I*-band magnitudes of the $z \simeq 3$ Lyα emitters range from $m_I \sim 23$ to $m_I > 28$. Of the 134 emitters in the two fields, 40 (30%) remained undetected (the hashed histogram in Fig. 6.3). Furthermore, only 20 (15%) of the emitters are brighter than $m_I = 25.5$. This magnitude is typically the spectroscopic limit for ground-based surveys for $z \simeq 3$ Lyman break galaxies (e.g., Shapley et al. 2003; Steidel et al. 2003; Cooke et al. 2004).

Fig. 6.4 shows the distribution of UV continuum luminosity at a rest-frame wavelength of 1500 Å of the 153 confirmed emitters in our protoclusters. For emitters that were imaged in only one broad-band filter, the contribution of the emission line was subtracted from the broad-band magnitude to derive the continuum luminosity. We further assumed that the UV continuum was flat (see §6.3.3). The QSOs dominate at the bright end of the distribution. The fraction of emitters that is undetected in the continuum is 29%. In Fig. 6.4 we also plotted the absolute magnitude of L^* at redshift of $z \simeq 3$ as derived by Steidel et al. (1999). Most likely, the value of L^* does not change significantly between $z = 3$ and $z = 4$ (Steidel et al. 1999). Of the confirmed Lyα emitters 95% are fainter than L^*, while most of the emitters that are brighter than L^* are QSOs. This shows that the Lyα search technique is very powerful in detecting (and confirming) galaxies at the faint end of the luminosity function.

The luminosity at 1500 Å can be used to calculate the SFR of of a galaxy (e.g., Madau et al. 1998). As can be seen in Fig. 6.4, most of the Lyα emitters form stars in a rate a few solar masses per year. This is lower than the average SFR of Lyman Break Galaxies, which is a few *tens* of solar masses per year (Giavalisco 2002; Shapley et al. 2003).

6.3.3   Continuum color

The 0316 protocluster at $z = 3.13$ and the 0052 protocluster at $z = 2.86$ were observed in two broad-band filters (Chapter 5). With the extra broad-band image an UV continuum slope can be derived. Chapter 3 describes in detail how the color, parameterized by
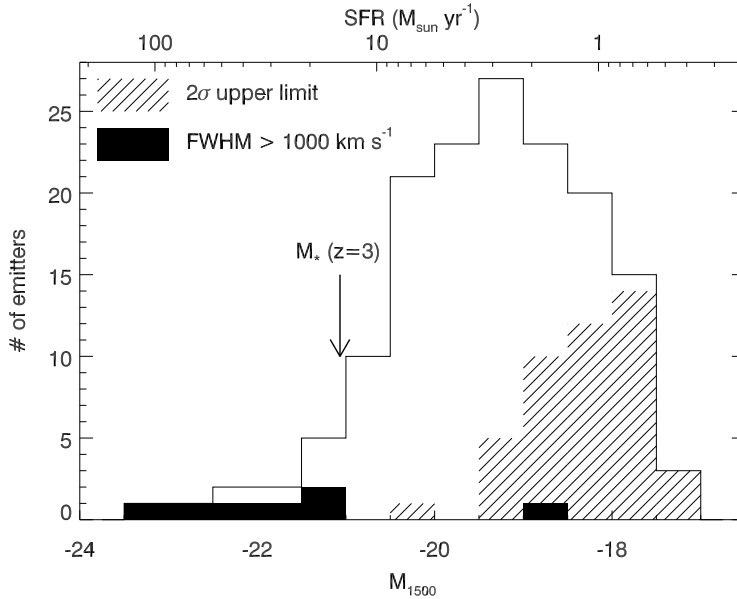
Figure 6.4 — Histogram of the absolute magnitude at a rest-frame wavelength of 1500 Å for 153 confirmed Lyα emitters. Emitters with a line width *FWHM* > 1000 km s^{-1}, which are likely to harbour an AGN, are represented by the filled histogram. Objects with an undetected UV continuum are shown in the hashed histogram.

β (with $f_\lambda \propto \lambda^\beta$), can be computed from the available data. In Fig. 6.5 the *I*-band magnitude of the confirmed emitters in the 0052 and 0316 fields are plotted against continuum slope. 14 of the 68 confirmed emitters (21%) remained undetected in both broad-band images and a slope could not be computed for these galaxies. Because the continuum of the emitters is faint (§6.3.2), the value of the continuum slope is not well constraint. The continuum slope ranges from $\beta = -4.9$ to $\beta = 0.6$. The median slope of the sample plotted in Fig. 6.5 is $\beta = -1.8$, very similar to the average of $\beta = -1.7$. The average color of $\beta = -1.7$ is much bluer than that of LBGs at redshift ~ 3 (Shapley et al. 2003). The sample of LBGs with Lyα in emission has a mean slope of $\beta = -1.1$ (Shapley et al. 2003).

Models of star burst galaxies predict UV continuum slopes of $\beta \simeq -2.1$ for constant star forming, dust free galaxies older than a few million years (Leitherer et al. 1999). Roughly 70% of the confirmed emitters for which we could compute a continuum slope, have within the uncertainty a slope that is consistent with that of an unobscured star burst galaxy.

6.4 Star formation rates

If it is assumed that the Lyα emission is caused by the emission of hot, massive stars, then the Lyα luminosity can be used to calculate the star formation rate (see Chapter 3). Assuming Case B recombination ($L_{\text{Ly}\alpha}/L_{\text{H}\alpha} = 8.7$, Brocklehurst 1971) and the empirical Hα luminosity to SFR conversion for a Salpeter initial mass function from Madau et al. (1998), the SFR of the Lyα emitters is in the range $0.2 < SFR_{\text{Ly}\alpha} < 11\ M_\odot$ yr^{-1} (Fig. 6.2). Because Lyα is a resonant line, the emission line can easily be extinguished due to absorption by dust in the galaxy. Even a small amount of dust could diminish the emission of Lyα. Therefore the SFR as calculated from the Lyα line probably underestimates the true SFR of a galaxy.

A more accepted method to derive a SFR is to use the UV continuum luminosity at

Figure 6.5 — *I*-band magnitude versus UV continuum slope β of 68 confirmed Lyα emitters in the 0052 and 0316 protoclusters.
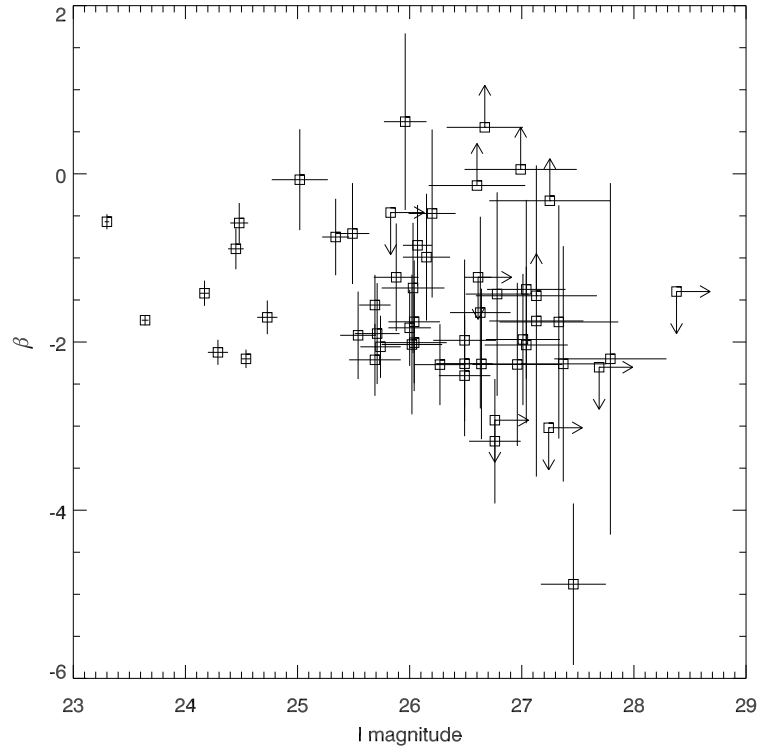
a rest-frame wavelength of 1500 Å (see §6.3.2). In Fig. 6.6 the two methods to calculate the SFR are plotted. The SFRs are broadly consistent with each other. On average, the SFR_{UV} is 1.3 times the SFR as calculated by the Lyα luminosity. Because, as mentioned above, it is much harder for a Lyα photon to escape the galaxy due to resonant scattering, this implies that the amount of dust in the galaxies must be small on average and that the extinction correction on the SFRs must be a factor $\ll 2$.

6.5 Discussion

We can summarize the properties of the Lyα emitters as faint and blue. The number of QSOs among the Lyα emitters, most of which can be identified by their broad emission line (*FWHM* > 1000 km s^{-1}), is small, and we estimate that a fraction of $\sim 5\%$ of the emitters are QSOs. The vast majority of the emitters are therefore star forming galaxies. These galaxies have typical star formation rates of a few $M_\odot$ yr^{-1}.

What can we deduce from these characteristics of Lyα emitters? The average blue color and the close relation between the SFRs as derived from the Lyα luminosity and the UV continuum, suggest that the amount of dust in these galaxies is small. The colors of 70% of the galaxies are consistent with that of an unobscured star forming galaxy. High resolution images of Lyα emitters taken with the *Hubble Space Telescope* further show that they are small compared to the bright star forming LBGs (Chapter 3, Overzier et al. in prep). The UV luminosities of the emitters are generally below L^*. These properties are consistent with the Lyα emitters being young star forming galaxies in their first starburst phase (see also Chapter 3).

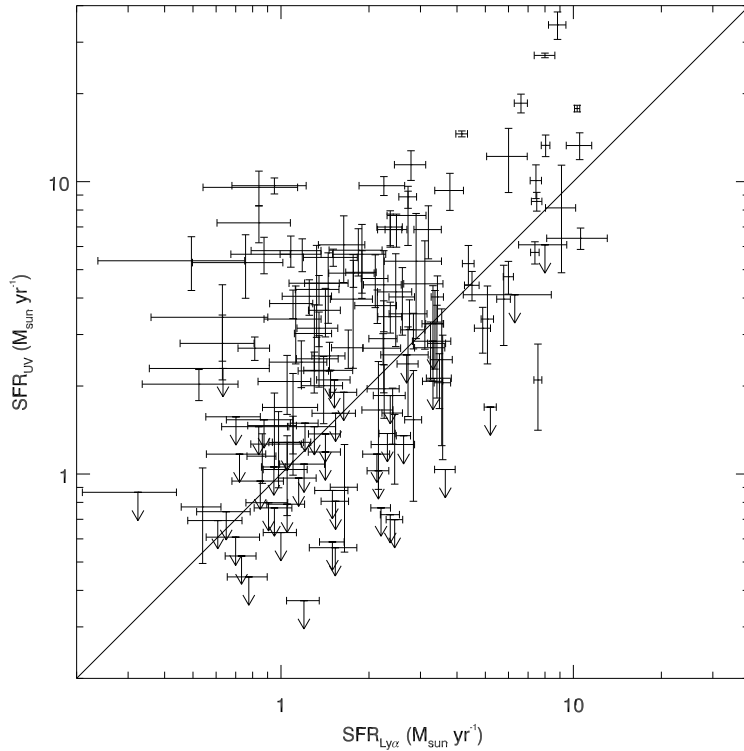The absence of a strong stellar continuum can be used to constrain the age of a

Figure 6.6 — Star formation rate as calculated by the Lyα luminosity plotted against the star formation rate as derived from the UV continuum at 1500 Å. The solid line shows where $SFR_{UV} = SFR_{Lyα}$.

Lyα emitter (Ellis et al. 2001). We illustrate this in Fig. 6.7, where we calculate the observed I-band magnitude of a galaxy at $z = 2.86$ and $z = 3.13$ that has a continuous star formation rate of $1\,M_\odot\,\mathrm{yr}^{-1}$. Models with different metallicities were used, ranging from $Z = 0.001$ to $Z = 0.04$. At galaxy ages < 10 Myr, the dependence of the predicted I-band magnitude on the metallicity is very weak. Following Ellis et al. (2001), we can now derive a maximum age for the emitters that are not detected in the I-band in the 0052 and 0316 fields. The number of confirmed emitters in these two fields is 68 (Chapter 3; Chapter 5). 17 of these (25%) are undetected in the I-band image down to 2σ upper limits of $m_I > 25.0 - 28.4$. Scaling the curves in Fig. 6.7 with the Lyα star formation rates, we find that 11 emitters (16%) have ages less than 10 Myr, otherwise we should have detected the emitters in the I-band images. If we now assume that emitters are only visible in Lyα when they undergo their first burst of star formation, then, based on the 16% that have an age of < 10 Myr, Lyα emitters should be younger than < 100 Myr.

An alternative explanation for the very faint continuum fluxes could be that the undetected Lyα emitters are dusty star burst galaxies, with the Lyα emission escaping the galaxy through outflows. Indeed, some of Lyα emitters have line profiles that are consistent with that of an outflow (see Chapter 3). In this scenario the emitters should be red which is a signature of the absorption. However, some of the emitters without an I-band flux were detected in a bluer broad-band image. Hence, they have a blue continuum slope (Fig. 6.5; Table 4 in Chapter 3), inconsistent with the color of a dusty star burst.

To resolve this issue, deep exposures are needed at longer wavelengths. If the undetected emitters are obscured star burst galaxies, they should appear in the rest-frame

Figure 6.7 — *I*-band magnitude as a function of age for a model galaxy from STARBURST99 (Leitherer et al. 1999) with a constant star formation rate of 1 $M_\odot$ yr^{-1} and a Salpeter initial mass function. The solid lines represent a galaxy at $z = 2.86$, and the dashed lines one at $z = 3.13$. The different lines at each redshift indicates the effect of a different metallicity, which ranges from $Z = 0.001$ (lowest solid and dashed lines) to $Z = 0.04$ ($= 2Z_\odot$, top lines).
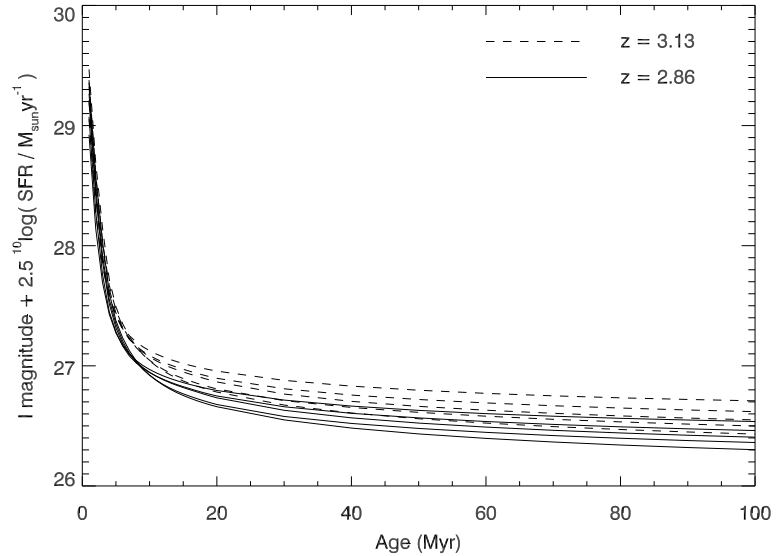
optical or infrared where the attenuation is less. If the Lyα emitters are detected in deep *Spitzer* observations, then it is unlikely that they are very young star forming galaxies.

6.5.1 Population III stars?

The Large Area Lyman Alpha (LALA) survey has found ~ 150 Lyα emitters at $z = 4.5$ (Rhoads & Malhotra 2001; Dawson et al. 2004). Interestingly, 60% of the Lyα emitters have a rest-frame equivalent width (EW_0) in excess of 240 Å (Malhotra & Rhoads 2002), which is the predicted maximum EW_0 in stellar models (Charlot & Fall 1993). Malhotra & Rhoads (2002) argue that the stellar initial mass function must have a very steep slope, or that the metallicity of stars is zero (Population III stars). We can compare the results from the LALA with our result. In Fig. 6.8 the distribution of EW_0 of the 298 candidate Lyα emitters is plotted. The overplotted grey histogram shows the distribution of the 153 confirmed emitters. In contrast to Malhotra & Rhoads (2002), we find that only a small fraction ($\lesssim 5\%$ of the confirmed emitters) of the emitters has an $EW_0 > 240$ Å. Also due to the very faint continuum, the error on the equivalent width is large for the high equivalent width objects, up to $\Delta EW_0 \sim 100$ Å. Our observation are therefore consistent with the predicted maximum EW_0 of 240 Å, and Population III stars are not needed to explain our results.

The results of the LALA survey in Malhotra & Rhoads (2002) could be explained in part by the method they used to calculate the EW_0. If an object was not detected in the broad-band image, they used the actual measured flux at the location of the narrow-band source, in stead of an upper limit on the flux. This sometimes made the EW_0 negative. Our approach was to set a 2σ upper limit to the flux if the object was not detected in the broad-band. Applying our method to the LALA data, the fraction of emitters with an $EW_0 > 240$ Å reduces to $\ll 10\%$ (see also Fig. 1 in Malhotra & Rhoads 2002).
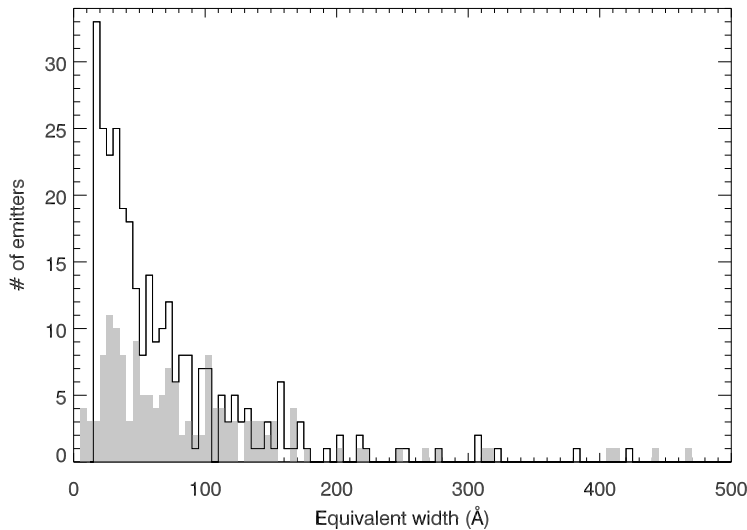
Figure 6.8 — The distribution of rest-frame equivalent width of 298 candidate Lyα emitters in eight high redshift radio galaxy fields. The solid grey histogram represents the equivalent width distribution of the 153 confirmed Lyα emitters in these fields.

Acknowledgments

References

Brocklehurst, M. 1971, MNRAS, 153, 471
Charlot, S. & Fall, S. M. 1993, ApJ, 415, 580
Cooke, J., Wolfe, A. M., Prochaska, J. X., & Gawiser, E. 2004, AJ accepted, astro-ph/0411681
Cowie, L. L. & Hu, E. M. 1998, AJ, 115, 1319
Dawson, S., Rhoads, J. E., Malhotra, S., et al. 2004, ApJ, 617, 707
de Propris, R., Pritchet, C. J., Hartwick, F. D. A., & Hickson, P. 1993, AJ, 105, 1243
Della Ceca, R., Braito, V., Beckmann, V., et al. 2003, A&A, 406, 555
Ellis, R., Santos, M. R., Kneib, J., & Kuijken, K. 2001, ApJ, 560, L119
Fujita, S. S., Ajiki, M., Shioya, Y., et al. 2003, AJ, 125, 13
Fynbo, J. P. U., Ledoux, C., Møller, P., Thomsen, B., & Burud, I. 2003, A&A, 407, 147
Fynbo, J. P. U., Møller, P., & Thomsen, B. 2001, A&A, 374, 443
Giavalisco, M. 2002, ARA&A, 40, 579
Hayashino, T., Matsuda, Y., Tamura, H., et al. 2004, AJ, 128, 2073
Hu, E. M., Cowie, L. L., Capak, P., et al. 2004, AJ, 127, 563
Hu, E. M., Cowie, L. L., & McMahon, R. G. 1998, ApJ, 502, L99
Hu, E. M., Cowie, L. L., McMahon, R. G., et al. 2002, ApJ, 568, L75
Jarvis, M. J., van Breukelen, C., & Wilman, R. J. 2005, MNRAS, L12
Kodaira, K., Taniguchi, Y., Kashikawa, N., et al. 2003, PASJ, 55, L17
Koo, D. C. & Kron, R. T. 1980, PASP, 92, 537
Kudritzki, R.-P., Méndez, R. H., Feldmeier, J. J., et al. 2000, ApJ, 536, 19
Leitherer, C., Schaerer, D., Goldader, J. D., et al. 1999, ApJ, 123, 3
Lowenthal, J. D., Hogan, C. J., Leach, R. W., Schmidt, G. D., & Foltz, C. B. 1990, ApJ, 357, 3
Madau, P., Pozzetti, L., & Dickinson, M. 1998, ApJ, 498, 106
Malhotra, S. & Rhoads, J. E. 2002, ApJ, 565, L71
Malhotra, S., Wang, J. X., Rhoads, J. E., Heckman, T. M., & Norman, C. A. 2003, ApJ, 585, L25
Meier, D. L. 1976, ApJ, 207, 343
Møller, P. & Fynbo, J. P. U. 2001, A&A, 372, L57

Norman, C., Hasinger, G., Giacconi, R., et al. 2002, ApJ, 571, 218

Oke, J. B. 1974, ApJ, 27, 21

Ouchi, M., Shimasaku, K., Akiyama, M., et al. 2005, ApJ, 620, L1

Ouchi, M., Shimasaku, K., Furusawa, H., et al. 2003, ApJ, 582, 60

Palunas, P., Teplitz, H. I., Francis, P. J., Williger, G. M., & Woodgate, B. E. 2004, ApJ, 602, 545

Pentericci, L., Kurk, J. D., Carilli, C. L., et al. 2002, A&A, 396, 109

Pritchet, C. J. 1994, PASP, 106, 1052

Pritchet, C. J. & Hartwick, F. D. A. 1987, ApJ, 320, 464

Rhoads, J. E., Dey, A., Malhotra, S., et al. 2003, AJ, 125, 1006

Rhoads, J. E. & Malhotra, S. 2001, ApJ, 563, L5

Shapley, A. E., Steidel, C. C., Pettini, M., & Adelberger, K. L. 2003, ApJ, 588, 65

Shimasaku, K., Ouchi, M., Okamura, S., et al. 2003, ApJ, 586, L111

Smith, H. E., Cohen, R. D., Burns, J. E., Moore, D. J., & Uchida, B. A. 1989, ApJ, 347, 87

Steidel, C. C., Adelberger, K. L., Giavalisco, M., Dickinson, M., & Pettini, M. 1999, ApJ, 519, 1

Steidel, C. C., Adelberger, K. L., Shapley, A. E., et al. 2000, ApJ, 532, 170

Steidel, C. C., Adelberger, K. L., Shapley, A. E., et al. 2003, ApJ, 592, 728

Stern, D., Moran, E. C., Coil, A. L., et al. 2002, ApJ, 568, 71

Thompson, D., Djorgovski, S. G., & Trauger, J. 1995, AJ, 110, 963

Thompson, D. & Djorgovski, S. G. 1995, AJ, 110, 982

Wang, J. X., Rhoads, J. E., Malhotra, S., et al. 2004, ApJ, 608, L21

Chapter 7

Radio galaxy protoclusters and models of structure formation

Abstract. Recently, we have discovered galaxy overdensities near seven luminous high redshift radio galaxies with $2.2 < z < 5.2$. The estimated masses of these forming clusters, or protoclusters, are consistent with the structures being the ancestors of present-day massive clusters of galaxies. In this chapter we compare high resolution N-body simulations of massive clusters combined with semi-analytical galaxy formation models with the observed protoclusters. We show that based on the observed properties of the Lyα emitters and their location in the protoclusters we can identify the Lyα emitting galaxies with the young (ages < 100 Myr) population of model galaxies in the simulations. The velocity dispersions of the confirmed galaxies in the observed protoclusters increase with decreasing redshift. A similar trend is seen in the velocity distribution of model cluster galaxies in the simulations. The agreement between theory and observations is strong additional evidence for the hypothesis that the radio galaxy protoclusters are forming massive clusters. We show that (a large fraction of) the confirmed Hα emitters near MRC 1138–262 at $z = 2.16$ lie in the region of the virialized core of a simulated forming massive cluster, implying that the Hα excess objects are likely to be the progenitors of old red cluster galaxies seen in $z < 1$ clusters.

B. P. Venemans, G. De Lucia, G. K. Miley & H. J. A. Röttgering

7.1 Introduction

U NDERSTANDING the formation and evolution of clusters and their galaxies is a key goal of cosmology. During the last decade significant progress has been made in studying clusters of galaxies up to redshifts of $z \sim 1$ (for a review, see Rosati et al. 2002). Unfortunately, conventional methods for finding distant clusters, including surveys for extended X-ray emission and galaxy overdensities are impractical for $z > 1$.

Luminous high redshift radio galaxies (HzRGs; $z > 2$) have properties consistent with them being the progenitors of local brightest cluster galaxies (see e.g. McCarthy et al. 1990, for a review). To search for distant clusters and their ancestors, we studied the environment of several radio galaxies in the redshift range $2.0 < z < 5.2$ (see Chapter 2 to 5). As a result, we found overdensities of Lyα emitting galaxies near at least six out of eight radio galaxy fields studied to sufficient depth (Chapter 5). The redshift distributions of the confirmed galaxies are narrow (velocity dispersions of $\sigma_v \sim 300 - 1000$ km s^{-1}), and the centres of the velocity distributions are located within a few hundred km s^{-1} of the redshift of the radio galaxies (Chapter 2 to 5). Based on the high density of galaxies near the radio galaxy combined with the narrow redshift distribution, we concluded that the Lyα emitters are members of forming clusters (protoclusters) that are physically associated with the radio galaxies. The estimated masses of the structures are in the range of $(2-9) \times 10^{14} \, M_\odot$ (Chapter 5). In the local Universe this mass scale corresponds to massive clusters of galaxies, and we concluded that the protoclusters are the progenitors of massive clusters.

In this chapter, we compare our observations with numerical simulations of the development of large scale structure in the Universe and show that the observed galaxy overdensities are consistent with forming massive clusters. §7.2 gives a brief description of the N-body simulations used and the semi-analytical models employed to provide catalogues with (properties of) cluster galaxies. We attempt to identify the observed Lyα emitters with model galaxies in §7.3. In §7.4 we compare the observed velocity distributions with those of the simulated model cluster galaxies and the virialized region of the protoclusters is studied in §7.5. The results are discussed in §7.6, followed by the conclusion in §7.7. Throughout this chapter, we adopt a standard Λ dominated, flat cosmology with $\Omega_M = 0.3$ and a Hubble constant of $70 \, \text{km s}^{-1} \, \text{Mpc}^{-1}$.

7.2 High resolution models of structure formation

7.2.1 N-body simulations of clusters

To compare the properties of the radio galaxy protoclusters with models of structure formation, we needed simulations with sufficient spatial and mass resolution to allow the identification of individual galaxies. For this purpose, five clusters with virialized masses at $z = 0$ of $\gtrsim 10^{15} \, M_\odot$ were randomly selected from the Very Large Simulation (Jenkins et al. 2001; Yoshida et al. 2001), a large (box size of ~ 700 Mpc) cosmological dark matter simulation. Next, the five selected clusters were resimulated with a higher resolution by applying the "zoom" technique (Katz & White 1993; Tormen et al. 1997). With this technique all the (dark matter) particles that make up each of the selected clusters were traced back to their initial position in the original simulation. The

particles were then replaced by a larger number of lower mass particles to obtain a better mass and spatial resolution. The region occupied by these low mass particles is called the "high resolution region". Because the spatial resolution has increased high frequency primordial fluctuations were added in the high resolution simulation. Outside the "high resolution region" particles of variable mass, increasing with distance were used. This allowed a faithful representation of the large scale density field of the original simulation to be maintained.

The high resolution simulation was then run using the tree code GADGET (Springel et al. 2001). The size of the "high resolution region" is roughly 13 comoving Mpc, which is the maximum size in the resimulation that only contains high resolution particles (see Clowe et al. 2004). The spatial and dark matter mass resolution was 7 kpc and $3 \times 10^9 \ M_\odot$ respectively. A detailed description of the "zoom" method and the properties of the resimulated clusters can be found in Lanzoni et al. (2003, 2004).

7.2.2 Galaxy modelling

The dark matter in the simulations was complemented by a baryonic component to follow the formation and evolution of galaxies in the clusters. Within cosmological simulations, the formation of large scale structure is driven by the hierarchical merging of the cold dark matter. However, the baryonic matter represents the direct observable (luminous) part of the clusters.

The evolution of the baryonic component was modelled using semi-analytical galaxy formation models (e.g. White & Rees 1978; White & Frenk 1991; Cole 1991). This technique avoids the complicated physics involved in galaxy formation and evolution. Instead, simplified, physically motivated prescriptions are adopted to describe the evolution of galaxies. The semi-analytic models used in the cluster simulations included gas cooling, star formation, feedback and metal production, and galaxy mergers (see De Lucia et al. 2004, for a detailed description of the semi-analytic models used). Subsequently, the Bruzual & Charlot stellar population models (Bruzual A. & Charlot 1993) were employed to calculate the spectral energy distributions of the cluster galaxies. Finally, the effects of dust extinction on the luminosity of the model galaxies were included.

The free parameters of the semi-analytical models were tuned to reproduce, among other things, the observed properties of the Milky Way, and several galaxy properties scaling relations such as the Tully-Fisher relation (which relates the luminosity to rotational velocity of late-type galaxies, Tully & Fisher 1977).

For each of the five simulated clusters, the properties of the model galaxies are extracted from the simulations at the redshifts that coincide with the redshifts of the observed protoclusters. In Fig. 7.1, an example of the properties (position, velocity, magnitude and color) of model galaxies in one of the simulated clusters at a redshift of $z \simeq 3$ are shown.

7.3 Lyα emitters in semi-analytical models

While the simulated clusters consist of hundreds of galaxies (e.g. Fig. 7.1), in the radio galaxy protoclusters are (at the moment) only < 80 Lyα and/or Hα emitters identified
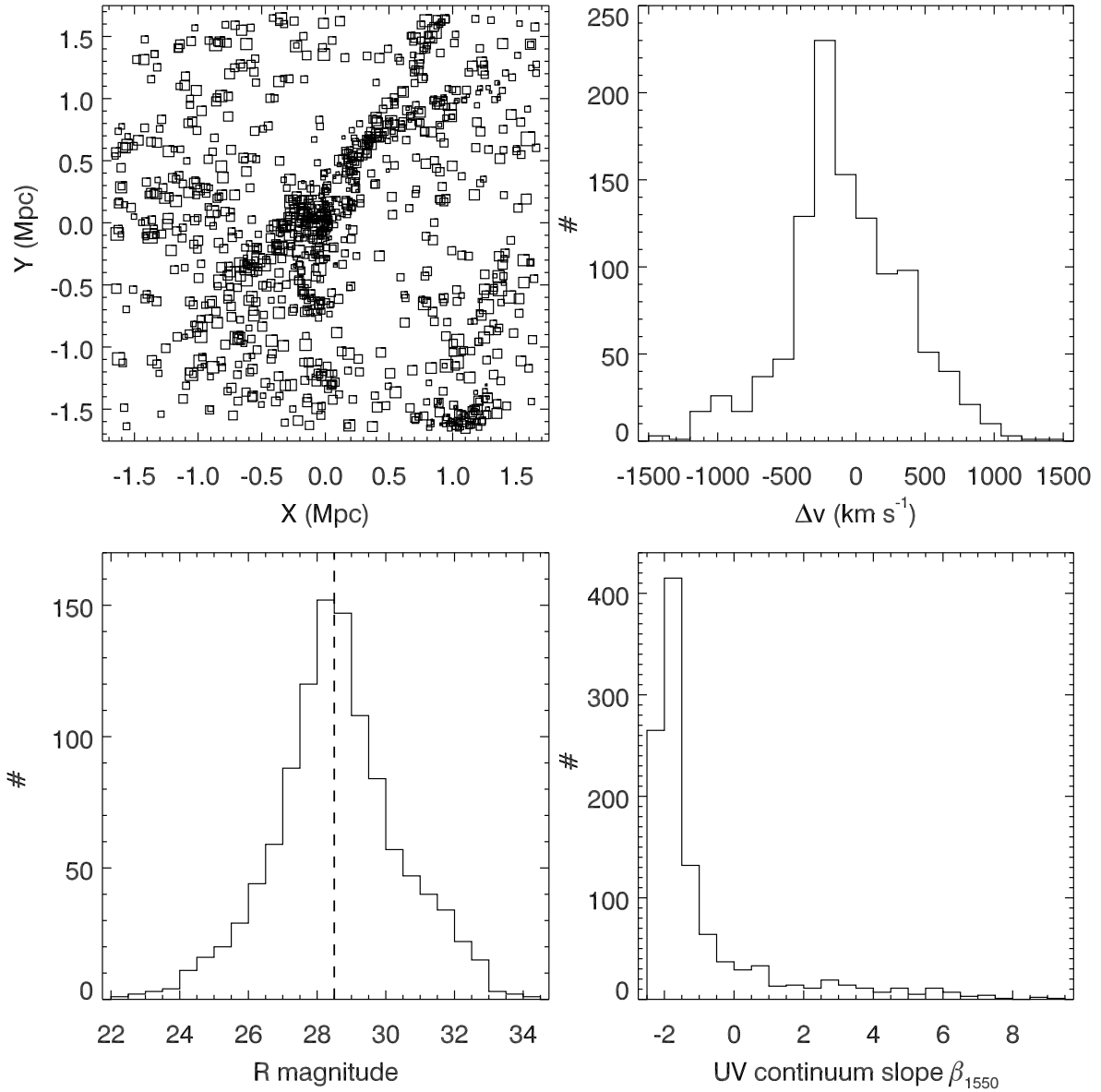
Figure 7.1 — Properties of model galaxies in one of the simulated clusters at $z \simeq 3$. (*Top left:*) Positions of the galaxies, relative to the position of the forming brightest cluster galaxy (BCG). The size of the symbol represents the UV luminosity of the galaxy at rest-frame wavelength of 1750 Å. (*Top right:*) Velocities of the galaxies relative to the BCG. The velocity dispersion of the galaxies is 425 $\mathrm{km\,s^{-1}}$. (*Bottom left:*) Observed *R*-band (rest-frame UV) magnitude of the model galaxies. The vertical dashed line indicates the magnitude where the semi-analytic model becomes incomplete due to the resolution limit of the simulation. (*Bottom right:*) distribution of the UV continuum slope near 1550 Å (β_{1550}, with $f_\lambda \sim \lambda^\beta$).

as (possible) cluster members. The number of spectroscopically confirmed members is < 40 in all cases. A question is whether we can identify galaxies in the simulations that could be associated with our relatively bright detected Lyα emitters.

The main difference between the hundreds of simulated galaxies and the Lyα emitters is the spatial distribution in the large scale structure. While the Lyα emitters are

either completely randomly distributed over the observed field or show a very modest increase towards the radio galaxy (Chapter 5), the simulated galaxies are concentrated near the central galaxy and show filamentary structure (see the top left panel in Fig. 7.1 for an example). Apparently, the Lyα emitters represent a population of galaxies in the forming cluster that is not very concentrated at the center of the structure. To illustrate this, we randomly selected 70 galaxies in the simulated clusters, which is roughly the number of (candidate) Lyα emitters in the protoclusters at $z \simeq 3$ (see Chapter 5). In the top panels of Fig. 7.2 an example is shown of the positions and radial profile of 70 model galaxies. The selected galaxies are strongly concentrated towards the cluster center, making it unlikely that the observed Lyα emitters are random cluster galaxies.

The properties of Lyα emitters at $z \simeq 3$ can be summarized as faint, blue and small galaxies, compared to the UV bright Lyman Break galaxies (LBGs) at similar redshifts (see e.g. Chapter 3 and 6). Can we use these properties to identify a population of galaxies in the simulated cluster with similar characteristics?

Because the semi-analytic models do not predict the size of galaxies, it is not possible to uniquely identify the Lyα emitters in the models based on their observed small size. However, a selection of galaxies based on their luminosity can be applied. The R-band magnitude of the Lyα emitters in the 0316 protocluster at $z = 3.13$ ranges from 24.2 to fainter than 28.5, which corresponds to a luminosity ranging from $1.3\,L^*$ to $< 0.03L^*$ (Chapter 3). Unfortunately, as can be seen in Fig. 7.1, nearly all model galaxies in the $z \simeq 3$ clusters have magnitudes in this range. The number of galaxies in simulated massive clusters at $z \simeq 3$ with $24 < m_R < 28.5$ is roughly $\sim 450 - 550$. If we assume that 20–25% of these galaxies have a high equivalent width Lyα emission line, which is the empirical fraction for $m_R < 25.5$ galaxies at $z \sim 3$ (e.g. Steidel et al. 2000; Shapley et al. 2003), then we find roughly $\sim 90 - 140$ possible Lyα emitters. This is only slightly higher than observed in the protoclusters (Chapter 5). However, the spatial distribution of a random subset of 70 of these R-magnitude selected galaxies is not uniform over the field as the observed Lyα emitters. An example is shown in Fig. 7.2. It seems that the selection on UV luminosity does not give a spatial distribution similar to the observed population of Lyα emitters in the forming clusters.

One of the other properties of the observed Lyα emitters is their nearly flat UV continuum ($\beta \simeq -2$ with $f_\lambda \sim \lambda^\beta$, see Chapter 3 and 6). However, most of the model galaxies have similar blue colors (Fig. 7.1). Selecting only the model galaxies with $\beta < -1.5$ vastly overestimates the number of galaxies, although the spatial distribution appears more uniform than that of the full sample of cluster galaxies (top panels in Fig. 7.3).

In Chapter 3 and 6 it is argued that the Lyα emitters might be young star forming galaxies in their first starburst phase. The possible young age of the Lyα emitters is supported by observations of Lyα emitters by other groups (e.g. Ellis et al. 2001; Keel et al. 2002; Malhotra & Rhoads 2002; Tapken et al. 2004). They also find that Lyα emitters might be very young, with ages as young as $< 10^7$ yr. Further support for this picture comes from models that try to explain the surface density of Lyα emitters at redshift $z > 3$ (e.g. Thommes & Meisenheimer 2005). In order to derive the correct number density of high redshift Lyα emitters, Thommes & Meisenheimer (2005) estimate that the Lyα bright phase of star forming galaxies lasts for only $\sim 10^8$ yr.
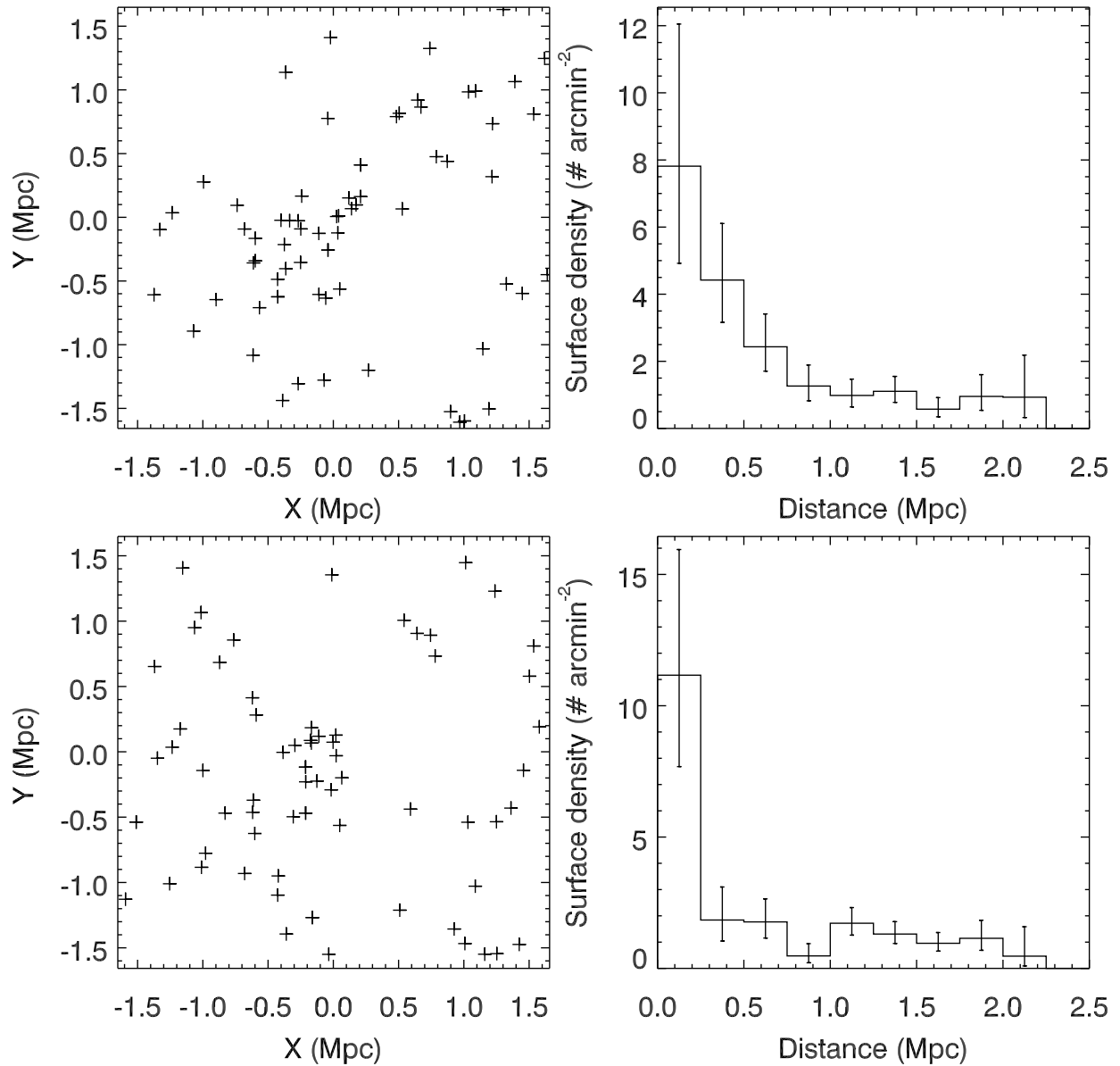
Figure 7.2 — (*Top left:*) Position of 70 randomly selected galaxies in one of the simulated clusters at $z \simeq 3$. (*Top right:*) Radial distribution of the 70 galaxies. The galaxies are concentrated toward the center, similar to the total population of cluster galaxies (see Fig. 7.1). (*Bottom left:*) Positions of 70 randomly selected galaxies with an $24 < m_R < 28.5$. (*Bottom right:*) Radial distribution of the 70 R-magnitude selected galaxies. The galaxies still follow the distribution of the full sample of cluster galaxies. The errors in the radial plots are Poissonian.

Most of the model galaxies in the simulated clusters at $z \simeq 3$ have ages between 300 Myr and 1 Gyr. If we select only the galaxies with ages younger than ~ 100 Myr as Lyα emitters, we roughly find the correct number of objects ($\sim 50 - 80$, the exact number depending slightly on the simulated cluster and redshift). Interestingly, the spatial distribution of these young model galaxies is more uniform over the field as compared to the distribution of all galaxies (see bottom panels of Fig. 7.3), in line with
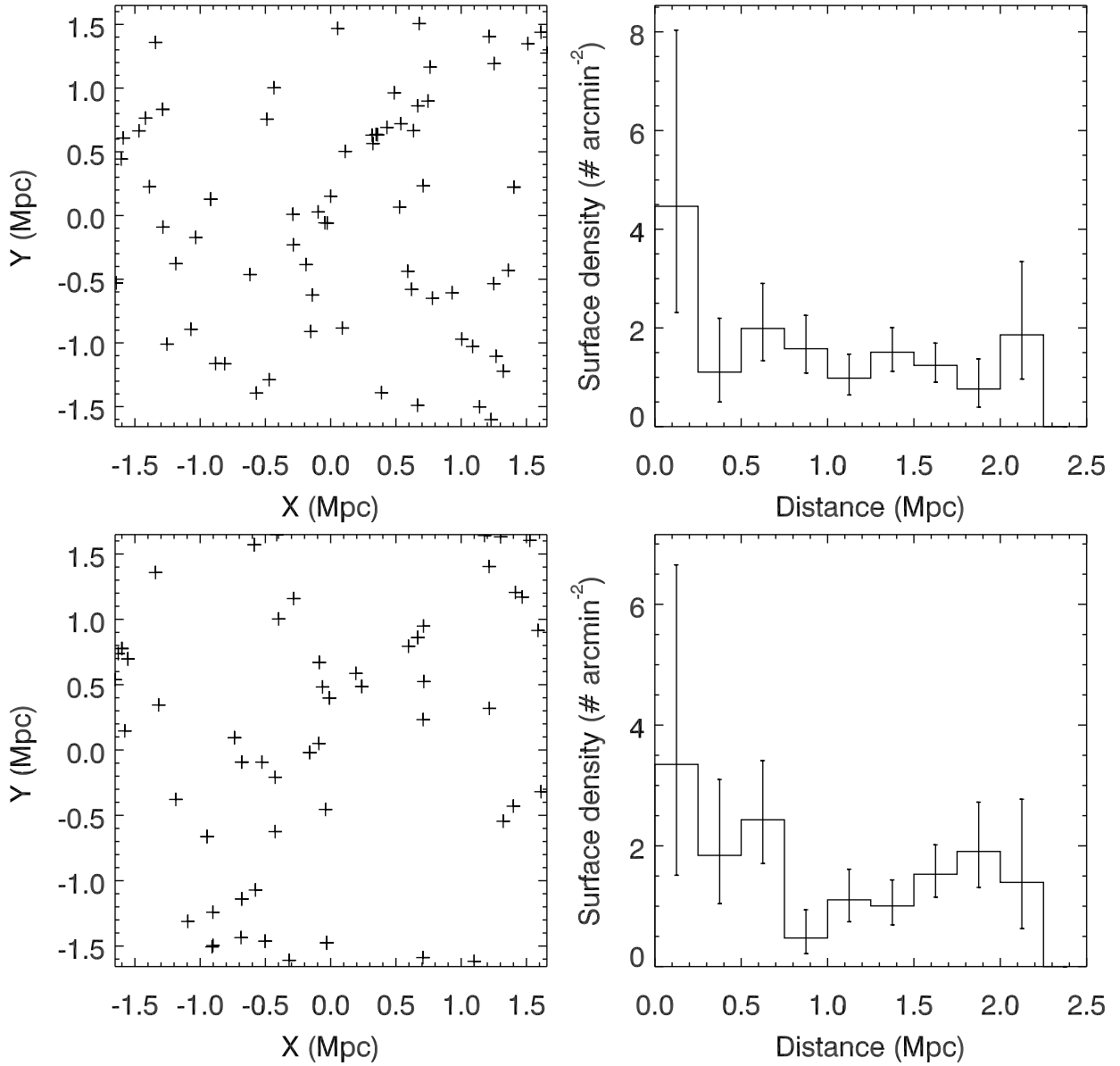
Figure 7.3 — (*Top left:*) Position of 70 galaxies with an UV continuum slope $\beta < -1.5$. (*Top right:*) Radial distribution of the 70 galaxies with $\beta < -1.5$. (*Bottom left:*) Positions of 70 galaxies with an age younger than 100 Myr and (*bottom right:*) radial distribution of the age < 100 Myr galaxies. The errors in the radial plots are Poissonian.

the spatial distribution of Lyα emitters in our protoclusters. This is consistent with the idea that the Lyα emitters are young galaxies, which are prodominantly located on the outskirts of the protoclusters, while the older, more evolved galaxies reside near the core of the protocluster.
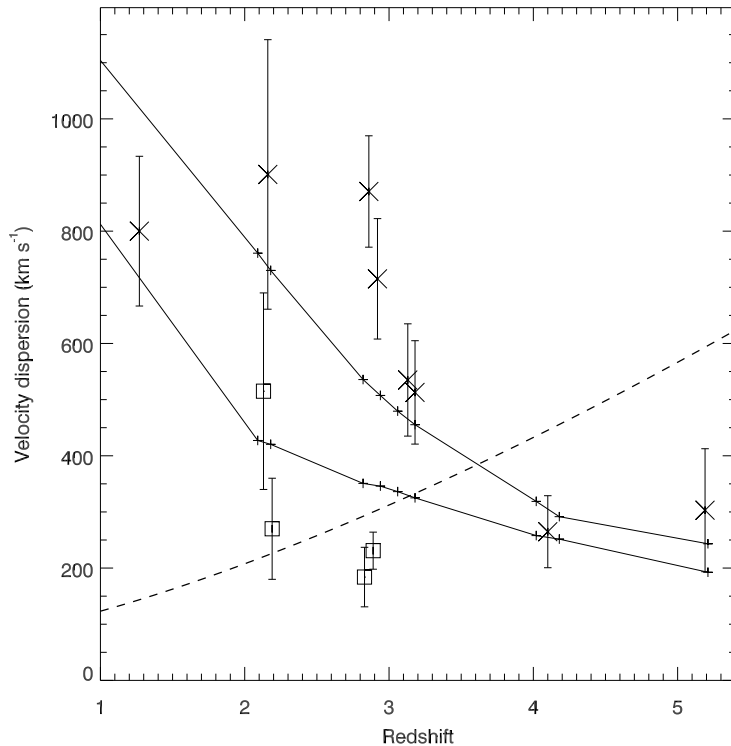
Figure 7.4 — Velocity dispersion of Lyα emitters in the radio galaxy protoclusters (*crosses*). The squares represent the velocity dispersion of the subgroups in the 1138 and 0052 fields (see Chapter 5 for the details). The data point near $z = 1.24$ represents the velocity dispersion in the X-ray cluster RDCS 1252.9-2927. The solid lines show the evolution of the velocity dispersion of the galaxies in two of the simulated clusters. The dashed line shows the Hubble flow over 1 Mpc as a function of redshift.

7.4   Galaxy velocity dispersion

In this section, we compare the observed properties of the protocluster with those of the simulated clusters. As mentioned in §7.2, the size of the high resolution simulation is 13 comoving Mpc, or 3.25 physical Mpc at $z = 3$. This is very similar to the size of our imaging of the radio galaxy protoclusters (e.g. Chapter 5). However, the size of the simulation is not large enough to show a clear edge of the forming clusters (e.g. top left panel in Fig. 7.1). We can therefore not derive a size from the protoclusters to compare our data to. Also, because the "field" (or an average density region) is outside the simulations, we can not predict how (over)dense our protoclusters should be.

One observation that we can compare is the velocity distribution of the cluster galaxies. The velocity dispersion of the Lyα emitters in the protoclusters seems to increase with decreasing redshift (Chapter 5). This increase was found to be very similar to the *dark matter* dispersion in numerical simulations of a massive cluster of galaxies (Eke et al. 1998, see Chapter 5). We can now look whether such a trend exists for the galaxy distributions in the (higher resolution) simulations presented in §7.2. We note that the velocity dispersion of the young (age < 100 Myr) model galaxies is generally consistent with the dispersion of all the cluster galaxies within 20%.

To compare the velocity dispersions, we need to analyze the velocity distribution of galaxies that reside in a similar sized region as modelled by the simulations. While our images have roughly the same size as that of the simulations ($\sim 3 \times 3$ Mpc^2), the redshift range that is probed by the narrow-band imaging is generally larger than the redshift depth of the simulations. The model cluster galaxies have velocities up to roughly 2000 km s^{-1} of that of the brightest cluster galaxy. We therefore only use emitters with

velocities within $2000 \, \mathrm{km \, s^{-1}}$ of the radio galaxy to calculate the velocity dispersion in the protoclusters.

This selection removed three emitters in the 0316 field (these galaxies were already marked as outliers, see Chapter 3) and two in 0052 field (see Chapter 5). In Fig. 7.4 the resulting velocity dispersion of the galaxies in the radio galaxy protoclusters is shown. Also plotted is the velocity dispersion of model galaxies in two simulated clusters, one with a dark matter halo mass of $3.3 \times 10^{15} \, M_{\odot}$ and one with $1.6 \times 10^{15} \, M_{\odot}$ at $z = 0$. Our data are consistent with the velocity dispersions as predicted for a $10^{15} \, M_{\odot}$ cluster, confirming our conclusions in Chapter 5 that the radio galaxy protoclusters are the progenitors of massive clusters.

7.5   Virialization

In Chapter 5, we assumed that the detected $\mathrm{Ly}\alpha$ emitters in the radio galaxy proto-clusters are far from virialization. The motivation for this assumption came from the estimated crossing time of a galaxy in the structure. The crossing time of a galaxy with a typical velocity ($\sim 500 \, \mathrm{km \, s^{-1}}$) in a protocluster is longer than the age of the Universe at high redshift ($z \sim 2 - 5$).

In the five simulated clusters, we can estimate the size of the region that is virialized. The virialized region in the simulation at a given redshift was defined as the region where the (dark matter) density was 200 times the critical density at $z = 0$. The spherical collapse model predicts that this region is virialized (e.g. Navarro et al. 1996; Lanzoni et al. 2004).

In Fig. 7.5, the "virial radius" R_{200} and the enclosed "virial mass" M_{200} of this high density region is plotted as a function of redshift. The "virial radius" is relatively small compared to the size of our imaging and ranges from $\lesssim 100$ kpc at $z = 4.1$ to $\lesssim 375$ kpc at $z = 2.2$. At redshifts $z \gtrsim 3$, the predicted "virial radius" of the protoclusters is $R_{200} \lesssim 200$ kpc. In the protoclusters, the number of $\mathrm{Ly}\alpha$ emitters within 200 kpc of the central (radio) galaxy is ≤ 2, of which at most one has a known redshift. It is therefore not possible to calculate a velocity dispersion in the virialized region.

At a redshift of $z \simeq 2.2$, R_{200} is $\lesssim 375$ kpc (Fig. 7.5). In the surroundings of the $z = 2.16$ radio galaxy MRC 1138–262 are three confirmed $\mathrm{Ly}\alpha$ emitters within a distance of 375 kpc from the radio galaxy (Pentericci et al. 2000; Kurk et al. 2004b), which is not enough to derive a velocity dispersion from. Fortunately, the 1138 field also contains forty candidate $\mathrm{H}\alpha$ emitters (Kurk et al. 2004b). Kurk et al. (2004b) already showed that the $\mathrm{H}\alpha$ emitters are concentrated within $40''$ (330 kpc) of the radio galaxy, within the "virial radius" at $z = 2.16$. Recently, redshifts were measured for nine of the $\mathrm{H}\alpha$ emitters (Kurk et al. 2004a). Of the nine confirmed $\mathrm{H}\alpha$ emitters, seven are located with 375 kpc of the radio galaxy. Despite the very small number of redshifts, we attempt to compute the velocity dispersion of these $\mathrm{H}\alpha$ emitters. The dispersion of the seven $\mathrm{H}\alpha$ emitters within the "virial radius" is $450 \, \mathrm{km \, s^{-1}}$. Using the gapper sigma, which is a better scale estimator for very small samples (Beers et al. 1990), the velocity dispersion is $480 \, \mathrm{km \, s^{-1}}$. Because of the low number of redshifts, the uncertainty in this dispersion using the bootstrap error analysis (e.g. Barrow et al. 1984) is $\sim 40\%$. Assuming the seven $\mathrm{H}\alpha$ emitters are within the virialized region of the protocluster (i.e. they are not
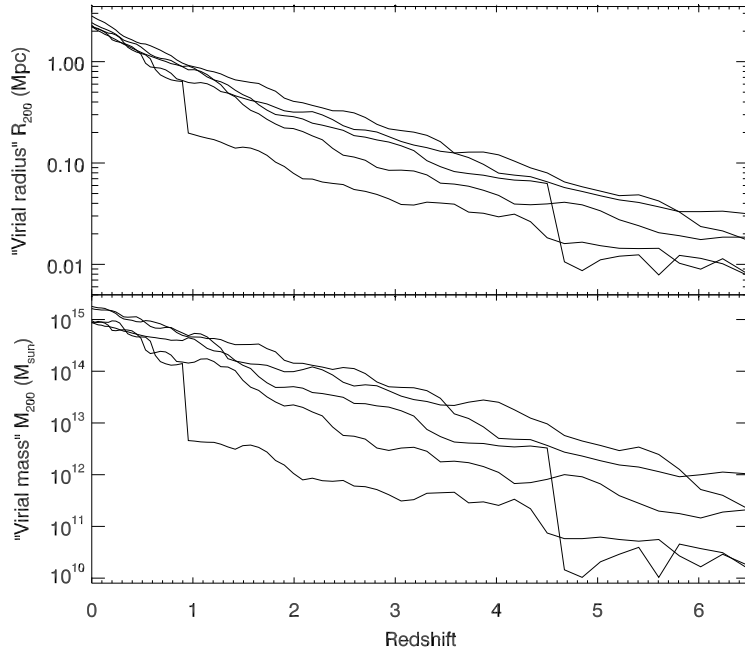
Figure 7.5 — Radius and mass of the region where in the simulations the density is 200 times the critical density at $z = 0$, as a function of redshift.

foreground or background galaxies), the virial mass is $(1.2 \pm 0.9) \times 10^{14}\, M_{\odot}$. If the three confirmed Lyα emitters within 375 kpc of the radio galaxy are included, the velocity dispersion increases to $635 \pm 190\ \mathrm{km\,s^{-1}}$. With this dispersion the estimated virial mass is $(2.1 \pm 1.2) \times 10^{14}\, M_{\odot}$. Although the errors are large due to the very small number of redshifts, these estimates of the virial mass are very similar to the "virial mass" M_{200} of $M_{200} \lesssim 1.9 \times 10^{14}\, M_{\odot}$ as derived from the simulations (Fig. 7.5). This could indicate that the Hα emitters are relatively old galaxies that will evolve into the central population of old red galaxies that is seen in $z < 1$ clusters (e.g. Holden et al. 2004; Gladders & Yee 2005).

7.6 Discussion

In §7.4 we conclude that the increase in velocity dispersion of the protocluster galaxies with cosmic time is consistent with simulations of a forming massive cluster. It is interesting to note that in two of our protoclusters (near the radio galaxies MRC 1138–262 at $z = 2.16$ and MRC 0052–241 at $z = 2.86$) the velocity distribution (with a dispersion of $900 - 1000\ \mathrm{km\,s^{-1}}$) of the confirmed Ly$\alpha$ emitters appears to be bimodal. In the 1138 field, the 14 emitters reside in two groups of seven emitters each (Pentericci et al. 2000), while in the 0052 field there are two groups with 12 and 19 members (Chapter 5). Such a bimodal distribution is rare in the simulations. The chance of finding a double peaked distribution of model galaxies or a distribution with a dispersion of $\sim 900\ \mathrm{km\,s^{-1}}$ by randomly selecting 20–40 model galaxies in the simulated clusters, is negligible ($< 0.01\%$).

It could be that we are observing some of the protoclusters just as two smaller subclusters are merging. As can be seen in Fig. 7.5, the clusters undergo several major mergers, in which the (virial) mass increases by a least 50%. For the five simulated clusters used in the chapter, between two and five major mergers occur at redshifts

$z < 5$. It is therefore plausible that we witness a major merging event in both the 0052 and 1138 fields. It is intriguing that we see such a rare event in two out of our seven (possible) protoclusters. A possible explanation could be that the merging triggers the activity of the central massive galaxy. As the two subgroups merge, the central galaxy is supplied with gas which could activate the central black hole. However, more radio galaxy protoclusters are needed to improve the statistics on this.

In the near future, the simulations will improve significantly. One of the most interesting next-generation large N-body simulations is the "Millennium Simulation"[1]. The size of the simulation is 700 Mpc on a side. The mass and spatial resolution of the entire simulation is 10^9 $M_\odot$ and 7 kpc respectively, which is equal or better than the (much smaller) resimulations used in this chapter. With this simulation, it will be possible to look at the extent and the galaxy content of tens of clusters that reside in the volume. Galaxies can be selected in both field environments and in clusters and the overdensity of different populations of cluster galaxies can directly be compared with the observations.

The more detailed simulations have to be matched with more observations. We need to observe more additional types of galaxies in the protoclusters. In the 1138 protocluster various galaxy populations are already detected (Kurk et al. 2004b), with very different spatial and velocity distributions (§7.5, Kurk et al. 2004b). In other radio galaxy protoclusters the Lyα emitting galaxies are supplemented by other populations of galaxies. For example, candidate UV bright star forming galaxies have been detected in the 1338 protocluster at $z = 4.1$ (Miley et al. 2004) complemented by very dusty galaxies (De Breuck et al. 2004). Also in the 0924 protocluster at $z = 5.2$ candidate UV bright cluster galaxies are detected (Overzier et al. 2005). The next step is to measure the redshifts of these additional galaxies to establish their velocity distribution. Combined with detailed simulations, this can lead to a better understanding of the formation of massive clusters and their galaxies.

7.7 Conclusion

This chapter presents a first order comparison between the observations of radio galaxy protoclusters with simulations of large scale structure. This comparison implies that (i) the Lyα emitting galaxies can be identified with the young galaxies in the simulations, and (ii) the change in the observed velocity dispersion with redshift is consistent with simulations of the most massive clusters. A more detailed comparison with the next generation simulations will be made in the near future.

References

Barrow, J. D., Bhavsar, S. P., & Sonoda, D. H. 1984, MNRAS, 210, 19P
Beers, T. C., Flynn, K., & Gebhardt, K. 1990, AJ, 100, 32
Bruzual A., G. & Charlot, S. 1993, ApJ, 405, 538
Clowe, D., De Lucia, G. , & King, L. 2004, MNRAS, 350, 1038
Cole, S. 1991, ApJ, 367, 45

---

[1]for details, see http://www.mpa-garching.mpg.de/mpa/research/current_research/hl2004-8/hl2004-8-en.html

De Breuck, C., Bertoldi, F., Carilli, C. L., et al. 2004, A&A, 424, 1
De Lucia, G., Kauffmann, G., & White, S. D. M. 2004, MNRAS, 349, 1101
Eke, V. R., Navarro, J. F., & Frenk, C. S. 1998, ApJ, 503, 569
Ellis, R., Santos, M. R., Kneib, J., & Kuijken, K. 2001, ApJ, 560, L119
Gladders, M. D. & Yee, H. K. C. 2005, ApJ, 157, 1
Holden, B. P., Stanford, S. A., Eisenhardt, P., & Dickinson, M. 2004, AJ, 127, 2484
Jenkins, A., Frenk, C. S., White, S. D. M., et al. 2001, MNRAS, 321, 372
Katz, N. & White, S. D. M. 1993, ApJ, 412, 455
Keel, W. C., Wu, W., Waddington, I., Windhorst, R. A., & Pascarelle, S. M. 2002, AJ, 123, 3041
Kurk, J. D., Pentericci, L., Overzier, R. A., Röttgering, H. J. A., & Miley, G. K. 2004a, A&A, 428, 817
Kurk, J. D., Pentericci, L., Röttgering, H. J. A., & Miley, G. K. 2004b, A&A, 428, 793
Lanzoni, B., Cappi, A., & Ciotti, L. 2003, Memorie della Societa Astronomica Italiana Supplement, 1, 145
Lanzoni, B., Ciotti, L., Cappi, A., Tormen, G., & Zamorani, G. 2004, ApJ, 600, 640
Malhotra, S. & Rhoads, J. E. 2002, ApJ, 565, L71
McCarthy, P. J., Kapahi, V. K., van Breugel, W. J. M., & Subrahmanya, C. R. 1990, AJ, 100, 1014
Miley, G. K., Overzier, R. A., Tsvetanov, Z. I., et al. 2004, Nature, 427, 47
Navarro, J. F., Frenk, C. S., & White, S. D. M. 1996, ApJ, 462, 563
Overzier, R. A., Zirm, A. W., Miley, G. K., et al. 2005, ApJ, submitted
Pentericci, L., Kurk, J. D., Röttgering, H. J. A., et al. 2000, A&A, 361, L25
Rosati, P., Borgani, S., & Norman, C. 2002, ARA&A, 40, 539
Shapley, A. E., Steidel, C. C., Pettini, M., & Adelberger, K. L. 2003, ApJ, 588, 65
Springel, V., Yoshida, N., & White, S. D. M. 2001, New Astronomy, 6, 79
Steidel, C. C., Adelberger, K. L., Shapley, A. E., et al. 2000, ApJ, 532, 170
Tapken, C., Appenzeller, I., Mehlert, D., Noll, S., & Richling, S. 2004, A&A, 416, L1
Thommes, E. & Meisenheimer, K. 2005, A&A, 430, 877
Tormen, G., Bouchet, F. R., & White, S. D. M. 1997, MNRAS, 286, 865
Tully, R. B. & Fisher, J. R. 1977, A&A, 54, 661
White, S. D. M. & Frenk, C. S. 1991, ApJ, 379, 52
White, S. D. M. & Rees, M. J. 1978, MNRAS, 183, 341
Yoshida, N., Sheth, R. K., & Diaferio, A. 2001, MNRAS, 328, 669

Nederlandse samenvatting

Astronomen houden zich bezig met het bestuderen van het Heelal. We willen het antwoord te weten komen op vragen zoals: Hoe is het Heelal ontstaan? Wanneer en hoe zijn sterren ontstaan? Op welke wijze vormen zich sterrenstelsels? Hoe ontstaan planeten? Bestaan er eigenlijk planeten die rond een andere ster dan de Zon draaien? En is er leven (mogelijk) op andere planeten? In dit proefschrift wordt stilgestaan bij de vraag hoe en wanneer groepen van sterrenstelsels zijn ontstaan, die ook wel clusters van sterrenstelsels worden genoemd.

Introductie

Eén van de problemen bij het zoeken naar antwoorden op de bovenstaande vragen is dat de onderzoeksmethoden, die astronomen ter beschikking staan, erg beperkt zijn. Zo is het helaas niet mogelijk om in een laboratorium een ster te maken of om te experimenteren hoe je het gemakkelijkst een planeet vormt.

Astronomen zijn geheel afhankelijk van wat er te zien is in de ruimte om ons heen. Dus om te zien hoe een ster ontstaat, moeten we dan ook proberen een ster waar te nemen juist op dat moment dat deze zich aan het vormen is. Een groot probleem daarbij is dat het ontstaan van een ster, evenals de meeste andere processen in het Heelal, heel erg lang duurt. Het is dus onmogelijk voor de mens om de volledige levensduur van een ster te observeren. De Zon bijvoorbeeld is al vijf miljard jaar oud en zal het nog zeker vijf miljard jaar volhouden.

Gelukkig kunnen astronomen gebruik maken van het feit dat licht zich voortbeweegt met "slechts" $300\,000$ km s^{-1}. Ook al is dit heel erg snel (het licht doet er maar een seconde over om van de Maan naar de Aarde te vliegen), toch geeft dit ons veel mogelijkheden. Om een voorbeeld te geven: het licht van de Zon doet er ongeveer 8 minuten over voor het de Aarde bereikt. Dat betekent dat we de Zon waarnemen, zoals deze was toen zij het licht 8 minuten geleden uitzond. En zo geldt dit voor alles wat we waarnemen in het Heelal: hoe verder we kijken, hoe verder we terugkijken in de tijd. Dit betekent dat het licht van heel ver weg staande sterrenstelsels ons informatie geeft over de tijd dat het Heelal en sterrenstelsels nog jong(er) waren. Eigenlijk zijn astronomen dus een soort historici.

Een volgend probleem is: hoe kunnen we nu zien of een sterrenstelsel ver weg staat of juist dichtbij? Zoals te zien is in Figuur 1 zijn er enorm veel zwakke stelsels aan de hemel. Gezien de vele verschillende vormen, helderheden en kleuren waarin sterrenstelsels voorkomen, is het niet mogelijk om de afstanden tot de stelsels aan de hand van dit soort foto's te bepalen.

Gelukkig worden we ook hier door de natuur geholpen. Begin jaren '30 ontdekte Edwin Hubble namelijk dat sterrenstelsels sneller van ons weg bewegen naarmate de afstand tot de Aarde groter is. Deze snelheid heeft invloed op de kleur (het spectrum)

Figuur 1 — Diepe opname van een klein stukje van de hemel (het oppervlak van deze opname is meer dan 100 keer zo klein als het oppervlak van de volle Maan). De sterrenstelsels op deze opname zijn alle verschillend van grootte en vorm. Ook alle kleine vlekjes op de foto zijn sterrenstelsels (credit: R. Williams, The HDF Team (STScI) en NASA).

van sterrenstelsels als gevolg van het zogenaamde Doppler-effect. Dit effect is het beste uit te leggen met behulp van het volgende voorbeeld: als een ambulance naar jou toe komt, dan klinkt de toon van de sirene hoog (een hoge frequentie). Nadat de ambulance je is gepasseerd, klinkt de toon van de sirene een stuk lager (een lage frequentie). Deze verschuiving van de toonhoogte is een manifestatie van het Doppler-effect. Dit geldt ook voor licht. Als een lichtbron naar je toe beweegt, verschuift het licht naar een hogere frequentie. Een bron die van je af beweegt, verschuift naar een lagere frequentie. Onze ogen nemen hoge frequenties van het licht waar als blauw, terwijl we lage frequenties als rood zien. Hubble ontdekte dat hoe verder weg de sterrenstelsels staan, hoe meer het spectrum van zo'n stelsel verschoven is naar het rood (lage frequentie). Dit fenomeen wordt "roodverschuiving" genoemd en kan dus gebruikt worden als een maat voor afstand. Omdat aan het spectrum van sterrenstelsels relatief gemakkelijk is af te lezen met welke snelheid deze van ons af bewegen, worden in de sterrenkunde alle afstanden uitgedrukt in roodverschuiving.

Oerknal

Sinds de ontdekking van Hubble weten we dus dat ver weg gelegen stelsels sneller van ons af bewegen dan dichterbij gelegen stelsels. Deze snelheden zijn het gevolg van de uitdijing van het Heelal. Dit betekent dat vroeger alle stelsels veel dichter bij elkaar hebben gestaan. En als je maar ver genoeg terug gaat, zullen alle stelsels zich op één punt bevinden. Dit besef leidde tot de Oerknaltheorie[2]. De Oerknaltheorie gaat er vanuit dat het Heelal is begonnen als een enorm hete, compacte soep van energie

---

[2]De term Oerknal ("Big Bang" in het Engels) is bedacht door Fred Hoyle in de jaren '50. Hij gebruikte de term echter op sarcastische wijze, aangezien hij een enorme tegenstander van de theorie was en deze met de term Oerknal belachelijk wilde maken.

en materie. Naarmate het Heelal expandeerde, werd de soep dunner en kouder. De theorie voorspelde dat het Heelal gevuld zou moeten zijn met achtergrondstraling die het overblijfsel is van het hete begin. En deze straling is ook waargenomen! Inmiddels is het Heelal afgekoeld tot zo'n 3 graden boven het absolute nulpunt. Door de helderheid van de genoemde straling te meten ontdekte men dat de hoeveelheid straling overal aan de hemel gelijk is. Dit wekte verbazing, aangezien de materie in het Heelal niet gelijkelijk verdeeld is en je daarom grote fluctuaties in de achtergrondstraling zou verwachten. Pas na heel nauwkeurig bestuderen van de achtergrondstraling heeft men heel kleine fluctuaties (kleiner dan 0.01%) gevonden. Omdat de fluctuaties in de straling zo klein zijn, kunnen ook dichtheidsveranderingen vlak na de Oerknal niet groter zijn geweest dan 0.01%. Tussen toen en nu is er duidelijk veel veranderd: overal om ons heen in het Heelal zien we grote concentraties van materie, zoals sterren, sterrenstelsels, planeten, enzovoorts. In de loop van de tijd zijn die kleine fluctuaties in dichtheid dus uitgegroeid tot grote klonten materie. En de grootste structuren die hierbij zijn ontstaan, zijn groepen van sterrenstelsels (clusters).

Door te onderzoeken wanneer en op welke manier de eerste groepen van sterrenstelsels zijn ontstaan, hopen we meer te weten te komen over de manier waarop structuur in het Heelal zich heeft ontwikkeld. Dit proefschrift heeft deze vraagstelling tot onderwerp.
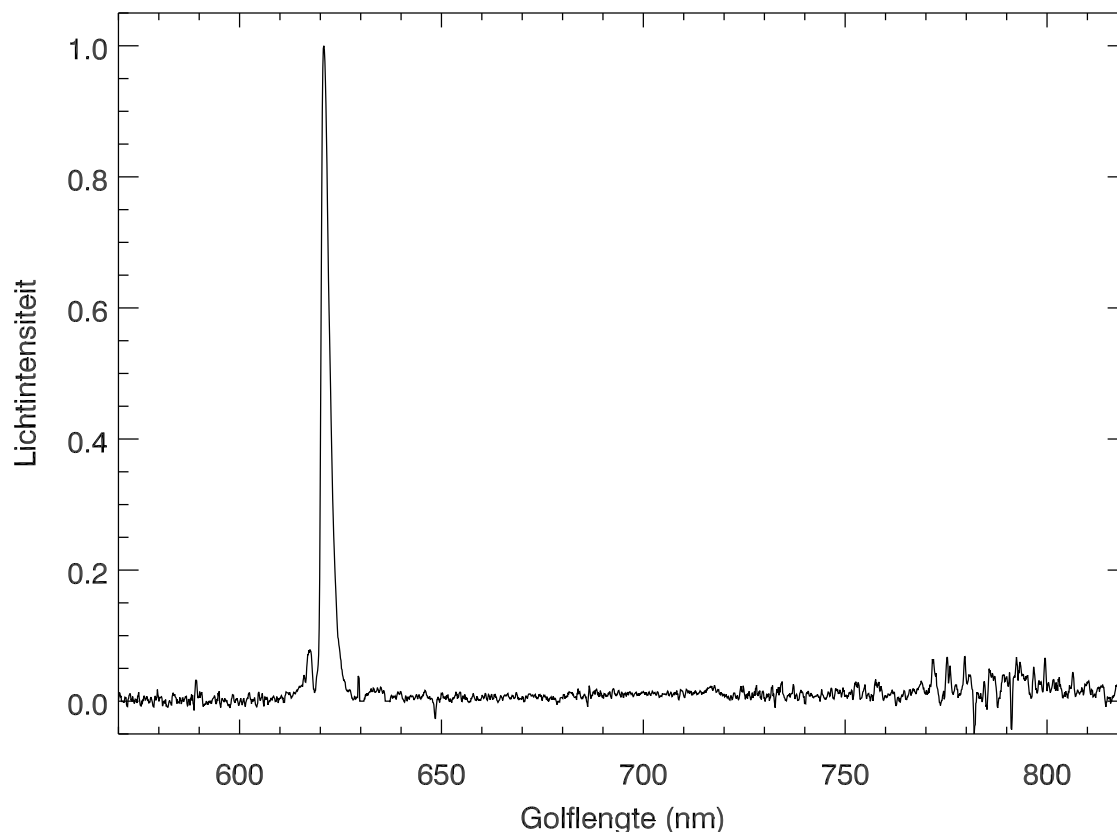
Radio sterrenstelsels

Om meer te weten te komen over het ontstaan van structuur in het vroege Heelal, bestuderen we groepen sterrenstelsels die ver weg staan en waarvan het door ons waargenomen licht dus informatie geeft over de tijd dat het Heelal nog erg jong was. Het is alleen moeilijk te bepalen waar die clusters van sterrenstelsels nu eigenlijk staan, omdat ze namelijk vrij zeldzaam zijn. We moeten er dus eerst achter komen waar we moeten zoeken. Radio sterrenstelsels kunnen hierbij helpen. Van dichtbijgelegen clusters van sterrenstelsels is namelijk gebleken dat zich in het centrum ervan enorme, massieve sterrenstelsels bevinden. Door te zoeken naar dit soort sterrenstelsels in het vroege Heelal kunnen we dus ook op het spoor komen van clusters. Maar hoe kunnen we nu dit soort sterrenstelsels localiseren? Het blijkt dat een massief sterrenstelsel in zijn kern een kolossaal zwart gat heeft, dat veel energie uitzendt op radiofrequenties; een dergelijk massief sterrenstelsel wordt dan ook een radio sterrenstelsel genoemd. De grote radiohelderheid van een dergelijk stelsel zorgt ervoor dat deze tot op grote afstand waar te nemen is.

Maar een ver radio sterrenstelsel is nog niet per definitie een ver cluster. Het laatste probleem is dan ook dat het lastig uit te maken is welke van de duizenden zichtbare stelsels behoren tot een bepaald cluster en welke niet. Deze clusterstelsels zijn namelijk niet helder op radiofrequenties, dus het is zaak om ze op een andere manier te localiseren.

Slimme truc

Radio sterrenstelsels zijn dus goede bakens om vormende, vroege clusters waar te nemen. Zoals te zien is in Figuur 1 is het moeilijk te bepalen welke stelsels eventueel in

Figuur 2 — Lichtintensiteit op iedere golflengte van een radio sterrenstelsel dat een roodverschuiving heeft van 4.1. De piek wordt veroorzaakt door de straling van heet waterstofgas.

een cluster zitten. Om stelsels te selecteren die samen met een radio sterrenstelsel een cluster vormen, hebben we een truc gebruikt. Deze truc maakt gebruik van de straling van heet waterstofgas. Een deel van de sterrenstelsels in het jonge Heelal blijkt veel straling van heet waterstofgas uit te zenden. Net zoals natriumlampen geel licht uitzenden (kijk bijvoorbeels 's avonds eens naar straatlantaarns), straalt heet waterstofgas ultra-violette straling uit, voornamelijk bij een golflengte van 121,6 nm. Op weg naar de Aarde wordt de straling van het hete waterstofgas verschoven naar het rood (roodverschuiving); dit komt doordat het Heelal uitdijt. Een voorbeeld hiervan is gegeven in Figuur 2. Te zien is de verdeling van de lichtintensiteit van een radio sterrenstelsel op iedere golflengte. De piek in deze verdeling is de waterstoflijn. Door de grote afstand van het radio sterrenstelsel (de roodverschuiving is 4.1) uit dit voorbeeld is de waterstoflijn roodverschoven naar een golflengte van ongeveer 620 nm. Door nu te zoeken naar sterrenstelsels met zo'n zelfde piek op dezelfde golflengte (dus met dezelfde roodverschuiving), selecteren we stelsels op gelijke afstand als het radiostelsel. We doen dit in de praktijk door de omgeving van het radio sterrenstelsel waar te nemen met een smalband filter, dat alleen licht doorlaat met een golflengte van 620 nm. Stelsels die opvallend helder zijn, gezien door dit smalband filter, hebben zeer waarschijnlijk een roodverschuiving die gelijk is aan dat van het radiostelsel en bevin-

den zich dus waarschijnlijk in hetzelfde cluster. Om daar helemaal zeker van te zijn, kan vervolgens de verdeling van de lichtintensiteit van deze stelsels worden bekeken om de roodverschuiving nog nauwkeuriger te meten.

Op deze wijze zijn wij erin geslaagd om groepen van sterrenstelsels te ontdekken in het vroege Heelal.

Dit proefschrift: verre clusters van sterrenstelsels rond radiostelsels

De afgelopen vier jaar hebben we de omgeving van radio sterrenstelsels met verschillende roodverschuivingen afgezocht op zoek naar clusters van sterrenstelsels. Hiervoor hebben we gebruik gemaakt van enkele van de grootste telescopen op Aarde, waaronder de Very Large Telescope (VLT) in Chili. In dit proefschrift worden de resultaten van dit project gepresenteerd.

In **hoofdstuk 2** worden de eerste resultaten van het project beschreven: de ontdekking van een zich vormend cluster rond een radio sterrenstelsel met een roodverschuiving van 4.1. Dit radiostelsel is heel bijzonder, omdat het één van de meest heldere waterstofgaslijnen heeft die we kennen (te zien in Figuur 2). Diepe opnames met een speciaal voor dit project gemaakt smalband filter laten een grote hoeveelheid sterrenstelsels zien die vlakbij het radiostelsel staan. Hieruit hebben we kunnen afleiden dat er zich al een cluster van stelsels had gevormd toen het Heelal nog maar 10% van zijn huidige leeftijd had. Een gedeelte van deze diepe opnames is afgedrukt op de voorkant van dit proefschrift.

In **hoofdstuk 3** wordt ingegaan op de ontdekking van een groep stelsels met een roodverschuiving van 3.1. Uit analyse van deze groep is gebleken dat we waarschijnlijk een voorouder hebben ontdekt van één van de grootste clusters van stelsels die bekend zijn in het nabije Heelal. Daarnaast hebben we door het combineren van diepe opnames van de VLT met foto's gemaakt door de Hubble Ruimtetelescoop gekeken naar de eigenschappen van de individuele stelsels in de groep. Het lijkt er op dat stelsels die straling van heet waterstofgas uitzenden erg jong zijn.

In **hoofdstuk 4** hebben we het allerverste radio sterrenstelsel, met een roodverschuiving van 5.2, geobserveerd. Door de enorme afstand tot het radiostelsel bleek het zelfs met onze slimme truc erg moeilijk om te ontdekken of er zich een cluster van sterrenstelsels in de omgeving bevond. Door verscheidene uren achter elkaar naar een klein gebiedje rond het radiostelsel te kijken met de VLT, hebben we toch aanwijzingen gevonden dat zelfs op deze grote afstand er zich al groepen begonnen te vormen.

In **hoofdstuk 5** beschrijven we alle data die we in de afgelopen jaren hebben verzameld. In totaal hebben we 25 nachten waargenomen met twee verschillende telescopen. Rond tenminste zes van de acht radiostelsels die we hebben bekeken, hebben we groepen van sterrenstelsels gevonden. Bij de overige twee konden we niet met zekerheid zeggen of er zich nu wel of niet een groep in de nabijheid bevond. Onze aanname dat radio sterrenstelsels gebruikt kunnen worden om clusters van sterrenstelsels te localiseren in het vroege Heelal blijkt juist te zijn, wat ons project tot een succes maakt.

Hoofdstuk 6 beschrijft de eigenschappen van de individuele sterrenstelsels die we hebben gevonden. Uit de data blijkt dat het waterstofgas waarvan we de straling

hebben waargenomen, verhit wordt door jonge, hete sterren. Daarnaast hebben we berekend dat deze sterrenstelsels erg jong zijn, waarschijnlijk niet veel ouder dan 100 miljoen jaar.

In **hoofdstuk 7** tenslotte vergelijken we de in het vroege Heelal gevonden groepen sterrenstelsels met modellen die beschrijven hoe clusters van sterrenstelsels ontstaan. De modellen en onze waarnemingen komen goed overeen, hetgeen onze conclusie versterkt dat we de voorouders hebben gevonden van de huidige massieve clusters van sterrenstelsels.

Curriculum vitae

Op de 20ste juni van het jaar 1977 ben ik geboren te Hoorn. Mijn eerste levensjaren heb ik doorgebracht in Medemblik, waarna ik naar Lelystad ben verhuisd. Vlak voor ik naar de middelbare school zou gaan, ben ik naar Amsterdam verhuisd. Van 1989 tot 1995 volgde ik het gymnasium aan het Spinoza Lyceum te Amsterdam. Na de middelbare school besloot ik sterrenkunde te gaan studeren aan de Universiteit Leiden. In 1996 behaalde ik mijn propedeuse en in het voorjaar van 1998 begon ik aan mijn afstudeeronderzoek "A Cluster of Galaxies around a High Redshift Radio Galaxy?" onder leiding van Dr. H. J. A. Röttgering. In het kader van dit onderzoek heb ik waargenomen met de New Technology Telescope op La Silla, Chili. In augustus 1999 rondde ik dit onderzoek en daarmee de studie sterrenkunde af.

Dankzij een beurs van het Talentenprogramma van het Nuffic kreeg ik de mogelijkheid om in oktober 1999 in Cambridge, Groot-Brittanië een eenjarige masteropleiding te doen in de astronomie. Als onderdeel van deze opleiding heb ik onderzoek gedaan naar het effect van stof op de straling van exploderende sterren onder leiding van Dr. A. W. Blain. Na het voltooien van de bijbehorende thesis "The visibility of gamma-ray burst afterglows in dusty star-forming regions", keerde ik terug naar Leiden om daar te starten op een promotieplek onder leiding van Prof. dr. G. K. Miley en Dr. H. J. A. Röttgering. De resultaten van dit onderzoek zijn gepresenteerd in dit proefschrift. Tijdens mijn promotie-onderzoek werd mij de gelegenheid geboden om regelmatig waar te nemen met 's werelds grootste optische telescopen. Acht keer heb ik het genoegen gehad om naar de Very Large Telescope in Chili te gaan, daarnaast heb ik mogen waarnemen met de Keck telescoop op Mauna Kea, Hawaii en met de Isaac Newton Telescope op La Palma, Spanje. Tevens heb ik werkbezoeken afgelegd aan de Lawrence Livermore National Laboratories, VS en de University of California Berkeley, VS. Om mijn werk te presenteren bezocht ik conferenties in Sesto (Italië), Lunteren, Santiago de Chile, Leiden, Venetië (Italië), Vlieland, Cambridge (Groot-Brittanië) en Oegstgeest. Ook heb ik een NOVA herfstschool in Dwingeloo bezocht. Daarnaast heb ik colloquia gegeven op de Carnegie Observatories (Pasadena, VS), Caltech (Pasadena, VS), University of California Santa Cruz (Santa Cruz, VS), Harvard-Smithsonian Center for Astrophysics (Cambridge, VS) en Johns Hopkins University (Baltimore, VS). In Leiden heb ik tijdens mijn promotie het werkcollege "Sterren" gegeven en het "Sterrenkundig Practicum 1" begeleid.

Na mijn promotie zal ik mijn onderzoek voortzetten als Postdoctoral Research Associate aan het Institute of Astronomy in Cambridge, Groot-Brittanië.

Nawoord

Er zijn veel mensen die ik wil bedanken voor het tot stand komen van dit proefschrift, al is het niet mogelijk om iedereen bij naam te noemen.

De Sterrewacht is een plezierige plek gebleken om onderzoek te doen. De goede werksfeer die steeds aanwezig is, is mede te danken aan de competente ondersteuning van de computergroep en het secretariaat. Maar ook de goede gesprekken, de wetenschappelijke discussies en het gezellige geklets in de pauzes, tijdens de lunch en op de borrel met vele andere Sterrewachters hebben hieraan zeker bijgedragen. In het bijzonder wil ik hiervoor bedanken: Andrew, Caroline, Jaron, Leonie, Mariska, Michiel en Roderik.

De financiële steun van onder andere het Kerkhoven-Bosscha Fonds en de Leidse Sterrewacht maakte het mogelijk om verschillende werkbezoeken af te leggen en internationale conferenties bij te wonen.

Naast het werk was er altijd tennis. Vele uren heb ik met mijn mede Qravelaars doorgebracht op de tennisbaan en in de kroeg. Onvergetelijk waren de heerlijke competitieweken in het voorjaar, die altijd het sportieve hoogtepunt van het jaar vormden.

Aan alle ex-Turf 10-ers: bedankt voor de gezelligheid en de vriendschappen door de jaren heen. Ik hoop dat we nog jaren met elkaar blijven huiseten, Kerstdineren en op weekend gaan.

Jantien: ik zal onze lunches en gesprekken over het promoveren en allerlei andere dingen erg gaan missen.

Mijn ouders wil ik bedanken voor het mij in contact brengen met de sterrenkunde. Ze hebben mij altijd gestimuleerd om in de wetenschap te gaan en te blijven. Hun steun was onmisbaar.

Nathalie, bedankt voor alles. Je was er altijd voor mij en zonder jou is mijn leven niet compleet. Ook al is de toekomst soms onzeker, we hebben altijd elkaar. Kocham cie.